Sphingolipid biosynthesis in *Physcomitrella patens*

Dissertation

for the award of the degree

“Doctor rerum naturalium”

of the University of Goettingen

within the GGNB doctoral program

“Microbiology and Biochemistry”

of the Georg-August University School of Science (GAUSS)

submitted by

Jasmin Gömann

born in

Holzminden

Göttingen 2020

Thesis Committee

Prof. Dr. Ivo Feußner
Department for Plant Biochemistry, Albrecht-von-Haller-Institute for Plant Science, University of Goettingen

Prof. Dr. Volker Lipka
Department of Plant Cell Biology, Albrecht-von-Haller Institute for Plant Science, University of Goettingen

Prof. Dr. Andrea Polle
Department for Forest Botany and Tree Physiology, Buesgen-Institute, University of Goettingen

Members of the Examination Board

Referee: Prof. Dr. Ivo Feußner
Department for Plant Biochemistry, Albrecht-von-Haller-Institute for Plant Science, University of Goettingen

2nd Referee: Prof. Dr. Volker Lipka
Department of Plant Cell Biology, Albrecht-von-Haller Institute for Plant Sciences, University of Goettingen

Further members of the Examination Board

Prof. Dr. Andrea Polle
Department for Forest Botany and Tree Physiology, Buesgen-Institute, University of Goettingen

Prof. Dr. Stefanie Pöggeler
Department for Genetics of Eukaryotic Microorganisms, Institute for Microbiology and Genetics, University of Goettingen

PD Dr. Till Ischebeck
Department for Plant Biochemistry, Albrecht-von-Haller-Institute for Plant Science, University of Goettingen

Jun.-Prof. Dr. Jan de Vries
Department of Bioinformatics (IMG), Institute for Microbiology and Genetics, University of Goettingen

Date of oral examination: November 16th, 2020

“ ‘Tell me, though, Miss Whittaker, what is it that you admire in mosses?’. ‘Their dignity,’ Alma replied without hesitation. ‘Also, their silence and intelligence. I like that—as a point of study—they are fresh. They are not like other bigger or more important plants, which have all been pondered and poked at by hordes of botanists already. I suppose I admire their modesty, as well. Mosses hold their beauty in elegant reserve. By comparison to mosses, everything else in the botanical world can seem so blunt and obvious. Do you understand what I am saying? Do you know how the bigger, showier flowers can look at times like dumb, drooling fools—the way they bob about with their mouths agape, appearing so stunned and helpless?’ […] ‘Somebody must defend them, Mr. Pike! For they have been so overlooked, and they have such a noble character! In fact, I find the miniature world to be a gift of disguised greatness, and therefore an honor to study.’ “

- Elizabeth Gilbert, *The Signature of All Things*

(S.201, Bloomsbury Publishing. Kindle-Version)

Affidavit

I hereby confirm that I wrote this dissertation entitled “Sphingolipid biosynthesis in *Physcomitrella patens*” on my own. No other sources and aids than quoted were used.

_____

Jasmin Gömann

Göttingen 2020

Table of Contents

1 Abstract

The complex sphingolipid classes glycosylceramides (GlcCers) and glycosyl inositolphosphorylceramides (GIPCs) are essential membrane components in plant cells. However, the regulation of their synthesis and their distinct physiological roles in plants is still poorly understood. GlcCers and GIPCs both contain a ceramide backbone consisting of a long-chain base (LCB) that is connected to a fatty acid. The syntheses of these two complex sphingolipids are alternative pathways in plant metabolism. It is assumed that distinct structural modifications in the LCB moiety determine the metabolic fate and physiological function of sphingolipids. In the bryophyte *Physcomitrella patens*, channelling of sphingolipid metabolites into complex sphingolipid formation appears to be stricter than in vascular plants. The physiological relevance of GlcCers, GIPCs, and their specific LCB moieties was therefore investigated in *P. patens*. *P. patens* GlcCers are enriched in ceramides with a dihydroxy, Δ4,8-diunsaturated LCB moiety while *P. patens* GIPCs mostly contain ceramides with a trihydroxy LCB moiety. The establishment of a sophisticated cultivation system and of various mutant characterisation assays is a prerequisite for in-depth examinations of *P. patens* mutants. *P. patens* knockout mutants were generated by homologous recombination that targeted key steps of sphingolipid biosynthesis. Disruption of the LCB C-4 hydroxylase, *Pp*S4H, which is involved in GIPC formation, resulted in plants that were severely impaired in growth and development. These growth impairments might have derived from cell plate formation defects during cytokinesis. Loss of the trihydroxy LCB moiety also caused global changes in all sphingolipid classes. Disruption of the LCB Δ4-desaturase, *Pp*SD4D, did not substantially affect plant viability. The mutant only showed mild cell elongation defects. However, *sd4d-1* mutants had substantially reduced GlcCer levels, which confirms that LCB Δ4-desaturation is important for channeling sphingolipids into GlcCer formation in *P. patens*. In contrast, *P. patens* plants that had a disturbed glycosylceramide synthase, *Pp*GCS, activity, were affected in plant growth and cell differentiation and showed cell death-like lesions. *gcs-1* plants lacked all GlcCers and accumulated precursor hydroxyceramides. Cumulative findings from this work show that disruption of individual steps in *P. patens* sphingolipid biosynthesis differently affect plant physiology. The results give first insights into sphingolipid biosynthesis in *P. patens*. While some aspects of plant sphingolipid metabolism known from studies in *Arabidopsis thaliana* have been confirmed in the bryophyte, novel features of the sphingolipid pathway could also be identified in *P. patens*. These new findings contribute to our knowledge on how sphingolipid synthesis and function have diversified during land plant evolution.

2 Introduction

2.1 Structure and function of biological membranes

Biological membranes are natural barriers that separate the inside of a cell from its external environment. They also act as an interface between the intracellular and extracellular space and therefore enable the exchange of nutrients and information. Intracellular membranes further restrict individual organelles and thereby establish compartmentalisation within a eukaryotic cell. The spatial restriction of subcellular compartments enables the simultaneous performance of numerous processes in close proximity to each other. Cell viability relies on the orchestration of these different physiological processes. Biological membranes play pivotal roles in synchronising cellular processes. The major constituent of biological membranes is a phospholipid bilayer. Phospholipids contain one or two hydrophobic hydrocarbon chains that are connected to a hydrophilic head group. The combination of hydrophilic and hydrophobic building blocks defines lipids as amphipathic molecules which is a crucial feature for membrane bilayer formation. The polar head group is oriented towards the surrounding aqueous phase, while the non-polar hydrocarbon chains face each other. They thereby form the inner and outer leaflets of biological membranes. The inner leaflet faces the cytosol of a cell or the lumen of an organelle while the outer leaflet faces the extracellular space or in case of plant cells, the apoplast.

The plasma membrane (PM) is a semipermeable lipid bilayer that defines the boundary of a cell. It separates the intracellular space from the extracellular environment. In plant cells the PM more accurately defines the symplast of a cell. The plant PM is additionally attached to a surrounding cell wall. The entirety of the intercellular space and all cell walls is called the apoplast. The PM is composed mainly of phosphoglycerolipids, sterols, sphingolipids, membrane proteins, and carbohydrates that are attached to some of the lipids and proteins at the exterior surface (Mamode Cassim *et al.*, 2019). At the cytoplasmic side the PM is connected to the cytoskeletal network and therefore offers structural support of the cell (Sackmann, 1990). Through incorporated ion channels and surface proteins the PM regulates the import and export of nutrients, metabolites, and signalling compounds and therefore has a vital role in the perception and transduction of incoming information.

Membrane lipids are not equally distributed between the two monolayers of the PM which results in lipid asymmetry. While phophatidylcholine (PC), sterols, and sphingolipids are prevalent lipids in the apoplastic outer monolayer of the PM, other unsaturated phospholipids like phosphatidylethanolamine (PE), phosphatidylinositol (PI) and phosphatidylserine (PS) are more abundant in the cytosolic inner monolayer (Devaux & Morris, 2004; Tjellström *et al.*, 2010; Cacas *et al.*, 2016; Mamode Cassim *et al.*, 2019). This

unequal distribution of membrane lipids equips each PM leaflet with distinct biophysical properties. The two monolayers have differing charges which together with incorporated ion channels contribute the establishment of the membrane potential. Furthermore, sugar residues and glycosylphosphatidylinositol- (GPI) anchored proteins at the outer monolayer serve in cell and pathogen recognition and hence in the activation of downstream signalling cascades (Borner *et al.*, 2005; Lenarčič *et al.*, 2017).

Plants are sessile organisms and are therefore restricted in their abilities to protect themselves against unfavourable environmental conditions. Therefore, they had to develop different adaptation strategies to surrounding putative threats. A major strategy is the dynamic adjustment of membrane properties. For instance, PM lipid composition can be adjusted to maintain membrane fluidity in changing temperatures, which increases plant tolerance of cold stress (Miquel *et al.*, 1993; Uemura *et al.*, 1995). Surface proteins embedded into the PM bilayer perceive pathogen components such as pathogen associated molecular patterns (PAMPs) and microbe-associated molecular patterns (MAMPs) which in turn initiates a signal transduction cascade that activates the plant's immune response (Gómez-Gómez & Boller, 2000; Sanabria *et al.*, 2010). The dynamic short-term adjustment of membrane properties underlies strict control mechanisms that mediate membrane organisation.

2.2 The evolution of membrane organisation models

The fluid-mosaic model proposed by Singer and Nicolson in 1972 describes a membrane as a heterogenous, fluid phospholipid bilayer into which membrane proteins are randomly incorporated in a mosaic-like pattern (Singer & Nicolson, 1972). The fluid-mosaic model is the first model that described the membrane as a dynamic compartment and has been a widely accepted concept of PM organisation. Following studies concerning lipid trafficking and membrane-associated signal transduction suggested that proteins may not be randomly distributed within membranes (van Meer & Simons, 1982; Lisanti & Rodriguez-Boulan, 1990). Based on these and other studies, the fluid mosaic model had been adjusted over the past decades. However, the basic principle has been maintained.

In 1997 Simons and co-workers proposed a new model of PM organisation, which is known as the 'lipid raft hypothesis' (Simons & Ikonen, 1997). The model describes the presence of micro- and nanoscale, temporary membrane regions, or 'lipid rafts', that are enriched in sterols, sphingolipids, and certain proteins (Simons & Vaz, 2004). According to this new concept, membrane proteins are distributed in these lateral lipid partitions instead of being randomly dispersed in the membrane. The proposed function of the sterol- and sphingolipid-rich domains is the lateral segregation and diffusion of membrane components,

especially of proteins. This becomes most important during membrane-associated signalling cascades that are induced by incoming stimuli (Simons & Toomre, 2000).

In lipid bilayers with high levels of sterols the co-existence of two liquid lipid phases is observed (Recktenwald & McConnell, 1981). Co-existence of distinct liquid phases is enabled by lateral phase separation. This means that different phases are laterally separated within the plane of the membrane. Two liquid crystalline lamellar phases are described: the liquid-ordered (Lo) phase and the liquid-disordered (Ld) phase (Ipsen *et al.*, 1987; Scheiffele *et al.*, 1997). The Lo phase is characterised by high levels of sterols, sphingolipids, and saturated phospholipids. Because of the high content of saturated lipids and the intercalation of sterols, Lo phases are more rigid due to tight lipid packaging and are therefore considered more ‘ordered’. The Ld phase has higher levels of unsaturated phospholipids. Lipids in the Ld phase can diffuse and rotate more freely within the bilayer plane and the phase is therefore more fluid, or ‘disordered’. Membrane domains can have either a Lo or a Ld phase-like structure. Lipid rafts have high levels of sterols and sphingolipids and are therefore considered to be in the Lo phase (Scheiffele *et al.*, 1997). The term ‘membrane domain’ is hence a more general description for regions with distinct lipid and protein composition, while ‘lipid rafts’ are a subtype of membrane domains. According to the raft hypothesis, membrane domains with distinct phase structures are considered to control membrane protein clustering.

Experimental evidence for the raft hypothesis has been provided by lipid purification studies using detergents. Detergents have a conical, amphiphilic molecular structure which causes spontaneous micelle formation in aqueous solutions. These compounds are therefore referred to as ‘curvophilic’. Phospholipids, however, form lipid bilayers and are therefore referred to as ‘curvophobic’ (Lichtenberg *et al.*, 2005). High detergent concentrations cause membrane solubilisation with phospholipids residing in detergent micelles. Membrane fractions with different lipid compositions are solubilised at different lipid/detergent ratios (Lichtenberg, 1985). This aspect has been used as a biochemical tool in studying the composition of biological membranes. Some membrane fractions are highly resistant against detergent solubilisation and stay in the lipid bilayer conformation at even high detergent levels. Lipid rafts that contain mixtures of sphingolipids, sterols, and GPI-anchored proteins are described as highly resistant to detergent solubilisation (Hanada *et al.*, 1995). Therefore, detergent-resistant membranes (DRMs) have often been identified as *in vitro* versions of lipid rafts. However, this association might be misleading since the experimental extraction procedure might induce artificial DRM formation which might not be found in native membranes (Lichtenberg *et al.*, 2005). This controversy caused many scientific debates over the existence of lipid rafts in biological membranes and called for new methods to investigate membrane lipid heterogeneity. Over the years, new

technologies including advanced lipid analytics, proteomics, and methods to visualise lipid raft markers *in vivo* have provided more evidence for lipid clustering in cell membranes (Pike, 2009; Cacas *et al.*, 2016). These studies have supported the lipid raft hypothesis. Especially investigations of model membranes that mimic the lipid composition of native membranes have been useful tools in improving our understanding of membrane organisation (Wesołowska *et al.*, 2009; Lin & London, 2014; Grosjean *et al.*, 2015; Grosjean *et al.*, 2018). Most membrane studies have been conducted on animal systems. However, animal membranes have different lipid compositions compared to plant membranes. In the mammalian PM cholesterol, sphingomyelin, and glycosphingolipids are the most abundant sterol and sphingolipid compounds. Hence, lipid rafts are considered to be mainly formed by the interaction between these compounds (Simons & Ikonen, 1997).

2.3 Plant lipid diversity

Plants contain a variety of lipids with different head group and backbone compositions (Table 1). These structurally varying lipid classes have different cellular distribution patterns and confer a multitude of physiological functions in the plant cell. Triacylglycerols (TAGs) are located in lipid droplets and are enriched in seeds where they serve as high-energy storage compounds (Xu & Shanklin, 2016). Diacylglycerols (DAGs) were described to act in lateral root development under mild salt stress in *A. thaliana* and may therefore play a role as second messengers in plants (Peters *et al.*, 2014). DAGs are further assumed to be important building blocks of plant cell membranes where they induce a negative curvature, which might be an important feature during membrane fusion events (Szule *et al.*, 2002). The majority of lipids have a function as structural elements in various membranes. Galactolipids such as monogalactosyldiacylglycerols (MGDGs) and digalactosyldiacylglycerols (DGDGs) represent highly abundant plant lipids that are enriched in thylakoid membranes where they have crucial roles in maintaining the integrity of photosynthetic active membranes (Dorne *et al.*, 1990; Joyard *et al.*, 1998; Dörmann & Benning, 2002). DGDGs are also found in minor amounts in the plasma membrane and are specifically enriched upon phosphate deprivation (Andersson *et al.*, 2003; Andersson *et al.*, 2005). Membranes of the endoplasmic reiticulum (ER), the Golgi apparatus, and the tonoplast are part of the secretory pathway and make up a big proportion of the lipid content of a plant cell. The organelle membranes contain large amounts of phosphoglycerollipids and minor amounts of sterols and sphingolipids. A gradient of sterols and sphingolipids is observed along organelles of the secretory pathway with highest levels being found in the plant plasma membrane. The two lipid classes define the thickness and rigidity of membranes which are critical features in membrane organisation (Casares *et al.*, 2019).

Table 1. Plant lipid classes, lipid composition, and abbreviations

Lipid classes		Lipid composition and abbreviations
	Sphingolipids	Long-chain bases (LCBs) Ceramides (Cers) Glycosylceramides (GlcCers) Glycosyl inositiolphosphorylceramides (GIPCs)
	Sterol lipids	Free sterols Steryl glycosides (SG) Acylated steryl glycosides (ASG) Steryl esters (SE)
Glycerolipids	Polar phosphoglycerolipids	Phosphatidylcholines (PC) Phosphatidylethanolamines (PE) Phosphatidylglycerols (PG) Phosphatidylinositols (PI) Phosphatidylserines (PS) Phosphatidic acid (PA) Lysoglycerophospholipids (LGPL)
	Polar glycoglycerolipids	Monogalactosyldiacylglycerols (MGDG) Digalactosyldiacylglycerols (DGDG) Sulfoquinovosyldiacylglycerols (SQDG) Diacylglyceryltrimethylhomo-Ser/-A (DGTS/A) Lysoglyceroglycolipids (LGGL)
	Neutral glycerolipids	Diacylglycerols (DAG) Triacylglycerols (TAG)

The plant PM has a specific lipid composition which is similar to animal PM lipid composition. Sterols represent 20–50 mol %; sphingolipids, 5–40 mol %; and phospholipids, 10–60 mol % of plant PM lipids (van Hooren & Munnik, 2017). The lipid constitution varies not only between different plant species but also between different tissue types (Sperling *et al.*, 2005; Markham *et al.*, 2006; Resemann, 2018). Furthermore, the composition is dynamically adjusted when plants are exposed to different biotic and abiotic stresses (Uemura *et al.*, 1995; Nagano *et al.*, 2014). As in animal systems, lipid asymmetry is proposed between the two monolayers of plant PM. DGDG and 60 % of the phospholipids are described to be located in the inner PM leaflet, while glycosylceramides (GlcCers), glycosyl inositolphosphorylceramides (GIPCs), and sterols are mainly found in the outer leaflet (Tjellström *et al.*, 2010; Cacas *et al.*, 2016).

The main phytosterol species are campesterol, ß-sitosterol, and stigmasterol (Furt *et al.*, 2011). The plant PM contains free phytosterols as well as the conjugated phytosterol forms steryl glycosides (SG) and acyl steryl glycosides (ASG) (Furt *et al.*, 2010). Sphingomyelin is not detected in plants. However, plants contain GIPCs which have varying head group compositions depending on the plant species (Buré *et al.*, 2011; Cacas *et al.*, 2013). The plant equivalent of mammalian glycosphingolipids are GlcCers. The major phospholipids in the plant PM are PC and PE. Phosphatidylglycerol (PG), phosphatidic acid

(PA), PS, PI, and phosphatidylinositol-phosphates (PIPs) are low abundant phospholipids (Mamode Cassim *et al.*, 2019).

The large diversity of the plant plasma membrane lipid composition has raised the question of the involvement of different lipid species in PM organisation. Similar to animal membranes, DRM fractions of plant PMs have been found to be enriched in sterols and sphingolipids (Mongrand *et al.*, 2004; Borner *et al.*, 2005; Minami *et al.*, 2009; Moscatelli *et al.*, 2015). Like the mammalian cholesterol, phytosterols have been described to be able to induce Lo phase formation (Roche *et al.*, 2008; Gerbeau-Pissot *et al.*, 2014). Recent studies on model membranes such as giant unilamellar vesicles (GUVs) and giant vesicles of native PMs (GVPMs) that mimic plant lipid mixtures reported varying abilities of different phytosterols to order membranes (Grosjean *et al.*, 2015; Grosjean *et al.*, 2018). Especially campesterol appears to strongly promote ordered domain formation. Interactions with the highly glycosylated GIPCs were described to enhance the ordering effect of campesterol (Grosjean *et al.*, 2015). In addition to that, immunogold electron microscopy in tobacco (*Nicotiana tabacum*) PM showed clustering of GIPCs in 35 nm diameter membrane domains (Cacas *et al.*, 2016). Other membrane sub compartments were also found to be enriched in phosphatidylinositol 4,5-bisphosphate (PIP2) (Furt *et al.*, 2010). Localisation studies on membrane proteins further revealed clustering of different proteins in distinct membrane domains (Raffaele *et al.*, 2009; Jarsch *et al.*, 2014; Noirot *et al.*, 2014).

These previous reports hint at lateral heterogeneity in the plant PM that is similar to that observed in animal cells. Membrane domains with different lipid and protein compositions and hence varying biophysical properties appear to co-exist in the plant PM. The contribution of individual lipid species to membrane organisation is a current research subject. Combining proteomics, lipidomics, and different imaging techniques with the study of mutant plants that are disturbed in PM organisation has greatly helped in understanding membrane dynamics (Grison *et al.*, 2015; Grosjean *et al.*, 2015; Grosjean *et al.*, 2018). However, the highly complex and dynamic nature of biological membranes poses major challenges to study *in vivo* mechanisms of plant membrane organisation and leave many unanswered questions that have to be addressed in the future.

2.4 The enigma of the plant sphingolipids

As described, sphingolipids are ubiquitous and essential membrane components in eukaryotes that play major roles in PM organisation. They were first described as lipid components of the brain tissue in the late nineteenth century by Johann Ludwig Wilhelm Thudichum (Thudichum, 1884). It is claimed that he named the newly discovered lipid class ‘sphingolipid’ in allusion to the Sphinx, a creature from Greek mythology. The unique structure of sphingolipids was equally cryptic to scientists at the time of their discovery as

the riddles of the Sphinx. Nowadays, the structure and function of sphingolipids in mammalian cells is well investigated, mainly because of their association with severe metabolic and nervous disorders, some of them known as sphingolipidoses. Lipid storage disorders are genetically inherited and affect various organs and the nervous system. Other disorders that affect sphingolipid metabolism include autoimmune diseases. Examples for sphingolipid-associated diseases are Tay-Sachs disease, Niemann-Pick disease, and Guillain-Barré syndrome (Yu & Ariga, 1998; Sandhoff & Harzer, 2013).

In plants, however, sphingolipids have been an overlooked lipid class for many years. Over the past three decades plant sphingolipids have been associated with multiple essential cellular processes and therefore attracted more attention by the plant science community. Plant sphingolipids may account for up to 10 % of total lipids from plant tissues (Lynch & Dunn, 2004). The structural diversity and complexity of plant sphingolipids requires powerful analytical tools. Up to 200 molecular species in the plant sphingolipidome have been described using advanced mass spectrometric approaches (Markham *et al.*, 2006; Markham & Jaworski, 2007; Cacas *et al.*, 2013). Several plant enzymes involved in sphingolipid biosynthesis have been identified by sequence similarity to characterised enzymes in the baker's yeast *Saccharomyces cerevisiae*. Mutants that are disturbed in different sphingolipid enzyme activities have been generated and showed major physiological and metabolic phenotypes (Luttgeharm *et al.*, 2016). The combination of analytical approaches, *in vitro* enzyme assays, and investigations of plant mutants that are compromised in sphingolipid metabolism have been valuable tools in expanding our understanding of plant sphingolipid structure, metabolism, and function.

2.5 Sphingolipid biosynthesis and structure

Sphingolipids are amphipathic compounds. Their hydrophobic backbone includes an amino alcohol, referred to as long-chain base (LCB). LCBs are the characteristic core of sphingolipids that identify them as a distinct lipid class. LCBs may be connected to a fatty acid moiety. The resulting product is referred to as ceramide, which is the hydrophobic component of sphingolipids. More complex sphingolipid classes are formed through the conjugation of hydrophilic polar head groups to the LCB moiety of the ceramide backbone. The polar head groups of sphingolipids largely differ between animal, yeast, and plant cells. Plant sphingolipids are categorised into the following four classes: LCBs, ceramides, GlcCers, and GIPCs (Fig. 1). LCBs and ceramides are minor sphingolipid compounds that constitute 0.5 % and 2 % of the total sphingolipid content in *Arabidopsis thaliana* leaf extract, respectively (Markham *et al.*, 2006). GlcCers and GIPCs are the most abundant plant sphingolipids and represent 34 % and 64 % of the total sphingolipid content in *A. thaliana* leaf extract, respectively (Markham *et al.*, 2006).

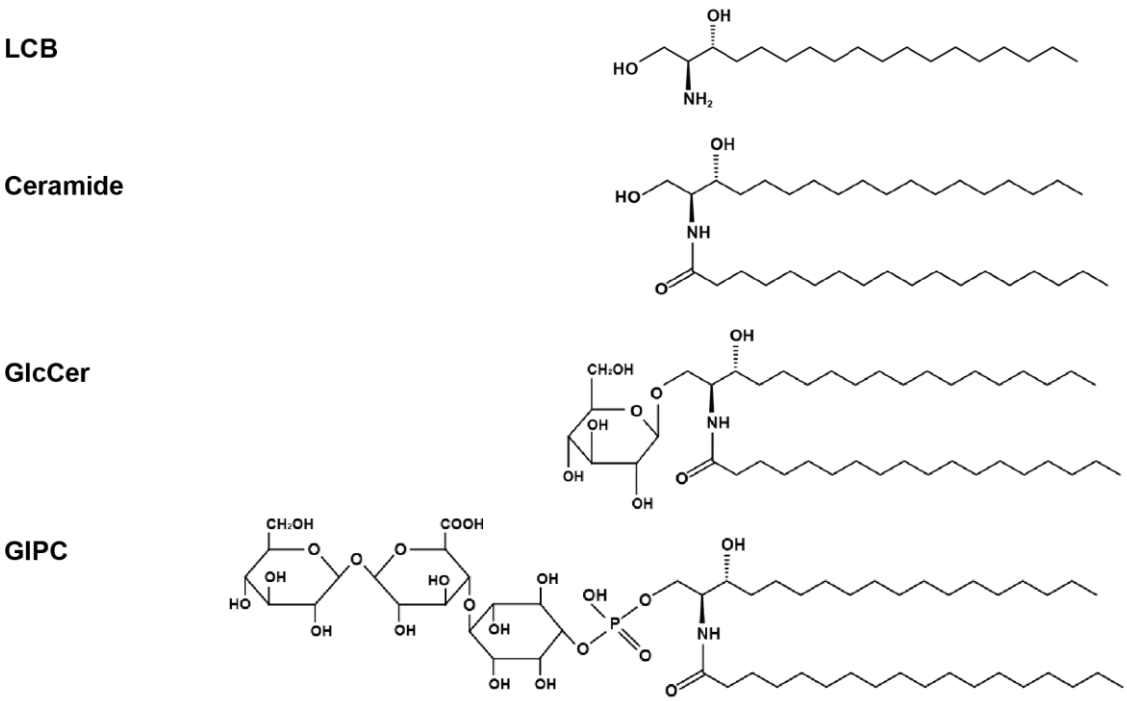

Fig. 1. Plant sphingolipids are divided into four main classes. Plant sphingolipids are categorised into long-chain bases (LCBs), ceramides, glycosylceramdies (GlcCers), and glycosyl inositolphosphorylceramides (GIPCs). The simplest sphingolipid compound, the LCB, is an amino alcohol. The LCB moiety may be connected via its amino group to a fatty acid moiety. The resulting product is called ceramide. Addition of a glucose moiety to the ceramide backbone results in the formation of GlcCers. Addition of an inositolphosphate and subsequent glycosylation results in the formation of GIPCs, whereby the number of added sugar groups may vary. The overview represents the four plant sphingolipid classes without detailed structural modifications on the ceramide backbone. Modified from (Lynch and Dunn, 2004).

The following description of sphingolipid biosynthesis in plants is based on findings from *A. thaliana*. Sphingolipids are mainly synthesised via the *de novo* pathway that is acyl-coenzyme A (CoA) dependent (Fig. 2). Sphingolipid biosynthetic enzymes are located in the membrane of the ER. The *de novo* pathway is initiated by the condensation of serine and palmitoyl-CoA. The reaction is catalysed by the serine palmitoyltransferase and results in the formation of the intermediate 3-ketosphinganine (Chen *et al.*, 2006; Dietrich *et al.*, 2008; Teng *et al.*, 2008). The enzyme 3-ketosphinganine reductase catalyses the reduction of 3-ketosphinganine to the simplest sphingolipid compound: the LCB sphinganine (Chao *et al.*, 2011). Sphinganine is also referred to as dihydrosphingosine, a dihydroxy LCB, or in short d18:0 (Fig. 2). As the name indicates, d18:0 has a chain length of 18 carbon atoms and contains two hydroxyl groups at the C-1 and C-3 positions. The two hydroxyl groups derive from the serine and palmitoyl-CoA precursors. Different modifications are introduced to the LCB moiety that define its downstream metabolic fate. A third hydroxyl group may be introduced to the C-4 position by an LCB C-4 hydroxylase (Sperling *et al.*, 2001; Chen *et al.*, 2008). The resulting LCB is referred to as phytosphinganine, a trihydroxy LCB, or in short t18:0 (Fig. 2). Most LCB moieties of plant sphingolipids are trihydroxylated (Markham *et al.*, 2006). Double bonds can be introduced to the LCB moiety by two distinct classes of

LCB desaturases. Double bonds may be inserted between the C-4 and C-5 position, designated as Δ4, and between the C-8 and C-9 position, designated as Δ8 (Sperling *et al.*, 1998; Ryan *et al.*, 2007; Michaelson *et al.*, 2009). The most common LCB moiety found in *A. thaliana* and other plants is trihydroxylated with a double bond in Δ8 position, t18:1 (Fig. 2) (Markham *et al.*, 2006). While the Δ4 double bond is only inserted in *trans* (*E*) configuration, the Δ8 double bond can be inserted in either *cis* (Z) or *trans* (*E*) configuration. The prevalence of the two Δ8 configuration states largely varies between different plant species and tissue types and may change when plants are exposed to external stresses (Markham *et al.*, 2006; Sato *et al.*, 2019).

N-acylation of LCBs is catalysed by ceramide synthases and results in the formation of ceramides (Fig. 2). In plants, LCBs may be connected to fatty acids with chain lengths varying from 16 to 26 carbon atoms. Fatty acids with chain lengths of 16 or 18 carbons (C16, C18) are called long-chain fatty acids (LCFAs), while fatty acids with chain lengths longer than 18 carbons (≥ 20C) are called very long-chain fatty acids (VLCFAs). In *A. thaliana* distinct ceramide synthases have been described that have different substrate preferences. The class I ceramide synthase generates ceramides with dihydroxy LCBs and LCFAs, while the class II ceramide synthases prefer trihydroxy LCBs and VLCFAs (Markham *et al.*, 2011; Ternes *et al.*, 2011a) (Fig. 2). LCBs and ceramides may also be phosphorylated at the C-1 position of the LCB moiety by the action of LCB and ceramide kinases and are subsequently referred to as LCB phosphates (LCB-Ps) and ceramide phosphates, respectively (Liang *et al.*, 2003; Imai & Nishiura, 2005; Worrall *et al.*, 2008). Structural modifications may also be introduced to the fatty acid moiety of ceramides. The acyl chain may be hydroxylated at the C-2 or ‘α’ position through the activity of a fatty acid hydroxylase. Ceramides with α-hydroxylated fatty acid moieties are often termed hydroxyceramides. In the nomenclature, a saturated, α-hydroxylated fatty acid moiety with a 24-carbon chain can be called h24:0. If the fatty acid moiety is not hydroxylated, it is often called c24:0. The fatty acid moiety may also carry a *cis* double bond in *n*-9 position (Imai *et al.*, 2000).

Ceramides are the precursor molecules for the more complex sphingolipid classes GlcCers and GIPCs. The formation of GlcCers and GIPCs are alternative routes within sphingolipid metabolism (Fig. 2). The second most abundant plant sphingolipid class, GlcCer, is generated by the attachment of a hexose moiety, mostly glucose and sometimes mannose, to the C-1 of the LCB moiety. The transfer of a sugar moiety from uridine diphosphate-glucose (UDP-Glc) is catalysed by a glucosylceramide synthase (Leipelt *et al.*, 2001; Melser *et al.*, 2010; Msanne *et al.*, 2015). The hexose is connected to the ceramide backbone by a 1,4-glycosidic linkage (Leipelt *et al.*, 2001) (Fig. 2).

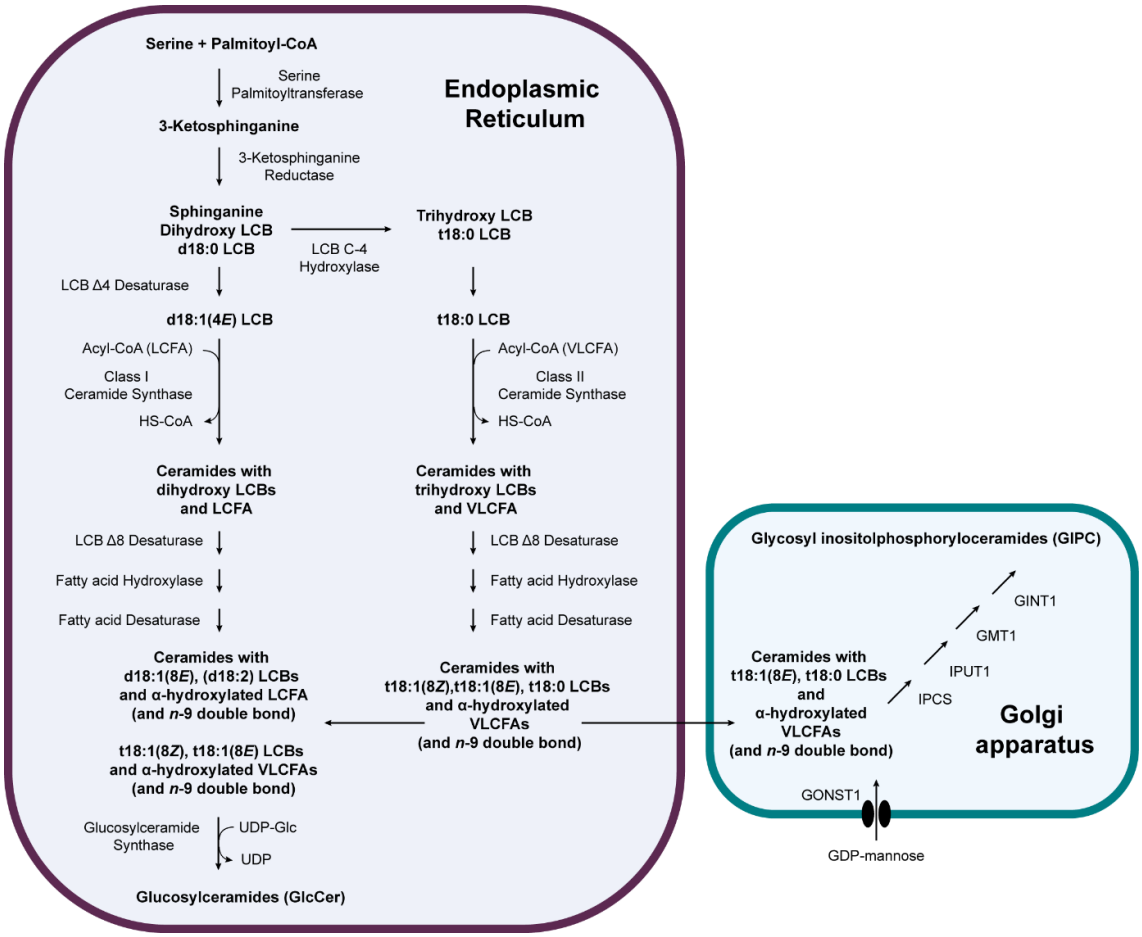

Fig. 2. Abbreviated *de novo* sphingolipid biosynthesis in *A. thaliana*. The majority of reactions within sphingolipid biosynthesis takes place in the endoplasmic reticulum (ER). During the initial steps, the simplest sphingolipid compound, the long-chain base (LCB) sphinganine (d18:0), is formed. The d18:0 LCB is subsequently applied to modifications such as Δ4-desaturation and C-4 hydroxylation. *N*-acylation of the LCB moiety results in ceramide formation. Depending on the structural features of the LCB, different ceramide synthases, class I or class II, are active that connect dihydroxy LCBs either with long-chain fatty acids (LCFAs), or trihydroxy LCBs with very long-chain fatty acids (VLCFAs). The ceramide backbone may subsequently be modified by additional Δ8-desaturation of the LCB moiety, fatty acid α-hydroxylation, or fatty acid *n*-9 desaturation. The combination of structurally different LCB and fatty acid moieties results in a large variety of ceramide species that are subsequently channelled into the glucosylceramide (GlcCer) or glycosyl inositolphosphorylceramide (GIPC) formation. The demonstrated pathway is an abbreviated version of sphingolipid biosynthesis, not including reactions such as phosphorylation, de-phosphorylation or breakdown of complex sphingolipids. Abbreviations are as follows: CoA: Coenzyme A; GDP-Man: Guanosine Diphosphate Mannose; GINT1: Glucosamine Inositolphosphorylceramide Synthase; GMT: GIPC Mannosyl Transferase; GONST1: GDP-Mannose Transporter; IPCS: Inositolphosphorylceramide Synthase; IPUT: Inositolphosphorylceramide Glucuronosyl Transferase; UDP-Glc: Uridine Diphosphate Glucose.

In contrast to the previous steps in sphingolipid biosynthesis that happen in the ER, modification of the most abundant plant sphingolipid class, GIPC, happens in the Golgi apparatus (Wang *et al.*, 2008). GIPC synthetic enzymes reside in the Golgi membrane and ceramide substrates are therefore exported from the ER and transported to the Golgi apparatus for further processing. Inositolphosphorylceramide synthases transfer an inositolphosphate head group from PI to the ceramide backbone (Wang *et al.*, 2008; Mina *et al.*, 2010). Subsequent glycosylation steps can add up to seven additional sugar residues to the inositolphosphorylceramide head group, leading to a variety of GIPC species with different head group compositions (Mortimer *et al.*, 2013; Rennie *et al.*, 2014; Fang *et al.*,

2016; Tartaglio *et al.*, 2017; Ishikawa *et al.*, 2018). The first sugar moiety linked to the inositolphosphorylceramide backbone is usually glucuronic acid. The following sugar moieties may be hexosamine, *N*-acetylhexosamine, or a variety of different pentoses and hexoses. If only one sugar moiety is attached to the glucuronic acid, the GIPCs are called series A GIPCs. If two sugar moieties are attached, GIPCs are termed series B GIPCs. The glycan head group composition varies between different plant species and tissue types (Buré *et al.*, 2011; Cacas *et al.*, 2013).

The introduced modifications in the ceramide backbone including the hydroxylation status (Fig. 3A), the number and position of inserted double bonds (Fig. 3B), the composition of polar head groups (Fig. 3C), and the variation of the acyl chain length (Fig. 3D) are the main causes for the diversity found among plant sphingolipids. The structural features of individual sphingolipid species offer them an array of different biophysical properties including size, charge, or polarity and are likely key to their varied physiological functions.

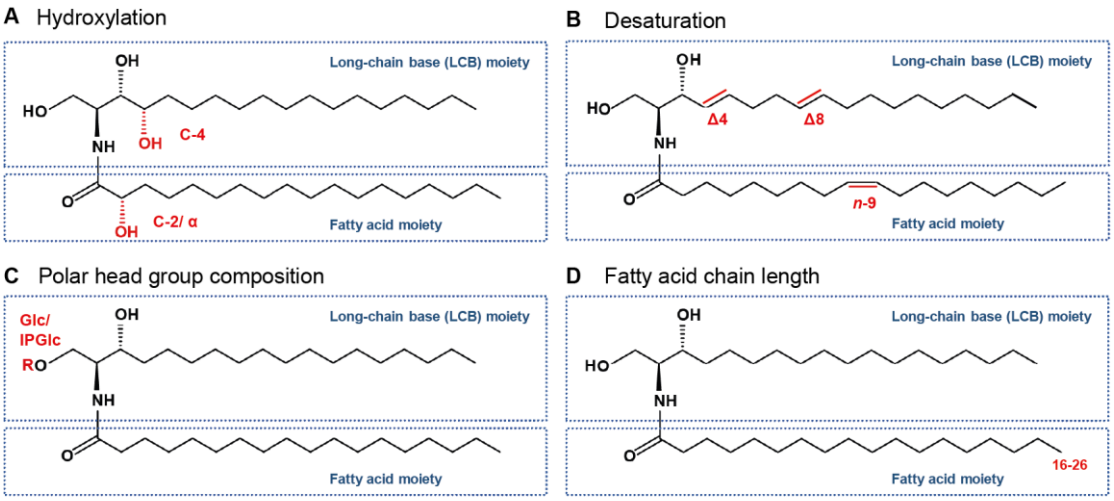

Fig. 3. Structural modifications on the ceramide backbone broadens variety of *A. thaliana* sphingolipids. Structural modifications on the ceramide backbone include (A) hydroxylation of the LCB and the fatty acid moieties, (B) desaturation of the LCB and the fatty acid moieties, (C) the composition of the polar head group, and (D) the chain length of the fatty acid moiety. (A) Hydroxylation can happen on the C-4 position of the LCB moiety or on the C-2 or α position of the fatty acid moiety. (B) Double bonds may be introduced at the Δ4 and Δ8 position of the LCB and at the *n*-9 position of the fatty acid moiety. (C) Different polar head groups (designated as R) such as glucose (Glc) or inositolphosphate and additional sugar residues (IPGlc) may be added to the C-1 of the LCB moiety. (D) In plants, the fatty acid chain length varies from 16 to 26 carbon atoms. Modified from (Berkey *et al.*, 2012).

Sphingolipids are involved in various signal transduction processes both during plant development as well as in immune responses. Especially LCBs and ceramides, which are believed to be second messengers in signalling cascades, are considered essential for the establishment of adaptive responses. Minor amounts of LCBs and ceramides may be provided by the breakdown of more complex sphingolipids which enables their re-entry into synthetic pathways. This process is referred to as salvage pathway. Different degradation

enzymes are active during the salvage pathway, including glucosylceramidases (Dai *et al.*, 2020), various ceramidases (Chen *et al.*, 2015; Li *et al.*, 2015; Wu *et al.*, 2015; Zienkiewicz *et al.*, 2020) and an LCB-P lyase (Tsegaye *et al.*, 2007; Nishikawa *et al.*, 2008). In contrast to the *de novo* biosynthesis pathway, the salvage pathway is fatty acid and not acyl-CoA dependent. To ensure fast responses of plants to their environment, conversion of sphingolipid compounds through anabolic and catabolic enzyme reactions has to adapt quickly.

2.6 Plant sphingolipids have diverse physiological and metabolic functions

Sphingolipids have roles as structural elements in membranes and as bioactive molecules during signal transduction (Greenberg *et al.*, 2000; Coursol *et al.*, 2003; Markham *et al.*, 2006; Shi *et al.*, 2007). Disruption of sphingolipid metabolism causes severe defects in essential cellular processes such as development and the plant's ability to respond to external stresses (Chen *et al.*, 2008; Msanne *et al.*, 2015; Gonzalez-Solis *et al.*, 2020). Alterations in sphingolipid structure may influence the overall biophysical properties of membrane domains. Furthermore, disruption of sphingolipid metabolism may interfere with signalling cascades during essential cellular processes. This shows that an imbalance of sphingolipid homeostasis has drastic and harmful effects on plant viability (Abbas *et al.*, 1994; Chen *et al.*, 2008; König *et al.*, 2012; Msanne *et al.*, 2015; Gonzalez Solis *et al.*, 2020; Zienkiewicz *et al.*, 2020). Therefore, the conversion of sphingolipids must be controlled in a dynamic manner to avoid an unusual accumulation of certain sphingolipid compounds that negatively affect plant viability (Abbas *et al.*, 1994; Liang *et al.*, 2003; Shi *et al.*, 2007; Chen *et al.*, 2008).

Because of their distinct structural features, the four plant sphingolipid classes and even certain sphingolipid species have been ascribed to different physiological functions. The less abundant LCBs and ceramides appear to mostly act as bioactive mediators of cellular functions. LCBs, ceramides and their phosphorylated forms seem to be antagonistic partners in these processes. Especially the balance between LCBs, ceramides and their phosphorylated counterparts are important factors in regulating physiological processes. The activity of sphingolipid kinases and lyases controls the ratio of the free and phosphorylated forms (Liang *et al.*, 2003; Imai & Nishiura, 2005; Worrall *et al.*, 2008). LCBs and ceramides both have been reported as triggers of programmed cell death (PCD) (Greenberg *et al.*, 2000; Liang *et al.*, 2003; Shi *et al.*, 2007; Alden *et al.*, 2011). First indications for the involvement of LCBs and ceramides in PCD induction were observed during studies with fungal-derived sphingosine analogues. The mycotoxins from *Alternaria alternata* f. sp. *lycopersic*i (AAL) and fumonisin B1 (FB1) from *Fusarium* species are able to elicit PCD in plants. The two mycotoxins have structural similarity to sphingosine and

therefore act by competitively inhibiting ceramide synthase activity. Blockage of ceramide synthesis resulted in elevated levels of LCBs (Abbas *et al.*, 1994; Stone *et al.*, 2000). Following studies reported the specific inhibition of the class II ceramide synthase LOH1 by FB1, which in turn resulted in elevated levels of dihydroxy ceramides with LCFAs (Markham *et al.*, 2011; Molino *et al.*, 2014). LCBs and ceramides were later also directly shown to elicit PCD symptoms. Exogenous application of LCBs to *A. thaliana* leaves resulted in the induction of reactive oxygen species (ROS) dependent PCD (Shi *et al.*, 2007). Conversely, simultaneous application of LCBs and LCB-Ps suppressed the onset of PCD, which indicated that LCBs and LCB-Ps appear to counteract with each other (Shi *et al.*, 2007; Alden *et al.*, 2011). Similarly, investigation of the ceramide kinase mutant *acd5* revealed accumulation of ceramides, which was accompanied by PCD symptoms (Greenberg *et al.*, 2000; Liang *et al.*, 2003). Analogous to the ratio of LCBs to LCB-Ps, the balance of ceramides and phosphorylated ceramides was also observed to be a critical factor in cell death induction (Liang *et al.*, 2003). In general, ceramides and LCBs appear to play crucial roles in plant resistance to pathogens. Elevated levels of LCBs and ceramides were not only associated with the onset of PCD but also with upregulation of defence-related genes and higher levels of certain phytohormones. Especially a correlation of sphingolipid metabolism and phytohormone signalling appears to be a key factor in mediating the plant immune response. The fatty acid hydroxylase mutant, *fah1 fah2*, was shown to accumulate LCBs and ceramides, had constitutive *PR1* and *PR2* expression, and higher salicylic acid (SA) levels (König *et al.*, 2012). More recently, *A. thaliana* mutants disrupted in neutral ceramidase activities, *ncer1* and *ncer2*, accumulated jasmonic acid-isoleucine (JA-Ile) and SA, respectively (Zienkiewicz *et al.*, 2020). *ncer1* plants had higher levels of hydroxyceramides, which was associated with early leaf senescence (developmentally controlled PCD), while *ncer2* plants had higher levels of t18:0 LCBs, which was associated with defence-related cell death (pathogen-triggered PCD). The differing cell death symptoms in the two independent neutral ceramidase knockouts indicate that elevated levels of LCBs and ceramides may elicit different downstream signalling cascades that include either JA or SA pathways. In addition to their role in plant immune responses, LCB-Ps were also associated with abscisic acid (ABA) dependent guard cell closure (Ng *et al.*, 2001; Coursol *et al.*, 2003). Mutants disrupted in their sphingosine kinase (SphK1) activity were less sensitive to ABA-promoted stomatal closure. ABA is proposed to activate SphK1 which in turn caused an increase in LCB/LCB-P ratio. The signalling cascade affected cytosolic ion levels and hence opened ion channels that in turn caused turgor reduction of the guard cells, resulting in stomatal closure. Cumulative findings concerning LCB and ceramide signalling in plant cells indicate the participation of different LCB and ceramide species in response to biotic and abiotic stresses.

The more abundant complex plant sphingolipid classes GlcCers and GIPCs are ubiquitous structural elements of the plant PM and of endomembrane systems. They have been detected as components of intracellular membranes, including ER, Golgi apparatus, tonoplast, and endosomes (Moreau *et al.*, 1998; Mongrand *et al.*, 2004; Sperling *et al.*, 2005; Bayer *et al.*, 2014). A sphingolipid gradient is observed along the secretory pathway with highest sphingolipid levels found in the PM. GlcCers and GIPCs compose around 5-10 % and 40 % of all plant PM lipids, respectively, and are considered to be enriched in the outer leaflet (Tjellström *et al.*, 2010; Cacas *et al.*, 2016). The relative abundances of GlcCer and GIPCs in the plant PM likely contribute to adaptive processes towards biotic and abiotic stresses. For instance, the ratio of GlcCers to GIPCs in the plant PM has been associated with membrane adjustments in response to cold stress. Nagano *et al*. (2014) reported an increase in GIPC levels and a decrease in GlcCer levels in *A. thaliana* cold acclimation(Nagano *et al.*, 2014). Although both complex sphingolipid classes are assumed to be enriched in the plasma membrane (Cacas *et al.*, 2016), the two classes are structurally distinguishable in their head group and in their ceramide backbone composition. Therefore, they might have different functions in plant physiology. However, differences in their physiological activities are still poorly understood.

GlcCers are described to be specifically enriched in *A. thaliana* pollen and floral tissue (Luttgeharm *et al.*, 2015b). GlcCer-deficient mutants cannot develop beyond seedling stage, are defective in organ-specific cell differentiation, have an altered Golgi morphology, and impaired pollen transmission (Msanne *et al.*, 2015). Inhibition of the glucosylceramide synthase, GCS, from *A. thaliana* with the chemical inhibitor D,L-threo-1-phenyl-2-palmitoylamino-3-morpholino-1-propanol (PDMP) was similarly associated with an altered Golgi morphology (Melser *et al.*, 2010). Cumulative findings indicate a role for GlcCers in Golgi-mediated protein secretion and subsequent vesicle trafficking to the plant PM. The desaturation status of GlcCers was also found to be important in plant response to chilling and freezing. While in chilling-resistant plants the fatty acid moiety of GlcCers was mainly composed of unsaturated α-hydroxylated fatty acids (Cahoon & Lynch, 1991; Imai *et al.*, 1995), GlcCers of chilling sensitive plants did not have those fatty acids (Imai *et al.*, 1995).

GIPCs are considered to be the most abundant plant sphingolipid class, however, the relative abundances of GlcCers and GIPCs may vary depending on the investigated plant species, the tissue type, and the applied external conditions (Sperling *et al.*, 2005; Markham *et al.*, 2006; Markham & Jaworski, 2007; Luttgeharm *et al.*, 2015b). Due to their complex, highly polar head group compositions, GIPCs have limited solubility in traditionally used extraction solvents. Only recently, extraction methods for plant GIPCs have been optimised and enabled first investigations on this long-overlooked plant sphingolipid class (Buré *et al.*, 2011; Cacas *et al.*, 2013). Their high abundance in the PM, which was recently

described to be around 40 mol % of tobacco PM lipids, puts them into the spotlight as most abundant plant sphingolipids (Cacas *et al.*, 2016; Gronnier *et al.*, 2016). As described in part 2.3, lipid rafts are highly enriched in sterols and sphingolipids. The biggest proportion of sphingolipids found in lipid rafts is represented by GIPCs. GIPCs were found to be enriched in DRM fractions of tobacco Bright Yellow 2 (BY-2) cell cultures (Cacas *et al.*, 2016). Microscopic evidence for GIPC enrichment in certain membrane domains was given by Cacas *et al*. (2016), who performed immunogold labelling of tobacco PM vesicles. Subsequent tissue investigation with electron microscopy revealed clustering of highly glycosylated GIPCs in distinct membrane domains (Cacas *et al.*, 2016). GIPCs were further reported to enhance the campesterol-induced ordering effect of membrane domains (Grosjean *et al.*, 2015). Through their structural function in lipid rafts, GIPCs are assumed to be involved in a multitude of PM-associated signal transduction processes. They are described as lipid anchors for GPI-anchored surface proteins (Borner *et al.*, 2005; Lefebvre *et al.*, 2007). Plant GIPCs might also act as cell wall anchors (Voxeur & Fry, 2014). Moreover, GIPCs were recently also identified as toxin receptors and are known to be involved in salt sensing (Lenarčič *et al.*, 2017; Jiang *et al.*, 2019). In addition to that, purification of plasmodesmata membrane fractions reported a similar lipid composition as described for membrane rafts (Grison *et al.*, 2015). GIPCs are therefore likely involved in plasmodesmal cell-to-cell transport of nutrients and signalling compounds (Yan *et al.*, 2019; Liu *et al.*, 2020).

2.7 Metabolic routing of sphingolipid intermediates

Apart from their physiological function in plants, structural modifications on the ceramide backbone may also have a role in channelling ceramide substrates into downstream complex sphingolipid synthesis. As mentioned, GlcCer and GIPC formation display two alternative pathways in sphingolipid metabolism (Fig. 2). Especially the hydroxylation and desaturation state of the LCB moiety is considered to be responsible for dictating the metabolic fate of precursor compounds. Previous studies on *A. thaliana* showed that the trihydroxy LCB, mostly t18:1 with the double bond in Δ8 position, is the most abundant moiety in GIPCs while LCB Δ4-desaturation likely plays a key role in channelling substrates into GlcCer formation (Chen *et al.*, 2008; Michaelson *et al.*, 2009). The t18:1 LCB moiety of GIPCs is mainly found in association with α-hydroxylated VLCFAs, while the d18:2 LCB moiety of *A. thaliana* pollen GlcCers and of species such as tomato (*Solanum lycopersicum*) and soybean (*Glycine max*) is mostly connected with the α-hydroxylated LCFA C16. The channelling function of the C-4 hydroxylation and the LCB Δ4-desaturation is supported by the fact that both reactions happen on the C-4 position of the LCB moiety which makes them mutually exclusive.

The prevalence of certain ceramide modifications in GlcCers and GIPCs appears to have direct effects on the physiological functions of the two complex sphingolipid classes. The typical ceramide backbone found in GlcCer and GIPC species is usually highly hydroxylated, both on the LCB as well as on the fatty acid side. The hydroxylation status of sphingolipids is considered essential for building up an extensive hydrogen bond network with other membrane components (Slotte, 1999; Mombelli *et al.*, 2003; Slotte, 2016). This is especially important for the interaction with phytosterols during lipid raft formation (Mamode Cassim *et al.*, 2019). *A. thaliana* has two functionally redundant LCB C-4 hydroxylases, SBH1 and SBH2. The combined activities of both enzymes account for all trihydroxy LCB formation in the plant. Both genes were able to complement the *S. cerevisae* LCB C-4 hydroxylase knockout *sur2Δ* (Sperling *et al.*, 2001). Knockout of both hydroxylase encoding genes led to severely dwarfed plants that were likely disturbed in cell elongation and division and that did not reach reproductive maturity (Chen *et al.*, 2008). Additionally, knockout plants showed necrotic cotyledon lesions which were accompanied by the up-regulation of defence-related marker genes. Knockout of both genes caused serious alterations in all sphingolipid classes (Chen *et al.*, 2008). The most prominent observation was a drastic accumulation of sphingolipids containing dihydroxy LCB moieties and C16 fatty acid moieties. Furthermore, the most abundant LCB moiety in all sphingolipid classes switched from trihydroxy LCBs to dihydroxy LCBs (Chen *et al.*, 2008). Since sphingolipid content and composition were both affected in the mutant, the phenotype was speculated to derive either from the unusual accumulation of sphingolipids with dihydroxy LCBs and C16 fatty acids or from a global change in the most abundant LCB moiety from trihydroxy to dihydroxy LCBs. Similar to the LCB C-4 hydroxylases, *A. thaliana* harbours two redundant fatty acid hydroxylases, FAH1 and FAH2 (König *et al.*, 2012). The *fah1 fah2* mutant has reduced levels of α-hydroxylated sphingolipids and instead showed elevated levels of sphingolipids with unhydroxylated fatty acid moieties. Furthermore, trihydroxy LCBs and ceramides were enriched five- and ten-fold, respectively, and total GlcCer levels were reduced by 25 % compared to the wild type. These alterations in the sphingolipidome were accompanied by reduced plant size, elevated SA levels, constitutive PR gene expression and an associated increased resistance against the obligate biotrophic pathogen *Golovinomyces cichoracearum* (König *et al.*, 2012).

Another important feature is the prevalence of VLCFAs in GlcCers and GIPCs. Longer acyl chains increase the hydrophobicity and the membrane transition from fluid to gel phase state (Pinto *et al.*, 2014; Mamode Cassim *et al.*, 2019). Additionally, the chain length of the fatty acid moiety is considered a crucial feature in the interdigitation and therefore in the connection of the inner and outer PM monolayers (Mamode Cassim *et al.*, 2019). Sphingolipids with VLCFAs are reported to have a crucial role in development

(Markham *et al.*, 2011; Molino *et al.*, 2014). Inhibition of ceramide synthases that are specific for VLCFA substrates caused defects in root-outgrowth. On a subcellular level, defects in VLCFA-containing sphingolipids resulted in impaired membrane trafficking of auxin proteins to the PM (Markham *et al.*, 2011). Molino *et al*. (2014) also demonstrated altered cell plate formation in plants whose VLCFA incorporating ceramide synthase LOH1 was blocked by the mycotoxin FB1 (Molino *et al.*, 2014). The authors propose a function for VLCFA-containing sphingolipids in lipid bilayer fusion and therefore in vesicle dynamics during development.

Although GlcCer and GIPC architectures share some structural features, the *A. thaliana* GlcCer pool differs in certain molecular species from the GIPC pool.

A. thaliana GlcCers are enriched in the Δ4,8-diunsaturated, d18:2, LCB moiety compared to GIPCs (Markham *et al.*, 2006). Plants lacking the two LCB Δ8-desaturases, SLD1 and SLD2, have GlcCer levels that are 50 % reduced compared to the wild type and the mutants are more sensitive to cold stress (Chen *et al.*, 2012). It might be that the configuration state of the Δ8 double bond plays a role in shunting t18:1 species into GlcCer or GIPC formation. In contrast to that, knockout mutants of the *A. thaliana* LCB Δ4-desaturase did not show any obvious phenotypes (Michaelson *et al.*, 2009). In *A. thaliana* the d18:2 LCB moiety is enriched in pollen and floral tissue (Michaelson *et al.*, 2009). GlcCer levels were also significantly reduced in the LCB Δ4-desaturase knockout plant, indicating that LCB Δ4-desaturation has indeed a channelling function for GlcCer formation (Michaelson *et al*., 2009). However, pollen and general plant viability was not affected in the *A. thaliana* mutant plants. While Δ8-desaturation is one of the most abundant LCB modifications found in *A. thaliana* sphingolipids, LCB Δ4-desaturation appears to not have a significant physiological role in Brassicaceae (Markham *et al.*, 2006). A lipidomics screen covering 21 plants from different lineages identified the prevalence of the LCB double bond position in d18:1 LCB moieties (Islam *et al.*, 2012). They revealed that LCB Δ4-desaturation is most common to non-vascular plants and to the Poales family whereas LCB Δ8-desaturation is most abundant in plants like Brassicaceae. The authors speculated that LCB Δ4-desaturation appears to be more ancient than LCB Δ8-desaturation. Interestingly, in plants like tomato and soybean ceramides with a Δ4,8-diunsaturated LCB moiety and C16 fatty acids are most abundant (Markham *et al.*, 2006). This suggests that the LCB desaturation state was subject to divergent evolution and that LCB Δ4-desaturation likely has a more important physiological role in plants outside the Brassicaceae family. In the filamentous fungus *Pichia pastoris* loss of LCB Δ4-desaturation has more pronounced metabolic effects resulting in complete abolishment of GlcCers (Michaelson *et al.*, 2009). Plants that lack all GlcCers are seedling lethal and plants with a disturbed GlcCer formation show defects in cell differentiation and organogenesis, likely due to an impaired intracellular

membrane trafficking (Melser *et al.*, 2010; Melser *et al.*, 2011; Krüger *et al.*, 2013). The structural features of GlcCers therefore appear to have an important role in vesicle dynamics.

GIPCs have a characteristic head group. The glycan residues of the GIPC head group might be important for pathogen perception and cell recognition (Lenarčič *et al.*, 2017). The head group composition is strongly specific for certain plant species and tissue types (Buré *et al.*, 2011; Cacas *et al.*, 2013; Luttgeharm *et al.*, 2015b). Alterations of the glycan head group composition is reported to have severe effects on plant viability. Knockout of one of the three inositolphosphoceramide synthases, ERH1, resulted in GIPC reduction and accumulation of the ceramide precursor, which was accompanied by the onset of cell death symptoms (Wang *et al.*, 2008). Knockout of subsequent enzymes that catalyse conjugation of different sugar residues resulted in mutants that were either lethal or had severe growth defects (Mortimer *et al.*, 2013; Rennie *et al.*, 2014; Tartaglio *et al.*, 2017).

Taken together, studies on distinct *A. thaliana* sphingolipid mutants indicate that LCB modifications have a strong influence on the metabolic flux of sphingolipid compounds, and that distinct structural features of GlcCers and GIPCs have important effects on their physiological function. Especially LCB C-4 hydroxylation and LCB Δ4-desaturation appear to be of great importance for the downstream metabolic fate of sphingolipids. In *A. thaliana*, the channelling of sphingolipid metabolites seems to also be partially controlled by the ratio of *cis* and *trans* Δ8 double bonds (Markham *et al.*, 2006; Markham & Jaworski, 2007). However, the exact channelling process of sphingolipid intermediates in plants is not yet fully elucidated, in part because of the large complexity of the *A. thaliana* sphingolipidome. Furthermore, although sphingolipid biosynthesis is broadly conserved among plants of different taxonomic groups, sphingolipid composition differs between plant species and even between different tissues of the same plant (Sperling *et al.*, 2005; Markham *et al.*, 2006; Markham & Jaworski, 2007; Luttgeharm *et al.*, 2015b). This underlines that distinct sphingolipid species have different physiological roles which may be more or less important in certain plants and plant tissues. This also includes a potential divergent evolution of different pathogen interaction systems in plants of different taxonomic groups. A recent study gave a great example for this and showed that GIPCs can act as necrosis and ethylene-inducing peptide 1–like (NLP) toxin receptors in eudicots but not in monocots (Lenarčič *et al.*, 2017). The authors concluded that this host selectivity may be due to the glycan head group composition which is known to be plant species- and tissue-dependent (Buré *et al.*, 2011; Cacas *et al.*, 2013). These observations indicate that sphingolipid metabolism diverged during land plant evolution. However, the functional relevance for this diversification is largely unknown.

2.8 The value of bryophytes in sphingolipid studies

Most findings on plant sphingolipid biosynthesis have been gained from studies on the vascular model *A. thaliana* (Luttgeharm *et al.*, 2016). While observations made in this commonly used model contributed greatly to our knowledge on plant sphingolipid metabolism, the sole focus on the *A. thaliana* sphingolipidome may also present some limitations. As the previous paragraph explained, sphingolipid metabolism in plants appears to have diverged during land plant evolution. Therefore, structural modifications such as LCB Δ4-desaturation, which is an essential feature for GlcCer formation in plants like tomato or soybean, is nearly absent in *A. thaliana* (Markham *et al.*, 2006; Michaelson *et al.*, 2009). To study the physiological relevance of compounds that are not important for Brassicaceae, it is therefore crucial to study plants beyond *A. thaliana* (Michaelson *et al.*, 2009; Islam *et al.*, 2012; Markham *et al.*, 2013). Another disadvantage of studying sphingolipid biosynthesis in vascular land plants is their complex body plan. Disruption of sphingolipid genes in vascular plants therefore often results in pleiotropic phenotypes, making it difficult to ascribe distinct sphingolipids to certain physiological functions (Chen *et al.*, 2008; König *et al.*, 2012; Msanne *et al.*, 2015). Our recently acquired knowledge on the importance of plant GIPCs in membrane organisation furthermore calls for novel tools to study *in planta* membrane dynamics. Previous studies focused on working with model membrane systems of decreasing complexity to decipher the role of individual sphingolipid classes on membrane organisation (Grosjean *et al.*, 2015; Grosjean *et al.*, 2018). While these studies gave undeniably valuable insights of how different sphingolipid classes influence the membrane order *in vitro*, they unfortunately omit the complex background of biological membranes in native tissues. This includes the presence of integral or peripheral membrane proteins and intercellular communication. The study of plants with simpler tissue types and a sphingolipidome of lower complexity might therefore be key in advancing our knowledge on the sphingolipid function in plants.

The study of different plant lineages displays a valuable tool in understanding the evolution of physiological processes. Around 400 million years ago the first plants conquered terrestrial environments as habitat. A sister lineage of vascular plants are the bryophytes that comprise three groups of non-vascular land plants: mosses, liverworts, and hornworts (Hedges, 2002). Emerging model organisms from this group are the liverwort *Marchantia polymoropha* and the moss *Physcomitrella patens*. Mosses share the same essential metabolic and physiological processes with vascular plants. However, their body plans are much simpler than the highly complex vascular tissues. *P. patens* has gained increased attention in plant research over the past three decades due to a plethora of advantageous properties (Cove, 2005; Cove *et al.*, 2006; Rensing *et al.*, 2008). In 2008 the

P. patens genome was completely sequenced (Rensing *et al.*, 2008). Since then an advanced molecular toolkit for gene editing of the plant has been developed. The moss has a haplodiplontic life cycle with the alternation of two generations: the haploid gametophyte and the diploid sporophyte. The dominant haploid gametophytic phase of the moss is easily accessible for genetic manipulation. Homologous recombination has for a long time been the method of choice for targeted gene disruption in *P. patens* (Schaefer & Zrÿd, 1997). More recently, the use of the CRISPR-Cas9 system has been established in the moss, enabling simultaneous disruption of numerous genes (Lopez-Obando *et al.*, 2016; Collonnier *et al.*, 2017).

Compared to vascular plants, the architectural design of *P. patens* is relatively simple. The gametophyte consists of two developmental stages: the initially formed protonema and the shoot-like gametophore (Prigge & Bezanilla, 2010) (Fig. 4). The protonema is a two-dimensional network of filamentous cells. Two cell types compose the protonema. The first cells to be generated are the assimilatory chloronema that harbour numerous chloroplasts. Chloronema cells gradually differentiate into the foraging caulonema cells, which are much longer and grow faster than chloronema cells (Fig. 4). In dark conditions, only caulonema cells are able to grow against the gravity vector and are then referred to as skotonema cells (Cove *et al.*, 1978; Rensing *et al.*, 2020). The filamentous cells grow via polarized tip growth and side-branching is initiated at subapical cells.

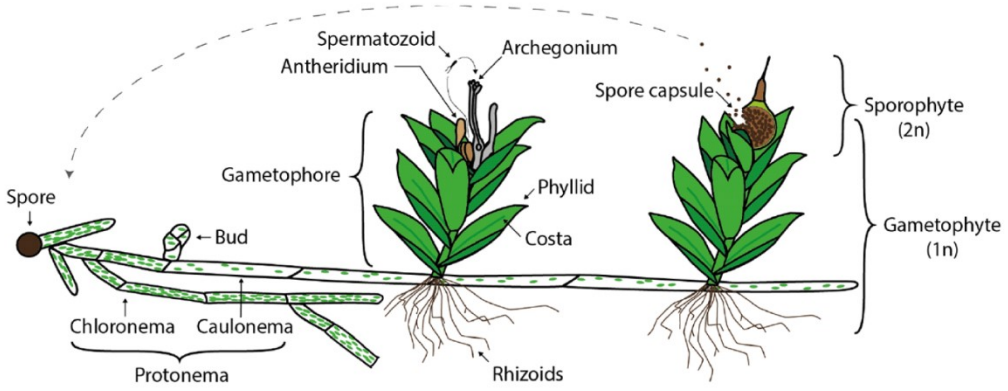

Fig. 4. *P. patens* life cycle. The haplodiplontic *P. patens* life cycle is dominated by the haploid gametophyte that consists of spores, protonema, and gametophore. It starts with a single spore that germinates into the filamentous protonema. The protonema is composed of two cell types: the chloronema and the caulonema cells. Buddings that emerge from the protonema grow out into the gametophore. The gametophore has leaf-like phyllids and root-like rhizoids. The reproductive organs, the female archegonia and the male antheridia, are located at the tip of the gametophore. After the egg inside the archegonium is fertilised by spermatozoids, the zygote matures into the spore capsule. The diploid sporophyte consists of a spore capsule and a short seta. Modified from (Rensing *et al*., 2020).

Once the protonema has ensured proper establishment of the plant, the development of the adult stage, the gametophore, is initiated (Fig. 4). The gametophore is a three-dimensional structure that is most similar to the shoot of vascular plants. However, the individual organs

of the plant have a much simpler architecture than the ones of vascular land plants. The gametophore shoot carries leaflets that are only one cell layer thick. They also have root-like structures, filamentous rhizoids, which anchor the shoot to the ground and ensure nutrient supply (Fig 4). Sexual reproduction of the moss is dependent on autumn-like environmental conditions. Colder temperatures induce the formation of the sexual organs, the gametangia, at the tip of the gametophore (Hohe *et al.*, 2002) (Fig 4). Subsequent submersion with water enables spermatozoids to swim from the male antheridia to the female archegonia and to fertilise the egg inside the female organ. The zygote matures into the sporophyte, the only diploid phase of the life cycle, which consists of a spore capsule and a short seta (Landberg *et al.*, 2013; Hiss *et al.*, 2017). Bursting of the spore capsule results in the release of haploid spores that initiate a new life cycle (Engel, 1968).

In addition to sexual reproduction *P. patens* can also be propagated vegetatively. Disruption of gametophytic tissue results in a high regeneration rate. This might be especially interesting for studying mutants disturbed in sphingolipid metabolism since many *A. thaliana* sphingolipid mutants are unable to reach reproductive maturity. Disturbed sexual reproduction is often associated with embryo lethal phenotypes. True *A. thaliana* sphingolipid knockout plants are therefore often not accessible for detailed phenotype characterisation, forcing scientists to instead work on knockdown plants. The life cycle of *P. patens* can easily be completed under laboratory conditions making each developmental stage easily accessible for thorough phenotypic investigations.

All these aspects have put *P. patens* into the spotlight for developmental and evolutionary genetic studies. Because of its anatomical simplicity, the yeast *S. cerevisiae* has been a valuable model in investigating the sphingolipid pathway (Riezman, 2006; Dickson, 2010). The same reasoning may be applied in using the bryophyte *P. patens* as plant model with a simple non-vascular anatomy. In terms of studying sphingolipid biosynthesis in plants, discoveries of individual reactions in *P. patens* sphingolipid biosynthesis may allow us to take a step back from the thoroughly investigated *A. thaliana* sphingolipidome and put new findings on plant sphingolipid biosynthesis into an evolutionary context. This might help us to understand the divergence of sphingolipid metabolism in different land plant lineages.

2.9 The *P. patens* sphingolipidome

A recent study conducted a global lipid analysis on *P. patens* protonema (Resemann, 2018). For the lipidomics screen a multiple reaction monitoring (MRM)-based ultra-performance liquid chromatography (UPLC) coupled with nanoelectrospray ionisation (nanoESI) and triple quadrupole tandem mass spectrometry (MS/MS) approach was applied that was adjusted from a screen for *A. thaliana* lipids (Tarazona *et al.*, 2015). The

authors described over 700 lipid species in the moss that were divided into 20 lipid classes (Resemann, 2018). These classes included the four introduced plant sphingolipid classes. One of the major differences to the sphingolipidome of vascular plants was the prevalence of the t18:0 LCB moiety in all sphingolipids instead of the t18:1 LCB moiety. The t18:1 LCB moiety was only detected in low amounts or did not exist in *P. patens*. Furthermore, unlike *A. thaliana*, *P. patens* GlcCers were mainly composed of a single molecular species with a d18:2/h20:1 ceramide backbone. This GlcCer composition rather resembles GlcCers found in plants such as tomato and soybean. In addition, *P. patens* sphingolipids mostly harbour VLCFAs (≥ 20C) while *A. thaliana* contains two main classes of ceramide species that derive from the activity of two distinct substrate-specific ceramide synthases (Markham *et al.*, 2011; Ternes *et al.*, 2011a). One class consists of ceramides with a dihydroxy LCB and LCFAs, the other one of ceramides with trihydroxy LCBs and VLCFAs (Markham *et al.*, 2011; Ternes *et al.*, 2011a). This structural distinction of ceramides was, however, not described for sphingolipids in *P. patens*.

Sphingolipid diversity in *A. thaliana* partially derives from the presence of redundant genes for key enzymes within the sphingolipid pathway. An aspect that may facilitate the study of sphingolipid enzymes in *P. patens* is the lack of redundant genes for some key steps in sphingolipid biosynthesis. The LCB-C4 hydroxylase, the LCB Δ4- and Δ8-desaturases, and the glycosylceramide synthase may all be represented by single genes in *P. patens*.

In addition to the determination of the lipid profile of *P. patens*, Resemann (2018) also identified the sphingolipid fatty acid desaturase, *Pp*SFD (Resemann, 2018). The gene was first described in a transcriptomic screen where it was upregulated when *P. patens* was exposed to cold temperatures (Beike *et al.*, 2015). While *sfd* mutants did not show growth defects under normal temperature, the plants were more sensitive to cold stress. *A. thaliana* plants that had a disturbed fatty acid desaturase activity, *ads2.1*, were similarly sensitive to cold stress (Chen & Thelen, 2013). Complementation of the *A. thaliana* mutant *ads2.1* with *Pp*SFD resulted in a rescue of the cold phenotype. Analytical investigation of the double bond position revealed that *Pp*SFD inserts the fatty acid double bond mainly at *n*-8 position. The *At*ADS2, however, specifically introduces the fatty acid double bond at position *n*-9. These findings indicate independent evolutionary backgrounds of the sphingolipid fatty acid desaturases of the two plant organisms. Although the two desaturases evolved convergently to each other, they appear to confer the same physiological function in both plants. This and other studies on convergent evolution demonstrate the utility of bryophytes as model organisms. They allow us to identify fundamental aspects of metabolic pathways and help us to understand how certain metabolic pathways evolved and adapted in the process of plant terrestrialisation and diversification.

2.10 Aim of this study

The metabolic routing of sphingolipid intermediates and the diversification of plant sphingolipid metabolism is still poorly understood in vascular plants. While *A. thaliana* has been an invaluable model that has helped us to broaden our knowledge of plant sphingolipid biosynthesis and function, it also shows clear limitations. The *A. thaliana* sphingolipidome is highly diverse and complex. *A. thaliana* sphingolipid mutants that are disturbed in single reactions hence often show global changes in all sphingolipid classes that cause pleiotropic downstream effects. Moreover, certain reactions that may not play an important physiological role in *A. thaliana* might be crucial for plants of other taxonomic groups. The physiological relevance of these compounds in other plants has therefore been largely omitted in previous studies.

The sphingolipidome of *P. patens* is much less complex than the sphingolipidome of *A. thaliana* (Resemann, 2018). The routing of structurally distinct sphingolipid compounds into complex sphingolipid formation appears stricter in *P. patens* than in vascular plants. GlcCers contain a ceramide backbone with a Δ4,8-diunsaturated LCB moiety and GIPCs a ceramide backbone with a t18:0 LCB moiety. LCB C-4 hydroxylation and LCB Δ4-desaturation therefore appear to dictate the metabolic fate of sphingolipids in *P. patens*. The predominance of GlcCer species with a d18:2 LCB moiety also indicates a greater physiological role for Δ4-unsaturated sphingolipids in *P. patens* than in *A. thaliana*. In *P. patens* the LCB C-4 hydroxylase and the LCB Δ4-desaturase are most likely single genes and are therefore both easy targets for genetic manipulation. Moreover, the first committed step of GlcCer synthesis is catalysed by the glycosylceramide synthase, which is also very likely represented by a single gene in *P. patens*. To study the metabolic routing and the physiological relevance of sphingolipid species with distinct structural features, null mutants of the three key enzymes within *P. patens* sphingolipid biosynthesis were generated by homologous recombination. In order to perform extensive examinations of the sphingolipid knockouts, *P. patens* cultivation and characterisation assays had to be established and optimised (chapter 1). The effects of disrupting the individual sphingolipid enzymes were assessed via macro- and microscopic investigation of different developmental stages of the mutants as well as by determination of the underlying lipid profiles by UPLC-nanoESI-MS/MS. The LCB C-4 hydroxylase, *Pp*S4H, is located in the pathway leading to GIPC formation. Investigation of the *s4h* mutant is described in chapter 2. The LCB Δ4-desaturase and the glycosylceramide synthase are both parts of the GlcCer synthetic pathway. Knockout mutants of the two genes were designated as *sd4d-1* and *gcs-1*, respectively, and mutant characterisations are shown in chapter 3. Comparison of all three mutants might help to dissect the specific physiological roles of GlcCers and GIPCs in plants. It may also

reveal if and how certain structural modifications of the LCB moiety influence the function of complex sphingolipids. Combining the findings from *P. patens* sphingolipid mutants with results from studies on the corresponding *A. thaliana* mutants may contribute to our understanding of how and why sphingolipid biosynthesis in plants diversified during land colonisation.

3 Chapter 1

Establishment and optimisation of *Physcomitrella patens* cultivation, characterisation assays, and analytic techniques

The following chapter demonstrates the establishment and optimisation of a toolkit for using *P. patens* as a model system in the department.

Author contribution:

Jasmin Gömann evaluated the liquid culture system for *P. patens* cultivation. She researched commonly used cultivation strategies and consequently replaced the liquid media cultivation system used in the department. She established and optimised *P. patens* cultivation on solidified mineral medium plates. She used the new system to selectively cultivate different developmental stages of *P. patens*. She maintained and cultivated the different *P. patens* tissues for lipid and phytohormone analyses. She planned and performed the lipid extractions and measurements using UPLC-nanoESI-MS/MS. She analysed and processed the lipid data. She maintained and cultivated the *P. patens* wild type and mutant material for macro- and microscopic phenotype investigation. She planned and performed the particle bombardment assay. Finally, she displayed, interpreted, and discussed the results and wrote the chapter.

Establishment and optimisation of *Physcomitrella patens* cultivation, characterisation assays, and analytic techniques

Jasmin Gömann[1], Cornelia Herrfurth[1,2], Agnieszka Zienkiewicz[1], Krzysztof Zienkiewicz[1], Tegan M. Haslam[1], Ivo Feussner[1,2,3*]

[1]University of Goettingen, Albrecht-von-Haller-Institute for Plant Sciences, Department of Plant Biochemistry, D-37077, Goettingen, Germany.
[2]University of Goettingen, Goettingen Center for Molecular Biosciences (GZMB), Service Unit for Metabolomics and Lipidomics, D-37077 Goettingen, Germany.
[3]University of Goettingen, Goettingen Center for Molecular Biosciences (GZMB), Department of Plant Biochemistry, D-37077 Goettingen, Germany.

E-mail address for each author:
jasmin.goemann@stud.uni-goettingen.de
cornelia.herrfurth@biologie.uni-goettingen.de
agnieszka.zienkiewicz@biologie.uni-goettingen.de
krzysztof.zienkiewicz@biologie.uni-goettingen.de

*Correspondence: Ivo Feussner, e-mail: ifeussn@uni-goettingen.de,
Tel: +49-551-3925743, ORCID iD: 0000-0002-9888-700

Abstract

Over the past few decades bryophyte model organisms attracted increased attention in the plant science community. By now, one of the most promoted models is *Physcomitrella patens*. The moss is a multicellular, terrestrial plant that shares fundamental metabolic and physiological processes with vascular plants. Its architectural design and some of its metabolic pathways are of lower complexity than in vascular plants. The *P. patens* genome is completely sequenced since 2008 and the life cycle of the moss is dominated by the haploid gametophyte. Both aspects make the plant easily accessible for genetic manipulation. Furthermore, the moss can be grown under laboratory conditions and individual developmental stages can be thoroughly investigated. *P. patens* therefore combines favourable aspects for genetic, developmental, and biochemical studies. Its phylogenetic position offers the opportunity to study diversification of metabolic pathways in different plant lineages. The establishment of appropriate cultivation conditions and characterisation assays is a time-consuming but essential aspect of implementing new model organisms in a laboratory. Luckily, the increased attention of *P. patens* in plant research resulted over the years in the publication of protocols and reviews concerning *P. patens* growth and mutant characterisation. However, depending on the anticipated purpose of certain studies, the conditions and characterisation assays need to be adjusted individually. Lipidomic screens often require large amounts of biological material. *P. patens* may be grown in bio reactors that are suited for the production of large amounts of biomass. However, the system displays limitations in terms of tissue and cell differentiation. Therefore, prior to sphingolipid mutant characterisation, the *P. patens* cultivation was shifted to a plate-based cultivation system, which enables completion of the *P. patens* life cycle. By this re-establishment, phenotype characterisations could be conducted on each developmental stage. Furthermore, upscaling of *P. patens* plate cultivation enabled sphingolipidomic profiling of individual developmental stages and tissues. New assays for analytical studies were applied and partially optimised. This work built the framework for the subsequent sphingolipid mutant characterisations and is the basis for future *P. patens* mutant studies.

Introduction

Plant sphingolipids are a lipid class with an exceptionally large structural diversity. This diversity arises from various modifications introduced to the sphingoid backbone. The backbone of sphingolipids consists of an amino alcohol or long-chain base (LCB), which is the characteristic subunit of all sphingolipids. LCBs may be esterified to a fatty acid moiety and are subsequently referred to as ceramides. Structural decorations are introduced to the LCB and/ or the fatty acid moieties. Modifications may be LCB C-4 hydroxylation, LCB Δ4- and Δ8-desaturation, phosphorylation or the addition of polar head groups to the C-1 of the LCB, and α-hydroxylation, desaturation, and chain length variation of the fatty acid. Different structural features affect the biophysical properties of individual sphingolipid species, including their size, charge and solubility (Luttgeharm *et al.*, 2016). There is a connection between this structural variability and the involvement of sphingolipids in a multitude of physiological processes like development (Chen *et al.*, 2008; Msanne *et al.*, 2015), programmed cell death (Brodersen *et al.*, 2002; Liang *et al.*, 2003; Shi *et al.*, 2007; Alden *et al.*, 2011), abscisic acid mediated stomatal closure, and tolerance towards drought (Ng *et al.*, 2001; Coursol *et al.*, 2003), cold (Chen *et al.*, 2012; Dutilleul *et al.*, 2012; Zhou *et al.*, 2016) and other biotic and abiotic stresses. Sphingolipids may have either a structural or a signalling function in these processes. Four main classes represent the plant sphingolipidome: LCBs, ceramides, and the two complex sphingolipid classes glycosylceramides (GlcCers) and glycosol inositolphosphorylceramides (GIPCs). LCBs, ceramides and their phosphorylated counterparts are only present in minor amounts in plant cells (Markham *et al.*, 2006; Markham & Jaworski, 2007). They mainly have roles as bioactive compounds mediating various processes (Ng *et al.*, 2001; Shi *et al.*, 2007). Complex sphingolipids, however, are the most abundant plant sphingolipids (Markham *et al.*, 2006). They mainly have roles as membrane components that maintain the structural integrity and permeability of plant membranes and that mediate membrane-bound signal transduction processes by the formation of micro- and nanodomains (Simons & Toomre, 2000).

Sphingolipids represent approximately 10 % of all plant lipids (Lynch & Dunn, 2004). The plant membrane lipid composition is specific for different organisms and tissues and may be dynamically altered in response to environmental and endogenous stimuli (Sperling *et al.*, 2005; Markham *et al.*, 2006). Differences between the sphingolipidomes of various plants may be found in the relative abundances of the individual sphingolipid classes. In *Arabidopsis thaliana* leaves, GIPCs represent two thirds and GlcCers represent one third of all sphingolipids (Markham *et al.*, 2006). In tomato (*Solanum lycopersicum*) leaves, however, GIPCs and GlcCers appear to be present in equal amounts (Markham *et al.*, 2006; Markham & Jaworski, 2007). The simpler sphingolipid classes, LCBs and ceramides, are

only found in low amounts (less than 3 % of the total sphingolipid content) in all plants (Markham *et al.*, 2006; Markham & Jaworski, 2007). Alterations between the sphingolipid profiles of different taxonomic groups may also be found in their specific LCB and fatty acid moieties. For example, the dihydroxy, Δ4,8-diunsaturated LCB moiety, d18:2, is detected in low to non-existent amounts in *A. thaliana* and other plants from the Brassicaceae family, in intermediate amounts in Fabaceae (pea and soybean), and in high amounts in Solanaceae (tomato and tobacco) (Markham *et al.*, 2006). A recent study further identified d18:2 as the exclusive LCB moiety in *Physcomitrella patens* GlcCers (Resemann, 2018). It was also shown that different tissues from *A. thaliana* have varying sphingolipid profiles. *A. thaliana* leaves have high levels of GIPCs (Markham *et al.*, 2006), while pollen and floral tissues are enriched in GlcCers (Michaelson *et al.*, 2009; Luttgeharm *et al.*, 2015b). Sphingolipids also have different subcellular distribution patterns with GIPCs and GlcCers being mainly enriched in the tonoplast and the plasma membrane (Tjellström *et al.*, 2010; Cacas *et al.*, 2016). These observations demonstrate that plant sphingolipid metabolism diverged during land colonisation and may have adapted according to the specific needs of individual plant species. The functional relevance of the varying sphingolipid profiles in different plants, tissues and membranes has, however, not yet been elucidated.

P. patens is a non-vascular model moss. It belongs to the group of bryophytes that diverged around 450 million years ago from vascular land plants (Rensing *et al.*, 2008). It has a haplodiplontic life cycle with the haploid gametophyte being the dominant phase of the cycle (Fig. 1) (Prigge & Bezanilla, 2010). Haploid spores or protoplasts (Fig. 1A, B) give rise to a two-dimensional filamentous network, the protonema. The protonema is the juvenile stage of the moss. Two functionally and morphologically distinct cell types constitute the protonema, the chloronema and the caulonema cells (Fig. 1C, D). Single spores or protoplasts first differentiate into highly photosynthetically active chloronema cells. These harbour many, well-developed chloroplasts and have cell plates that are oriented in a perpendicular angle to the surrounding cell wall. Chloronema cells differentiate gradually into caulonema cells. This cell type has fewer and poorly developed chloroplasts, is much longer and thinner, grows faster than chloronema cells, has an exploratory growth behaviour and has cell plates that are oriented in an oblique angle to the surrounding cell wall. Protonema cells grow via polarised growth during which cell wall material is transported to the tip of the apical cell (Menand *et al.*, 2007). Branching of filaments happens at the subapical cell. Bud initials mark the transition to three-dimensional growth. Outgrowth of the buddings results in the formation of gametophores, the adult stage of the life cycle (Fig. 1E). The gametophore is a shoot-like structure that is anchored to the soil or medium through root-like rhizoids. The shoot carries little leaflets or phyllids that are only a single cell layer thick. Transition to the diploid sporophyte is induced by transferring fully grown

gametophores to autumn-like conditions and flooding them with water. The reproductive organs, gametangia, then develop at the tip of the gametophore (Hohe *et al*., 2002) (Fig. 1F). Female gametangia are referred to as archegonia and male gametangia as antheridia. The water submersion enables spermatozoids that are released by the antheridia to swim to and fertilise the egg that is located within the archegonium. Subsequently, the maturing zygote develops into the diploid sporophyte which is composed of the mature spore capsule and a short seta (Landberg *et al*., 2013; Hiss *et al*., 2017) (Fig. 1G). After the spore capsule releases the haploid spores, the life cycle starts from the beginning (Engel, 1968).

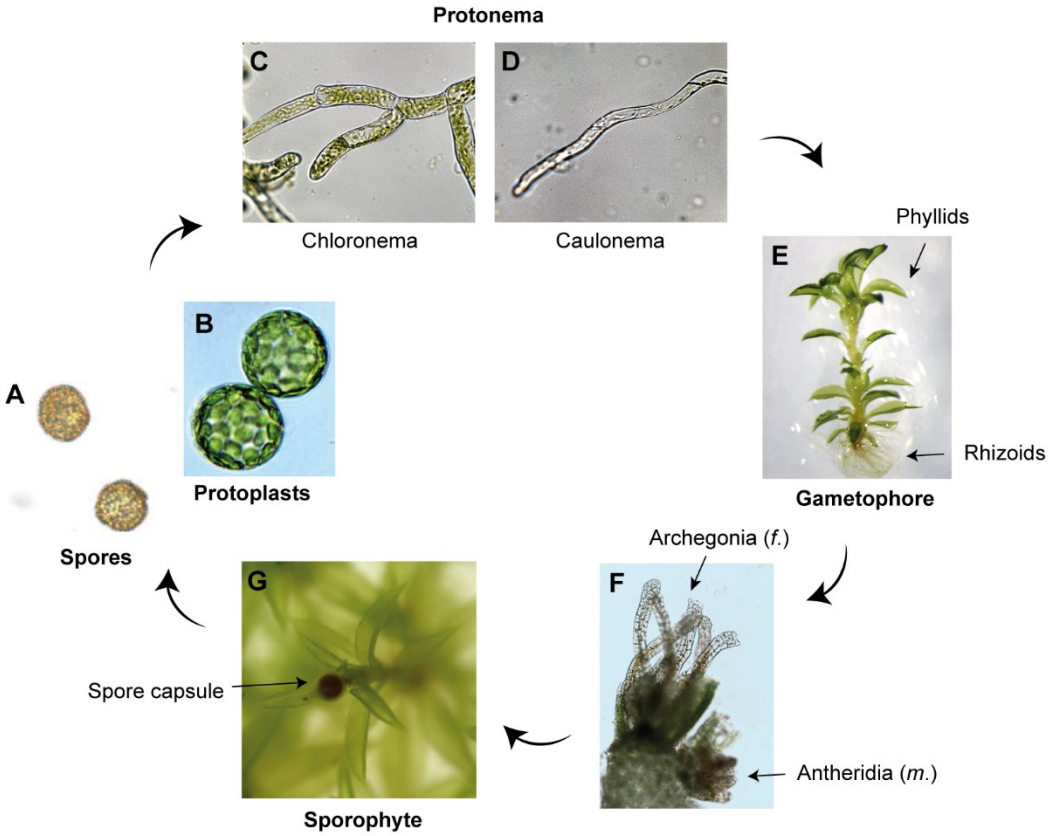

Fig. 1. *P. patens* life cycle. (A) Haploid spores or (B) protoplasts differentiate into filamentous protonema cells. Protonema is composed of (C) photosynthetically active chloronema and (D) explorative caulonema. (E) Gametophores emerge from the protonema and mark a transition to three-dimensional growth. (F) Male (antheridia) and female (archegonia) gametangia are located at the tip of the gametophore. (G) The diploid sporophyte develops after fertilisation and is composed of a spore capsule and a short seta. Haploid spores are released from the spore capsule and initiate the next life cycle. Stages A-F belong to the haploid stage. F is the only diploid stage of the life cycle. A was taken from (Stumpe *et al.*, 2010).

The non-vascular morphology of *P. patens* enables visualisation of subcellular mechanisms on a single cell level. The unique evolutionary position of *P. patens*, the tools available for the genetic manipulation of the haploid gametophyte, and its simple morphology may put this model plant into the spotlight of studies concerning plant sphingolipid metabolism. Findings about *P. patens* sphingolipids may help to shed light onto the general roles of sphingolipids in plants.

A recent study conducted in our department focused on the description of the *P. patens* lipidome (Resemann, 2018). Along with other lipids, the study revealed the

sphingolipid composition of *P. patens* protonema. The moss protonema can be easily propagated under laboratory conditions and may even be cultivated in large-scale bioreactors (Decker & Reski, 2004). A similar cultivation procedure was applied to collect *P. patens* material for the lipidomics screen. Protonema tissue was grown in liquid medium using aerated glass columns. While this cultivation was suitable to generate large amounts of biomass for performing the global lipid analyses, it is less appropriate for phenotype studies. The system promotes protonema growth but neglects differentiation into other developmental stages like the gametophore or the sporophyte generation. While the study revealed the lipid composition of *P. patens* protonema, it could not give any information about lipids of other growth stages of the moss. Additonally, the system does not represent the natural growth condition of the moss.

Classical small-scale *P. patens* cultivation is performed on agar-based medium in petri dishes. The two most commonly used media for *P. patens* cultivation are the Knop medium (Reski & Abel, 1985) and the BCD medium (Ashton & Cove, 1977) that only vary in minor ingredients. For protonema growth, medium dishes are overlaid with sterile cellophane. The protonema is cultivated on top of the cellophane and can be easily harvested by scraping off the plant material. Gametophores are grown on medium without cellophane so that they can anchor with their rhizoids into the agar and thereby allow full expansion of the shoot.

P. patens growth and tissue differentiation is strongly influenced by external conditions. Nutrient supply and light conditions are critical factors that determine protonema cell differentiation in *P. patens*. For example, the presence of ammonium tartrate as nitrogen source promotes chloronema growth and branching, while differentiation into caulonema cells and gametophores is favoured in the absence of ammonium tartrate (Thelander *et al.*, 2005). Sporophyte induction is dependent on moist and autumn-like conditions. Therefore, gametophore colonies are moved to 15-19 °C, with a photo period of 8 h light/ 16 h dark and a lower light intensity. Moss development and cell differentiation is also controlled by the presence of different phytohormones (Decker *et al.*, 2006). Auxin levels mediate the transition from chloronema to caulonema cells, cytokinin is responsible for bud induction, and abscisic acid initiates the formation of vegetative cells that are resistant to unfavourable conditions (Decker *et al*., 2006). Changes in the cultivation conditions are essential tools to manipulate the development of *P. patens*.

As mentioned, sphingolipid profiles and the presence of specific molecular species may vary greatly between organisms and tissue types. To fully understand the divergent evolution of plant sphingolipid metabolism and the physiological role of different sphingolipid species, it is of great importance to describe the sphingolipid profiles of different *P. patens* tissues and to investigate different sphingolipid mutant phenotypes. This chapter

demonstrates differences in the sphingolipidomes of *P. patens* wild type protonema and gametophores. Furthermore, relevant aspects of the *P. patens* cultivation in respect to phenotype characterisations such as cell differentiation ability are demonstrated and discussed. These aspects are exemplified by describing mutant phenotypes of three *P. patens* sphingolipid mutants that are defective in distinct sphingolipid enzyme activities: the LCB C-4 hydroxylase mutant *s4h*, the LCB Δ4-desaturase mutant *sd4d-1*, and the glycosylceramide synthase mutant *gcs-1*. Thorough examinations of the three enzymes and the corresponding mutant phenotypes are found in chapter 2 and chapter 3 of this thesis.

Materials and methods

Plant material and growth conditions

The *P. patens* 'Gransden' strain (Hedw.) Bruch & Schimp was used as wild type. Plants were grown in a 16 h light/ 8 h dark photoperiod at 25 °C and with a light intensity of 50–70 µmol m^2 s^{-1}. Protonema was regularly sub-cultivated on BCD agar medium plates (90 mm diameter) supplemented with 1 mM $CaCl_2$ and 5 mM ammonium tartrate (BCDAT) (Ashton & Cove, 1977). Protonema was grown on medium plates that were covered with sterile cellophane discs (folia, Wendelstein, Germany). Protonema sub-cultivation was achieved by harvesting one- to two-week-old tissue and disrupting the material in sterile water for 20 s using a tissue lyser (Ultra Turrax, Ika, Staufen, Germany). The cell suspension was spread onto fresh BCDAT plates. Plates were sealed with micropore tape before incubation.

Lipid and phytohormone measurements were conducted on protonema that was cultivated on cellophane-covered BCD plates. For direct comparison of different mutant lines, the dry weight of the cell suspension was determined after tissue lyser treatment. Plate cultures were subsequently inoculated with a volume equal to 5 mg dry weight. After ten days of incubation, protonema material from eight 90 mm plates was pooled. After the harvest the plant material was frozen in liquid nitrogen and subsequently lyophilised. Gametophores that were used for lipid analyses were induced by placing spot inocula (around 1 mm) on BCD medium. Culture plates were enclosed with micropore tape and gametophores were grown for 42 days. Rhizoids were cut off during the harvest. 200 Gametophore colonies were collected during one cultivation round. Gametophores were frozen in liquid nitrogen and lyophilised.

For imaging of protonema and gametophore development, 1 mm spot inocula of seven- to ten-day-old protonemal tissue were placed on plates containing BCD medium with 1 mM $CaCl_2$. For protonema development, colonies were imaged after one to two weeks. Fully grown gametophores were imaged after six weeks. Plates were sealed with micropore tape during cultivation.

Selective induction of skotonema cells followed the protocol described in (Saavedra *et al.*, 2015). In short, protonema spot inocula of around 1 mm diameter were placed on square BCDAT plates supplemented with 2 % sucrose. *P. patens* colonies were grown in horizontal position under continuous light for one week. Afterwards, plates were rotated into vertical position and moved to the dark. Growth was continued for another four weeks. Images were recorded as described above. Images were recorded with a binocular (Olympus SZX12 binocular, Olympus Corporation, Tokio, Japan) attached to a camera (R6 Retiga camera, QImaging, Surrey, Canada) with the Ocular scientific image acquisition software (version 1.0, Digital Optics Ltd, Auckland, New Zealand). Images were processed with ImageJ 1.52b software (Schneider *et al.*, 2012).

Fluorescence microscopy

One- to two-week-old protonema was bleached overnight in ethanol/acetic acid (3:1) prior to callose labelling. Callose staining was adjusted from a protocol described before (Schuette *et al.*, 2009). The moss tissue was incubated for 30 min at room temperature in 0.1 % aniline blue solution in 50 mM sodium phosphate buffer (pH 9). After aniline blue staining, the plant tissue was washed in in 50 mM sodium phosphate buffer (pH 9). Images were visualised using an excitation wavelength at 405 nm and an emission wavelength at 500 nm. Images were recorded with a fluorescence microscope (Olympus BX51, Olympus Corporation, Tokio, Japan) attached to a camera (C11440, ORCA-flash 4.0, Hamamatsu Photonics, Hamamatsu, Japan) with the HOKAWO scientific image acquisition software (version 2.10, Hamamatsu Photonics, Hamamatsu, Japan). Images were processed with ImageJ 1.52b software (Schneider *et al.*, 2012).

Cloning and transient transformation via particle bombardment

PpS4H and *PpSD4D* coding sequences were cloned into a pEntry vector that contained a sequence encoding a C-terminal yellow fluorescent protein (YFP). *PpS4H* was cloned with restriction sites *Apa*I/*Xho*I into the vector system using the following primer combinations: *Apa*I S4H-fw: 5'-GGAgggccc ATGGTGTTCTGGG-3' and *Xho*I S4H-rev: 5'-GGActcgagCCTCGATCTTCTTC-3'. *PpSD4D* was cloned with restriction sites *Apa*I/ *Xho*I into the vector system using the following primer combinations: *Apa*I SD4D-fw: 5'-GGAgggcccATGAGTGATGTTGG-3' and *Xho*I SD4D-rev: 5'-GGActcgagCGTTGGTTTTGCC-3'. Successful cloning was confirmed by sequencing of the plasmids.

50 mg of gold particles were prepared by washing three times with 96 % ethanol and dividing them into 10 µL aliquots. 50 ng/µL plasmid DNA, 1 M $CaCl_2$ and 10 mM spermidine were added to one 10 µL gold particle aliquot and the mixture was vortexed thoroughly. The mixture was centrifuged for 10 s at 10000 g.

The supernatant was discarded, and particles were washed twice with 96 % ethanol. The particles were finally re-suspended in 20 µL 96 % ethanol and ready to use for the bombardment. 4 µL of the DNA-coated gold particles were used for each shot. The macro carrier and rupture discs of 900 or 1000 psi were soaked in propan-2-ol, and dried. The gold suspension was pipetted onto the centre of the macro carrier and dried again. The components of the particle gun (Bio-Rad Laboratories, Inc., Hercules, California, USA) were assembled. One-week-old protonema grown on cellophane-covered BCD medium was transiently transformed. After bombardment, the tissue was incubated for 12 h before visualisation with a confocal laser scanning microscope. Images were analysed with Leica TCS SP5 confocal microscope (Leica Microsystems GmbH, Wetzlar, Germany) and processed with ImageJ 1.52b software (Schneider *et al.*, 2012).

Sphingolipid extraction and analysis

Sphingolipid extraction from different *P. patens* tissues was achieved by performing a monphasic extraction as described by (Grillitsch *et al.*, 2014) with minor modifications. 20 mg of lyophilised and homogenised protonema and gametophore material were immersed in propan-2-ol/hexane/water (60:26:14, v/v/v) and incubated at 60 °C for 30 min. After incubation, samples were centrifuged for at 20 °C for 20 min at 635 g. The supernatant was collected into new glass vials. After solvent evaporation under a nitrogen stream, lipids were re-suspended in 800 µL tetrahydrofuran/methanol/water (4:4:1, v/v/v). Samples were centrifuged for 10 min at 635 g and 20 °C before transferring them to glass micro-vials. Samples were directly used for ultra-performance liquid chromatography (UPLC) coupled with nanoelectrospray ionisation (nanoESI) and triple quadrupole tandem mass spectrometry (MS/MS) (UPLC-nanoESI-MS/MS) analysis (AB Sciex, Framingham, Massachusetts, USA).

UPLC-nanoESI-MS/MS molecular species analysis was performed as previously described (Resemann, 2018). Separation of constituents was achieved by UPLC using an ACQUITY UPLC® I-class system (Waters Corp., Milford, Massachusetts, USA) equipped with an ACQUITY UPLC® HSS T3 column (100 mm × 1 mm, 1 µm; Waters Corp., Milford, Massachusetts, USA). The flow rate was set to 0.1 mL/min and the injection volume to 2 µL. The separation temperature was 35 °C. Solvent B was tetrahydrofuran/methanol/ammonium acetate (20 mM) (6:3:1; v/v/v) containing 0.1 % (v/v) acetic acid; and solvent A was methanol/ammonium acetate (20 mM) (3:7; v/v) containing 0.1 % (v/v) acetic acid. All sphingolipids were separated with linear binary gradients following the same scheme: start conditions (40, 65, or 80 % solvent B) held for 2 min, linear increase to 100 % solvent B for 8 min, 100 % solvent B held for 2 min and re-equilibration

to start conditions in 4 min. The start conditions were 40 % solvent B for LCB, 65 % solvent B for inositol-containing sphingolipids and 80 % solvent B for ceramides and GlcCers.

Chip-based nanoelectrospray ionisation was achieved with a TriVersa Nanomate® (Advion, Inc., Ithaca, New York, USA) in the positive ion mode with 5 µm internal diameter nozzles. By using a post-column splitter 255 nL/min of the eluent were directed to the nanoESI chip. Sphingolipid molecular species were detected with a 6500 QTRAP® tandem mass spectrometer (AB Sciex, Framingham, Massachusetts, USA) by monitoring (i) the transition from [M+H]+ molecular ions to dehydrated LCB fragments for ceramides, GlcCers and LCBs; and (ii) the transition of $[M+NH_4]^+$ molecular ions to ceramide fragments as loss of phosphoinositol-containing head groups for inositol-containing sphingolipids. Determination of head group-specific ions was done as described (Buré *et al.*, 2011). Dwell time was either 5 ms (ceramide/ GlcCer), 15 ms (inositol-containing sphingolipids) or 20 ms (LCB) and MS parameters were optimised to maximise detector response. The integration workflow made use of the Analyst® IntelliQuan (MQII) peak-finding algorithm.

For data acquisition Analyst 1.6.2 (AB Sciex, Framingham, Massachusetts, USA) was used. The chip ion source TriVersa Nanomate® was controlled with ChipSoft 8.3.1 (Advion, Inc., Ithaca, NY, USA)

LC-MS data was processed using Analyst 1.6.2 and MultiQuant 3.0.2 software (both AB Sciex, Framingham, Massachusetts, USA).

Phytohormone extraction and analysis

Phytohormone extraction was achieved by a two-phase extraction method using methyl *tert*-butylether (MTBE) according to (Matyash *et al.*, 2008) with minor modifications. 10 mg of lyophilised and homogenised *P. patens* protonema was immersed in 0.75 mL methanol. After addition of an internal standard mixture containing: 10 ng D4-SA, 10 ng D6-ABA (both from C/D/N Isotopes Inc., Pointe-Claire, Canada), 30 ng D5-OPDA (kindly provided by Otto Miersch, Halle/Saale, Germany), 20 ng D_5-IAA (Eurisotop, Freising, Germany), 2.5 mL of MTBE was added, and the mixture was covered with argon. Extraction was performed for 1 h at 4 °C while shaking in the dark. Subsequent phase separation was achieved by the addition of 0.6 mL of water. The sample was mixed and incubated for 10 min at room temperature. After centrifuging for 15 min at 450 g, the upper phase was collected and transferred to a new vial. The lower phase was re-extracted by the addition of 0.7 mL methanol/water (3:2.5, v/v) and 1.3 mL MTBE. Upper phases were combined and evaporated under a stream of nitrogen. The residue was resuspended in 200 µL methanol. Prior to measurements, the sample was centrifuged at 16000 g for 2 min and the methanol was evaporated. The sample was dissolved in 20 µL solvent B (acetonitrile/water, 90:1, v/v, containing 0.3 mmol/L NH_4HCOO, adjusted to pH 3.5 with formic acid). After adding 80 µL

of solvent A (water containing 0.3 mmol/L NH_4HCOO, adjusted to pH 3.5 with formic acid) the mixture was vortexed and centrifuged for 10 min at 16000 g. Samples were transferred to glass micro-vials and used for phytohormone analysis.

Phytohormone measurement and analysis was done according to (Herrfurth & Feussner, 2020). In short, reversed phase separation of constituents was achieved by UPLC using an ACQUITY UPLC® system (Waters Corp., Milford, Massachusetts, USA) equipped with an ACQUITY UPLC® HSS T3 column (100 mm x 1 mm, 1.8 µm; Waters Corp., Milford, Massachsetts, USA). Aliquots of 10 µL were injected in a partial loop with needle overfill mode. Elution was adapted to (Balcke *et al.*, 2012). The flow rate was set to 0.16 mL/min and the injection volume to 3 µL. The sample manager temperature was set to 18 °C and the column oven temperature was constantly at 40 °C. The solvent gradient used as mobile phase for chromatographic separation was as follows: for 0.5 min at 10 % solution B, followed by a linear increase to 40 % solution B in 2 min, this condition was held for 2 min, followed by a linear increase to 95 % solution B in 1 min, this condition was held for 2.5 min. The column was re-equilibrated for start conditions in 3 min.

Nanoelectrospray analysis was achieved using the chip ion source TriVersa Nanomate® (Advion Inc., Ithaca, New York, USA). For stable nanoESI, 70 µL/min of 2-propanol/acetonitrile/water (70:20:10, v/v/v) containing 0.3 mmol/L NH_4HCOO (adjusted to pH 3.5 with formic acid) delivered by Agilent 1100 HPLC isocratic pump (Agilent, Waldbronn, Germany) with mixing tee valve and equipped with nanoESI chip with 5 µm internal diameter nozzles. Ionisation voltage was set to -1.7 kV. Phytohormones were ionised in a negative mode and determined in scheduled multiple reaction monitoring (MRM) mode with an AB Sciex 4000 QTRAP® tandem mass spectrometer (AB Sciex, Framingham, Massachsetts, USA). Mass transitions were as previously described (Iven *et al.*, 2012), with some modifications and were as follows: 141/97 [declustering potential (DP) -25 V, entrance potential (EP) -6 V, collision energy (CE) -22 V] for D4-SA, 137/93 (DP -25 V, EP -6 V, CE -20 V) for SA, 179/135 (DP -35 V, EP -9 V, CE -14 V) for D5-IAA, 269/159 (DP -30 V, EP -5 V, CE -16 V) for D6-ABA and 263/153 (DP -35 V, EP -4 V, CE -14 V) for ABA. The mass analysers were adjusted to a resolution of 0.7 amu full width at half-height. The ion source temperature was 40 °C, and the curtain gas was set at 10 (given in arbitrary units). Quantification was carried out using a calibration curve of intensity (m/z) ratios of [unlabelled]/[deuterium-labelled] vs. molar amounts of unlabelled (0.3-1000 pmol). For data acquisition Analyst 1.6.2 (AB Sciex, Framingham, Massachsetts, USA) was used. nanoESI was controlled with ChipSoft 8.3.1 (Advion, Inc., Ithaca, New York, USA).

LC-MS data was processed using Analyst 1.6.2 and MultiQuant 3.0.2 software (both AB Sciex, Framingham, Massachsetts, USA).

Results and discussion

Previous *P. patens* studies performed in our department focused on describing the lipidome and required the generation of large amounts of biomass for extraction. *P. patens* cultivation in liquid cultures produces large amounts of biomass in relatively short time. Cultivation of *P. patens* in aerated glass columns was therefore the method of choice for generating protonema biomass for the global lipid profiling of *P. patens* performed by Resemann (2018). While this research laid the groundwork for our understanding of the *P. patens* lipidome, it just represents a snapshot of the lipid composition in *P. patens* during a specific time of development. Furthermore, the natural habitats of mosses are terrestrial ecosystems. Although mosses are mostly found in moist environments, they can also withstand prolonged exposure to drought. The laboratory cultivation in liquid culture is therefore a rather artificial system and may not reflect the endogenous membrane compositions under natural conditions. The next steps in the *P. patens* lipidome research would therefore benefit from the establishment of a cultivation system that resembles the natural growth conditions of *P. patens*.

P. patens cultivation was changed from liquid cultures to solidified medium

P. patens has been used for decades as a model organism in plant biology research. Cultivation methods are therefore thoroughly described in several publications and reviews (Frank *et al.*, 2005; Strotbek *et al.*, 2013). Literature research revealed a common technique for small-scale *P. patens* cultivation on solidified medium plates. In the beginning of this study the established liquid culture system used in the department was therefore evaluated for its applicability and suitability for *P. patens* mutant characterisation. The following section demonstrates the advantages of *P. patens* cultivation on solidified medium plates over cultivation in liquid cultures.

Phenotype investigations of mutant plants require the establishment of a highly controllable cultivation system. In liquid cultures, *P. patens* only grows in the filamentous protonema stage. Routine disruption of the plant material for plant propagation prevents gametophore development. Furthermore, gametophores are shoot-like structures with assimilatory rhizoids that anchor into solid ground or medium. In liquid cultures, gametophores are floating and therefore do not have defined anchor points. Since the gametophores are the adult stage of the moss that carry the gametangia, liquid cultivation also neglects sporophyte development. Moreover, monitoring of *P. patens* growth is a challenge with liquid cultures because samples are taken from the sterile culture for microscope imaging. This increases the chance of contamination. Additionally, time course visualisation of *P. patens* growth cannot be performed because the liquid culture samples always contain a new set of cells whose growth cannot be continued after they were

removed from the sterile culture. In contrast to that, *P. patens* growth on solidified medium can be easily controlled. Colonies are started from spores, protoplasts, single leaflets, or protonema spot inocula. *P. patens* development is influenced by medium supplements. During the first two weeks, protonema growth can be monitored. Afterwards, gametophore growth is initiated. Plates with fully expanded gametophores can be transferred to autumn-like conditions to induce sporophyte development. The *P. patens* life cycle can therefore be completed during cultivation on solidified medium plates. Furthermore, growth of a single colony or even single cells can be visualised over long periods of time. Plate cultivation represents a highly controllable system that allows the identification of morphological and physiological peculiarities of mutant plants. Different developmental stages can be selectively cultivated which allows for in-depth investigations of distinct growth patterns and differentiation processes of *P. patens*.

Moreover, the lipid profiles of different growth stages can be assessed. Therefore, plate cultivation allows a direct connection between the morphological phenotypes observed in the mutants and the underlying metabolic changes in lipid metabolism.

Another important consideration is the maintenance and propagation of *P. patens* mutants. Mutants may be affected in their growth and development and therefore might have special requirements for cultivation. In the course of this study, it was observed that the investigated sphingolipid mutants had substantial variations in their growth behaviours. *P. patens s4h* mutants were not able to develop fully grown gametophores and had to be maintained in protonema stage (chapter 2). *gcs-1* mutants, however, could not be kept for a long time in protonema stage without showing cell death-like symptoms (chapter 3). Although reduced in size, *gcs-1* gametophores had a normal morphology and plants could easily be maintained in this developmental stage over longer time periods. The specific requirements for maintenance of different mutant lines can therefore only be identified and fulfilled when plants are grown on solidified medium plates.

Additionally, application of external stressors and investigation of the responses of *P. patens* to these stresses can be performed on colonies grown on solid medium without having to account for the added stresses introduced by the continuous, artificial liquid environment.

In light of these observations made during the first months of the study, the established liquid culture system used in the department was found unsuitable for the planned sphingolipid mutant characterisation studies. The system was therefore replaced by a more appropriate cultivation system that is based on *P. patens* growth on solidified mineral medium plates. Change of the cultivation system may give a more elaborate picture of the involvement of distinct sphingolipids in various plant developmental and physiological processes.

Establishment of a regular *P. patens* maintenance system

Before phenotype studies of *P. patens* mutants could be addressed, regular plant maintenance had to be established. The applied continuous plant propagation system ensured a constant provision of fresh *P. patens* material for phenotype and chemotype investigations.

A scheme of the regular sub-cultivation cycle is depicted in Fig. 2. *P. patens* protonema has a high regeneration rate. The regular propagation of the plant material was therefore performed with protonema material. The protonema was cultivated for one to two weeks on cellophane-covered solidified mineral medium supplemented with ammonium tartrate (BCDAT) (Fig. 2A). Ammonium tartrate is a nitrogen source that promotes growth of photosynthetically active chloronema cells. The cellophane is permeable for water and nutrients. Cultivation of *P. patens* protonema on sterile cellophane discs prevents the filamentous tissue to grow into the agar medium and therefore enables easy harvesting of the plant material. For sub-cultivation, the material was scraped off the cellophane and was immersed in 10 mL sterile water (Fig. 2B). The protonema was subsequently disrupted using a homogeniser to generate a cell suspension (Fig. 2C). The protonema suspension was applied to fresh medium plates that were overlaid with cellophane (Fig. 2D). The tissue was allowed to dry before enclosing the cultivation plates with micropore tape to enable aeration during the cultivation period (Fig. 2E). Standard growth conditions for *P. patens* cultivation were a 16 h light/ 8 h dark long-day cycle with a light intensity of 50–70 µmol m^2 s^{-1} and a temperature of 25 °C. The protonema was maintained on the plates for one to two weeks until the next sub-cultivation round was performed.

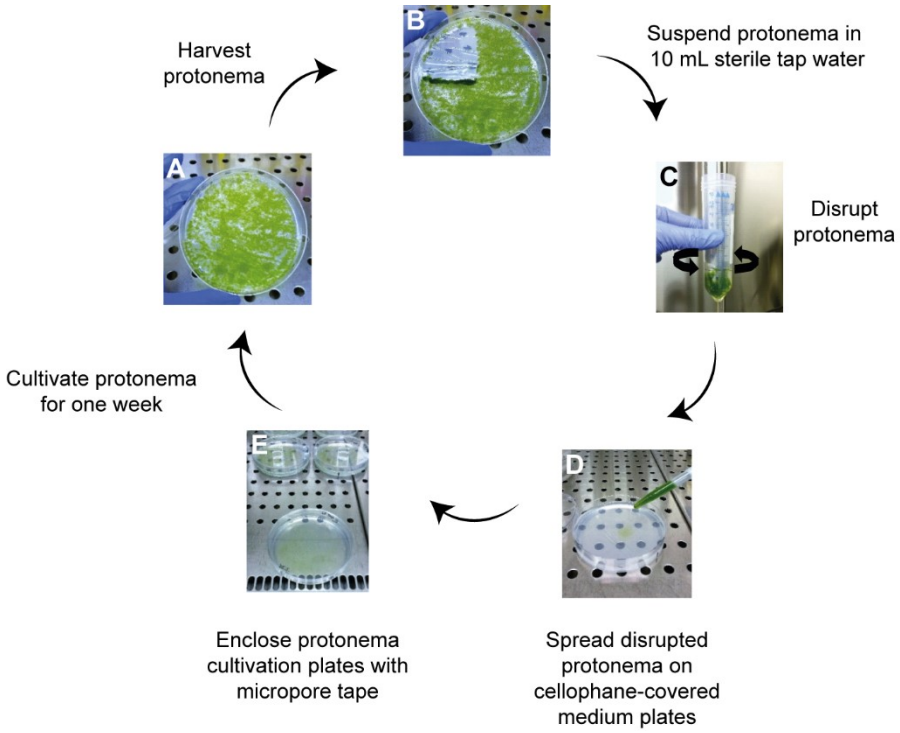

Fig. 2. Regular sub-cultivation of *P. patens*. (A) A one- to two-week-old protonema plate is used for sub-cultivating *P. patens* tissue. (B) The protonema is harvested by scraping off the material from the cellophane. (C) The material is immersed in 10 mL sterile water and treated with a tissue lyser for disruption. (D) The cell suspension is applied to a fresh plate overlaid with cellophane. (E) Cultivation plates are allowed to dry and are enclosed with micropore tape to allow aeration. Cultures are incubated for one to two weeks.

The routinely cultivated protonema was used for different applications. It was used as starting material for phenotype studies or to start cultures for the collection of material used in lipid analyses. The material was also directly applied for the isolation of protoplasts. Usually, five- to seven-day-old protonema is used during the protoplasting procedure. Protoplasts were subsequently used for polyethylene-glycol (PEG) mediated transformations or directly regenerated for phenotype studies. Before the switch from liquid to solid medium cultures, protonema was grown and routinely sub-cultivated in non-aerated liquid cultures for around three months until the tissue was ready for transformation. Protonema growth on solidified medium therefore greatly shortened the cultivation period of tissue used for transformations and allowed for more flexible and efficient *P. patens* transformations.

Protonema cultivation for lipid analyses

As explained, plate cultivation is an appropriate system for phenotype characterisations. Sphingolipid mutant characterisations of this study involved the description of their lipid profiles. However, the solid medium cultivation system is only a small-scale method. To obtain sufficient amounts of plant material for lipid extractions, the cultivation needed to be scaled up. A critical aspect to be considered in the work with mutants is that the plants might be affected in their growth and development. This was especially true for the investigated

sphingolipid mutants, since the corresponding *A. thaliana* knockout plants also exhibited severe growth defects (Chen *et al.*, 2008; Msanne *et al.*, 2015). To ensure comparable cultivation, inoculation of the cultivation plates had to be normalised. For normalisation, the dry weight of the protonema cell suspension was determined. Normalisation was modified from the procedure described in the dissertation of Dr. Anna Ostendorf (née Beike) from 2013 (Beike, 2013). In that study, liquid cultures were inoculated with a certain amount of tissue that was determined by drying the cell suspension on filter paper. A drawback of filter paper is, however, that it tends to soak up moisture from its environment quickly after being dried and therefore may falsify the dry weight determination. Aluminium cups were used in this study for tissue drying and dry weight determination (Fig. 3F). After treatment with the tissue lyser, 1 mL of the cell suspension was transferred to the aluminium cups and dried at 110 °C for 45 min. After the liquid was completely evaporated, the dry weight of the cell suspension was determined. Volumes that corresponded to 5 mg dry weight proved ideal for starting the plate cultures (Fig. 3G). Larger amounts turned out to be disadvantageous for protonema growth indicated by browning and hence putative cell death of the tissue. This might have been due to a too high density of the tissue. Lower amounts, however, resulted in a too low recovery rate of protonema tissue. The protonema of all plant lines was harvested after ten days (Fig. 3H). Longer incubation resulted in browning of *gcs-1* protonema tissue and was therefore avoided. Tissue cultivation for lipid analyses was performed on mineral medium without ammonium tartrate (BCD). The presence of ammonium tartrate enhances growth of chloronema cells but inhibits differentiation into caulonema cells. Absence of ammonium tartrate in the medium allows for protonema cell differentiation. Lipid screens performed on BCD medium grown tissue therefore covered all protonema cell types. Several plates were inoculated for each plant line. The tissue from all plates was pooled after harvesting and the fresh weight was determined. Subsequently, the plant material was frozen in liquid nitrogen and stored at -80 °C. After the material was lyophilised, the dry weight was determined, and the material was used for lipid and phytohormone analyses.

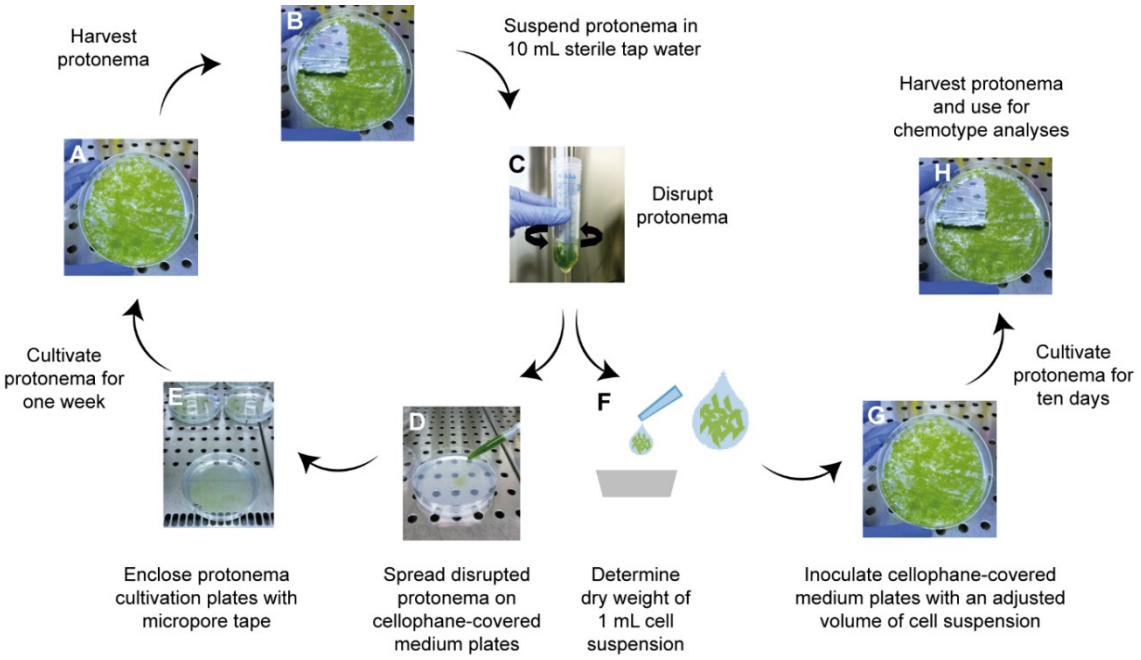

Fig. 3. Cultivation of protonema for lipid analyses. (A) A one- to two-week-old protonema plate is used for sub-cultivating *P. patens* tissue. (B) The protonema is harvested by scraping off the material from the cellophane. (C) The material is immersed in 10 mL sterile water and treated with a tissue lyser for disruption. (D) The cell suspension is applied to a fresh plate overlaid with cellophane. (E) Cultivation plates are allowed to dry and are enclosed with micropore tape to allow aeration. Cultures are incubated for one to two weeks. (F) To standardise cultivations, 1 mL of the cell suspension prepared in (C) is dried in aluminium cups at 110 °C for 45 min. (G) Cultivation plates are subsequently inoculated with a volume corresponding 5 mg dry weight. (H) Protonema is harvested after ten days of incubation, weighed for fresh weight determination, lyophilised and used for chemotype analyses.

Gametophore cultivation for lipid analyses

Gametophore induction was achieved by placing protonema spot inocula of around 1 mm in diameter onto BCD plates that were not overlaid with cellophane. Growth on medium plates without cellophane allowed gametophores to anchor through their rhizoids into the solidified medium. The plates were enclosed with micropore tape to ensure aeration during the cultivation period. The first gametophores emerged two weeks after inoculation. Fully grown and expanded gametophores are obtained after five-to seven weeks incubation (Fig. 4F). To obtain sufficient amounts of gametophore material for lipid extractions, around 200 wild type colonies were collected during one cultivation round. Gametophores were harvested by cutting the colonies at their basis to avoid collection of rhizoids. Gametophore tissue was subsequently lyophilised and used for lipid analyses.

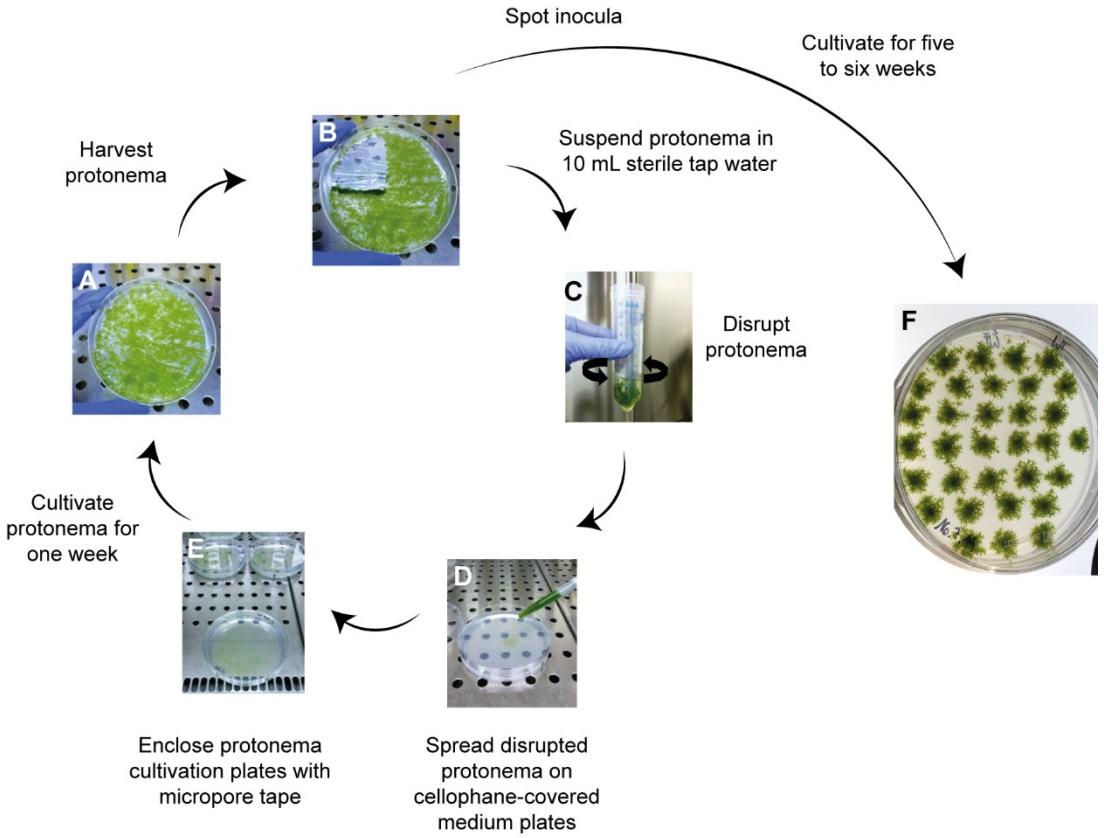

Fig. 4. Cultivation of gametophores for lipid analyses. (A) A one- to two-week-old protonema plate is used for sub-cultivating *P. patens* tissue. (B) The protonema is harvested by scraping off the material from the cellophane. (C) The material is immersed in 10 mL sterile water and treated with a tissue lyser for disruption. (D) The cell suspension is applied to a fresh plate overlaid with cellophane. (E) Cultivation plates are allowed to dry and are enclosed with micropore tape to allow aeration. Cultures are incubated for one to two weeks. For gametophore induction, protonema is taken from (B) and spot inocula of around 1 mm in diameter are placed on BCD plates without cellophane. Gametophore plates are enclosed with micropore tape and incubated for five to six weeks. (F) Fully expanded gametophore colonies are harvested but cutting the gametophores at their bases. The gametophore tissue was then frozen in liquid nitrogen, lyophilised and used for chemotype analyses.

Sphingolipid profiles vary in different *P. patens* tissues

Sphingolipids were extracted from wild type protonema and gametophores and lipid profiles were determined using UPLC-nanoESI-MS/MS.

LCB profiles of protonema and gametophores were very similar with the t18:0 LCB predominating in both tissues at around 90 % and the d18:0 LCB being found in minor amounts (Fig. 5A).

The most significant differences between protonema and gametophores were found in the fatty acid composition of ceramides (Fig. 5B). In protonema, ceramides with a t18:0 LCB moiety predominated. The five most abundant fatty acid moieties were h24:0 (52 %), h22:0 (10 %), c24:0 (10 %), h24:1 (10 %), and c24:1 (4 %). All other molecular species represented less than 4 % of all ceramides. The ceramide profile of gametophores showed major variations compared to the ceramide profile of protonema. The three most abundant ceramide species in gametophores were only found in trace amounts in the protonema.

They had the following LCB/fatty acid moiety combinations: t18:0/c20:0 (21 %), d18:0/h20:0 (20 %), and d18:0/c20:0 (19 %). The next two most abundant ceramide species were t18:0/h24:0 (15 %) and t18:0/c24:0 (10 %). The remaining profile was composed of minor molecular species each representing less than 5 % of total ceramides.

The GlcCer profiles of protonema and gametophores looked the same (Fig. 5C). A single species composed of d18:2/h20:0 represented more than 90 % of all GlcCers in both tissues. All other molecular species were only detected in trace amounts.

GIPC profiles with a head group composition consisting of one hexose (Hex) moiety connected to a glucuronic acid (GlcA) linked to the inositolphosphate ceramide (IPC) backbone (Hex-GlcA-IPC) were analysed in both tissue types. Hex-GlcA-IPC profiles of gametophores differed slightly from Hex-GlcA-IPC profiles of protonema (Fig. 5D). The most abundant Hex-GlcA-IPC species in the protonema were composed of a t18:0 LCB moiety and the following fatty acid moieties: h24.0 (45 %), h24:1 (35 %), h22:0 (8 %), and h20:0 (5 %). Most abundant Hex-GlcA-IPC species in the gametophores also had a t18:0 LCB moiety that was connected to the following fatty acid moieties: h24:0 (52 %), h20:0 (18 %), h24:1 (13 %), h26:0 (7 %), and h22:0 (6 %). The other Hex-GlcA-IPC species in the protonema and the gametophore profiles represented each less than 5 % of total Hex-GlcA-IPCs.

The different ceramide profiles of protonema and gametophores raised the question why ceramide species composed of fatty acids with a 20-carbon chain length were significantly enriched in the gametophore. This is especially interesting since not all of these enriched ceramide species were found in significantly larger amounts in the downstream complex sphingolipid classes. It indicated that these species are not channelled into GlcCer or GIPC synthesis but that they might have immediate activities as ceramides. Ceramides are usually only found in minor amounts in plants and as those they mainly function as signalling molecules (Liang *et al*., 2003). This suggested that the identified enriched ceramide species might have signalling activities in *P. patens* gametophores. However, this does not exclude a putative structural role of those compounds. Gametophores are differently structured than the protonema. While the protonema consists of filamentous cells, gametophores have leaflets that are a single cell layer thick. Cells in these tissues are therefore connected in different patterns, and it would not be surprising if the membranes of leaflets and protonema cells have different lipid compositions. Ceramides lack a polar head group and therefore induce a negative membrane curvature. This might suggest an increased vesicular transport in tissues with higher ceramide levels. While the comparison of the relative profiles of different sphingolipid classes in *P. patens* tissues revealed a different distribution of specific molecular species, the results cannot be interpreted quantitatively. The individual sphingolipid classes and molecular species have different

ionisation efficiencies in the UPLC-nanoESI-MS/MS. In future, combination with other measuring techniques might help to provide a quantitative description of single sphingolipid classes and species in *P. patens*. It could further be assessed whether the absolute amounts of individual classes vary significantly among different developmental stages of *P. patens*. The varying sphingolipid profiles in different *P. patens* tissues may represent a useful tool in future sphingolipid mutant studies. Depending on the target gene, the focus may be put on distinct developmental stages in which the gene seems more active according to the wild type lipid profile. Furthermore, since different sphingolipid profiles were identified in different *P. patens* tissues, it might also be worthwhile to look at other lipid classes outside the sphingolipids. This will greatly extend our knowledge on the *P. patens* lipidome.

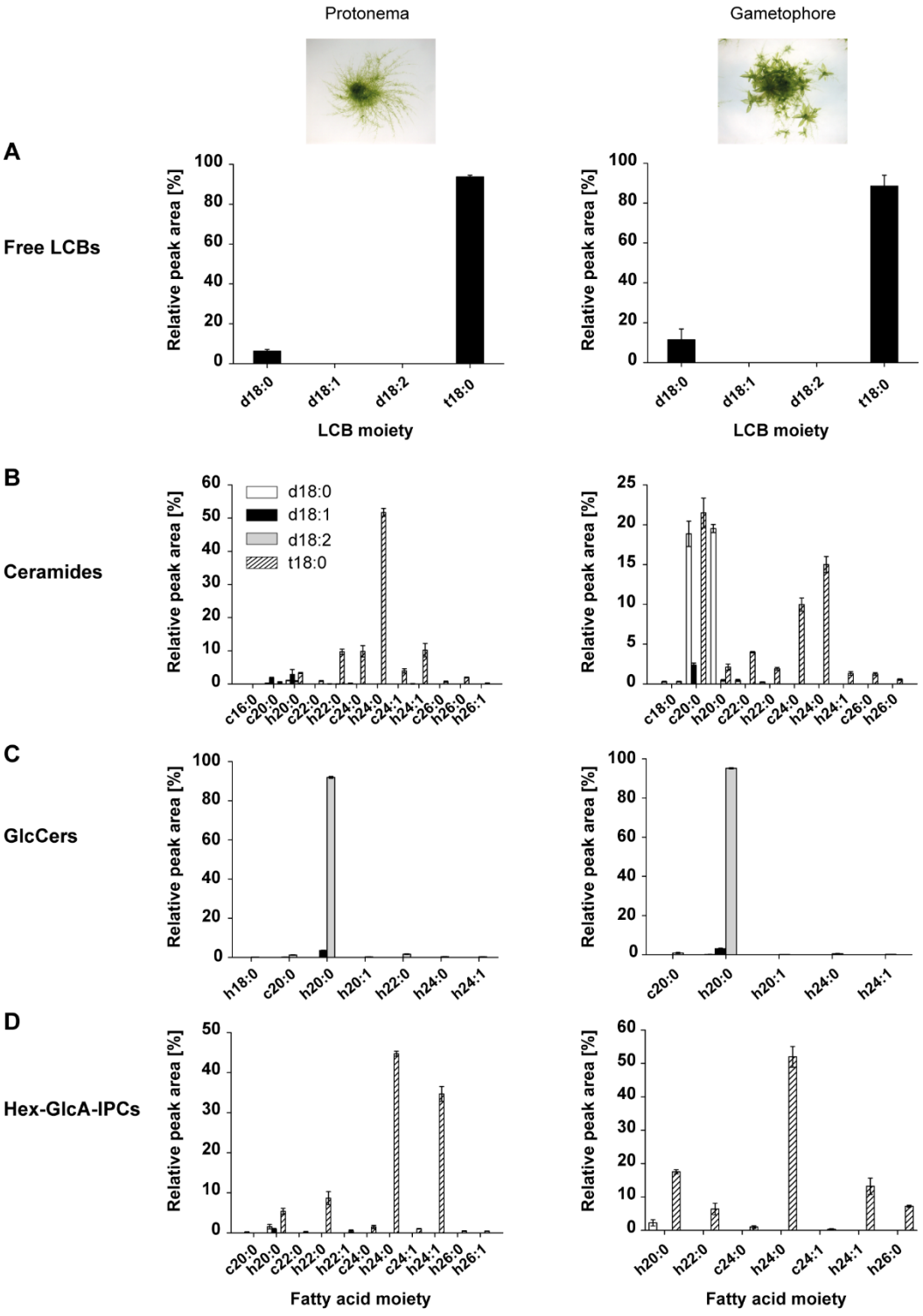

Fig. 5. Sphingolipid profiles of *P. patens* wild type protonema and gametophores. (A-D) Ceramides were extracted from ten-day-old wild type (WT) protonema and from 45-day-old WT gametophores and analysed with UPLC-nanoESI-MS/MS. Relative profiles of (A) long-chain bases (LCBs), (B) ceramides, (C) glycosylceramides (GlcCers), and (D) glycosyl inositolphosphorylceramides (GIPCs). Ceramide, GlcCer, and GIPC molecular species are shown with their LCB (column colour) and fatty acid (x-axis) moieties. Dihydroxy LCB moieties are indicated by a 'd' and trihydroxy LCB moieties are indicated by a 't'. Molecular species with an unhydroxylated fatty acid moiety are indicated by a 'c' and molecular species with an α-hydroxylated fatty acid moiety are indicated by an 'h'. Protonema sphingolipid data represent the mean ± SD of measurements from four independent cultivations each containing protonema material from eight cultivation plates. Gametophore sphingolipid data represent the mean ± SD of measurements from three independent cultivations each containing gametophore material from approximately 200 gametophore colonies. Abbreviations are as follows: GlcA: glucuronic acid, Hex: hexose, IPCs: inositolphosphorylceramides.

Phenotype characterisation of different developmental stages

Phenotype investigations were started with protonema spot inocula. Spot inocula of around 1 mm in diameter were placed onto BCD medium plates and incubated for five to six weeks. During the first two weeks, protonema development was investigated (Fig. 6F). After approximately two weeks, gametophore growth initiated in wild type plants (Fig. 6G). Gametophores were fully expanded after five to six weeks of incubation. The growth and development of the different tissue types was monitored using different macro- and microscopic observation techniques and revealed substantially different growth behaviours in all investigated sphingolipid mutants (chapter 2 Fig. 7, chapter 3 Fig. 5).

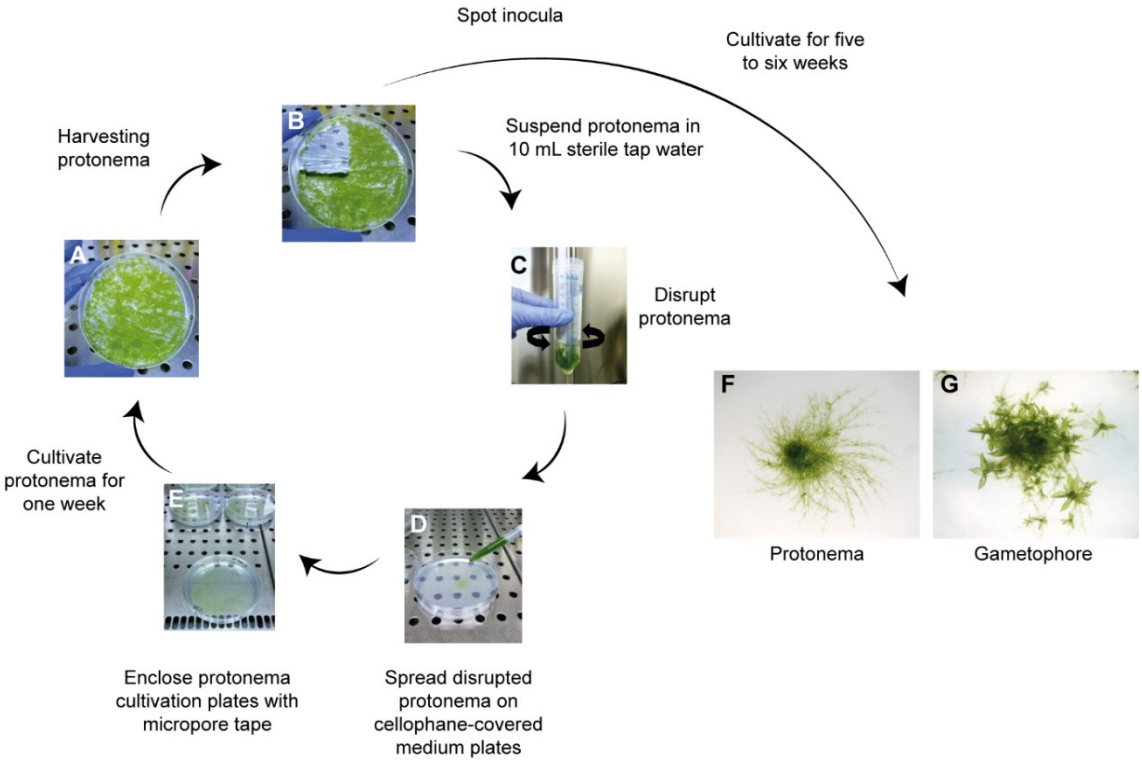

Fig. 6. Cultivation of protonema and gametophores for phenotype analyses. (A) A one- to two-week-old protonema plate is used for sub-cultivating *P. patens* tissue. (B) The protonema is harvested by scraping off the material from the cellophane. (C) The material is immersed in 10 mL sterile water and treated with a tissue lyser for disruption. (D) The cell suspension is applied to a fresh plate overlaid with cellophane. (E) Cultivation plates are dried and are enclosed with micropore tape to allow aeration. Cultures are incubated for one to two weeks. For phenotype analysis of protonema and gametophore development, protonema is taken from (B) and spot inocula of around 1 mm in diameter are placed on BCD plates without cellophane. (F) Protonema development can be monitored during the first two cultivation weeks. (G) Gametophore development can be observed from the onset of buddings after two weeks until full gametophore expansion after five to six weeks.

Protonema cell types are identified by their cross-wall orientation

As discussed, protonema and gametophore tissues are anatomically very different structures and can therefore be easily distinguished. The two protonema cell types can be identified by the orientation of the cross-wall that separates two adjacent filamentous cells. Chloronema cells have a cross-wall that is oriented perpendicular to the surrounding cell wall (Fig. 7A, B). Caulonema cells are identified by cross-walls that are oriented in an oblique angle to the surrounding cell wall (Fig. 7C, D). Initially, this characteristic feature was used for determining if the investigated sphingolipid mutants had cell differentiation defects. A unique component of protonema cross-walls is the polysaccharide callose (ß-1→3-glucan). Callose is deposited after phragmoplast and subsequent cell plate formation at newly synthesised cell walls. To accurately identify the cross-wall orientation, the tissue was therefore stained with 0.1 % aniline blue which is a fluorescent stain for callose.

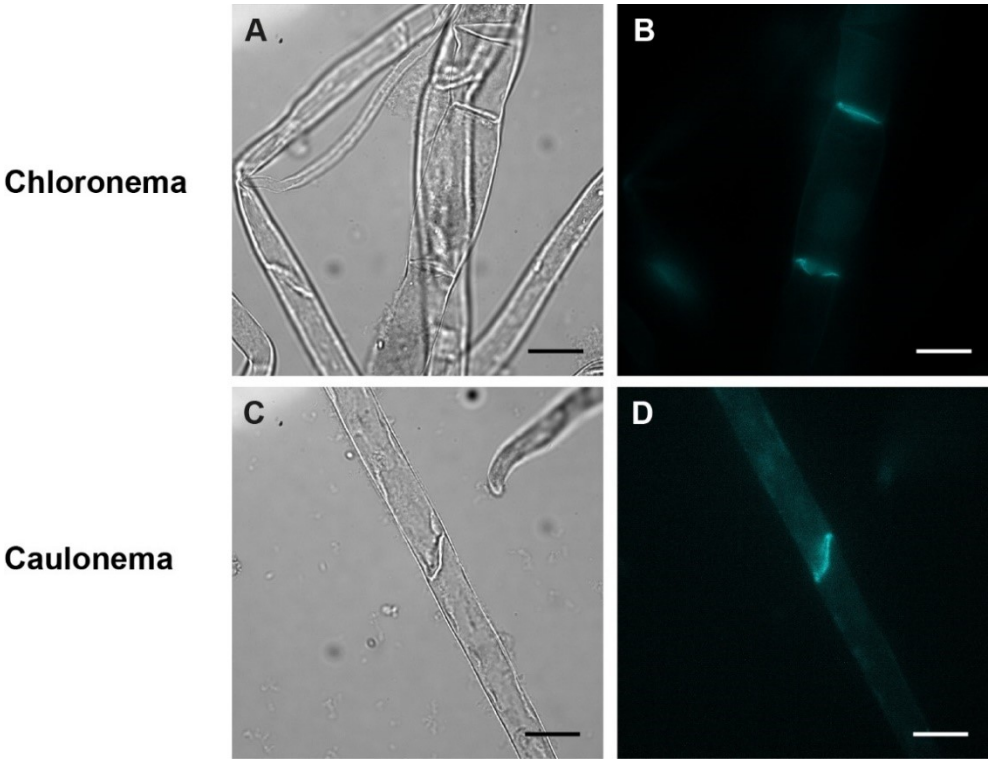

Fig. 7. Cross-wall orientation in chloronema and caulonema cells. Callose in the cross-walls of *P. patens* protonema cells was stained with 0.1 % aniline blue. The orientation of the cross-walls indicates the identity of protonema cell types. Pictures were taken as bright field (A, C) and fluorescent (B, D) images. Perpendicular cross-walls are characteristic to chloronema cells (A, B), oblique cross-walls are characteristic to caulonema cells (C, D). Scales bars are 20 µm. Staining of the cross-walls with aniline blue was regularly performed with the same results. Pictures are representative images for at least three independent experiments.

Microscopic channels, plasmodesmata, traverse cross-walls of plant cells. Plasmodesmata enable communication and transport between two adjacent cells. Callose deposition at plasmodesmata neck regions regulates permeability of the symplastic channels (Vatén *et al.*, 2011; De Storme & Geelen, 2014). The level of deposits influence plasmodesmata structure and therefore cause narrowing or opening of the channels. Sphingolipids and sterols were recently found enriched in the plasmodesmata membrane in *A. thaliana*

(Grison *et al.*, 2015; Liu *et al.*, 2020). Furthermore, changes in sphingolipid metabolism affect plasmodesmata ultrastructure and consequently influence plasmodesmal cell-to-cell transport (Yan *et al.*, 2019; Liu *et al.*, 2020). In addition to determining the cross-wall orientation, the callose stain can therefore be applied to investigate plasmodesmata defects in sphingolipid mutants. Callose deposition in *s4h* protonema cells indicated altered cross-walls in the mutant. This phenotype is demonstrated and discussed in chapter 2 (Fig. 8).

Protonema cell differentiation ability is determined in a dark growth assay

Although the cross-wall can be specifically stained with aniline blue, the protonema cell type identity could not always be determined with absolute certainty. The transition from chloronema to caulonema cells happens gradually and is represented in a transition zone. The onset of differentiation can therefore not be determined accurately. Cross-wall staining could hence not be used to determine the protonema cell differentiation ability in the sphingolipid mutants as initially expected.

For a more detailed analysis of the cell differentiation ability of different plant lines, a dark growth assay was performed that promotes selective cultivation of caulonema cells. The assay was described in (Saavedra *et al.*, 2015). Caulonemata that are grown in the dark are referred to as skotonema cells. To start the assay, spot inocula were placed on BCDAT medium that was supplemented with 2 % sucrose as external carbon source. Colonies were grown for the first week under continuous light to generate enough tissue for skotonema induction. After one week, the light was switched off and cultivation plates were rotated to a vertical position. Colonies were incubated for another three to four weeks. After the cultivation period, the wild type generated long, brown filaments that reached upwards. As skotonema cells grow straight upwards, cell length measurements could easily be performed on individual cells. This assay is therefore a suitable approach to observe protonema cell differentiation and elongation and revealed developmental defects in the different sphingolipid mutants that are described in chapter 2 (Fig. 7b) and chapter 3 (Fig. 6, 7).

Determination of phytohormone levels in *P. patens* sphingolipid mutants

Another idea to examine the cell differentiation ability of sphingolipid mutants was to determine their phytohormone levels. External and internal phytohormones influence a wide variety of physiological processes in *P. patens* (Decker *et al.*, 2006). Phytohormones like auxin, cytokinin, and abscisic acid have different effects on early moss development. Auxin is a thoroughly studied and versatile phytohormone in *P. patens*. A major role of auxin in *P. patens* physiology is the regulation of protonema cell differentiation, where it is responsible for the transition from chloronema to caulonema cells and in maintenance of caulonema cell identity (Ashton *et al.*, 1979). Endogenous auxin levels were therefore of

particular interest during the characterisation of the different sphingolipid mutants. Especially the *gcs-1* mutant, which was unable to generate skotonema cells, was expected to have altered auxin levels compared to the wild type. The tightly controlled and standardised cultivation conditions were considered appropriate to detect differences in auxin levels and hence to explain the inability of *gcs-1* plants to generate skotonema cells. Phytohormones were extracted from protonema that was cultivated for ten days on cellophane-covered BCD plates. As already explained, BCD medium lacks ammonium tartrate and should therefore promote the transition from chloronema to caulonema cells. Unfortunately, measurements of the bioactive auxin compound indole-3-acetic acid (IAA) in the protonema of different sphingolipid mutants did not lead to conclusive results. IAA levels were very low in all analysed plant lines (0.1-0.2 nmol/ g d.w.) (Fig. 8). Furthermore, drastic variations between different replicates were observed, which resulted in substantial error. These variations in IAA levels inhibited proper interpretation of the data. Previous studies on *P. patens* auxin metabolism measured the auxin levels in the protonema tissue and in the medium (Viaene *et al.*, 2014). It appears that IAA is released by *P. patens* to the surrounding medium (Reutter *et al.*, 1998; Viaene *et al.*, 2014). Therefore, a future approach might be to target the determination of IAA levels in liquid culture grown protonema and to determine IAA levels in the moss tissue as well as in the medium. It would further be interesting to determine the levels of conjugated IAA, which was previously found in larger amounts in *P. patens* than free IAA (Ludwig-Müller *et al.*, 2009). It might also be that differences in IAA cannot be determined by measuring total free IAA content. Auxin gradients are assumed to be the driving force for differentiation and polar growth processes. It is therefore possible that the distribution of auxin within the cell may not be established properly in sphingolipid mutants. A failed establishment of an auxin gradient can, however, not be determined by extraction and analysis of total auxin. Another way to determine changes in auxin metabolism could be to target the gene expression of different auxin metabolic genes in *P. patens* sphingolipid mutants by qRT PCR analysis. Various genes involved in auxin metabolism have already been identified and studied in *P. patens* (Thelander *et al.*, 2018). The subcellular localisation of the auxin efflux carriers (PIN proteins) may also be determined to assess whether sphingolipid mutants have problems in directional auxin transport. The PIN-dependent intercellular transport was shown to be important for developmental processes in tip-growing filaments in *P. patens* (Viaene *et al.*, 2014).

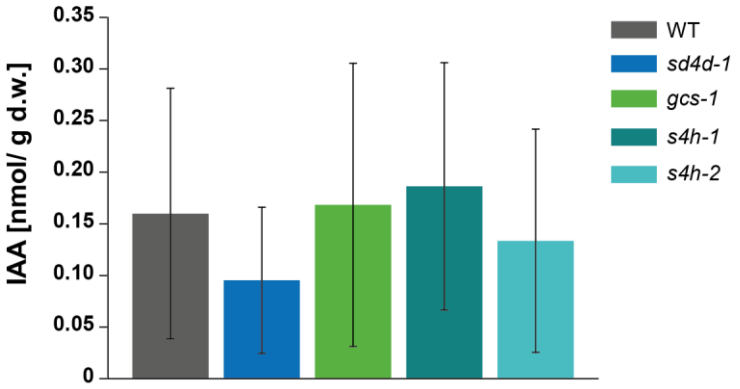

Fig. 8. Free IAA levels in *P. patens* wild type, *sd4d-1*, *gcs-1*, *s4h-1*, *and s4h-2* plants. Free indole-3-acid (IAA) was extracted from ten-day-old protonema grown on cellophane-covered BCD medium and analysed using UPLC-nanoESI-MS/MS. Data represent the mean ± SD of measurements from four independent cultivations each containing protonema material from eight cultivation plates.

Other phytohormone levels were determined in addition to auxin, including abscisic acid and salicylic acid levels. As observed for IAA levels, most of the determined phytohormone levels did not give any conclusive results. However, levels of the jasmonate precursors 12-oxo-phytodienoic acid (OPDA) and *dinor*-OPDA (*dn*-OPDA) were significantly increased in the *gcs-1* mutant. The results are presented and discussed in chapter 3.

Phytohormone measurements demonstrated that the standardised cultivation method using solidified medium plates can only partially be used for the analysis of phytohormone levels in *P. patens*. Future studies should focus on optimising phytohormone measurements and on detection of hormone derivatives that were previously described in *P. patens* (von Schwartzenberg *et al.*, 2007; Ludwig-Müller *et al.*, 2009).

Subcellular localisation of *Pp*S4H and *Pp*SD4D in *P. patens* protonema cells

Another approach investigated the subcellular localisation of the sphingolipid enzymes within the *P. patens* protonema. The simple anatomy of *P. patens* allows for transient expression assays. Therefore, the protonema was transiently transformed through particle bombardment using DNA-coated gold particles. Subcellular localisation studies on sphingolipid metabolic enzymes in *A. thaliana* showed localisation in the membrane of the endoplasmic reticulum (ER) (Chen *et al.*, 2008; Melser *et al.*, 2010). However, while most *A. thaliana* sphingolipid enzymes are located in the ER (Luttgeharm *et al.*, 2016), individual enzymes may also reside in the membrane of the Golgi apparatus. For instance, GIPC synthetic enzymes that transfer GIPC head group units to the ceramide backbone are found exclusively in the Golgi membrane (Wang *et al.*, 2008; Rennie *et al.*, 2014). This shows that sphingolipid metabolic enzymes may either be located in the ER or in the Golgi apparatus.

In general, plant sphingolipid enzymes are highly conserved. The corresponding *A. thaliana* enzymes of the investigated *P. patens* sphingolipid enzymes are described in the ER (Chen *et al.*, 2008; Melser *et al.*, 2010). Moreover, all of the investigated enzymes

in *P. patens* had predicted transmembrane domains (chapters 2 and 3). Therefore, it was expected that these would also localise to the ER.

A YFP fluorescent tag was attached to the C-terminus of *Pp*S4H and *Pp*SD4D. The gene constructs were cloned into a pEntry vector backbone (pUC18 derived, approximately 4.5 kb) provided by Dr. Ellen Hornung. *PpS4H* and *PpSD4D* expression was driven by a 35S promoter. The gene constructs were co-transformed with a CFP-tagged ER marker in a pCAT vector backbone (approximately 6.2 kb) provided by Dr. Martin Fulda. The protonema was grown for one to two weeks on cellophane covered BCD medium before the bombardment. The transformed protonema was incubated for twelve hours under standard conditions before visualisation using a confocal laser scanning microscope. Several cells showed clear YFP signals that indicated successful transformation of the *PpS4H-YFP* and the *PpSD4D-YFP* constructs (Fig. 9).

The *Pp*S4H-YFP signal was found distributed throughout the cell in globular structures (Fig. 9D). The signal was also detected at the cell border. The observed structures might have been ER aggregates. Unfortunately, the used ER marker did not label the ER (Fig. 9B). Since the ER marker did not show ER localisation, it cannot be concluded with absolute certainty that *Pp*S4H really locates to the ER.

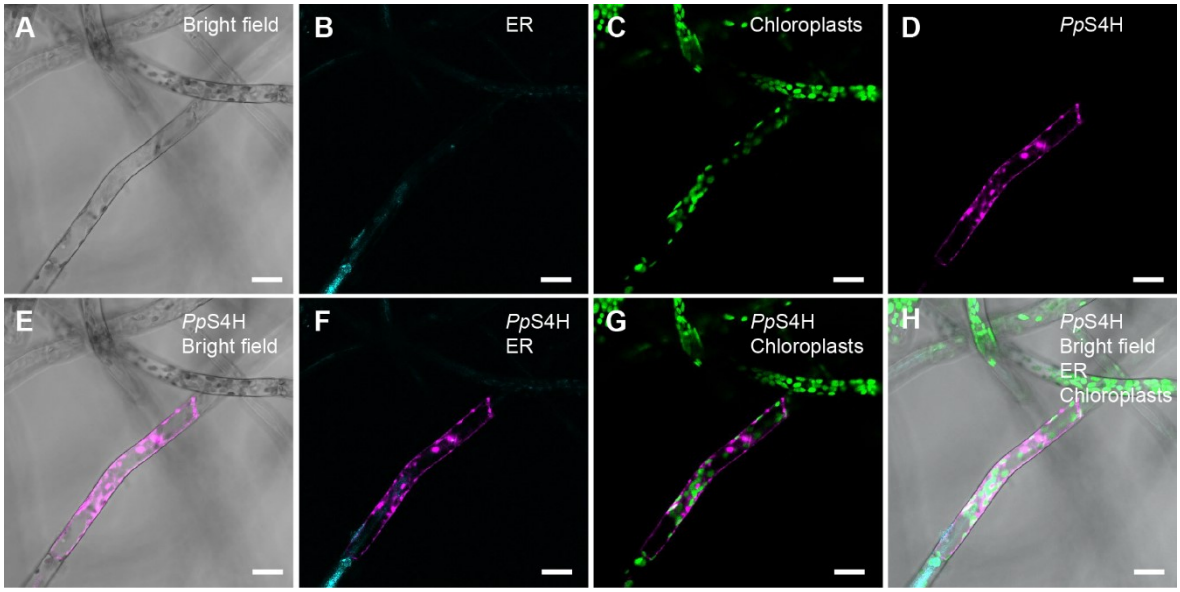

Fig. 9. Subcellular localisation of *Pp*S4H and ER marker in a transiently transformed *P. patens* protonema cell. Transient transformation of *P. patens* was achieved through particle bombardment of one- to two-week-old protonema tissue. A transformed protonema cell is shown as (A) bright field, and (B-D) fluorescence images. (B) shows localisation of the endoplasmic reticulum (ER) that was tagged with CFP (cyan). (C) shows chloroplast autofluorescence (green). (D) shows the *Pp*S4H localisation that was tagged with YFP (magenta). (E) shows the merged image of the bright field image and the *Pp*S4H signal (magenta). (F) shows the merged image of *Pp*S4H signal (magenta) and the ER signal (cyan). (G) shows the merged image of the *Pp*S4H signal (magenta) and the chloroplast autofluorescence (green). (H) shows the merged image of the *Pp*S4H signal (magenta), the ER signal (cyan), the chloroplast autofluorescence (green), and the bright field image. The scale bars represent 20 µm. The experiment was done once. The bombardment resulted in fluorescent signal detection in several protonema cells. Pictures are representative images for at least three transformed cells.

The *Pp*SD4D-YFP signal showed a more network-like pattern throughout the protonema cell (Fig. 10D). Within the network were also small globular structures that might have represented ER aggregates. The signal was also observed at the border of the cell and around a spherical structure within the cell, which most likely represented the nucleus. The fluorescent signal within the cell was only detected in one half which might be due to the fact that only one part of the filamentous cell was in the focus plane. As with the *PpS4H-YFP* construct, the CFP-tagged ER marker did, unfortunately, not visualise the ER (Fig. 10B). However, the spherical structure in the centre of the cell might represent the nuclear envelope, which is a hallmark of ER localisation.

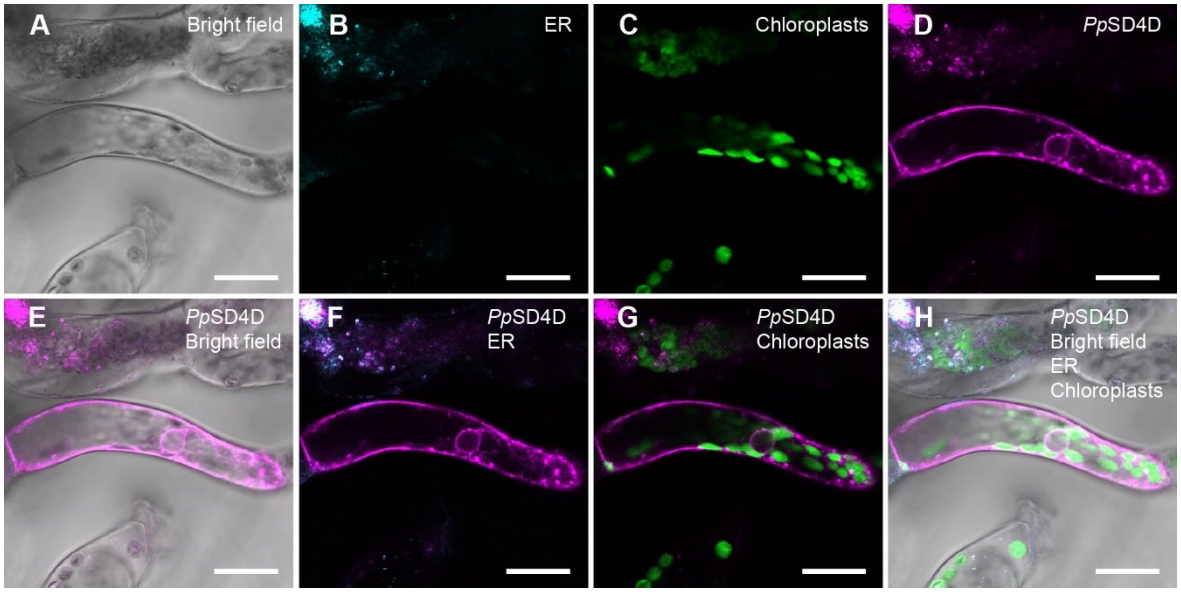

Fig. 10. Subcellular localisation of *Pp*SD4D and ER marker in a transiently transformed *P. patens* protonema cell. Transient transformation of *P. patens* was achieved through particle bombardment of one- to two-week-old protonema tissue. A transformed protonema cell is shown as (A) bright field, and (B-D) fluorescence images. (B) shows localisation of the endoplasmic reticulum (ER) that was tagged with CFP (cyan). (C) shows chloroplast autofluorescence (green). (D) shows the *Pp*SD4D localisation that was tagged with YFP (magenta). (E) shows the merged image of the bright field image and the *Pp*SD4D signal (magenta). (F) shows the merged image of *Pp*SD4D signal (magenta) and the ER signal (cyan). (G) shows the merged image of the *Pp*SD4D signal (magenta) and the chloroplast autofluorescence (green). (H) shows the merged image of the *Pp*SD4D signal (magenta), the ER signal (cyan), the chloroplast autofluorescence (green), and the bright field image. The scale bars represent 20 µm. The experiment was done once. The bombardment resulted in fluorescent signal detection in several protonema cells. Pictures are representative images for at least three transformed cells.

Both of the sphingolipid enzymes were expected to locate to the ER. The *Pp*S4H-YFP and *Pp*SD4D-YFP fluorescent signals showed similar distribution patterns within the cell. The observed spherical structures likely represented ER aggregates. ER aggregation may occur when overexpression of genes affects cell viability and results in subcellular rearrangements. *PpS4H* and *PpSD4D* overexpression might have interfered with the structural organisation of the cellular elements, causing reshaping of the ER. However, ER morphology may also change over the course of cell growth and development. It might

therefore also be that cells bombarded with *PpS4H* and *Pp*SD4D constructs were in certain developmental stages. Finally, also the particle bombardment itself may cause a shift in subcellular arrangement.

Of the investigated sphingolipid enzymes only *Pp*S4H and *Pp*SD4D were examined for their subcellular localisation. Subcellular localisation of *Pp*GCS was not determined because the gene could not be amplified from *P. patens* cDNA.

To confirm the subcellular localisations of *Pp*S4H and *Pp*SD4D to the ER, a co-localisation to the organelle would need to be observed. Since the used plasmid harbouring the ER marker did not work in the applied assay, another plasmid carrying an ER marker sequence should be designed that properly labels the ER. Ideally, the pEntry vector system should be used as it proved functional in *P. patens* for the gene constructs. For future studies, it would even be reasonable to generate a plasmid library consisting of pEntry vectors that harbour marker sequences for different organelles. That way, the subcellular localisation of future proteins of interest can be identified that are expected to localise to different cellular organelles. Another possibility would be to generate stable *P. patens* marker lines that constitutively express fluorescent proteins targeted to various cellular organelles.

Conclusion and outlook

In summary, the establishment and optimisation of an appropriate toolkit for using *P. patens* as model system in the department proved to be essential in the beginning of the study for the subsequent sphingolipid mutant characterisations. A thorough understanding of *P. patens* growth and development mechanisms was beneficial to target selective cultivation of different tissues. Growth on solidified medium greatly facilitated the maintenance of *P. patens* sphingolipid mutant lines that showed different growth behaviours and therefore had varying cultivation requirements. The highly standardised cultivation procedure enabled comprehensive and quantitative mutant phenotype investigations of *s4h* (chapter 2), *sd4d-1*, and *gcs-1* (chapter 3) mutants and laid the groundwork for future *P. patens* mutant characterisation studies. Furthermore, the identified *P. patens* sphingolipid profile from Resemann (2018) was extended by performing separate lipid extractions and analyses on protonema and gametophore tissue.

Although the newly established cultivation system enabled thorough examination of sphingolipid mutants, future work needs to target optimisation of cultivation conditions for certain applications, such as phytohormone measurements. Future studies concerning *P. patens* sphingolipid metabolism may also reveal even more detailed analytics of distinct tissue types, such as the sporophyte, rhizoids, or skotonema cells. Advanced microscopic studies of membrane dynamics may be key in determining the role of sphingolipids in

membrane organisation. *P. patens* represents a model plant that may be easily accessible for *in planta* membrane studies.

Acknowledgements

We are grateful to Lina Helwig who assisted in the subcellular localisation studies and to Nina Zaremba who assisted in optimising the callose staining. J.G. has been a doctoral student of the Ph.D. program "Microbiology and Biochemistry" from the Göttingen Graduate Center for Neurosciences, Biophysics, and Molecular Biosciences (GGNB) at the Georg August University Göttingen. I.F. acknowledges funding through the German Research Foundation (DFG, INST 186/822-1 and INST 186/1167-1).

Author contribution

J.G. designed and performed the experiments. A.Z. performed CLSM examinations. K.Z. performed phytohormone measurements. J.G. performed and analysed the lipid measurements with the assistance of C.H.. J.G. wrote the chapter. T.M.H. and I.F. edited the chapter and I.F. supervised the study.

4 Chapter 2

Sphingolipid long-chain base hydroxylation influences plant growth and cross-wall formation in *Physcomitrella patens*

The article is ready for submission. The supplemental material can be found at the end of the main part.

Author contribution:

Jasmin Gömann generated *s4h* knockout mutants by homologous recombination. She confirmed the mutant identity by investigating the *s4h* genotype and chemotype. She complemented the *Saccharomyces cerevisiae* LCB C-4 hydroxylase mutant with *Pp*S4H. She maintained and cultivated the *P. patens* and *S. cerevisiae* wild type and transgenic line material for subsequent lipid analyses. She planned and performed the lipid extractions and measurements using UPLC-nanoESI-MS/MS. She analysed and processed the lipid data. She further maintained and cultivated the *P. patens* wild type and mutant material for subsequent macro- and microscopic phenotype investigation. She designed and performed the experiments for the phenotypic characterisation of the *P. patens s4h* mutant using different cultivation strategies to selectively analyse various developmental stages. Finally, she displayed, interpreted and discussed the results and wrote the first draft of the manuscript.

The work of this chapter was first published in *New Phytologist* on the 1st of June 2021. The published paper ist a shortened version of this chapter. It furthermore contains additional data concerning subcellular localisation and quantified lipid data.

Gömann, J., Herrfurth, C., Zienkiewicz, A., Ischebeck, T., Haslam, T.M., Hornung, E. and Feussner, I. (2021), Sphingolipid long-chain base hydroxylation influences plant growth and callose deposition in *Physcomitrium patens*. *New Phytologist*, 231: 297-314. https://doi.org/10.1111/nph.17345

Sphingolipid long-chain base hydroxylation influences plant growth and cross-wall formation in *Physcomitrella patens*

Jasmin Gömann[1], Cornelia Herrfurth[1,2], Agnieszka Zienkiewicz[1], Ellen Hornung[1], Tegan M. Haslam[1], Ivo Feussner[1,2,3*]

[1]University of Goettingen, Albrecht-von-Haller-Institute for Plant Sciences, Department of Plant Biochemistry, D-37077, Goettingen, Germany.
[2]University of Goettingen, Goettingen Center for Molecular Biosciences (GZMB), Service Unit for Metabolomics and Lipidomics, D-37077 Goettingen, Germany.
[3]University of Goettingen, Goettingen Center for Molecular Biosciences (GZMB), Department of Plant Biochemistry, D-37077 Goettingen, Germany.

E-mail address for each author:
jasmin.goemann@stud.uni-goettingen.de
cornelia.herrfurth@biologie.uni-goettingen.de
agnieszka.zienkiewicz@biologie.uni-goettingen.de
ehornun@biologie.uni-goettingen.de
tegan.haslam@biologie.uni-goettingen.de

*Correspondence: Ivo Feussner, e-mail: ifeussn@uni-goettingen.de,
Tel: +49-551-3925743, ORCID iD: 0000-0002-9888-700

Summary

- Sphingolipids and sterols are enriched in microdomains in the plant plasma membrane. Lipid microdomains are assumed to be important sorting platforms for proteins involved in cellular processes such as signalling, responses to biotic and abiotic stresses and cell wall synthesis and degradation. Free hydroxyl groups in the characteristic long-chain base (LCB) moiety of sphingolipids are believed to be essential for the interaction network between sphingolipids and sterols. The hydroxylation status of the LCB moiety of sphingolipids therefore influences the biophysical properties of the plant plasma membrane and thus affects membrane-associated cellular signalling cascades.
- *Physcomitrella patens* null mutants for the LCB C-4 hydroxylase *S4H* were generated by homologous recombination. The mutants were characterised chemically by identification of their sphingolipid and glycosylated sterol (SG) profiles, and phenotypically by macro- and microscopic investigation of different developmental stages (protonema, gametophore).
- *s4h* mutants lost the hydroxyl group at the C-4 position of their LCB moiety in sphingolipids. Loss of the t18:0 LCB moiety caused global changes in all sphingolipid classes. The predominant t18:0 LCB moiety was replaced by the d18:0 LCB moiety in LCBs, phosphorylated LCBs (LCB-Ps), ceramides, and glycosyl inositolphosphorylceramides (GIPCs). These changes in the *P. patens* sphingolipidome were correlated with alterations in the SG composition. As physiological consequence, *s4h* mutants were substantially impaired in growth and development. Growth defects may possibly be triggered by an impaired cell division as indicated by the misplacement of the cell-plate marker callose resulting in malformed cross-walls in protonema cells.
- Loss of LCB-C4 hydroxylation substantially changes the *P. patens* sphingolipidome and reveals a key role for S4H during cell division and general growth in non-vascular plants. *P. patens* represents a valuable model organism for studying the diversification of the plant sphingolipid metabolism. Compared to *Arabidopsis thaliana* the simple structural design of *P. patens* greatly facilitates visualisation of physiological processes in biological membranes.

Key words: callose, long-chain base (LCB) hydroxylation, LCB C-4 hydroxylase, microdomain, non-vascular plants, plasma membrane, plant development, *Physcomitrella* patens, sphingolipid metabolism

Introduction

Sphingolipids are involved in essential cellular and subcellular processes in eukaryotes, some prokaryotes and viruses (Smith & Merrill, 2002; Lynch & Dunn, 2004; Sperling *et al.*, 2005). As abundant lipid molecules their predominant role is to maintain the structural integrity of the plasma membrane and of endomembrane systems. Their amphipathic nature arises from their unique hydrophobic sphingoid backbone that is connected to hydrophilic head groups (Lynch & Dunn, 2004). The backbone contains an *N*-acylated amino alcohol, also known as long-chain base (LCB). LCBs are characteristic for sphingolipids and therefore define them as a distinct lipid class. Sphingolipids account of around 40 mol % of plasma membrane lipids in plants (Sperling *et al.*, 2005; Cacas *et al.*, 2016) and are believed to play a key role in membrane organisation by participating in micro- and nanodomain formation. In addition to their structural role, some sphingolipids act as signalling molecules during processes including programmed cell death (PCD) (Liang *et al.*, 2003; Shi *et al.*, 2007; Zienkiewicz *et al.*, 2020) and responses to biotic and abiotic stresses (Huby *et al.*, 2020). They further play a role as necrosis and ethylene-inducing peptide 1-like toxin receptors during plant pathogen interactions (Lenarčič *et al.*, 2017).

The plant sphingolipidome can be broken down into four classes which are sorted in the following according to their relative abundance in *Arabidopsis thaliana* leaf extract: LCBs (0.5 %), ceramides (2 %), glycosylceramides (GlcCer) (34 %), and glycosyl inositolphosphorylceramides (GIPC) (64 %) (Markham *et al.*, 2006; Markham & Jaworski, 2007). Sphingolipid biosynthesis takes place in the endoplasmic reticulum (ER) and starts with the condensation of palmitoyl-CoA and serine forming 3-ketosphinganine. This is reduced to the LCB sphinganine, which is also referred to as dihydroxy LCB, or in short d18:0. Plant LCBs typically have a hydrocarbon chain length of 18 carbon atoms. The LCBs are the core structure of ceramides and complex sphingolipids and can be *N*-acylated through the action of ceramide synthases. *N*-acylation of LCBs to long-chain fatty acids (LCFAs) or very long-chain fatty acids (VLCFAs) results in the formation of ceramides. In plants, the pool of acyl chain lengths of sphingolipids typically ranges from 16 to 26 carbons. Complex sphingolipids (GlcCers and GIPCs) are generated through the attachment of a polar head group to the C-1 position of the LCB moiety. Sphingolipids are a diverse lipid class in part due to different structural modifications on either their LCB or fatty acid moiety. These include phosphorylation, hydroxylation and desaturation and are usually introduced at the level of LCBs, acyl-CoAs or ceramides. Even small modifications have a great impact on the biophysical properties of sphingolipids. Structural changes in the sphingoid backbone therefore determine the metabolic and physiological fate of individual sphingolipid species.

Most of our knowledge of plant sphingolipid metabolism has been gained from studying the vascular model plant *A. thaliana*. Many different enzymes within the

sphingolipid pathway have been thoroughly investigated, and a multitude of mutants with severe, pleiotropic phenotypes haven been identified (Luttgeharm *et al.*, 2016). However, the tissue and organ complexity of vascular plants has made it difficult to assign specific sphingolipid molecules distinct functions. Furthermore, many *A. thaliana* sphingolipid mutants are embryo lethal or severely dwarfed making it challenging or even impossible to perform phenotypic characterisation on true knockout plants (Msanne *et al.*, 2015; Tartaglio *et al.*, 2017; Gonzalez-Solis *et al.*, 2020). Thus, there are clear limitations to the utility of *A. thaliana* as model organism to study sphingolipid functions.

The moss *Physcomitrella patens* belongs to the group of bryophytes and can be used as amodel organism with a remarkably simple morphology. Its dominant haploid life cycle starts with a single spore that develops into a two-dimensional filamentous network, the protonema. From this juvenile stage buddings arise that induce three-dimensional growth. The buddings grow out into the gametophore, a shoot-like structure with leaflets or phyllids that consist of only a single cell layer (Prigge & Bezanilla, 2010). In contrast to the more complex organs of vascular plants, the simplicity of these different moss tissue types greatly facilitates visualisation of inter- and intracellular processes. Additionally, *P. patens* can be propagated vegetatively, meaning that mutants which do not reach reproductive maturity can still be investigated. Bryophytes and vascular plants began to diverge early in land plant evolution, around 450 million years ago (Rensing *et al.*, 2008). Therefore, studying a bryophyte model, in addition to the work carried out in classical, vascular plant models, is going to provide insight into conserved features of land plants.

A recent study conducted a global lipid profile analysis in *P. patens* (Resemann, 2018). Besides glycerolipids and sterol lipids, the identified lipids include the four plant sphingolipid classes: LCBs, ceramides, GlcCers and GIPCs. The analysis revealed that most essential and characteristic parts of plant sphingolipid metabolism are conserved from non-vascular to vascular land plants. An overview of the *P. patens* sphingolipid metabolism with focus on trihydroxy sphingolipids is depicted in Fig. 1. The figure combines the findings on *P. patens* sphingolipid metabolism from the lipidomics approaches from (Resemann, 2018) and (Cacas *et al.*, 2013) with current knowledge on plant sphingolipid metabolism in general (Luttgeharm *et al.*, 2016). While GlcCers contain with over 90 % the dihydroxy LCB moiety with two double bonds, d18:2, GIPCs contain mainly the saturated trihydroxy LCB moiety t18:0 (Resemann, 2018). This observation of distinct LCB moieties in different sphingolipid pools may facilitate studying specific enzymatic reactions in sphingolipid metabolism. Furthermore, the *P. patens* sphingolipidome may be considered less complex than the *A. thaliana* sphingolipidome regarding the combination variety of different LCB and fatty acid moieties.

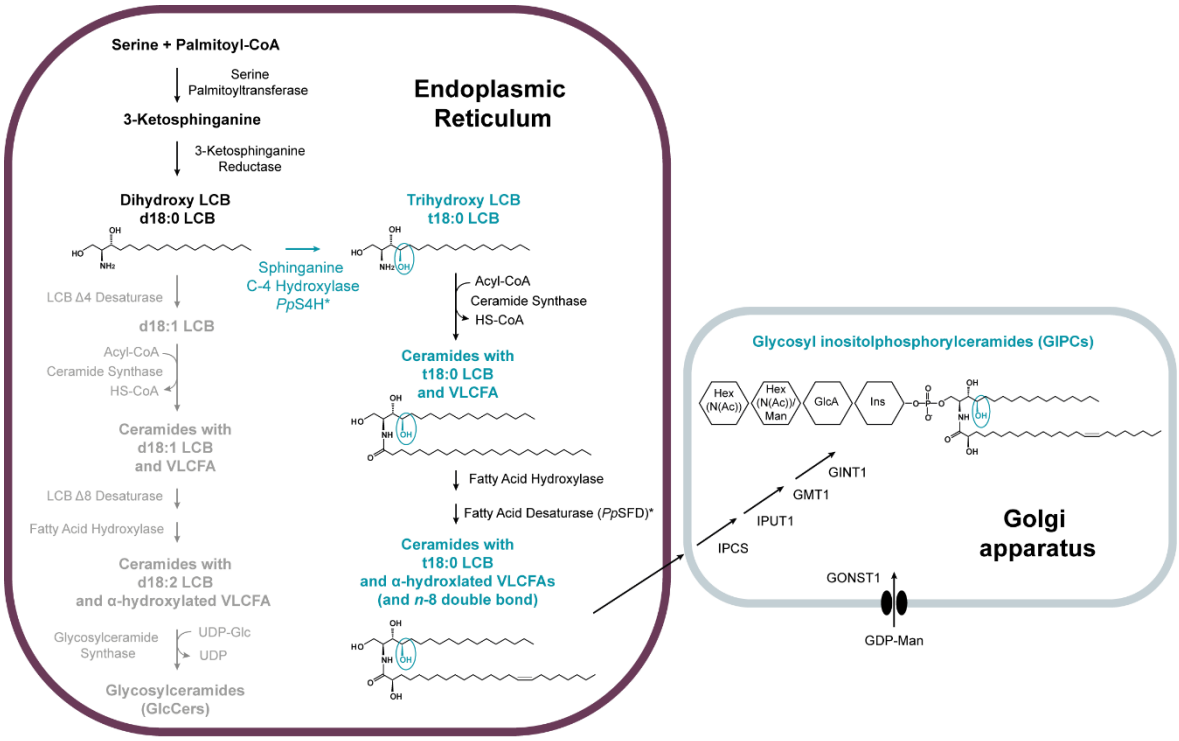

Fig. 1. Trihydroxy sphingolipids are mainly channelled into GIPC formation in *P. patens*. The depicted sphingolipid metabolism shows the two pathways for glycosylceramide (GlcCer) and glycosyl inositolphosphorylceramide (GIPC) synthesis in *P. patens*. Dihydroxy long-chain bases (LCBs) are channelled into GlcCer formation (grey) and trihydroxy LCBs are channelled into GIPC formation (blue). Asterisks indicate functionally characterised enzymes in *P. patens*. Abbreviations are as follows: HS-CoA: Coenzyme A; GDP-Man: Guanosine Diphosphate Mannose; GINT1: Glucosamine Inositolphosphorylceramide Synthase 1; GlcA: Glucuronic Acid; GMT1: GIPC Mannosyl Transferase 1; GONST1: GDP-Mannose Transporter 1; Hex: hexose; HexNAc: *N*-acetylhexosamine; IPCS: Inositolphosphorylceramide Synthase; Ins: Inositol; IPUT1: Inositolphosphorylceramide Glucuronosyl Transferase 1; Man: Mannose; SFD: Sphingolipid Fatty acid Desaturase; VLCFA: Very Long-Chain Fatty Acid; UDP-Glc: Uridine Diphosphate Glucose.

Resemann (2018) also characterised the first sphingolipid enzyme from *P. patens*: SPHINGOLIPID FATTY ACID DESATURASE (*Pp*SFD). *Pp*SFD and its *A. thaliana* counterpart ADS2 introduce double bonds at different positions of the fatty acid backbone and are therefore believed to have independent evolutionary backgrounds (Fukuchi-Mizutani *et al.*, 1995; Heilmann *et al.*, 2004; Resemann, 2018). However, both mutants exhibit a cold-sensitive phenotype and *ads2.1* plants complemented with *Pp*SFD re-established resistance to cold stress (Resemann, 2018). This confirms that both enzymes confer the same physiological function despite their independent evolutionary origin.

One essential modification of plant sphingolipids is the hydroxylation of the LCB and fatty acid moieties. Following initial formation, the LCB moiety contains two hydroxyl groups and is referred to as d18:0 LCB or sphinganine. The C-1 and C-3 hydroxyl groups result from the precursor molecules serine and palmitoyl-CoA, respectively (Dunn *et al.*, 2004; Lynch & Dunn, 2004). A hallmark of plant and yeast sphingolipids is a third hydroxyl group added to C-4 of the LCB moiety by an LCB hydroxylase (Haak *et al.*, 1997; Sperling *et al.*, 2001; Markham *et al.*, 2006; Chen *et al.*, 2008). This LCB moiety is referred to as t18:0 LCB or phytosphingosine. Around 90 % of all LCB moieties found in total leaf extract from

A. thaliana contain trihydroxy LCBs (Markham *et al.*, 2006; Tarazona *et al.*, 2015). Trihydroxy LCBs are mainly acylated to VLCFA and are mostly found in the GIPC pool (Buré *et al.*, 2011).

GIPCs are the most abundant plant sphingolipids and account for ~64 % of total sphingolipids in *A. thaliana* leaves (Markham *et al.*, 2006). Furthermore, they make up 30 to 40 mol % of the plasma membrane lipids of *Nicotiana tabacum* and represent 60 % to 80 % of the total outer leaflet lipids (Cacas *et al.*, 2016). The presence of additional hydroxyl groups in the sphingoid backbone allows sphingolipids to form more hydrogen bonds with other membrane components, such as sterols and saturated phospholipids, which affects the biophysical properties of the membrane in a dynamic manner (Quinn & Wolf, 2009; Klose *et al.*, 2010; Mamode Cassim *et al.*, 2019). Membrane fractions enriched in sterols and sphingolipids form stable gel phases with increased melting temperatures, so called liquid-ordered domains or lipid rafts (Simons & Ikonen, 1997; Pike, 2009). These domains have a role as protein sorting platforms in the plasma membrane (Simons & Ikonen, 1997; de Almeida *et al.*, 2003; Huang *et al.*, 2019). *A. thaliana* mutants with altered sphingolipid homeostasis that affect GIPC structure exhibit severe growth and developmental phenotypes, which could be caused by defects in cytokinesis, involving altered cell plates and impaired plasmodesmal cell-to-cell transport (Chen *et al.*, 2008; Molino *et al.*, 2014; Liu *et al.*, 2020; Yan & Liu, 2020). GIPCs are therefore believed to have an important role in orchestrating membrane dynamics during plant developmental processes.

Even though the presence of three hydroxyl groups in the LCB moiety is considered a characteristic and crucial feature for plants, sphingolipid C-4 hydroxylases have only been characterised in *A. thaliana* (Sperling *et al.*, 2001; Chen *et al.*, 2008). *A. thaliana* SPHINGOID BASE HYDROXYLASE1 (*At*SBH1) and *At*SBH2 are functionally redundant LCB C-4 hydroxylases. Only knockout of both genes led to a complete loss of trihydroxy LCBs. This resulted in disruption of the overall sphingolipid composition of *sbh1 sbh2* double mutants. The mutants were severely dwarfed, were impaired in cell expansion and division, and failed to transition from vegetative to reproductive development. The authors concluded that LCB C-4 hydroxylation is crucial for *A. thaliana* growth and viability.

The following study shows the significance of the t18:0 LCB moiety in sphingolipids of the bryophyte model *P. patens*. By generating a loss-of-function mutant of the single gene *Sphinganine C-4 Hydroxylase* (*S4H*) via homologous recombination, a complete loss of t18:0 LCB containing sphingolipids was achieved. This resulted in global changes across all sphingolipid classes. Expression of S4H in the *Saccharomyces cerevisiae* LCB C-4 hydroxylase knockout mutant *sur2Δ* restored the formation of t18:0 LCB containing sphingolipids in yeast. Similar to the *A. thaliana sbh1 sbh2* mutant, the *P. patens s4h* mutants showed severely stunted growth in all developmental stages. The growth

phenotype might be attributed to impaired cytokinesis as indicated by altered deposition of the cell plate marker callose. The study highlights the advantages of *P. patens* as model plant to investigate the role of sphingolipids in membrane dynamics.

Materials and methods

Plant material and growth conditions

In this study the 'Gransden' wild type strain of *P. patens* (Hedw.) Bruch & Schimp was used. Plant material was grown per default at 25 °C in long-day conditions (16 h light/ 8 h dark) with a photon flux of 50–70 µmol m^{-2} s^{-1}. Protonema material was weekly cultivated on BCD agar medium plates (90 mm diameter) containing 1 mM $CaCl_2$ and 5 mM ammoniumtartrate (BCDAT) (Ashton & Cove, 1977) covered with sterile cellophane discs (folia, Wendelstein, Germany). Regular maintenance was achieved by collecting one-to two-week-old protonema tissue and disrupting it for 20 s using a tissue lyser (Ultra Turrax, Ika, Staufen, Germany). The cell suspension was spread onto fresh medium plates.

For lipidomics analysis of protonema and determination of fresh weight, BCD plates covered with sterile cellophane were inoculated with a volume of tissue suspension corresponding to 5 mg dry weight. The protonema material was harvested after ten days, weighed for fresh weight biomass determination and frozen in liquid nitrogen. Collected tissue was lyophilised and weighed again for determination of dry weight. To obtain enough material for analyses, tissue from eight plates were pooled during each cultivation round.

For imaging of protonemal development, approximately 1 mm spot inocula of one-to two-week-old protonema were placed on plates containing BCD medium with 1 mM $CaCl_2$. Plates were sealed with micropore tape and imaged after the indicated time points. For induction of gametophores, spot inocula were incubated on BCD medium plates for five to six weeks.

For targeted cultivation of skotonema filaments, spot inocula were placed on square petri dishes containing BCDAT medium with 2 % (w/v) sucrose and were grown horizontally for one week under continuous light. Plates were subsequently shifted into vertical position and grown in darkness for another three to four weeks.

Images were taken with a binocular (Olympus SZX12 binocular, Olympus Corporation, Tokio, Japan) linked to a digital camera (R6 Retiga camera, QImaging, Surrey, Canada). Pictures were acquired with the Ocular scientific image acquisition software (version 1.0, Digital Optics Ltd, Auckland, New Zealand). Images were processed using ImageJ 1.52b software (Schneider *et al.*, 2012).

Generation of targeted knockout plasmids

To construct the vector for targeted knockout of the *S4H* gene, 750 bp genomic DNA fragments of the 5' region and the 3' region of *S4H* were amplified using the primer pairs 5' *Apa*I S4H-fw (5'-atgggcccATGGGCCCATGGTGTTCTGGGAGGATTATGTC-3')/ 5' *Sal*I S4H-rev (5'-atgtcgacACCATGTTTAACCTAGAGCCCGC-3') and 3' *BamH*I S4H-fw (5'-atggatccGTGGCGGCTTATCGCCTAATTAC-3')/ 3' *Xba*I S4H-rev (5'-attctagaCACTCGATCTTCTTCACAGGCATG-3'), respectively. The fragments were cloned into a pBluescript vector flanking a kanamycin cassette under the control of a 35S promotor. Correct cloning of the fragments into the destination vector was confirmed via sequencing. Prior to transformation into the *P. patens* wild type strain, the fragment used for homologous recombination, containing the 5' and the 3' flanking regions, was linearised using the restriction enzymes ApaI and XbaI.

***P. patens* transformation and molecular characterisation of knockout mutants**

Transgenic plants were generated via polyethylene glycol (PEG)-mediated transformation of protoplasts according to (Schaefer *et al.*, 1991).

The linearised fragment containing the 5' and 3' *S4H* flanking regions and the kanamycin selection cassette was used for PEG-mediated transformation.

The used protonema material was cultivated in non-aerated, shaking liquid cultures in sterile Erlenmeyer flasks under long-day conditions (16 h light, 8 h dark) at 25 °C and a photon flux of 50–70 µmol m^{-2} s^{-1}. The protonema was routinely sub-cultivated in liquid Knop medium (Reski & Abel, 1985) until transformation. One week prior to the transformation, the plant material was transferred to liquid Knop medium containing 1/10 of the original $Ca(NO_3)_2$ amount. Protonema was harvested using a 100 µm mesh size nylon sieve and immersed in 1.3 % (w/v) sterile driselase in 0.5 % (w/v) mannitol solution for protoplast isolation. After overnight incubation, the protoplast suspension was applied consecutively to a 100 µm and a 50 µm sieve. Protoplasts were washed in 0.5 % mannitol solution and centrifuged after each wash at 50 g without acceleration and break. Cell number was determined using a Fuchs-Rosenthal cell count chamber (Paul Marienfeld GmbH&Co.KG, Lauda-Königshofen, Germany). Protoplasts were adjusted with MMM solution (15 mM $MgCl_2$, 0.1 % (w/v) MES, 0.48 M Mannit, pH 5.6) to a cell count of 1.2 *10^6 protoplasts/mL. 3*10^5 protoplasts/mL were gently mixed with 20-30 µg plasmid DNA in sterile 0.1 M $Ca(NO_3)_2$ and 350 µL sterile 40 % (w/v) PEG 4000 solution. Transformation mixture was incubated in the dark for 30 min with occasional gently mixing. The PEG in the transformation mixture was gradually diluted by adding in total 10 mL of MMM solution over 30 min. The diluted mixture was centrifuged at 50 g for 10 min. Protoplasts were re-suspended in MMM solution and incubated for 24 h in the dark.

Protoplasts were maintained in liquid medium for another week under long-day conditions (16 h light, 8 h dark) and were subsequently spread on cellophane-covered Knop medium plates. After one week, the cellophane with the regenerating protoplasts was transferred to selection plates containing the selection agent G418 (Geneticin) (40 mg/L). The selection pressure was released after one week by transferring cellophanes back to medium plates without G418. After growing the moss for two weeks without antibiotics, another two-week selection round on G418-containing plates was applied. Individual plants were subsequently separated and transferred to medium plates without cellophane.

Molecular characterisation of targeted gene disruption

A small explant of regenerated protonemal tissue was used for DNA isolation. Genomic DNA was extracted using the cetyl trimethylammonium bromide (CTAB) extraction method. First, integration of the kanamycin cassette into the *P. patens* genome was checked by PCR using a primer pair combination that was specific for the selection cassette (fw: ATGGGGATTGAACAAGATGGATTGCAC/ rev: TCAGAAGAACTCGTCAAGAAGGC). Subsequently, insertion of the selection cassette into the correct locus was confirmed by PCR using primer pair combinations specific for the selection cassette and the corresponding untranslated regions of *S4H* 5’ (fw: 5’-GAGGGCTTCGACAAAAGAAG-3’/ rev: 5’-GATAGCTGGGCAATGGAATCCG-3’) and 3’ (fw: 5’-TAGGGTTCCTATAGGGTTTCGCTC-3’/ rev: 5’-GTAAAAACCAGGTCCAGCCC-3’).

Reverse transcriptase PCR for mutant characterisation

Total RNA was extracted from wild type and mutant gametophytic tissue using TRIzol™ reagent (Thermo Fisher Scientific, Waltham, Massachusetts, USA). Prior to cDNA synthesis RNA was treated with DNaseI (Thermo Fisher Scientific, Waltham, Massachusetts, USA) according to manufacturer’s instructions. 1 µg of DNA-free RNA was applied for cDNA synthesis using RevertAid H Minus First Strand cDNA Synthesis Kit (Thermo Fisher Scientific Waltham, Massachusetts, USA). The following primer pairs were used for determination of *S4H* (fw: 5'-ATGTCAGCGATGAGGTGCTG-3'/ rev: 5'-AACATGGCCACCACAAACTG-3') and for determination of *ACTIN8* transcripts (fw: 5'-GCTGGTTTCGCTGGAGACGATGC-3'/ rev: 5'-ATCGTGATCACCTGCCCGTCC-3').

Heterologous expression in *S. cerevisiae* LCB C-4 knockout mutant *sur2*Δ

P. patens S4H gene was synthesised and codon usage optimised for *S. cerevisiae* expression (Genscript, Piscataway Township, New Jersey, USA) and cloned into the pYES2-CT vector (Thermo Fisher Scientific, Waltham, Massachusetts, USA) using *BamH*I and *Xho*I restriction sites. The Kozak consensus sequence was added to enhance protein translation initiation. The following primer pairs were used for molecular cloning of *P. patens*

S4H into into the pYES2-CT vector: fw: 5'-GGAggatccAAACGATGGTATTCTGGGAAG-3'/ rev: 5'-GGActcgagTTCTATTTTCTTGACTGG-3'. Successful cloning was confirmed by sequencing of the plasmid. The empty vector and the *S4H*-containing plasmid were transformed into the *sur2*Δ-null mutant (Desfarges *et al.*, 1993; Haak *et al.*, 1997) using LiAc/SS carrier DNA/PEG method according to (Gietz & Schiestl, 2007). Transformed yeast and the corresponding wild type strain (BY4741) were cultivated in pre-cultures for 24 h in single dropout (SD) medium lacking uracil and containing 2 % glucose. For gene induction, yeast main cultures were inoculated to a final OD_{600} of 0.02 in SD dropout medium lacking uracil and containing 2 % galactose and 2 % raffinose and grown for another 24 h. Yeast cultivations were performed at 30 °C in shaking flasks. Cells were harvested at 3000 g for 10 min, washed with water and stored at -80 °C. Yeast cells were lyophilised prior to lipid extraction and analysis.

Lipid extraction

Lipids were extracted using a monophasic extraction method according to (Grillitsch *et al.*, 2014) with minor modifications. 20 mg lyophilised and homogenised *P. patens* or *S. cerevisiae* material were immersed in a 60 °C pre-heated solvent mixture containing propan-2-ol/hexane/water (60:26:14, v/v/v). The mixture was incubated for 30 min at 60 °C with every 10 min vortexing. The solution was centrifuged, the supernatant was collected and evaporated under a stream of nitrogen. Dried lipids were dissolved in 800 µL tetrahydrofuran/methanol/water (4:4:1, v/v/v). Extracts were directly applied for LCB measurement by ultra-performance liquid chromatography (UPLC) coupled with nanoelectrospray ionisation (nanoESI) and triple quadrupole tandem mass spectrometry (MS/MS) (UPLC-nanoESI-MS/MS) analysis (AB Sciex, Framingham, Massachusetts, USA) or further processed as described in the following.

Methylamine treatment

For ceramide and GlcCer analysis 50 µL of the lipid extract were evaporated. 1.4 mL 33% (w/v) methylamine dissolved in ethanol together with 600 µL H_2O were added to the dried extract (Markham and Jaworski, 2007). The mixture was incubated for 1 h at 50 °C in a water bath. After methylamine treatment the solvent was evaporated, dried lipids were dissolved in 50 µL tetrahydrofuran/methanol/water (4:4:1, v/v/v) and applied for UPLC-nanoESI-MS/MS.

Derivatisation with acetic anhydride

Acetic anhydride treatment was performed according to (Berdyshev *et al.*, 2005; Yanagawa *et al.*, 2017). For detection of LCB phosphates (LCB-Ps) 50 µL of the lipid extract were evaporated and subsequently re-suspended in 100 µL pyridine and 50 µL acetic anhydride.

The mixture was incubated for 30 min at 50 °C. After solvent evaporation samples were dissolved in 50 µL tetrahydrofuran/methanol/water (4:4:1, v/v/v). The samples were applied for UPLC-nanoESI-MS/MS analysis.

Microsome preparation

For enhanced detection of GIPC and SG species, microsomal fractions were prepared from the collected protonemal tissue. Microsome preparation was done according to (Abas & Luschnig, 2010). All steps were performed at 4 °C. A 1.5x fractionation buffer (FB) stock containing 150 mM Tris-HCl (pH 7.5), 37.5 % (w/w), 7.5 % glycerol, 15 mM EDTA (pH 8.0), 15 mM EGTA (pH 8.0) and 7.5 mM KCl was prepared. 1.1x and 1x solutions were diluted from the 1.5x stock. 20 mg of homogenised material were mixed with 1.5x FB, vortexed, and centrifuged at 600 g for 3 min. The supernatant was collected into a new tube. The pellet was re-extracted with 1.1x FB and the supernatant was combined with the first one. The pellet was re-extracted a last time with 1x FB and centrifuged at 2.000 g for 30 s. Combined supernatants were diluted 1:1 with water and divided into 600 µL aliquots. Supernatant samples were centrifuged at 20817 g for 2 h. The supernatant (soluble fraction) was discarded and the pellet was washed with water. The sample was centrifuged again at 20817 g for 45 min. The wash was discarded, and the sample was stored at -80 °C until further processing.

The microsomal pellet was dissolved in water and lipids were extracted according to lipid extraction described above. Samples were applied for UPLC-nanoESI-MS/MS analysis.

Lipid analysis

Measurement of targeted molecular lipid species was performed using the multiple reaction monitoring (MRM)-based UPLC-nanoESI-MS/MS approach described in (Resemann, 2018). LCB-Ps were measured in negative ionisation mode with $[M-H]^-$ as precursor ions. The more complex GIPC classes Hex(NAc)-GlcA-IPCs and Hex-Hex(NAc)-GlcA-IPCs were measured in positive ionisation mode with $[M+NH_4]^+$ as precursor ions and ceramide fragments as product ions. Head group-specific ions were detected as described before (Buré *et al.*, 2011). LC-MS data was processed using Analyst 1.6.2 and MultiQuant 3.0.2 software (both AB Sciex, Framingham, Massachusetts, USA).

Confocal Laser Scanning Microscopy (CLSM)

For callose labelling one- to two-week-old protonema was bleached overnight in ethanol/acetic acid (3:1, v/v). Callose labelling was modified from the protocol described in (Schuette *et al.*, 2009). The bleached plant tissue was incubated in 0.1 % (w/v) aniline blue in 50 mM sodium phosphate buffer (pH 9) for 30 min at room temperature. Before

visualisation, the tissue was rinsed in 50 mM sodium phosphate buffer (pH 9). Images were captured using an excitation wavelength at 405 nm and an emission wavelength at 500 nm. Images were analysed with Leica TCS SP5 confocal microscope (Leica Microsystems GmbH, Wetzlar, Germany) and processed with ImageJ 1.52b software (Schneider *et al.*, 2012).

Webtools

BLAST search

Sphinganine C-4 hydroxylases were searched by BLAST of *A. thaliana* SBH1 and SBH2 in the NCBI proteome database (National Center for Biotechnology Information (NCBI), U.S. National Library of Medicine, Maryland, USA) (http://www.ncbi.nlm.nih.gov/BLAST/) for *P. patens* (Altschul *et al.*, 1990).

Conserved domain prediction (CDD)

S4H was assigned to “Fatty acid hydroxylase superfamily” with CDD database (Marchler-Bauer *et al.*, 2015; Lu *et al.*, 2020).

Membrane protein topology prediction

Membrane protein topology was predicted with TMHMM software (Sonnhammer *et al.*, 1998; Krogh *et al.*, 2001).

Electronic fluorescent pictograph (eFP) browser

Gene expression information was obtained using *P. patens* eFP browser at: http//www.bar.utoronto.ca (Winter *et al.*, 2007; Ortiz-Ramírez *et al.*, 2016).

Results

Pp*S4H is a putative LCB C-4 hydroxylase in *P. patens

In *A. thaliana* LCB C-4 hydroxylation is catalysed by two redundant LCB C-4 hydroxylases SBH1 and SBH2 (Sperling *et al.*, 2001; Chen *et al.*, 2008). BLAST search using both proteins revealed the presence of only one putative LCB C-4 hydroxylase in the *P. patens* proteome with 68 % and 63 % identity, respectively. *The P. patens* protein has a length of 256 amino acids and is annotated in the NCBI database as Sphinganine C4-Monooxygenase 1-like (XP_024362887.1). Here, the protein is designated as Sphinganine C-4 Hydroxylase (S4H). Exploration of the organ-specific gene expression pattern of *S4H* in *P. patens* using the gene investigation tool eFP browser (Winter *et al.*, 2007; Ortiz-Ramírez *et al.*, 2016), revealed a strong expression of *S4H* in all organs (Fig. S1a). Highest expression could be detected in the protonema, the gametophore, and the mature spore

capsule. The constitutive expression pattern confirms with the expression of *SBH1* and *SBH2* in *A. thaliana* and suggests an important role of S4H function in all developmental stages of *P. patens*. Similar to other identified membrane-bound hydroxylases and desaturases, S4H contains three characteristic histidine motifs within its hydroxylase domain that are believed to be responsible for coordinating the di-iron cluster in the active site (Shanklin & Cahoon, 1998; Bai *et al.*, 2015) (Fig. S1b, c). S4H further contains two transmembrane domains as predicted by the TMHMM web tool (Fig. S1d). Since most identified plant sphingolipid enzymes are located in the ER membrane (Luttgeharm *et al.*, 2016), including the *A. thaliana* SBH1 and SBH2, S4H likely localises within the membrane of the ER as well.

*Pp*S4H restores trihydroxy LCB formation in *S. cerevisiae* LCB C-4 hydroxylase knockout mutant *sur2Δ*

To confirm the annotated LCB C-4 hydroxylase function of S4H, its coding sequence was codon usage optimised for *S. cerevisiae* expression. The optimised gene was expressed in the LCB C-4 hydroxylase *S. cerevisiae* knockout mutant *sur2Δ*. *sur2Δ* lacks all trihydroxy LCBs but the yeast cells remain viable (Haak *et al.*, 1997). Expression of *P. patens* S4H in *sur2Δ* successfully restored formation of trihydroxy LCBs, both in the ceramide pool (Fig. 2) as well as in the LCB pool (Fig. S2). Notably, plants usually exclusively contain C18 LCBs, while *S. cerevisiae* contains both C18 and C20 LCBs. Both C18 and C20 LCBs were hydroxylated in *S. cerevisiae* by *P. patens* S4H. This confirms the predicted enzymatic activity of S4H and shows that S4H is independent from the LCB carbon chain length.

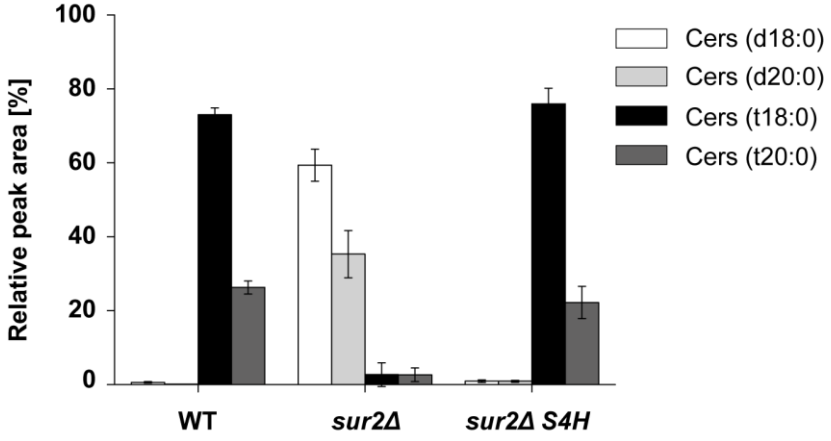

Fig. 2. Complementation of *S. cerevisiae* LCB C-4 hydroxylase knockout mutant *sur2Δ* with *P. patens* S4H restores formation of trihydroxy ceramides. Ceramide profiles of *S. cerevisiae* wild type (WT), *sur2Δ* knockout strain, and *sur2Δ* knockout strain complemented with *P. patens* LCB C-4 hydroxylase S4H are shown. Ceramide species (Cers) with the same LCB moiety are summed up and are categorised into dihydroxy (d18:0, d20:0) or trihydroxy (t18:0, t20:0) ceramides with 18 or 20 LCB carbon chain lengths. Data represent the mean ± SD of four independent biological replicates.

Loss of trihydroxy LCBs reshapes sphingolipid metabolism in *P. patens*

After the enzymatic activity of S4H was confirmed in *S. cerevisiae*, *P. patens* loss-of-function *s4h* mutants were generated by homologous recombination. Two independent mutant lines (*s4h-1* and *s4h-2*) were obtained. In both lines the *S4H* transcript was completely absent, as determined by reverse transcriptase PCR analysis (Fig. 3a, Fig. S3a). To study the *in vivo* effects of the complete loss of LCB C-4 hydroxylation on the sphingolipidome of *P. patens*, protonema was cultivated for ten days on BCD medium covered with cellophane. Covering of the agar medium with cellophane enabled agar-free and easy harvesting of the protonema tissue. After lipid extraction, the sphingolipid profiles were determined using the UPLC-nanoESI-MS/MS approach described in (Resemann, 2018). Relative profiles and fold changes of absolute peak areas compared to the wild type were analysed for all four plant sphingolipid classes (LCBs, ceramides, GlcCers and GIPCs). LCBs, LCB-Ps, ceramides, and GlcCers were analysed in crude protonema lipid extract. GIPC content was measured in microsomes prepared from protonema to enrich these membrane-bound sphingolipids.

The simplest sphingolipid classes LCBs and LCB-Ps are depicted in Fig. 3b-e. While in the wild type t18:0 LCBs accounted for 94 % and d18:0 LCBs for 6 % of the total, *s4h-1* and *s4h-2* had no t18:0 LCBs and instead contained 99 % d18:0 LCBs (Fig. 3b). The mutants additionally contained minor amounts of d18:1 and d18:2 LCBs (0.5 % and 0.1 %, respectively). In the wild type LCB-P profile t18:0 LCB-P also predominated with more than 60 % of the total (Fig. 3c). d18:0 LCB-P accounted for around 30 % of the total in the wild type. In *s4h-1* and *s4h-2* no t18:0 LCB-P were detected. Instead, over 99 % were d18:0 LCB-P and around 0.3 % d18:1 LCB-P. d18:2 LCB-P were only detected in trace amounts in the *s4h* mutants. Overall, there was a > 60-fold accumulation of LCBs and a > 2000-fold accumulation of LCB-Ps in the *s4h* mutants compared to the wild type (Fig. 3d, e).

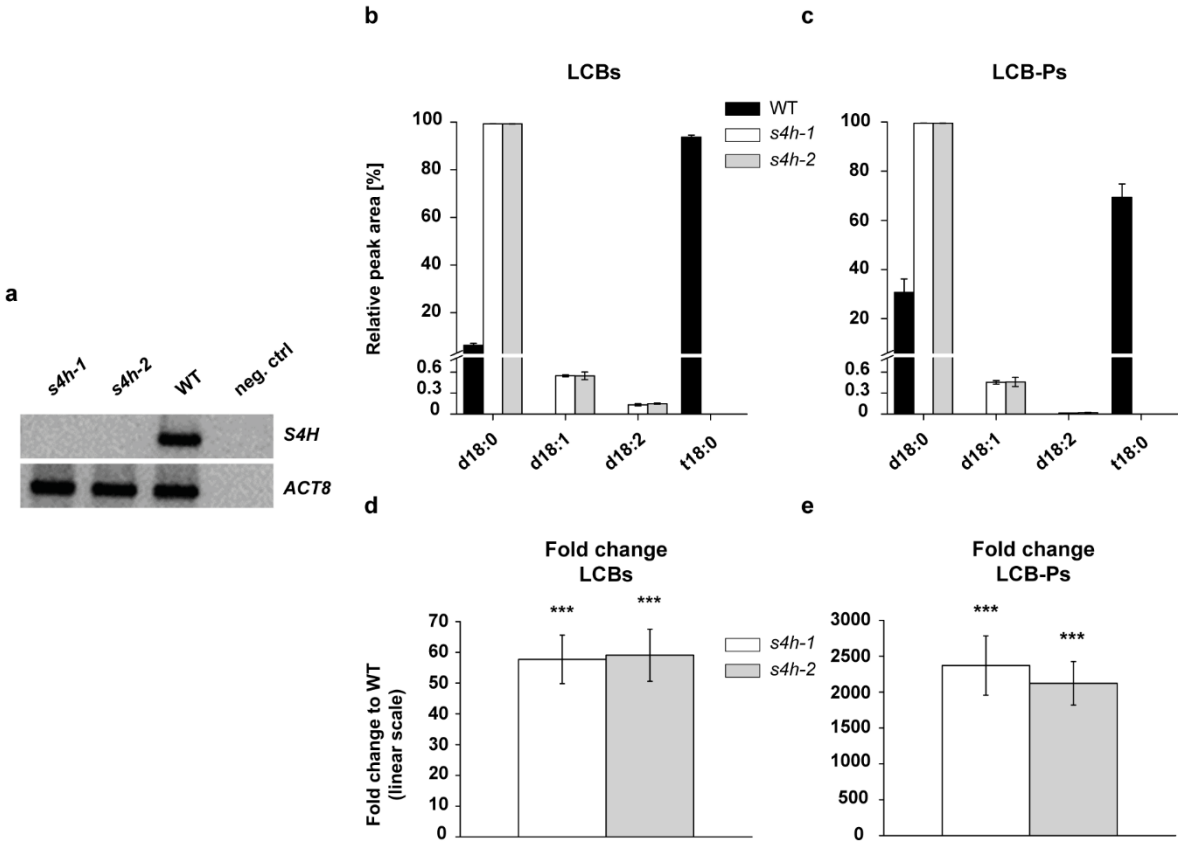

Fig. 3. *s4h* mutant characterisation and altered LCB content of *s4h-1* and *s4h-2*. (a) *S4H* transcript determination by reverse transcriptase PCR. *ACTIN8* (*ACT8*) was used as reference gene and water as negative control (neg. ctrl). (b-e) Long-chain bases (LCBs) and phosphorylated LCBs (LCB-Ps) were extracted from protonema of ten-day-old wild type (WT), *s4h-1*, and *s4h-2 P. patens* and analysed with UPLC-nanoESI-MS/MS. Dihydroxy LCBs are indicated by a 'd' and trihydroxy LCBs are indicated by a 't'. Relative profiles of (b) LCBs and (c) LCB-Ps in WT, *s4h-1*, and *-2* lines. Fold changes of (d) LCBs and (e) LCB-Ps to the WT were calculated using absolute peak areas. Fold changes are depicted in linear scale. The WT, which is not shown, is set to 1. Sphingolipid data represent the mean ± SD of measurements from four independent cultivations each containing protonema material from eight cultivation plates. Statistical analysis was done using Student's *t*-test. Asterisks indicate different significance levels with *** significance at $P < 0.001$ compared to the WT.

The drastic increase of LCBs and LCB-Ps is consistent with findings from *A. thaliana sbh1 sbh2* double knockout mutant (Chen *et al.*, 2008). Since the absolute content of downstream sphingolipid classes was also affected in the *sbh1 sbh2* double mutant in *A. thaliana,* it was hypothesised, that this might also be the case in *P. patens*. Surprisingly, there was no change in the total ceramide amount of the *s4h* mutants compared to the wild type (Fig. S3b). In the wild type, ceramides with the t18:0 LCB moiety predominated (Fig. 4a, d), while in the *s4h* mutants the most abundant LCB moiety was majorly d18:0 and in minor amounts d18:1 and d18:2 (Fig. 4b, c, e, f).

Ceramides were grouped according to the hydroxylation state of their fatty acids. By this categorisation, ceramides contain unhydroxylated fatty acids, which is indicated by a 'c' in front if the chain length number (Fig. 4a-c), and hydroxyceramides contain α-hydroxylated fatty acids, which is indicated by an 'h' in front of the chain length number (Fig. 4d-f). Relative ceramide and hydroxyceramide profiles revealed that the wild type contained more

hydroxyceramides, while the *s4h* mutants contained more ceramides (Fig. 4a-f). Fold change calculations confirmed this observation with *s4h-1* having 4.7-fold more and *s4h-2* having 4.4-fold more ceramides than the wild type (Fig. 4g). Hydroxyceramides decreased in *s4h-1* to 40 % and in *s4h-2* to 35 % of the wild type content. In logarithmic scale this corresponds to an increase in ceramide content in *s4h* mutants by around 0.65 (Fig. 4g) and a reduction of hydroxyceramide content in *s4h* mutants by around 0.42 (Fig. 4h).

The wild type fatty acid profile of all ceramides was mainly composed of saturated fatty acids and a few unsaturated fatty acids ranging from C20 to C26 (Fig. 4a, d). Ceramides in *s4h-1* and s*4h-2* mutants showed a similar fatty acid profile with c16:0 emerging additionally in minor amounts (Fig. 4b, c, e, f).

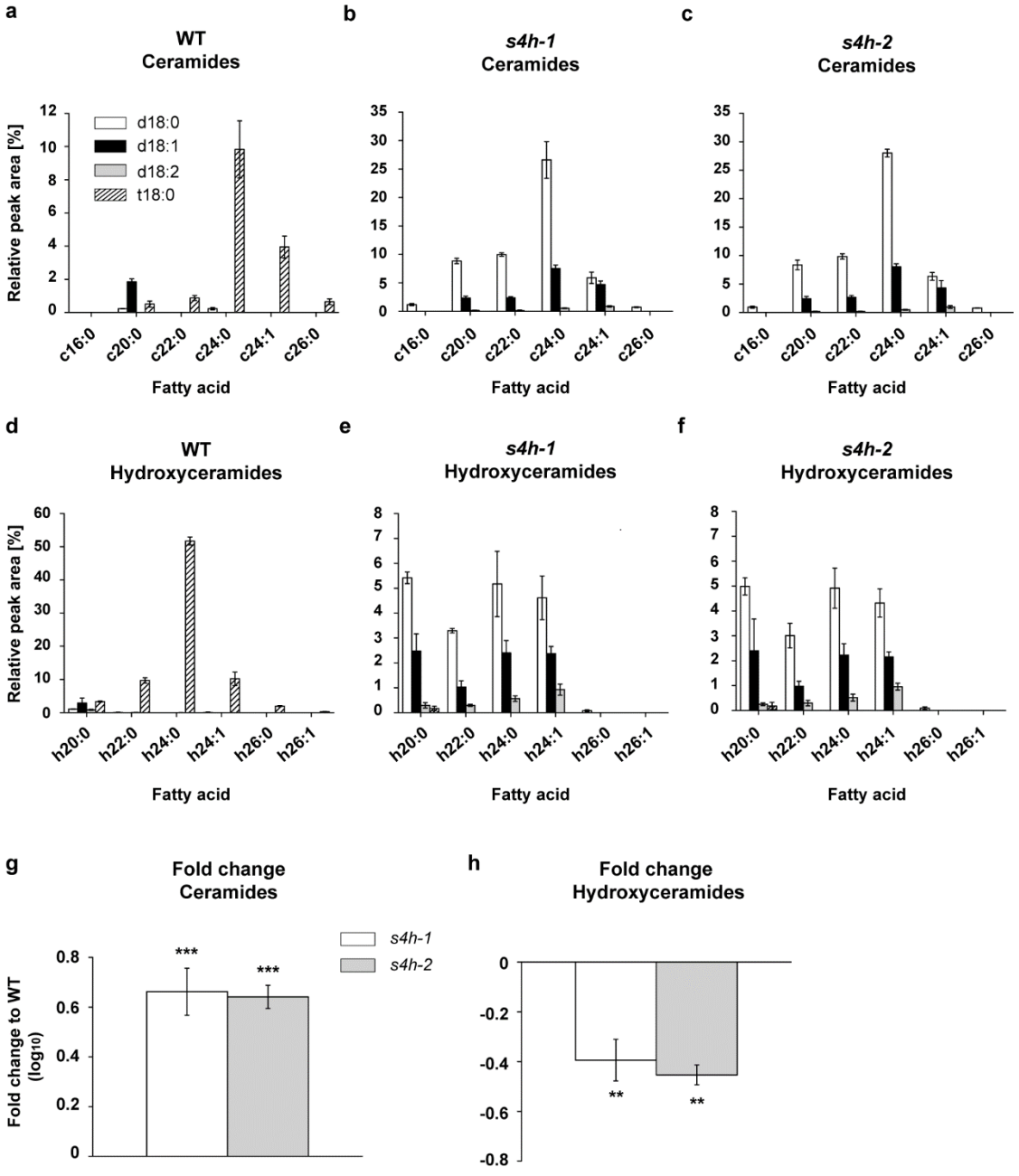

Fig. 4. *s4h-1* and *s4h-2* have an altered ceramide content. (a-h) Ceramides were extracted from protonema of ten-day-old wild type (WT), *s4h-1*, and *s4h-2 P. patens* and analysed with UPLC-nanoESI-MS/MS. Relative profiles of (a-c) ceramide and (d-f) hydroxyceramide molecular species are shown with their long-chain base (LCB) (column colour) and fatty acid (x-axis) moieties. Dihydroxy LCB moieties are indicated by a 'd' and trihydroxy LCB moieties are indicated by a 't'. Molecular species with an unhydroxylated fatty acid moiety are indicated by a 'c' and molecular species with an α-hydroxylated fatty acid moiety are indicated by an 'h'. Relative profiles of (a) WT, (b) *s4h-1*, and (c) *s4h-2* ceramides with unhydroxylated fatty acid moieties. Relative profiles of (d) WT, (e) *s4h-1*, and (f) *s4h-2* hydroxyceramides with α-hydroxylated fatty acid moieties. (g) Ceramide and (h) hydroxyceramide fold changes to the WT were calculated using absolute peak areas and are depicted in $\log_{10}$ scale. The WT, which is not shown, is set to 0. Sphingolipid data represent the mean ± SD of measurements from four independent cultivations each containing protonema material from eight cultivation plates. Statistical analysis was done using Student's *t*-test. Asterisks indicate different significance levels with *** significance at $P < 0.001$ and ** significance at $P < 0.01$ compared to the WT.

Relative profiles of the complex sphingolipid classes GlcCers and GIPCs are shown in Fig. 5. Shown GIPCs have a head group composition consisting of a hexose unit (Hex) that is connected to glucuronic acid (GlcA) linked IPC. Over 90 % of the GlcCer profile of the

wild type was made up by a single molecular species, with a sphingoid backbone consisting of a d18:2 LCB moiety and a h20:0 fatty acid moiety (Fig. 5a). The predominant LCB moiety found in GlcCers of *s4h* mutants was also d18:2. The fatty acid profile of the *s4h* GlcCers was substantially broadened compared to the wild type profile (Fig. 5b, c). The most abundant fatty acids in the mutants were saturated and unsaturated fatty acids ranging from C20 to C24 chain length. Total GlcCer levels were not significantly changed in *s4h* mutants compared to the wild type control (Fig. S3c).

Over 90 % of the Hex-GlcA-IPC molecular species of wild type *P. patens* had a t18:0 LCB moiety (Fig. 5d). Similar to alterations in ceramide profiles, the predominant LCB moiety was changed from t18:0 to d18:0 in the *s4h* mutants. In contrast to the LCB moiety, the fatty acid composition of Hex-GlcA-IPCs was not changed in *s4h* mutants compared to the wild type (Fig. 5d, e, f). The four most abundant fatty acids found in the Hex-GlcA-IPC pool were h20:0, h22:0, h24:0 and h24:1. Relative profiles were also determined for GIPCs with different polar head groups (Fig. S4). GIPCs may be grouped according to the complexity of their head group composition. Series A GIPCs contain one additional sugar residue, Hex-GlcA-IPCs, which may also be converted to *N*-acetylhexosamine (HexNAc), HexNAc-GlcA-IPCs. Series B GIPCs contain two additional sugar residues, Hex-Hex-GlcA-IPCs, of which one may be converted to HexNAc, Hex-HexNAc-GlcA-IPCs. The relative profiles of these complex GIPCs in the wild type and in the *s4h* lines were comparable to the described Hex-GlcA-IPC profiles (Fig. S4). Interestingly, fold change calculations revealed a slight increase (around 1- to 2-fold) of series A GIPCs and a significant accumulation (around 6-fold) of series B GIPCs in *s4h* lines compared to the wild type (Fig S5).

Analogous to ceramides, molecular species of GlcCers and Hex-GlcA-IPCs were sorted according to the hydroxylation status of their fatty acid moieties. Again, an increase in species with unhydroxylated fatty acids and a decrease in species with hydroxylated fatty acids was observed in the *s4h* lines (Fig. S6).

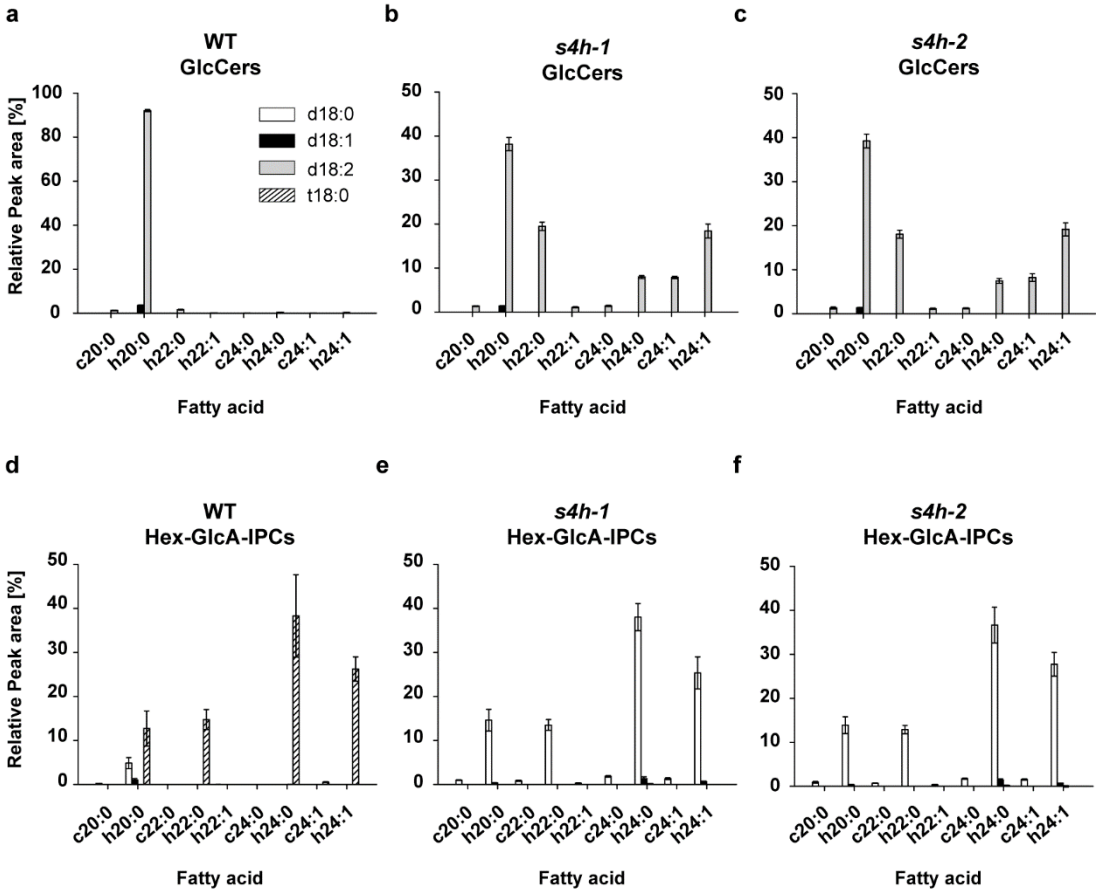

Fig. 5. *s4h-1* and *s4h-2* have altered GlcCer and Hex-GlcA-IPC profiles. (a-c) Glycosylceramides (GlcCers) were extracted from protonema of ten-day-old wild type (WT), *s4h-1*, and *s4h-2 P. patens*. (d-f) Glycosyl inositolphosphorylceramides (GIPCs) were extracted from microsomes prepared from protonema of ten-day-old WT, *s4h-1*, and *s4h-2 P. patens*. Sphingolipids were analysed with UPLC-nanoESI-MS/MS. GlcCer and Hex-GlcA-IPC molecular species are shown with their long-chain base (LCB) (column colour) and fatty acid (x-axis) moieties. Dihydroxy LCB moieties are indicated by a 'd' and trihydroxy LCB moieties are indicated by a 't'. Molecular species with an unhydroxylated fatty acid moiety are indicated by a 'c' and molecular species with an α-hydroxylated fatty acid moiety are indicated by an 'h'. (a-c) Relative GlcCer profiles of (a) WT, (b) *s4h-1*, and (c) *s4h-2*. Only molecular species with a peak area ≥ 1 % in at least one of the three lines were included in the GlcCer graphs. (d-f) Relative Hex-GlcA-IPC profiles of (d) WT, (e) *s4h-1*, and (f) *s4h-2*. Only molecular species with a peak area ≥ 0.5 % in at least one of the three lines were included in the Hex-GlcA-IPC graphs. Sphingolipid data represent the mean ± SD of measurements from four independent cultivations each containing protonema material from eight cultivation plates. Abbreviations are as follows: GlcA: glucuronic acid; Hex: hexose; IPCs: inositolphosphorylceramides.

Taken together, these results demonstrate that loss of LCB C-4 hydroxylation in *P. patens* causes a substantial shift in the composition of all sphingolipid classes. Depending on the sphingolipid class, most obvious changes were observed in either the LCB (LCBs, LCB-Ps, ceramides, GIPCs) or in the fatty acid moiety (GlcCers). There was a substantial increase of LCBs as potential substrates of S4H. Except for significant accumulation of series B GIPCs, loss of LCB C-4 hydroxylation had no substantial effect on total content of downstream sphingolipid classes.

Loss of trihydroxy LCBs causes change in composition of conjugated sterols

Several studies on plasma membrane organisation have demonstrated a strong interaction network between different free and conjugated phytosterols and sphingolipids (Grosjean *et al.*, 2015; Grosjean *et al.*, 2018). A result of these interactions is the formation of micro- and nanodomains, which are considered to be important sorting platforms for membrane proteins (Simons & Ikonen, 1997; Cacas *et al.*, 2012). Connections between sterols and sphingolipids are believed to take place in form of hydrogen bonds (Slotte, 2016). The change of the hydroxylation pattern of sphingoid backbones in the *s4h* mutants was therefore expected to influence interactions between sterols and sphingolipids in the plasma membrane, and perhaps, by extension, sterol content. To test this hypothesis, the relative profile of steryl glycosides (SGs) was analysed in microsomes obtained from protonema of wild type and *s4h* plants (Fig. 6). At 47 % of the total, campesteryl represented the most abundant steryl moiety of SGs in the wild type, followed by isofucosteryl (27 %), sitosteryl (15%), stigmasteryl (9 %) and brassicasteryl (2 %). Cholesteryl was only detected in trace amounts (0.07 %). While the general SG profile was maintained in *s4h* mutants, a significant increase compared to the wild type was observed for sitosteryl and isofucosteryl. A significant decrease was observed for stigmasteryl and brassicasteryl. However, changes in SG composition had no significant effect on total SG content (Fig. S7).

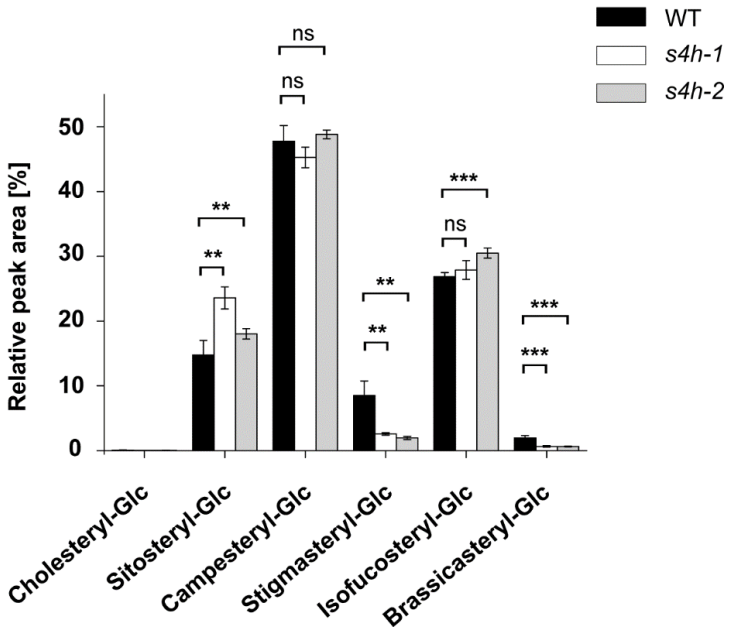

Fig. 6. *s4h-1* and *s4h-2* have altered steryl glycoside profiles. Steryl glycosides (SGs) were extracted from microsomes prepared from protonema of ten-day-old wild type (WT), *s4h-1*, and *s4h-2 P. patens* and analysed with UPLC-nanoESI-MS/MS. Relative SG profiles of WT, *s4h-1*, and *s4h-2*. SG data represent the mean ± SD of measurements from four independent cultivations each containing protonema material from eight cultivation plates. Statistical analysis was done using Student's *t*-test. Asterisks indicate different significance levels with *** significance at $P < 0.001$, ** significance at $P < 0.01$ and not significant (ns) at $P > 0.05$ compared to the WT. Abbreviation is as follows: Glc: glycoside.

s4h mutants show impaired growth and development in all tissues

The observed changes in sphingolipid and sterol composition suggest a change in membrane organisation, which could affect cell growth and division. Furthermore, the *A. thaliana* double knockout mutant *sbh1 sbh2* showed defects in cell elongation and division causing severely dwarfed plants that fail to reach reproductive maturity (Chen *et al.*, 2008). Gametophyte development of the *P. patens s4h* mutants was studied to determine whether they were similarly affected. Protonema spot inocula of around 1 mm in diameter were placed on BCD medium and incubated for up to five weeks. After 12 days of growth the wild type plant developed a star-shaped colony with long, branched protonemal filaments that reached outwards from the dense centre (Fig. 7a). Small gametophores were observed developing in the centre of the colony. *s4h* mutants also developed protonemal filaments from the dense centre, however colonies had a rounded, less branched appearance than the wild type. Furthermore, no gametophores could be observed emerging from the centre of the colony. After 24 days of growth, the wild type showed fully developed gametophores that completely overgrew the protonemal tissue. *s4h* mutants showed no gametophore development and protonema filaments still grew in a stunted manner. After 37 days of growth severely dwarfed gametophores were observed in *s4h* colonies. The gametophores had diameters of around 0.4 mm. A photo taken with the same magnification of a wild type gametophore of the same age could only capture the phyllids at the tip of the shoot. Gametophytic development, including both gametophore and protonemal tissues, was drastically impaired in *s4h* mutants.

Protonema consists of two cell types: chloroplast-rich chloronema cells and caulonema cells that contain fewer and less-well developed chloroplasts. Regarding *s4h* colony growth behaviour it was speculated that the transition from chloronema to caulonema cells might be impaired. To have a more extensive look at protonema differentiation, a dark growth experiment was performed. Protonema spot inocula of the wild type, *s4h-1*, and *s4h-2* lines were placed on BCDAT medium supplemented with 2 % sucrose. After growth for one week under continuous light the wild type and *s4h* mutant colonies looked alike (Fig. 7b). Colonies developed a dense green centre consisting of filamentous protonema cells. Subsequently, plates were transferred to the dark and put into vertical orientation. Cultivation under these conditions was continued for three weeks. The developing filamentous cells in the wild type did not contain chloroplasts and had a brownish appearance. The developed cells are a subtype of caulonema, specified as skotonema. Wild type skotonema cells formed numerous long filaments reaching upwards. Although *s4h* mutants were able to generate skotonema cells, their filaments were much smaller, and with an altered morphology compared to wild type cells. Although counting of filaments was

not feasible with this experimental setup, their number appeared to be drastically reduced in *s4h* mutants.

To quantify the growth defect of *s4h* mutants, protonema biomass production was determined. Protonema cultures were inoculated on cellophane-covered BCD medium plates. Each plate was inoculated with a protonemal cell suspension that was adjusted to a volume corresponding to 5 mg dry weight. Protonemal tissue was maintained on plates for ten days before harvesting and determination of fresh weight. In four independent experiments, wild type tissue reached a mean biomass of around 4.4 g (Fig. 7c). *s4h* mutants generated with a mean biomass of around 2.3 g significantly less material than the wild type. Determination of the dry weight confirmed the observed effect (Fig. S8).

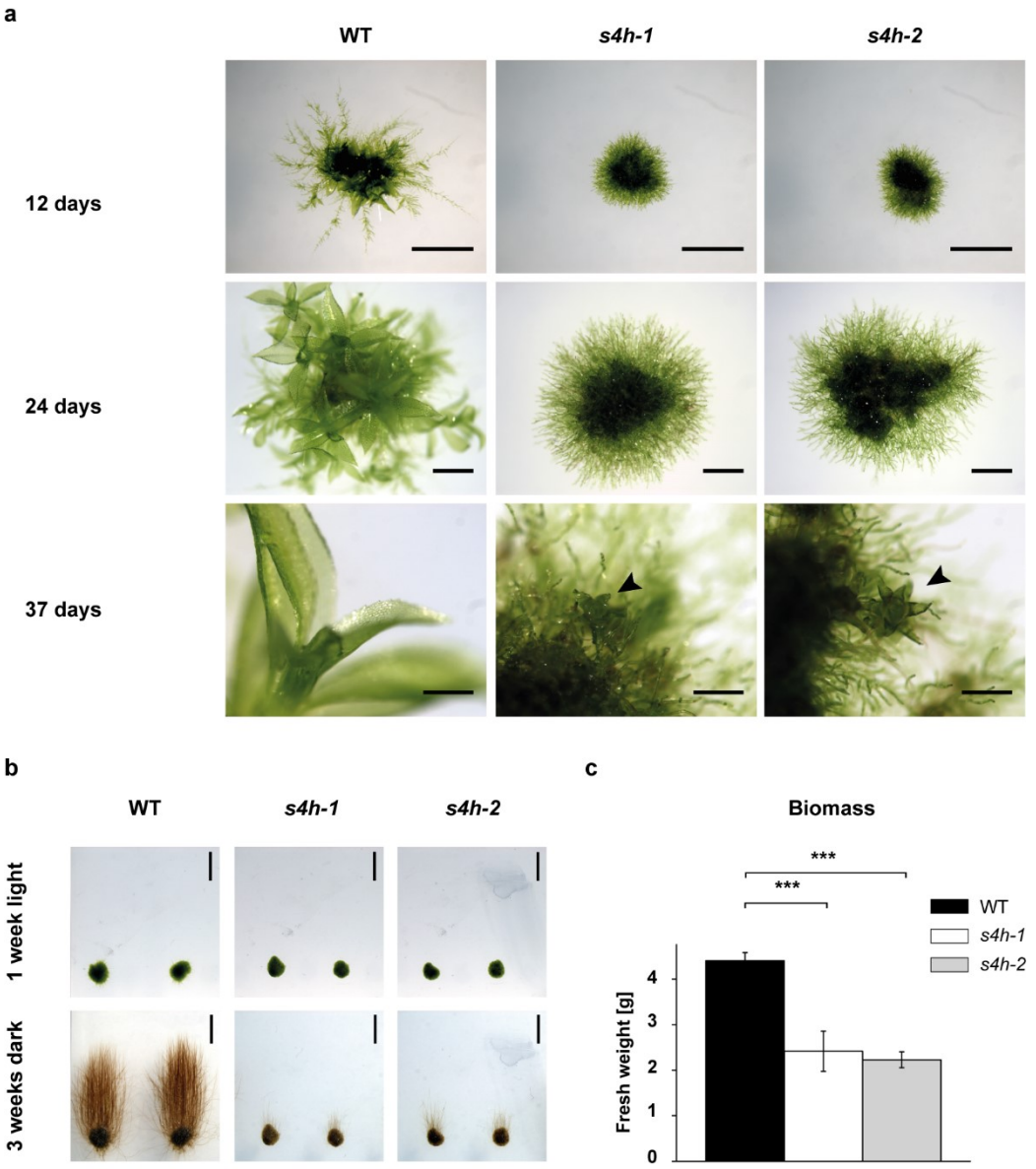

Fig. 7. *s4h-1* and *s4h-2* lines exhibit a growth phenotype in all gametophytic stages. (a) 1 mm protonema spot inocula of wild type (WT), *s4h-1* and *s4h-2* were placed on BCD medium and grown for the indicated time periods. Scale bars in 12-day colony pictures are 4 mm. Scale bars in 24-day colony pictures are 1 mm. Scale bars in 37-day colony pictures are 0.4 mm. Arrowheads indicate gametophores on *s4h-1* and *s4h-2* colonies. (b) Spot inocula of *P. patens* WT, *s4h-1*, and *s4h-2* were placed on BCDAT+ 2 % sucrose and grown under continuous light for one week (upper row). Plates were moved to the dark and rotated into vertical position. Colonies were grown for another three weeks to induce skotonema development (lower row). Scale bares are 0.5 cm. (c) Growth of WT, *s4h-1*, and *s4h-2* was quantified by collecting ten-day-old protonema tissue grown on cellophane-covered BCD medium and determining the fresh weight. Data represent the mean ± SD of measurements from four independent cultivations each containing protonema material from eight cultivation plates. Statistical analysis was done using Student's *t*-test. Asterisks indicate significance level with *** significance at $P < 0.001$ compared to the WT.

Imbalance of sphingolipid metabolism alters callose deposition at protonema cross-walls

P. patens s4h mutants have severe growth defects, similar to *A. thaliana* sphingolipid mutants (Chen *et al.*, 2008). In *A. thaliana sbh1 sbh2* these growth defects were attributed to impaired cell elongation and division (Chen *et al.*, 2008). Another study showed that inhibition of VLCFA sphingolipid synthesis caused abnormal cell plate formation in root tips

(Molino *et al.*, 2014). Defects in cell plate formation are believed to arise from impaired vesicle and membrane trafficking affecting the deposition of cell wall material during cell division. Callose is a cell wall component deposited during plant cytokinesis; in *P. patens* protonema, callose is deposited during cell division at the cross-walls separating two filamentous cells (Scherp *et al.*, 2001; de Keijzer *et al.*, 2017). To determine whether *s4h* mutants also have abnormal cell plate formation, callose was stained using aniline blue in protonema tissue. Protonema was cultivated on cellophane-covered BCD medium for one to two weeks before visualisation using confocal laser scanning microscopy. In wild type protonema cells callose was exclusively found in the cross-walls between two filamentous cells (Fig. 8). The cross-wall displayed a plain line-shaped structure without irregularities. Cross-walls in *s4h* mutants, however, were abnormally shaped. Callose was still deposited at cross-walls but irregular stretches could be seen on both sides of the wall. Callose expansions were oriented perpendicular to the cross-wall and extended towards the centre of both adjacent filamentous cells. A vast majority of *s4h* protonema cells showed cross-wall malformations of different degrees.

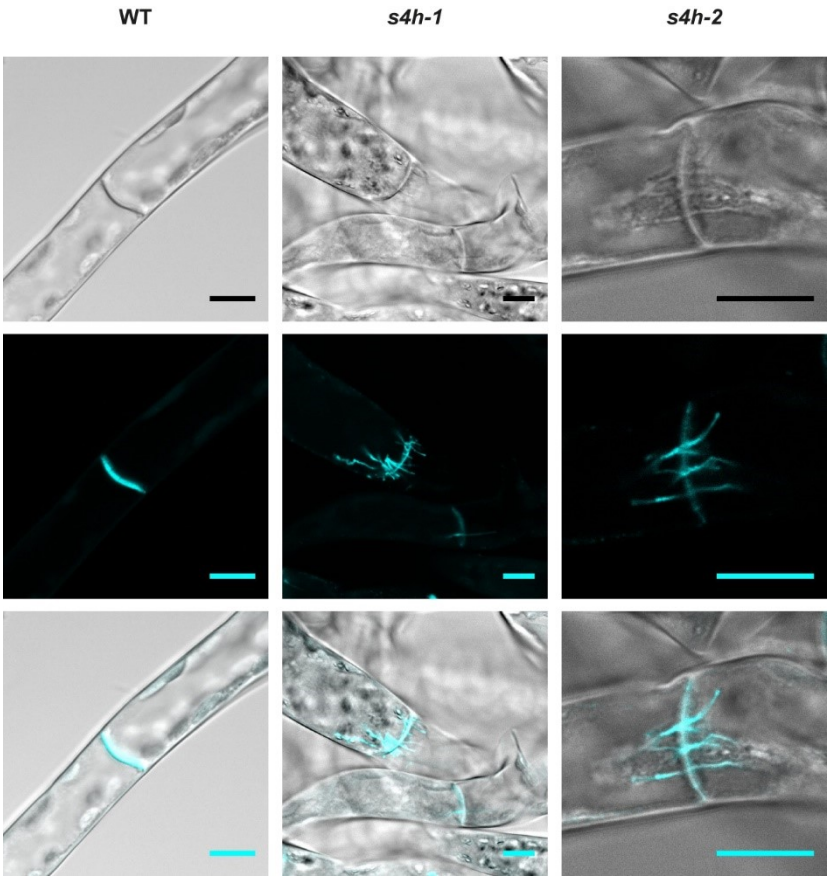

Fig. 8. Irregular callose deposition at cross-walls of *s4h-1* and *s4h-2* protonema cells. Cross-walls of one- to two-week-old filamentous wild type (WT), *s4h-1*, and *s4h-2* protonema cells were captured using confocal laser scanning microscopy. Callose was stained with aniline blue. Pictures are shown in bright field (upper row), in aniline blue fluorescence (middle row) and as merge of both (lower row). Scale bars are 10 µm. Pictures are representative for three independent experiments.

Discussion

Sphingolipids containing trihydroxy LCB moieties predominate in plants (Markham *et al.*, 2006). From characterisation of the *A. thaliana sbh* knockout and knockdown mutants it is known that trihydroxy sphingolipids are crucial for plant growth and development (Chen *et al.*, 2008). To examine the role of trihydroxy sphingolipids in non-vascular plants, the LCB C-4 hydroxylase S4H from *P. patens* was characterised. The enzyme was identified based on sequence homology, and its metabolic activity was confirmed by complementation of the *S. cerevisiae sur2Δ* mutant. Sphingolipid analysis of *s4h* null mutants revealed complete depletion of trihydroxy sphingolipids, and substantial enrichment of LCB substrates. Consistent with *sbh1 sbh2* in *A. thaliana, s4h* plants were impaired in growth and development. The developmental phenotype was accompanied by irregular callose depositions at the cross-walls of filamentous *s4h* protonema cells.

Disruption of *P. patens S4H* resulted in loss of all t18:0 LCB-containing sphingolipids. This confirmed that the LCB C-4 hydroxylase is encoded by a single gene in *P. patens*. As in *A. thaliana sbh1 sbh2*, loss of the trihydroxy LCB moiety in *s4h* caused a shift of most abundant species from tri- towards dihydroxy LCB moieties. The shift was observed in *P. patens* for LCBs, ceramides, and GIPCs, but not for GlcCer. This can be explained by the fact that the wild type *P. patens* GlcCer pool only contains d18:2 LCBs but no t18:0 LCBs (Resemann, 2018).

Loss of trihydroxy LCBs in *A. thaliana* was accompanied with a total increase of all sphingolipid classes (Chen *et al.*, 2008). In *P. patens* only LCBs, LCB-Ps and series B GIPCs were found to have strongly elevated levels in *s4h* mutants compared to the wild type. The total contents of ceramides, GlcCers and series A GIPCs were only slightly or not significantly affected. *P. patens s4h* had a much higher fold change for LCB-Ps (around 2000-fold) than for LCBs (around 60-fold) compared to the wild type. One explanation may be that several substrate-specific ceramide synthases are active in wild type *P. patens*. The excess of d18:0 LCBs may exceed the capacity of d18:0-specific ceramide synthases to incorporate all LCBs into ceramides. It is known from vascular plants that application of LCBs induces PCD (Shi *et al.*, 2007). Application of LCB-Ps suppresses the LCB-induced PCD (Shi *et al.*, 2007; Alden *et al.*, 2011). The balance of LCBs and LCB-Ps is therefore believed to be an important factor in PCD induction (Shi *et al.*, 2007; Alden *et al.*, 2011). To dispose of excess LCBs in *P. patens s4h*, it could be that a large portion is phosphorylated. Resulting higher levels of LCB-Ps might outweigh accumulation of LCBs and therefore suppress LCB-induced cell death. This is supported by the phenotype since no cell death was observed in *s4h* mutants.

It should further be noted that LCB-Ps are very low abundant molecules in plants, representing around 0.03 % of total sphingolipids in *A. thaliana* leaf extracts (Markham *et*

al., 2006; Yanagawa *et al.*, 2017). Their detection in wild type plants therefore requires optimised extraction conditions, derivatisation techniques, and a high detection sensitivity. Although the detection of LCB-Ps in *A. thaliana* has been improved over the past years (Yanagawa *et al.*, 2017; Zienkiewicz *et al.*, 2020), these sphingolipid compounds have not yet been identified in *P. patens* (Resemann, 2018). This study identified LCB-Ps for the first time in *P. patens*. The strongly elevated levels of LCB-Ps in *s4h* mutants largely facilitated the detection of the molecular species that are only present in minor amounts in the wild type. This underlines the utility of sphingolipid mutants in the technical establishment of sphingolipid detection.

A. thaliana sbh1 sbh2 showed an accumulation of sphingolipids with C16 fatty acids (Chen *et al.*, 2008). Chen *et al*. (2008) therefore speculated that the growth phenotype resulted from accumulation of LCFAs, likely due to the action of different substrate specific ceramide synthases. In the *P. patens* sphingolipidome, C16 fatty acids only represent a minor fatty acid moiety that was not enriched in *s4h* mutants. Therefore, it appears unlikely that the growth phenotype observed in *A. thaliana* and *P. patens* results from accumulation of LCFAs.

Another important aspect was that *P. patens s4h-1* and *s4h-2* showed accumulation of ceramides, Hex-GlcA-IPCs, and GlcCers with unhydroxylated fatty acids. While this was not observed for *A. thaliana sbh1 sbh2*, it was, however, described for *S. cerevisiae sur2Δ* cells (Haak *et al.*, 1997). It indicates that the fatty acid hydroxylase might prefer ceramides containing trihydroxy LCBs as substrates. The sphingolipid profiles of the *A. thaliana* fatty acid hydroxylase mutant *fah1 fah2* were investigated by König *et al*. (2012). Indeed, the mutant had elevated levels of sphingolipids with trihydroxy LCB moieties, indicating that these compounds are the favoured substrates of fatty acid hydroxylases. To test whether this is also true for fatty acid hydroxylases in non-vascular plants, further studies would have to be conducted on fatty acid hydroxylase function in *P. patens*.

The LCB profiles in the complex sphingolipids GlcCers and GIPCs indicated that enzymes adding different head groups to the ceramide backbone have preferences for ceramides with certain LCB modifications; while *P. patens* homologues for inositolphosphorylceramide synthases prefer ceramides with a t18:0 LCB moiety, the glycosylceramide synthase homologue works on ceramides with a d18:2 LCB moiety. Another notable observation was that series B GIPCs (Hex-Hex(NAc)-GlcA-IPCs) accumulated more strongly in *s4h-1* and *s4h-2* than series A GIPCs (Hex(NAc)-GlcA-IPCs). Since detection of GIPC classes with more complex head groups is a recent achievement (Buré *et al.*, 2011; Cacas *et al.*, 2013), it is not known whether GIPC classes in *A. thaliana sbh1 sbh2* were also differently affected. To learn more about the impact of different GIPC

head groups on the physiology of non-vascular plants, enzymes involved in GIPC head group assembly will have to be investigated in *P. patens*.

LCB C-4 hydroxylases are functionally related to sphingolipid Δ4-desaturases. In mammals, LCB C-4 hydroxylase and sphingolipid Δ4-desaturase activities are carried out by a bifunctional enzyme, designated DES2 (Ternes *et al.*, 2002; Mizutani *et al.*, 2004). In *A. thaliana* sphingolipid Δ4-desaturase is only expressed in flowers and its activity might therefore not have been detected in the sphingolipid analyses conducted by Chen *et al*. (2008), which was performed on vegetative tissue. The authors could therefore not exclude that the sphingolipid Δ4-desaturase from *A. thaliana* also contributes a portion of hydroxylated LCBs. They speculated that sphingolipid Δ4-desaturase might exhibit a more prominent hydroxylase activity in plants containing high amounts of Δ4-unsaturated LCBs such as Solanaceae (Dunn *et al.*, 2004; Sperling *et al.*, 2005; Markham *et al.*, 2006; Markham & Jaworski, 2007). In these plants, the desaturase may be ubiquitously expressed, and could contribute either or both hydroxylase/desaturase functions in different tissues. The *P. patens* sphingolipidome more closely resembles that of Solanaceae than of Brassicaceae with d18:2 LCB being the only LCB moiety identified in the GlcCer pool of *P. patens* (Markham *et al.*, 2006; Resemann, 2018). This hints at a high sphingolipid Δ4-desaturase activity in *P. patens*. However, with respect to hydroxylase/desaturase bifunctionality, the fact that the knockout of *S4H* in *P. patens* resulted in loss of all detectable trihydroxy LCBs indicates that S4H likely accounts for all trihydroxy LCB synthesis. Sphingolipid Δ4-desaturase, however, probably does not contribute to LCB hydroxylation in *P. patens.*

Loss of trihydroxy LCBs caused fundamental alterations of the sphingolipid homeostasis in *A. thaliana* and *P. patens* resulting in severe growth phenotypes. Cumulative findings from both organisms indicate that defects in growth and development may be caused by the shift from tri- to dihydroxy LCB moieties and the accompanied biophysical changes in the membrane. Changes in the SG composition in *P. patens s4h* mutants is evidence of this. Free phytosterols and their conjugated forms, SGs and acylated SGs (ASGs), were shown to induce microdomain formation (Grosjean *et al.*, 2015; Grosjean *et al.*, 2018). These domains are enriched in sterols and hydroxylated sphingolipids, mainly GIPCs (Cacas *et al.*, 2016). Microdomains are believed to be formed and maintained in part through an intermolecular hydrogen bond network (Slotte, 1999; Mombelli *et al.*, 2003; Slotte, 2016). As indicated by the lipidomics data in this study, loss of one hydroxyl group in the sphingoid backbone of GIPCs may not only reduce the strength of the hydrogen bond network between sterols and sphingolipids, but also changes the membrane sphingolipid composition. A resulting failure of microdomain formation might hamper protein sorting downstream and therefore influence developmental processes.

Altered membrane composition would explain the observed impaired callose deposition in the *s4h* mutants. Callose is a cell wall component that is deposited at the cell plate during plant cytokinesis (Scherp *et al.*, 2001). Several mutations that affect GIPC structure (head group, trihydroxy LCB moiety, α-hydroxylated VLCFA moiety) cause developmental phenotypes in *A. thaliana* (Chen *et al.*, 2008; Bach *et al.*, 2011; Markham *et al.*, 2011; König *et al.*, 2012; Molino *et al.*, 2014). Molino *et al*. (2014) observed malformed cell plates in root tip cells in which synthesis of VLCFA-containing sphingolipids, mainly GIPCs, is inhibited by fumonisin B1. Cell plates were either incomplete or were tilted, and their alteration was explained by defects in membrane fusion and vesicle trafficking. In *P. patens s4h* protonema cells the cross-walls resulting from cytokinesis still appeared to be formed normally, however, stretches of callose were observed reaching into the centre of both adjacent cells. The stretches resembled the microtubule network, which is responsible for transporting vesicles loaded with cell wall material towards the cell plate during cytokinesis. This phenotype suggests disturbed vesicle trafficking during cell division. The altered callose deposition at newly formed cross-walls in *P. patens* is a valuable indicator of the involvement of trihydroxy LCB-containing sphingolipids in cell division. Consistent with this hypothesis are findings from Luttgeharm *et al*. (2015), who reported that overexpression of the ceramide synthases LOH1 and LOH3 resulted in accumulation of sphingolipids with trihydroxy LCBs and VLCFAs (Luttgeharm *et al.*, 2015a). In consequence, the transgenic plants had higher biomasses that resulted in part from increased cell division. However, more detailed investigation of *P. patens* sphingolipid biosynthesis should be done to finally confirm the involvement of certain sphingolipid species in cytokinesis.

Callose deposition regulates the size exclusion limit of plasmodesmata (Vatén *et al.*, 2011; De Storme & Geelen, 2014). Plasmodesmata are symplastic channels that traverse the cell wall between two adjacent cells. They enable intercellular transport during growth and development by linking the cytoplasm and the ER of two cells (Gallagher *et al.*, 2014; Tilsner *et al.*, 2016). Their membrane is enriched in sterols and sphingolipids, the same lipids found in microdomains (Grison *et al.*, 2015; Liu *et al.*, 2020). Callose deposition is regulated by biosynthesis and degradation enzymes, which were found to be glycosylphosphatidylinositol- (GPI) anchored proteins (Simpson *et al.*, 2009; Zavaliev *et al.*, 2011). Impaired sterol biosynthesis affects localisation of callose metabolic enzymes, causing abnormal callose accumulation and thereby limiting plasmodesmal transport (Grison *et al.*, 2015). Recent studies confirmed that disruption of sphingolipid metabolism also alters callose deposition in response to *Botrytis cinerea* infection and at plasmodesmal sites (Bi *et al.*, 2014; Grison *et al.*, 2015; Liu *et al.*, 2020). If the callose dislocation in *P. patens s4h* also influenced plasmodesmal transport must be targeted in future studies.

Membrane studies in vascular plants like *A. thaliana* and *N. tabacum* are mainly restricted to protoplasts, root tips, or pollen tubes (Molino *et al.*, 2014; Moscatelli *et al.*, 2015; Lenarčič *et al.*, 2017; Huang *et al.*, 2019). Many studies also focused on mimicking lipid interactions by generating membrane model systems such as giant unilamellar vesicles (Wesołowska *et al.*, 2009; Grosjean *et al.*, 2015; Grosjean *et al.*, 2018). These systems, however, might not reflect the complexity and high dynamics of biological membranes in plant tissues. Studying the involvement of different sphingolipids in lateral partitioning and in interactions between domains of various order is still a challenging task. *P. patens* with its simple non-vascular morphology may facilitate detailed investigation of sphingolipid interactions *in planta*.

In summary, LCB hydroxylation has an important role in maintaining sphingolipid homeostasis in vascular and non-vascular plants, and loss of trihydroxy sphingolipids causes substantial growth defects. *P. patens* with its simple non-vascular morphology offers a valuable platform to study physiological and biochemical processes in complex and highly dynamic biological membranes. Together with findings from vascular plants and simple model membrane systems this may contribute in future studies to fully elucidate the physiological and metabolic function of sphingolipids.

Acknowledgements

We are grateful to Kirstin Feussner for critical reading of the manuscript and to Volker Lipka and Elena Petutschnig from the Central Microscopy Facility of the Faculty of Biology & Psychology for the use of CLSM microscope. J.G. has been a doctoral student of the Ph.D. program "Microbiology and Biochemistry" from the Göttingen Graduate Center for Neurosciences, Biophysics, and Molecular Biosciences (GGNB) at the Georg August University Göttingen.

FUNDING

I.F. acknowledges funding through the German Research Foundation (DFG, INST 186/822-1 and DFG, INST 186/1167-1).

Author Contribution

I.F. and J.G. designed the experiments. J.G. performed the experiments. E.H. assisted in designing the knockout construct that was used for homologous recombination. A.Z. performed CLSM investigations. J.G. performed and analysed the lipid measurements with the assistance of C.H.. J.G. wrote the manuscript. T.M.H. and I.F. edited the manuscript and I.F. supervised the study.

Supplemental material

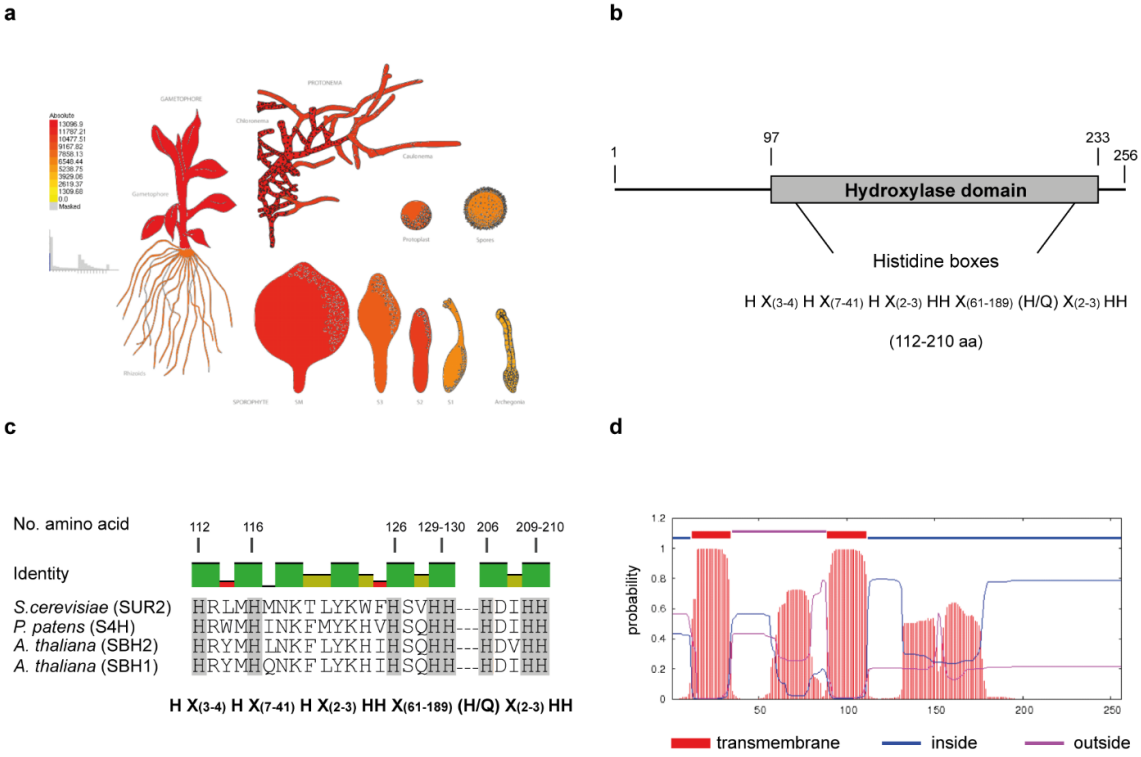

Fig. S1. Prediction data for gene expression, functional domains, and transmembrane domains. (a) Gene expression atlas was generated using eFP browser. (b) Information about hydroxylase domain prediction was found in the NCBI database. (c) Three characteristic histidine motifs were identified in *P. patens* S4H by alignment with amino acid sequences from *S. cerevisiae* SUR2 and *A. thaliana* SBH1 and SBH2. Histidine residues are highlighted in grey. (d) Transmembrane domain prediction was done using TMHMM webtool.

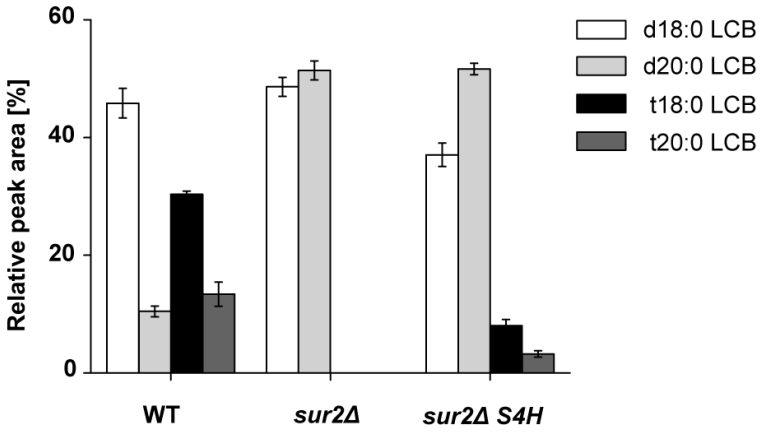

Fig. S2. Complementation of *S. cerevisiae sur2Δ* with *P. patens* S4H restores formation of free trihydroxy LCBs. Long-chain base (LCB) profiles of *S. cerevisiae* wild type (WT), *sur2Δ* knockout strain and *sur2Δ* knockout strain complemented with *P. patens* S4H are shown. LCB species are categorised into dihydroxy (d18:0, d20:0) or trihydroxy (t18:0, t20:0) LCBs with 18 or 20 LCB carbon chain lengths. Data represent the mean ± SD of four biological replicates.

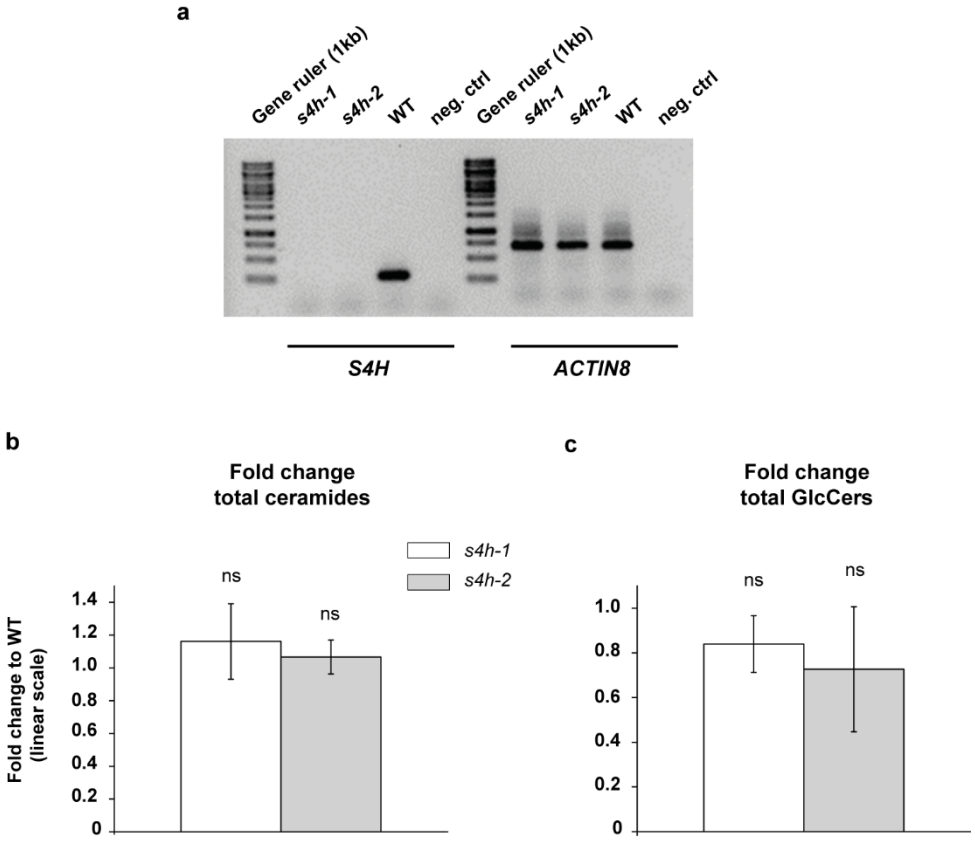

Fig. S3. *s4h* mutant characterisation and ceramide and GlcCer fold changes in *s4h* lines. (a) Complete gel picture of *S4H* transcript determination by reverse transcriptase PCR. *ACTIN8* was used as reference gene and water as negative control (neg. ctrl). (b, c) Ceramides and glycosylceramides (GlcCers) were extracted from protonema of ten-day-old wild type (WT), *s4h-1*, and *s4h-2 P. patens* and analysed with UPLC-nanoESI-MS/MS. Fold changes of (b) total ceramides and (c) GlcCers were calculated using absolute peak areas. Fold changes are depicted in linear scale. The WT, which is not shown, is set to 1. Sphingolipid data represent the mean ± SD of measurements from four independent cultivations each containing protonema material from eight cultivation plates. Statistical analysis was done using Student's *t*-test. Asterisks indicate different significance levels with not significant (ns) at $P > 0.05$ compared to the WT. Abbreviations are as follows: kb: kilo base.

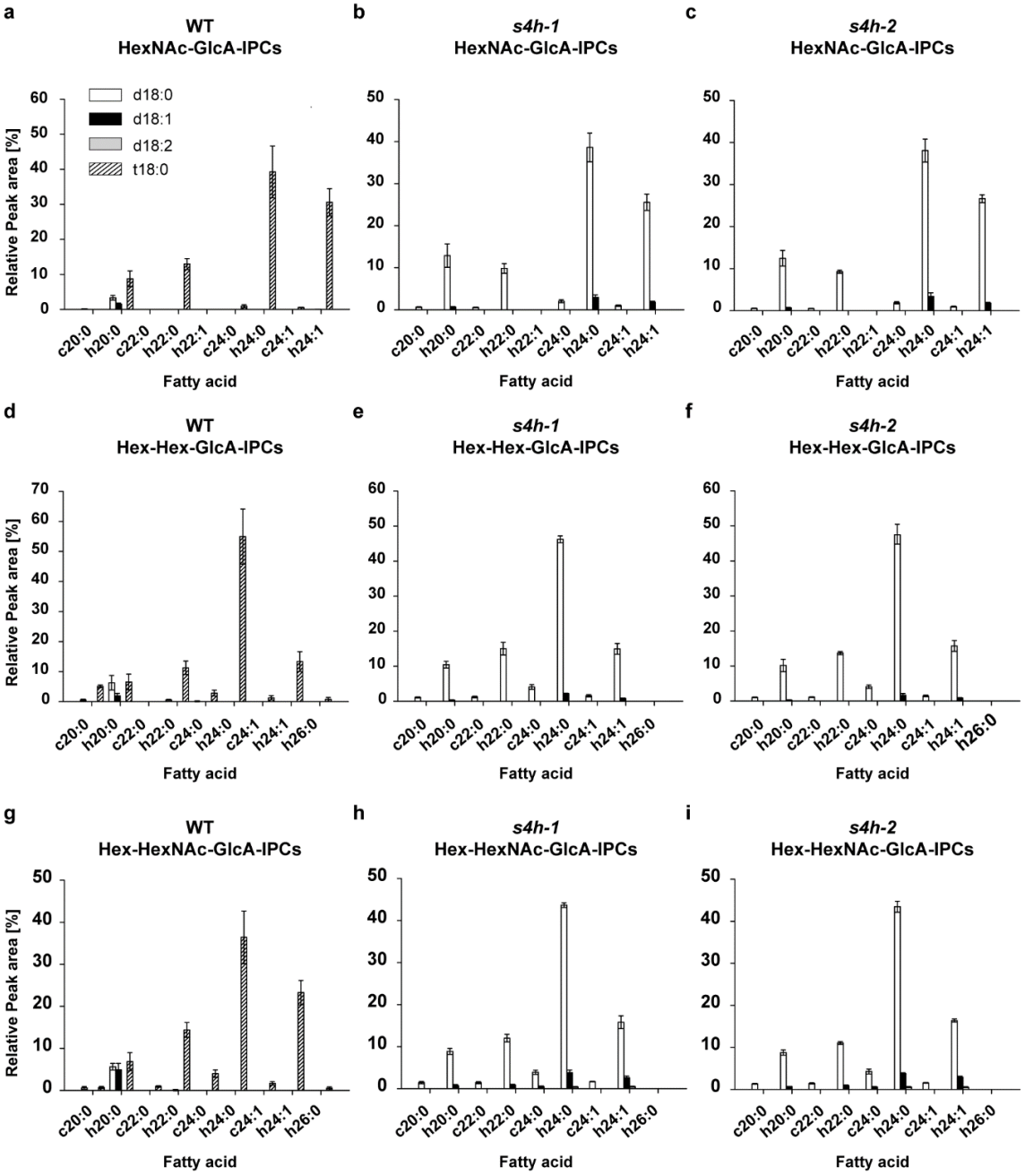

Fig. S4. *s4h-1* and *s4h-2* have altered GIPC profiles. Glycosyl inositolphosphorylceramides (GIPCs) were extracted from microsomes prepared from protonema of ten-day-old wild type (WT), *s4h-1*, and *s4h-2 P. patens* and analysed with UPLC-nanoESI-MS/MS. GIPC molecular species are shown with their long-chain base (LCB) (column colour) and fatty acid (x-axis) moieties. Dihydroxy LCB moieties are indicated by a 'd' and trihydroxy LCB moieties are indicated by a 't'. Molecular species with an unhydroxylated fatty acid moiety are indicated by a 'c' and molecular species with an α-hydroxylated fatty acid moiety are indicated by an 'h'. Relative HexNAc-GlcA-IPC profiles of (a) WT, (b) *s4h-1*, and (c) *s4h-2*. (d-f) Relative Hex-Hex-GlcA-IPC profiles of (d) WT, (e) *s4h-1*, and (f) *s4h-2*. (g-i) Relative Hex-HexNAc-GlcA-IPC profiles of (g) WT, (h) *s4h-1*, and (i) *s4h-2*. Only molecular species with a peak area ≥ 0.5 % in at least one of the three lines were included in the GIPC graphs. Sphingolipid data represent the mean ± SD of measurements from four independent cultivations each containing protonema material from eight cultivation plates. Abbreviations are as follows: GlcA: glucuronic acid; Hex: hexose; HexNAc: *N*-acetylhexosamine; IPCs: inositolphosphorylceramides.

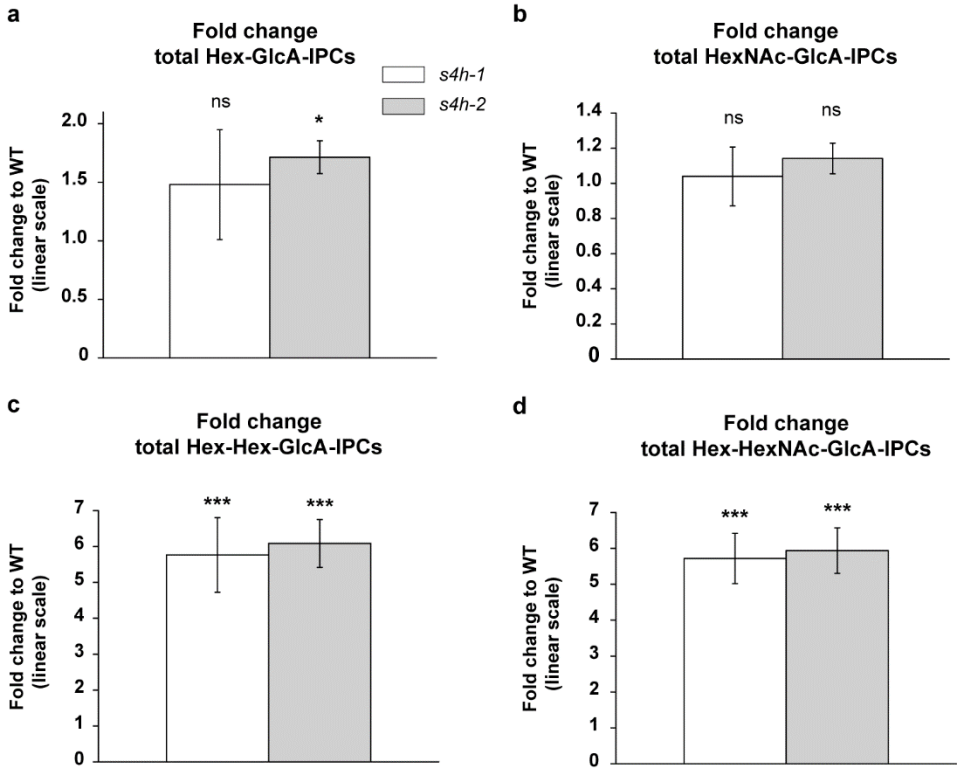

Fig. S5. Series B GIPCs strongly accumulate in *s4h-1* and *s4h-2*. Glycosyl inositolphosphorylceramides (GIPCs) were extracted from microsomes prepared from ten-day-old wild type (WT), *s4h-1*, and *s4h-2 P. patens* protonema and analysed with UPLC-nanoESI-MS/MS. Fold changes of (a) Hex-GlcA-IPCs, (b) HexNAc-GlcA-IPCs, (c) Hex-Hex-GlcA-IPCs, and (d) Hex-HexNAc-GlcA-IPCs were calculated using absolute peak areas. Fold changes are depicted in linear scale. The WT, which is not shown, is set to 1. Sphingolipid data represent the mean ± SD of measurements from four independent cultivations each containing protonema material from eight cultivation plates. Statistical analysis was done using Student's *t*-test. Asterisks indicate different significance levels with *** significance at $P < 0.001$, * significance at $P < 0.05$ and not significant (ns) at $P > 0.05$ compared with the WT. Abbreviations are as follows: GlcA: glucuronic acid; Hex: hexose; HexNAc: *N*-acetylhexosamine; IPCs: inositolphosphorylceramides.

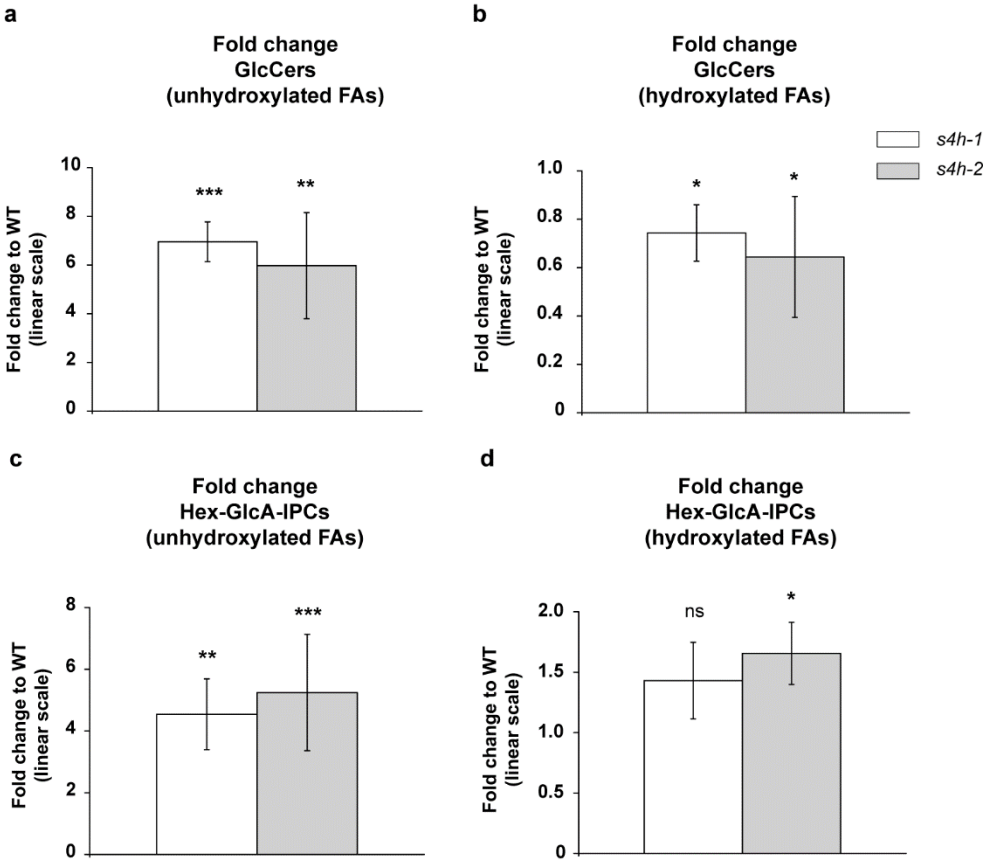

Fig. S6. Molecular species with unhydroxylated fatty acid accumulate in *s4h-1* and *s4h-2*. Sphingolipids were analysed with UPLC-nanoESI-MS/MS. (a, b) Glycosylceramides (GlcCers) were extracted from ten-day-old wild type (WT), *s4h-1*, and *s4h-2 P. patens* protonema. (c, d) Hex-GlcA-IPCs were extracted from microsomes prepared from ten-day-old WT, *s4h-1*, and *s4h-2 P. patens* protonema. (a-d) Fold changes of (a) GlcCers with unhydroxylated fatty acids (FAs), (b) GlcCers with hydroxylated FAs, (c) Hex-GlcA-IPCs with unhydroxylated FAs, and (d) Hex-GlcA-IPCs with hydroxylated FAs were calculated using absolute peak areas. Fold changes are depicted in linear scale. The WT, which is not shown, is set to 1. Sphingolipid data represent the mean ± SD of measurements from four independent cultivations each containing protonema material from eight cultivation plates. Statistical analysis was done using Student's *t*-test. Asterisks indicate different significance levels with *** significance at $P < 0.001$, ** significance at $P < 0.01$, * significance at $P < 0.05$, and not significant (ns) at $P > 0.05$ compared with the WT. Abbreviations are as follows: GlcA: glucuronic acid; Hex: hexose; HexNAc: *N*-acetylhexosamine IPCs: inositolphosphorylceramides.

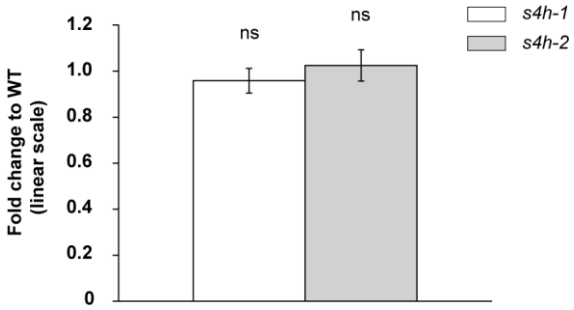

Fig. S7. Total levels of steryl glycosides are not affected in *s4h-1* and *s4h-2*. Steryl glycosides (SG) were extracted from microsomes prepared from ten-day-old wild type (WT), *s4h-1*, and *s4h-2 P. patens* protonema and analysed with UPLC-nanoESI-MS/MS. SG fold changes were calculated using absolute peak areas. Fold changes are depicted in linear scale. The WT, which is not shown, is 1. SG data represent the mean ± SD of measurements from four independent cultivations each containing protonema material from eight cultivation plates. Statistical analysis was done using Student's *t*-test with not significant (ns) at $P > 0.05$ compared to the WT.

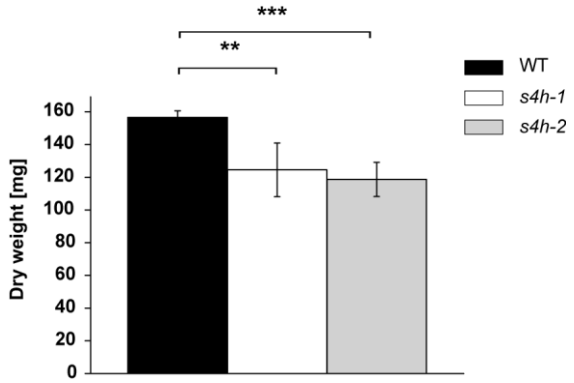

Fig. S8. Dry weight protonema biomass of *P. patens* wild type, *s4h-1*, *and s4h-2*. Growth of the wild type (WT), *s4h-1*, and *s4h-2* lines was quantified by collecting and lyophilising ten-day-old protonema grown on cellophane-covered BCD medium and determining the dry weight. Data represent the mean ± SD of measurements from four independent cultivations each containing protonema material from eight cultivation plates. Statistical analysis was done using Student's *t*-test. Asterisks indicate significance level with *** significance at $P < 0.001$ and ** significance at $P < 0.01$ compared to the WT.

5 Chapter 3

Sphingolipid Δ4-desaturation is an important regulatory mechanism in *Physcomitrella patens* for GlcCer formation

The article is ready for submission. The supplemental material can be found at the end of the main part.

Author contribution:

Jasmin Gömann generated additional *gcs* knockout mutants by CRISPR-Cas9. She confirmed the mutations in all used mutant lines by investigating the *sd4d and gcs* genotype and chemotype. She maintained and cultivated the *P. patens* wild type and mutant material for subsequent lipid and phytohormone analyses. She planned and performed the phytohormone and lipid extractions. She performed lipid measurements using UPLC-nanoESI-MS/MS. She analysed and processed the lipid data. She further maintained and cultivated the *P. patens* wild type and mutant material for subsequent macro- and microscopic phenotype investigation. She designed and performed the experiments for the phenotype characterisation of the *P. patens sd4d-1 and gcs-1* mutants using different cultivation strategies to selectively analyse various developmental stages. Finally, she displayed, interpreted, and discussed the results and wrote the first draft of the manuscript.

The work of this chapter was first published online as accepted manuscript by *Journal of Experimental Botany* on the 10th of June 2021. The accepted manuscript is a shortened version of this chapter. It additionally contains an overview of the sphingolipid metabolic pathway.

Gömann, J., Herrfurth C., Zienkiewicz, K., Haslam, T.M. and Feussner, I. (2021), Sphingolipid Δ4-desaturation is an important metabolic step for glycosylceramide formation in *Physcomitrium patens*, *Journal of Experimental Botany*, erab238, https://doi.org/10.1093/jxb/erab238

Sphingolipid Δ4-desaturation is an important regulatory mechanism in *Physcomitrella patens* for GlcCer formation

Jasmin Gömann[1], Cornelia Herrfurth[1,2], Krzysztof Zienkiewicz[1], Tegan M. Haslam[1], Ivo Feussner[1,2,3*]

[1]University of Goettingen, Albrecht-von-Haller-Institute for Plant Sciences, Department of Plant Biochemistry, D-37077, Goettingen, Germany.
[2]University of Goettingen, Goettingen Center for Molecular Biosciences (GZMB), Service Unit for Metabolomics and Lipidomics, D-37077 Goettingen, Germany.
[3]University of Goettingen, Goettingen Center for Molecular Biosciences (GZMB), Department of Plant Biochemistry, D-37077 Goettingen, Germany.

E-mail address for each author:
jasmin.goemann@stud.uni-goettingen.de
cornelia.herrfurth@biologie.uni-goettingen.de
krzysztof.zienkiewicz@biologie.uni-goettingen.de
tegan.haslam@biologie.uni-goettingen.de

*Correspondence: Ivo Feussner, e-mail: ifeussn@uni-goettingen.de,
Tel: +49-551-3925743, ORCID iD: 0000-0002-9888-700

Abstract

Glycosylceramides (GlcCers) are abundant components of plant membranes. They were associated with processes such as cell differentiation, organogenesis, intracellular membrane trafficking, and protein secretion. LCB Δ4-desaturation was described as a crucial structural feature responsible for metabolic channeling of sphingolipids into GlcCer formation in plants and fungi. However, LCB Δ4-unsaturated GlcCers are restricted in *Arabidopsis thaliana* to pollen and floral tissue, indicating that LCB Δ4-desaturation has a less important overall physiological role in *A. thaliana*. In *P. patens*, Δ4-desaturation is a typical structural modification of the LCB moiety of most abundant GlcCers. The *P. patens* sphingolipid Δ4-desaturase, *Pp*SD4D, and the glycosylceramide synthase, *Pp*GCS were identified as single genes via sequence similarity to the respective, characterised *A. thaliana* proteins. *P. patens* null mutants of the two genes, *sd4d-1* and *gcs-1*, were generated by homologous recombination and CRISPR-Cas9. Changes in the sphingolipidomes of both mutants were determined via UPLC-nanoESI-MS/MS measurements. *sd4d-1* and *gcs-1* plants were both devoid of almost all GlcCers. *gcs-1* plants additionally accumulated hydroxyceramides relative to the wild type. *gcs-1* mutants were strongly impaired in growth and development. The mutant plants were unable to differentiate into skotonema cells, they had dwarfed gametophores, and showed cell death-like lesions. Additionally, *gcs-1* plants had elevated levels of OPDA and *dn*-OPDA and showed upregulation of the defence-related marker genes. *sd4d-1* plants, however, mostly resembled wild type morphology and only exhibited minor cell elongation defects. Taken together, the results indicate that LCB Δ4-desaturation is a prerequisite for GlcCer formation in *P. patens*. Similar to the situation in vascular plants, *P. patens* GlcCers are likely involved in cell differentiation processes, however, their quantitative relevance in the moss has yet to be determined.

Key words: LCB desaturation, glycosylceramide (GlcCer), non-vascular plants, *Physcomitrella patens*, plant development, programmed cell death (PCD), sphingolipid Δ4-desaturase, sphingolipid metabolism

Introduction

Sphingolipids are essential structural elements in eukaryotic membranes. They represent up to 40 mol % of plant plasma membrane lipids (Tjellström *et al.*, 2010; Cacas *et al.*, 2016; Luttgeharm *et al.*, 2016). Together with sterols they form so called micro- and nanodomains that are thought to act as sorting platforms for membrane proteins (Borner *et al.*, 2005; Grosjean *et al.*, 2015; Grosjean *et al.*, 2018). Sphingolipids can further act as second messengers during developmental processes, abscisic acid-mediated guard cell closure, and in response to biotic and abiotic stresses (Shi *et al.*, 2007; Alden *et al.*, 2011; Chen *et al.*, 2012; Guo *et al.*, 2012; Guo & Wang, 2012).

Their involvement in a multitude of plant physiological processes likely results from the large structural diversity among sphingolipids. All plant sphingolipids have the same characteristic non-polar backbone consisting of a long-chain base (LCB). Plant LCBs typically have a chain length of 18 carbon atoms and may be *N*-acylated to a long-chain fatty acid (LCFA) or a very-long-chain fatty acid (VLCFA). LCBs that are connected to fatty acids are called ceramides. The chain length of the fatty acid moiety of plant sphingolipids ranges from 16 to 26 carbon atoms. Structural modifications such as hydroxylation and desaturation in the LCB and in the fatty acid moieties substantially increase the diversity of the sphingolipid pool.

The simpler sphingolipid classes, LCBs and ceramides, are low abundant molecules which represent around 2 % and 0.5 %, respectively, of all sphingolipids in *Arabidopsis thaliana* leaves (Markham *et al.*, 2006; Markham & Jaworski, 2007). They are important messenger molecules in different cellular functions including programmed cell death (PCD) (Greenberg *et al.*, 2000; Liang *et al.*, 2003; Shi *et al.*, 2007; Alden *et al.*, 2011).

Most plant sphingolipids have a polar head group attached to their non-polar ceramide backbone. These sphingolipids are referred to as complex sphingolipids and are divided into two classes: Glycosylceramides (GlcCers) and glycosyl inositolphosphorylceramides (GIPCs). GlcCers contain one sugar residue as head group and are the simplest complex sphingolipids. GIPCs contain an inositol-1-phosphate with up to seven different sugar moieties (Buré *et al.*, 2011; Cacas *et al.*, 2013). GlcCers and GIPCs are the most abundant plant sphingolipids and represent around 34 % and 64 % of all sphingolipids in *A. thaliana* leaves, respectively (Markham *et al.*, 2006). Complex sphingolipids have structural functions in plant membranes and the relative abundance and composition of each class influences the plant's ability to respond to abiotic stresses such as drought and cold stress (Ng *et al.*, 2001; Coursol *et al.*, 2003; Nagano *et al.*, 2014). Complex sphingolipid composition likely affects trafficking of secretory proteins and signal transduction during cellular processes through the formation of microdomains (Simons & Toomre, 2000; Melser *et al.*, 2010).

Whether sphingolipid species are channelled into GlcCer or GIPC formation is determined by certain LCB modifications. After their formation, LCBs harbour two hydroxyl groups at the C-1 and C-3 position that derive from their precursor molecules serine and acyl-CoA. The initial LCBs are thus referred to as dihydroxy LCBs, or in short d18:0 when palmitoyl-CoA was the acyl-CoA substrate. A third hydroxyl group may be introduced at the C-4 position through the action of an LCB C-4 hydroxylase (Sperling *et al.*, 2001; Chen *et al.*, 2008). The resulting LCBs are referred to as trihydroxy LCBs, or in short t18:0. The dihydroxy LCB moiety is enriched in GlcCers while trihydroxy LCBs are enriched in GlcCers and GIPCs (Markham *et al.*, 2006).

Another crucial modification is the insertion of double bonds into the LCB moiety. Double bonds may be introduced at the Δ4 or at the Δ8 position by the activity of distinct LCB desaturases (Napier *et al.*, 2002). LCB C-4 hydroxylation and LCB Δ4-desaturation both act on the C-4 position of d18:0 LCBs and are therefore mutually exclusive. Hence, insertion of two double bonds can only occur in a d18:0 but not in a t18:0 LCB moiety. Resulting LCBs are referred to as d18:1 or d18:2 and t18:1, depending on the hydroxylation state of the LCB moiety and on the number of inserted double bonds. Sphingolipids with a $t18:1^{\Delta 8}$ LCB moiety predominate in all *A. thaliana* sphingolipid classes and in other Brassicaceae species (Imai *et al.*, 2000). LCB Δ8-desaturation is therefore considered an important reaction during *A. thaliana* sphingolipid biosynthesis. Expression of the LCB Δ4-desaturase (At4g04930), however, is limited to *A. thaliana* floral and pollen tissue (Michaelson *et al.*, 2009). LCB Δ4-desaturation is therefore considered a less important LCB modification during *A. thaliana* sphingolipid biosynthesis. However, the LCB Δ4-desaturase appears to play a more important role in other plant species outside the Brassicaceae family. In tomato (*Solanum lycopersicum*) and soybean (*Glycine max*), LCB Δ4-desaturation mostly occurs in combination with LCB Δ8-desaturation and the resulting Δ4,8-diunsaturated LCB moiety is enriched in GlcCers throughout the plant (Sperling *et al.*, 2005; Markham *et al.*, 2006). Marine plants may further contain sphingolipid species with an LCB moiety that contains more than two double bonds. For instance, in the alga *Thalassiosira pseudonana* a diglycosylceramide was detected that had a ceramide backbone composition with a d18:3 LCB moiety and a C24:0 fatty acid moiety (Hunter *et al.*, 2018).

The physiological role of the LCB Δ4-desaturase was investigated in *A. thaliana*. In contrast to the LCB Δ8-desaturase, the LCB Δ4-desaturase is not a cytochrome b5-fusion protein and exclusively introduces the double bond in *trans* configuration. LCB Δ4-desaturases therefore define a new class of desaturases (Napier *et al.*, 2002). Orthologs of mammalian and fungal LCB Δ4-desaturases were identified by sequence homology in plants like *A. thaliana*, rice (*Oryza sativa*) and tomato (Ternes *et al.*, 2002). Functional

characterisation of the *A. thaliana* LCB Δ4-desaturase was achieved by heterologous expression in a *Pichia pastoris* LCB Δ4-desaturase knockout mutant (Michaelson *et al.*, 2009). The *P. pastoris* LCB Δ4-desaturase knockout not only lacks Δ4-unsaturaturated sphingolipids but is also devoid of GlcCers. Expression of *A. thaliana* LCB Δ4-desaturase in the *P. pastoris* LCB Δ4-desaturase knockout restored GlcCer formation (Michaelson *et al.*, 2009). LCB Δ4-desaturase expression in *A. thaliana* is restricted to floral and pollen tissues. Although knockout of the LCB Δ4-desaturase caused a significant reduction in pollen GlcCer levels compared to the wild type, it had no effect on plant viability (Michaelson, 2009). Together, these studies suggest that LCB Δ4-desaturation has a minor role in the Brassicaceae family, but that it is a crucial modification for channelling ceramides into GlcCers in some plants and fungi.

The occurrence of LCB Δ4-unsaturated sphingolipids exemplifies how sphingolipid composition is tissue and organism dependent (Sperling *et al.*, 2005; Luttgeharm *et al.*, 2015b). This highlights the importance of choosing appropriate model systems to study individual molecular species and classes. While *A. thaliana* has been an invaluable model for studying plant metabolism in general, it has clear limitations for the study of sphingolipids, in particular Δ4-desaturation of LCBs.

To better understand the physiological role of Δ4-desaturation of LCB moieties, the research focus should therefore be directed towards plants outside the Brassicaceae family. Islam *et al*. (2012), surveyed 21 plant species from different phylogenetic groups to analyse the position of the double bond in the d18:1 LCB moiety to determine the prevalence of d18:1$^{\Delta4}$ and d18:1$^{\Delta8}$ in different plants. They found that d18:1$^{\Delta4}$ is evolutionary more ancient than d18:1$^{\Delta8}$. Among the 21 surveyed plants in that study was the bryophyte *Physcomitrella patens*. The d18:1 LCB moiety of *P. patens* has the double bond at the Δ4 position and therefore qualifies as suitable plant system to study the role of Δ4-unsaturated sphingolipids in land plants.

A recent study described the lipidome of *P. patens*, including the four sphingolipid classes: LCBs, ceramides, GlcCers, and GIPCs (Resemann, 2018). In the *P. patens* sphingolipidome ceramides with specific LCB modifications show distinct channelling into either the GlcCer or the GIPC pool. This observation is consistent with findings from fungi and vascular land plants, however, the presence of exclusive LCB modifications in distinct complex sphingolipid classes is stricter in *P. patens*. GlcCers exclusively carry a d18:2 LCB moiety in their backbone, whereas GIPCs only carry a t18:0 LCB moiety. This simplifies the study of physiological functions of distinct sphingolipid species. The data further suggests that LCB Δ4-desaturation is a requirement for GlcCer formation in *P. patens*. The physiological role of Δ4-unsaturated sphingolipids is therefore expected to be tightly bound to the role of GlcCers in plants.

Although GlcCers are the second most abundant sphingolipids found in *A. thaliana*, their physiological function is not fully understood. GlcCers are generated by the transfer of a glucose residue from uridine diphosphate (UDP)-glucose to the ceramide backbone. This reaction is catalysed by a glucosylceramide synthase (GCS). *A. thaliana* only has one *GCS* gene (At2g19880). *gcs* null mutants lacked all GlcCers and had a higher GIPC content than wild type plants. The mutants were seedling lethal and were impaired in cell-type differentiation and organogenesis (Msanne *et al.*, 2015).

In this study, the physiological roles of sphingolipids with a Δ4-unsaturated LCB moiety and of GlcCers were investigated in *P. patens*. The LCB Δ4-desaturase and the glycosylceramide synthase, designated here as *Pp*SD4D and *Pp*GCS, respectively, were both identified in *P. patens* by sequence similarity to their *A. thaliana* orthologs. Loss-of-function mutants were generated by homologous recombination and by CRISPR-Cas9. In both knockout mutants GlcCer formation was inhibited. The *sd4d-1* mutant additionally lacked Δ4-unsaturated LCB moieties in other sphingolipid classes. Although GlcCers were nearly absent in both mutants, *sd4d-1* and *gcs-1* plants were differently affected in their growth and development. *sd4d-1* plants had almost no morphological impairments whereas *gcs-1* plants had substantial growth and development defects. This indicates a less important role for Δ4-unsaturated LCB moieties in *P. patens* GlcCers than expected.

Materials and methods

Plant material and growth conditions

The *P. patens* ‘Gransden’ strain (Hedw.) Bruch & Schimp was used as wild type. Plants were grown at 16 h light/ 8 h dark cycle at 25 °C and with a light intensity of 50–70 µmol m^{-2} s^{-1}. Protonema was cultivated on BCD agar medium plates (90 mm diameter) containing 1 mM $CaCl_2$ and 5 mM ammoniumtartrate (BCDAT) (Ashton & Cove, 1977). For protonema cultivation, the medium plates were covered with sterile cellophane discs (folia, Wendelstein, Germany). For protonema maintenance and propagation one- to two-week-old tissue was scraped off the cellophane and disrupted in sterile water for 20 s using a tissue lyser (Ultra Turrax, Ika, Staufen, Germany). The cell suspension was spread onto fresh BCDAT plates. Plates were sealed with micropore tape before incubation.

Protonema material for lipid analysis was cultivated on cellophane-covered BCD plates. To be able to compare measurements of different mutant lines, the dry weight of the disrupted material was determined after tissue lyser treatment. All plate cultures were subsequently started with a cell suspension volume equal to 5 mg dry weight. To obtain enough amounts for lipid measurements, plant material grown on eight plates was pooled. The protonema was cultivated for ten days before harvesting, and the material was immediately frozen in liquid nitrogen after the harvest. Prior to lipid extraction, plant material

was lyophilised. Plant growth capacities were determined by determination of the fresh weight after harvesting and before freezing material in liquid nitrogen. Protonema was weighed again after lyophilisation for determination of the dry weight. This experiment was part of a larger experiment and the lipid data for wild type protonema were used recently in a different study as well (Gömann *et al.*, 2021).

For imaging of gametophore development, 1 mm spot inocula of seven- to ten-day-old protonemal tissue were placed on plates containing BCD medium with 1 mM $CaCl_2$. Fully grown gametophores were imaged after six weeks. For visualisation of protonema development, colonies were imaged after one to two weeks. Plates were sealed with micropore tape during cultivation.

For sporophyte induction, gametophores were cultivated as described above. After fully grown gametophores were observed five to six weeks after inoculation, plates were transferred to short day cultivation conditions with a light cycle of 8 h light/ 16 h hour dark at 17 °C and lower light intensity. Gametophores were grown under these conditions until gametangia development was observed. Plant colonies were subsequently flooded with sterile tap water and kept under the described conditions for another month before imaging.

Dark growth experiments for skotonema induction were performed as described in (Saavedra *et al.*, 2015). For this, protonema spot inocula were placed on square BCDAT plates supplemented with 2 % sucrose. Colonies were grown for one week under continuous light and subsequently moved to the dark and rotated into vertical orientation. Colonies were grown for another four weeks before imaging.

Images were captured using a binocular (Olympus SZX12 binocular, Olympus Corporation, Tokio, Japan) or a microscope (Olympus Corporation, Tokio, Japan) that were connected to a camera (R6 Retiga camera, QImaging, Surrey, Canada). Images were analysed with the Ocular scientific image acquisition software (version 1.0, Digital Optics Ltd, Auckland, New Zealand). Images were processed using ImageJ 1.52b software (Schneider *et al.*, 2012).

Generation of targeted knockout plasmids

Targeted knockout plasmids were assembled by cloning 750 bp fragments from the 5’ and the 3’ genomic DNA untranslated regions (UTR) of the respective *SD4D* and *GCS* genes into a pBluescript vector backbone. The 5’ and 3’ fragments flanked a kanamycin cassette for future selection of knockout mutants. The following primer pairs were used for *SD4D* cloning: 5' *Sac*I SD4D-fw (5'-gagctcATGGACTTCTACTGGGCTGAGG-3')/ 5' *BamH*I SD4D-rev (5'-ggatccTCCTGACTCTAAGAAAGAAAAGTATAG-3') and 3' *Hind*III SD4D-fw (5'-gtcgacCTTCTATGCGTTCAGGCCTCTC-3')/ 3' *Apa*I SD4D-rev (5'-gggcccTCAGTTGGTTTTGCCATGCTTTGTC-3'). The following primer pairs were used for

GCS cloning: 5' *Sac*I GCS-fw (5'-gagctcATGGCGTTTGTGGAGGCCATG -3')/ 5' *Xba*I GCS-rev (5'-tctagaCCAATACCTGACTACGCCAATTGC-3') and 3' *Hind*III GCS-fw (5'-aagcttGTGATTTTTGTGAACTCAGTGAAATTG-3')/ 3' *Apa*I GCS-rev (5'-gggcccTCATTGTACCTGACAAATGTTTCCATT-3'). Correct cloning of the fragments into the destination vector was confirmed by plasmid sequencing. To linearise the *SD4D* and *GCS* fragments used for *P. patens* homologous recombination, the restriction enzymes SacI and ApaI were used for both gene constructs.

P. patens transformation and molecular characterisation of knockout mutants

Knockout plants were generated via polyethylene glycol (PEG)-mediated transformation of *P. patens* protoplasts according to (Schaefer *et al.*, 1991).

The knockout constructs containing the 5' and 3' *SD4D* and *GCS* flanking regions and the kanamycin selection cassette were used for homologous recombination in *P. patens*.

To confirm the correct insertion of the selection cassette into the *P. patens* genome, genomic DNA (gDNA) was extracted from a small sample of gametophytic tissue. gDNA was isolated using cetyl trimethylammonium bromide (CTAB) extraction. In a first step, successful integration of the kanamycin selection cassette was confirmed by PCR using the following primer combination: (kan fw: 5'-ATGGGGATTGAACAAGATGGATTGCAC-3'/ kan rev: 5'-TCAGAAGAACTCGTCAAGAAGGC-3'). In a second PCR, insertion of the selection cassette into the *SD4D* and *GCS* sites was confirmed. Following primer combinations were used to confirm insertion into the *SD4D* locus: 5' UTR region (fw: 5'-GTGGTGTGGTTGCCGTCAAGAC-3'/ rev: 5'-TAGGGTTCCTATAGGGTTTCGCTC-3'), 3' UTR region (fw: 5'-GATAGCTGGGCAATGGAATCCG-3'/ rev: 5'-GCATATTGTGGGTGCTGATGATTAGG-3'). Following primer combinations were used to confirm insertion into the *GCS* locus: 5' UTR region (fw: 5'-GCAACAATGTGCCCGAGCAGATC-3'/ rev: 5'-TAGGGTTCCTATAGGGTTTCGCTC-3'), 3' UTR region (fw: 5'-GATAGCTGGGCAATGGAATCCG-3'/ rev: 5'-GATGCAGATGATAAGGAGAATCTCAGC-3').

Reverse transcription PCR verification of mutants

RNA was obtained from *P. patens* wild type and mutant gametophytic tissue using TRIzol™ Reagent according to manufacturer's instructions (Thermo Fisher Scientific, Waltham, Massachusetts, USA). Total RNA was treated with DNAseI (Thermo Fisher Scientific, Waltham, Massachusetts, USA) prior to cDNA synthesis. 1 µg of the DNAseI-treated RNA was used for cDNA synthesis. cDNA was synthesised using the RevertAid H Minus First Strand cDNA Synthesis Kit (Thermo Fisher Scientific, Waltham, Massachusetts, USA). The following primer pairs were used for amplification of *SD4D* (fw: 5'-

CCGGTTGCTTGGCATATTCG-3'/ rev: 5'-CAATGGGGTGCATACCACCT-3'), *GCS* (fw: 5'-CGCGTTATCAGCTCACCAGA-3'/ rev: 5'-TCCTTCCCAGGTGACAATGC-3') and *ACTIN8* transcript (fw: 5'-GCTGGTTTCGCTGGAGACGATGC-3'/ rev: 5'-ATCGTGATCACCTGCCCGTCC-3').

Gene editing by CRISPR-Cas9

CRISPR-Cas9 was performed using the plasmid pUC57-PpU6pro-2XBbsI-etracRNA obtained from and designed by Tegan M. Haslam. Gene expression was driven by the U6 promoter used in (Collonnier *et al.*, 2017). The inserted etracRNA was described in (Castel *et al.*, 2019). A dual *Bbs*I site was further introduced into the plasmid for cloning. Prediction of protospacers was done using the CRISPOR software (Haeussler *et al.*, 2016) (http://tefor.net/crispor/crispor.cgi). The single-guide RNA (sgRNA) gcs-1 was designed to target the first exon of *PpGCS*. Oligos for gcs-1 sgRNA Oligo 1 (5'-AACCGGGATGGCAGAACACTAAGC-3')/ gcs-1 Oligo 2 (5'-AAACGCTTAGTGTTCTGCCATCCC-3') were aligned and cloned into the pUC57-PpU6pro-2XBbsI-etracRNA vector. Successful cloning was confirmed by sequencing. The plasmid carrying the sgRNA was co-transformed with pAct-Cas9 (Collonnier *et al.*, 2017) and pBNRF (Schaefer *et al.*, 2010) that carries resistance to G418 (Geneticin) into *P. patens* protoplasts. PEG-mediated protoplast transformation was performed as described before. Putative knockout mutants were confirmed by sequencing of the PCR product using the following primer combination that surrounded the target sequence: gcs-1-fw (5'-GGAGATGCGGTGAGAAGAAAC-3')/ gcs-1-rev (5'-TAAACCCCCACGATCACTGC-3').

Heterologous expression in *S. cerevisiae sur2*Δ

The *P. patens SD4D and GCS* genes were artificially synthesised (Genscript, Piscataway Township, New Jersey, USA). During synthesis, genes were codon usage optimised for *S. cerevisiae* expression. *PpSD4D* and *PpSD8D* were cloned into the pESC-His yeast expression vector (Thermo Fisher Scientific, Waltham, USA). *PpGCS* was cloned into the pYES2-CT yeast expression vector (Thermo Fisher Scientific, Waltham, USA). *P. patens PpSD8D* was amplified from *P. patens* cDNA and the first 60 bp of the coding sequence were codon usage optimised for *S. cerevisiae* gene expression using the following primer combination: PpSD8D-fw (5'-ATGGGTCCATTGGCTGCTGAAGACGAATTGGGTTCTTTCCCACAAGAATTGAAGGTTGAC-3')/ PpSD8D-rev (5'-TCAACCCTTGGAGTTCACAG-3') The following primer combinations were used to clone the genes into the multiple cloning sites (MCS) of the pESC-His vector. *PpSD4D* was cloned into MCS2 with *BamH*I-SD4D-fw (5'-GGAGGATCCAAACGATGTCAGATGTTGGAG-3')/ *Sal*I-SD4D-rev (5'-

GGAGTCGACGTTAGTTTTTCCGTGTTT-3'). PpSD8D was cloned into MCS1 with *Not*I-SD8D-fw (5'-GGAGCGGCCGCAAACGATGGGTCCATTGGCTGCTG-3')/ *Spe*I-SD8D-rev (5'-GGAACTAGTGCACCCTTGGAGTTCACAGC-3'). *PpGCS* was cloned into the pYES2-CT vector with *BamH*I-GCS-fw (5'-GGAGGATCCAAACGATGGCATTCGTTGAAGC-3')/ *Xho*I-GCS-rev (5'-GGACTCGAGAGAGTTTTTCAATTTACAAGA-3'). Gene constructs were transformed into the *S. cerevisiae* LCB C-4 hydroxylase *sur2*Δ mutant (Desfarges *et al.*, 1993; Haak *et al.*, 1997) using LiAc/SS carrier DNA/PEG method according to (Gietz & Schiestl, 2007). The BY4741 *S. cerevisiae* strain was used as corresponding wild type strain for the *sur2*Δ knockout. Yeast cells were grown in pre-cultures for 24 h in the respective single dropout (SD) medium (for pYES2-CT transformants without uracil, for pESC-His transformants without histidine) and with 2 % glucose. Main cultures were inoculated with the cells to a final OD_{600} of 0.02 in SD dropout medium without uracil and with 2 % galactose and 2 % raffinose. Main cultures were grown for 24 h. All yeast cultivations were performed at 30 °C in non-aerated shaking flasks. Harvesting was done by spinning cells down at 3000 g for 10 min. Cells were washed with water and stored at -80 °C. Yeast cells were lyophilised before lipids were extracted.

Sphingolipid extraction and analysis

Sphingolipid extraction was achieved by application of the lipid extraction protocol described in (Grillitsch *et al.*, 2014) with minor modifications. Lipids were extracted from 20 mg of lyophilised and homogenised *P. patens* protonema or *S. cerevisiae* material. The tissue was extracted at 60 °C using an extraction solvent composed of propan-2-ol/hexane/water (60:26:14, v/v/v). Lipids were re-suspended in 800 µL of a final solvent mixture composed of tetrahydrofuran/methanol/water (4:4:1, v/v/v). Samples were chemically modified or directly analysed with ultra-performance liquid chromatography (UPLC) coupled with nanoelectrospray ionisation (nanoESI) and triple quadrupole tandem mass spectrometry (MS/MS) (AB Sciex, Framingham, Massachsetts, USA) for LCB measurement.

Methylamine treatment

Lipid extracts were treated with methylamine solution for the analysis of ceramides, GlcCers and GIPCs. 50 µL of the lipid extract were evaporated. Dried lipids were re-suspended in 1.4 mL 33 % (w/v) methylamine dissolved in ethanol and 600 µL of water (Markham & Jaworski, 2007). The methylamine/lipid mixture was incubated for 1 h at 50 °C. The solvent was subsequently evaporated and dried lipids were dissolved in 50 µL of the final solvent mixture composed of tetrahydrofuran/methanol/water (4:4:1, v/v/v). The samples were used for UPLC-nanoESI-MS/MS analysis.

Derivatisation with acetic anhydride

Phosphorylated LCBs (LCB-Ps) were detected after acetic anhydride derivatisation using a modified protocol from (Berdyshev *et al.*, 2005). After 50 µL of the lipid extract were evaporated, the dried lipids were dissolved in 100 µL pyridine and 50 µL acetic anhydride. Derivatisation was performed at 50 °C for 30 min. The solvent mixture was subsequently evaporated, and samples were dissolved in 50 µL tetrahydrofuran/methanol/water (4:4:1, v/v/v). The samples were used for UPLC-nanoESI-MS/MS analysis.

Lipid analysis

Molecular lipid species measurement was performed using the UPLC-nanoESI-MS/MS with multiple reaction monitoring (MRM) approach described in (Resemann, 2018). LCB-Ps were measured in negative ionisation mode with $[M-H]^-$ as precursor ions. Series A and series B GIPC classes were analysed in positive ionisation mode with $[M+NH_4]^+$ as precursor ions and ceramide fragments as fragment ions. Determination of head group-specific ions was done as described before (Buré *et al.*, 2011). LC-MS data were processed using Analyst 1.6.2 and MultiQuant 3.0.2 software (both AB Sciex, Framingham, Massachusetts, USA).

Gene expression analysis by quantitative real-time PCR (qRT PCR)

RNA was extracted from two-week-old protonema tissue grown on cellophane-covered BCDAT medium using the TRIzol™ Reagent (Thermo Fisher Scientific, Waltham, USA) and cDNA was synthesised as described before. qRT PCR analyses were done using the Takyon™ No Rox SYBR® MasterMix dTTP Blue (Eurogentec Deutschland GmbH, Köln, Germany) in the iQTM5 RT PCR detection system according to the manufacturer's instructions. Adenine phosphoribosyltransferase (Ade PRT) (Le Bail *et al.*, 2013) was used as reference gene. Normalisation was done using the 2-ΔΔCT method (Livak & Schmittgen, 2001). The following primer combination was used for *Ade PRT* amplification: Ade PRT_fw: 5'-AGTATAGTCTAGAGTATGGTACCG-3' and Ade PRT_rev: 5'-TAGCAATTTGATGGCAGCTC-3' (Le Bail *et al.*, 2013). Primer combinations for amplification of the defence-related marker genes phenylalanine lyase 4 (*PAL4*), chalcone synthase (*CHS*), and the transcription factor ethylene-responsive element-binding factor 5 (*ERF5*) were: PAL4_fw: 5'-TGGCCTACTCGGTAATGGAG-3'/ PAL4_rev: 5'-GTCAACCATCCGCTTGATTT-3', CHS_fw: 5'-GGCATGGAACGAGATGTTCT-3'/ CHS_rev: 5'-CCTTGCATCTTGTCCTTGGT-3', ERF5_fw: 5'-GCTCCGCTGTATCGAAAGTC-3'/ ERF5_rev: 5'-TCGAAGTTGCTGACAAGGTG 3' all from (Bressendorff, 2012).

Phytohormone extraction and analysis

Phytohormone extraction was done according to (Matyash *et al.*, 2008) with minor modifications. Phytohormones were extracted from 10 mg of lyophilised and homogenised *P. patens* protonema. The protonema was grown for ten days on cellophane-covered BCD medium. The material was pooled from eight 90 mm petri dishes. Phytohormone measurement and analysis was done according to (Herrfurth & Feussner, 2020).

Webtools

BLAST search

P. patens sphingolipid Δ4-desaturase, sphingolipid Δ8-desaturase and glycosylceramide synthase were identified via sequence homology to the corresponding *A. thaliana* proteins. BLAST search using the NCBI proteome database for *P. patens* from the National Center for Biotechnology Information (NCBI) (U.S. National Library of Medicine, Maryland, USA) (http://www.ncbi.nlm.nih.gov/BLAST/) for *P. patens* (Altschul *et al.*, 1990).

Transmembrane domain prediction

Transmembrane domain prediction for *Pp*SD4D and *Pp*GCS was done using the TMHMM software (Sonnhammer *et al.*, 1998; Krogh *et al.*, 2001).

Gene expression

Information about *PpSD4D* and *PpGCS* gene expression was obtained using *P. patens* electronic fluorescent pictograph (eFP) browser (http://www.bar.utoronto.ca) (Winter *et al.*, 2007; Ortiz-Ramírez *et al.*, 2016).

Results

Sequence similarity indicates *PpSD4D* and *PpGCS* are single genes with similar expression patterns in *P. patens*

Candidate proteins homologous to the characterised sphingolipid Δ4-desaturase (At4g04930) (Michaelson *et al.*, 2009) and the glucosylceramide synthase (GCS) (At2g19880) (Msanne *et al.*, 2015) from *A. thaliana* were identified in the *P. patens* proteome via BLAST search in the NCBI database. *Pp*SD4D (XP_024361943.1) and *Pp*GCS (XP_024399720.1) had 63 % and 57 % identity, respectively, to their corresponding *A. thaliana* orthologs. Based on sequence similarity of the *P. patens* enzymes, both proteins are considered to be encoded by single genes. The cDNA of *PpSD4D* encoded an enzyme of 382 amino acids. Like its *A. thaliana* counterpart, *Pp*SD4D did not have an N-terminal cytochrome b5 fusion domain (Napier *et al.*, 1999; Sperling *et al.*, 2003). *Pp*SD4D included three histidine boxes that are characteristic for membrane-bound desaturases and

hydroxylases and that coordinate the di-iron cluster in the active site (Shanklin & Cahoon, 1998; Bai *et al.*, 2015). The cDNA of *Pp*GCS encodes an enzyme of 518 amino acids with a conserved glycosyl transferase domain.

Using the webtool TMHMM, transmembrane domains were predicted for both proteins (Fig. S1A, B). According to this prediction, *Pp*SD4D contained four and *Pp*GCS contained two transmembrane domains. Enzymes involved in sphingolipid biosynthesis, including the GCS, are located in the endoplasmic reticulum (ER) in *A. thaliana* (Melser *et al.*, 2010). The presence of transmembrane domains in the *P. patens* proteins is therefore consistent with the assumption that they are also localised to the ER. The expression pattern reported in the eFP browser (Winter *et al.*, 2007; Ortiz-Ramírez *et al.*, 2016) revealed that *PpSD4D* and *PpGCS* had similar expression in *P. patens* tissues (Fig S1C, D). Highest expression was found in the protonema, the spores, and the sporophyte generation. *PpGCS* had a generally higher expression than *PpSD4D*. *PpSD4D* appeared to be especially upregulated in caulonema cells whereas *PpGCS* is highly expressed throughout the whole protonema. These similar expression patterns are in agreement with the notion that both genes could contribute to the same processes. This idea is supported by the *P. patens* sphingolipid profile identified by (Resemann, 2018), in which LCB Δ4-desaturation seems to be a prerequisite for GlcCer formation.

S. cerevisiae is an unsuitable host for functional characterisation of *Pp*SD4D and *Pp*GCS

To confirm the predicted enzymatic activities of both proteins, the open reading frames were codon usage optimised and heterologously expressed in *S. cerevisiae*. *S. cerevisiae* does endogenously not contain an LCB Δ4-desaturase. However, LCB C-4 hydroxylation, which is an abundant modification in yeast sphingolipids, and LCB Δ4-desaturation both work on the C-4 LCB position and therefore exclude each other. Functional characterisation of the LCB Δ4-desaturase therefore had to be performed with the LCB C-4 hydroxylase knockout mutant *sur2Δ* (Haak *et al.*, 1997). The enzymatic functions of several mammal and fungal LCB Δ4-desaturases were already successfully verified using this yeast expression system (Ternes *et al.*, 2002). However, *S. cerevisiae* turned out to be an unsuitable host for the functional characterisation of vascular plant LCB Δ4-desaturases, including the *A. thaliana* and the tomato enzymes (Sperling & Heinz, 2003). Napier *et al*. (2002) speculated that plant LCB Δ4-desaturases might require some plant-specific substrates or co-factors that are yet unknown. Dunn *et al*. (2004) further suggested that the substrate for LCB Δ4-desaturases in vascular plants might be the d18:1$^{\Delta 8}$-unsaturated LCB moiety. This was speculated because the Δ4,8-diunsaturated LCB moiety is common in plants while the d18:1$^{\Delta 4}$ LCB moiety is only found in trace amounts. *S. cerevisiae* does endogenously not contain

GlcCers and Δ8-unsaturated LCBs. To overcome this issue, Ternes *et al*. (2006) engineered a *S. cerevisiae* strain for the functional characterisation of the *P. pastoris* C9-methyltransferase. C9-methylation is an abundant LCB modification in GlcCers of fungi sphingolipids (Ternes *et al.*, 2006). *In vitro* characterisation of the enzyme activity required the presence of GlcCers with a Δ4,8-diunsaturated LCB moiety. The authors successfully expressed the *P. pastoris* LCB Δ4- and Δ8-desaturases, the human glucosylceramide synthase, and the *P. pastoris* C9-methyltransferase in *S. cerevisiae sur2Δ* cells. They thereby confirmed the formation of GlcCers in *S. cerevisiae*, showing that the engineered strain is an appropriate host for the confirmation of GlcCer production. Taking these results into consideration, *PpSD4D* was expressed alongside the *P. patens* LCB Δ8-desaturase in *sur2Δ* cells. Having both double bonds integrated into the LCB backbone would also putatively enable *Pp*GCS activity in this system. The composition of the *P. patens* GlcCer pool (Resemann, 2018) suggested that the preferred substrate of *Pp*GCS is a ceramide with a d18:2 LCB moiety. In this study, a similar attempt to the strategy from Ternes *et al*. (2006) was therefore applied to confirm *Pp*SD4D and *Pp*GCS enzymatic activities (Ternes *et al.*, 2006). *Pp*GCS and the two sphingolipid desaturases, *Pp*SD4D and *Pp*SD8D were simultaneously expressed in *S. cerevisiae sur2Δ*. Unfortunately, neither *Pp*GCS activity nor *Pp*SD4D or *Pp*SD8D activities were detected. Further work should determine whether the transcripts and proteins were present in the transgenic lines. However, since heterologous expression of other plant LCB Δ4-desaturases also failed in *S. cerevisiae*, it is likely that the yeast is an inappropriate host system to determine the enzymatic activity of plant LCB desaturases. In conclusion, to determine the enzyme activities of *Pp*SD4D and *Pp*GCS *in vitro*, another host system might be required. A suitable yeast host that was already used to confirm the activity of the LCB Δ4-desaturase from *A. thaliana* is *P. pastoris* (Michaelson *et al.*, 2009).

GlcCers are nearly absent in *sd4d* and *gcs* plants

To determine the enzymatic function of *Pp*SD4D and *Pp*GCS *in vivo*, knockout mutants for both single genes were generated by homologous recombination. Seven independent *sd4d* knockouts were obtained. Absence of the transcript was confirmed by semiquantitative reverse transcriptase PCR (Fig. 1A, Fig. S2A). In contrast, only a single true *gcs* mutant was obtained by homologous recombination (Fig. 1B, Fig. S2B), and so CRISPR-Cas9 genome editing was additionally applied to target *PpGCS*. Three more mutants were generated using CRISPR-Cas9 targeting the first exon (Fig. S2C) that showed the same growth phenotype as the *gcs-1* mutant from homologous recombination. The knockout was confirmed by sequencing of the targeted gene region (Fig. S2D). All three mutants had frame-shift deletions that intervened with proper translation of the protein.

Sphingolipid measurements were conducted on *P. patens* wild type, *sd4d*, and *gcs* mutants to determine their sphingolipid composition. For better visualisation of the ceramide backbone composition, molecular species of GlcCers (Fig. 1C), ceramides (Fig. 2C-H), and GIPCs (Fig. 3) were divided into species with unhydroxylated fatty acids, indicated by a 'c' in front of the chain length number and species with α-hydroxylated fatty acids, indicated by an 'h' in front of the chain length number. Lipids were extracted from ten-day-old protonema grown on cellophane-covered BCD medium and applied to UPLC-nanoESI-MS/MS. Growth on cellophane-covered solid medium enabled easy harvesting of the filamentous tissue. Previous sphingolipid analyses on *P. patens* showed that around 94 % of GlcCers contain the d18:2 LCB moiety (Resemann, 2018).

The *P. patens* wild type GlcCer profile was confirmed in this study (Fig. 1C). The profile suggested that GlcCer formation might be disturbed in *sd4d-1* and *gcs-1* mutants. The lipid data served as second line of evidence for the functional disruption of *PpSD4D* and *PpGCS* genes in the mutant lines. Fold changes compared to the wild type were determined to show the abolishment of GlcCers. All tested *sd4d* and *gcs* lines had substantially reduced GlcCer levels compared to the wild type (Fig. 1D, Fig S3A, B). After confirmation of several independent knockout lines for each gene, all following mutant characterisations were performed only on the *sd4d-1* and *gcs-1* alleles. In *sd4d-1* and *gcs-1* GlcCer levels were reduced by 99.8 % and 99.9 %, respectively (Fig. 1D). More than 92 % of the wild type GlcCer pool consisted of a single sphingolipid species (Resemann, 2018). This had a Δ4,8-diunsaturated LCB moiety with two hydroxyl groups, d18:2, conjugated to an α-hydroxylated 20-carbon fatty acid with no double bonds, h20:0 (together d18:2/h20:0). Minor species like d18:1/h20:0, d18:2/h22:0, and d18:2/c20:0 accounted for 4 %, 2 %, and 1 % of *P. patens* GlcCers, respectively. All other detected species represented < 1 % of all GlcCers. Interestingly, the *sd4d-1* mutant still had residual amounts of GlcCer d18:2/h20:0 that might derive from a putative desaturase activity of the LCB C-4 hydroxylase (Ternes *et al.*, 2002). *sd4d-1* plants also contained GlcCer species with a d18:0 LCB moiety that were not affected by the mutation. However, all GlcCer species found in *sd4d-1* were in trace amounts and therefore did not produce a substantial GlcCer pool. The residual GlcCer amounts found in the *gcs-1* mutant were attributed to background signals. The GlcCer results verified the generation of null mutants for both genes and confirmed that *Pp*SD4D and *Pp*GCS are the only enzymes in *P. patens* that catalyse the respective reactions in the tested conditions and tissues.

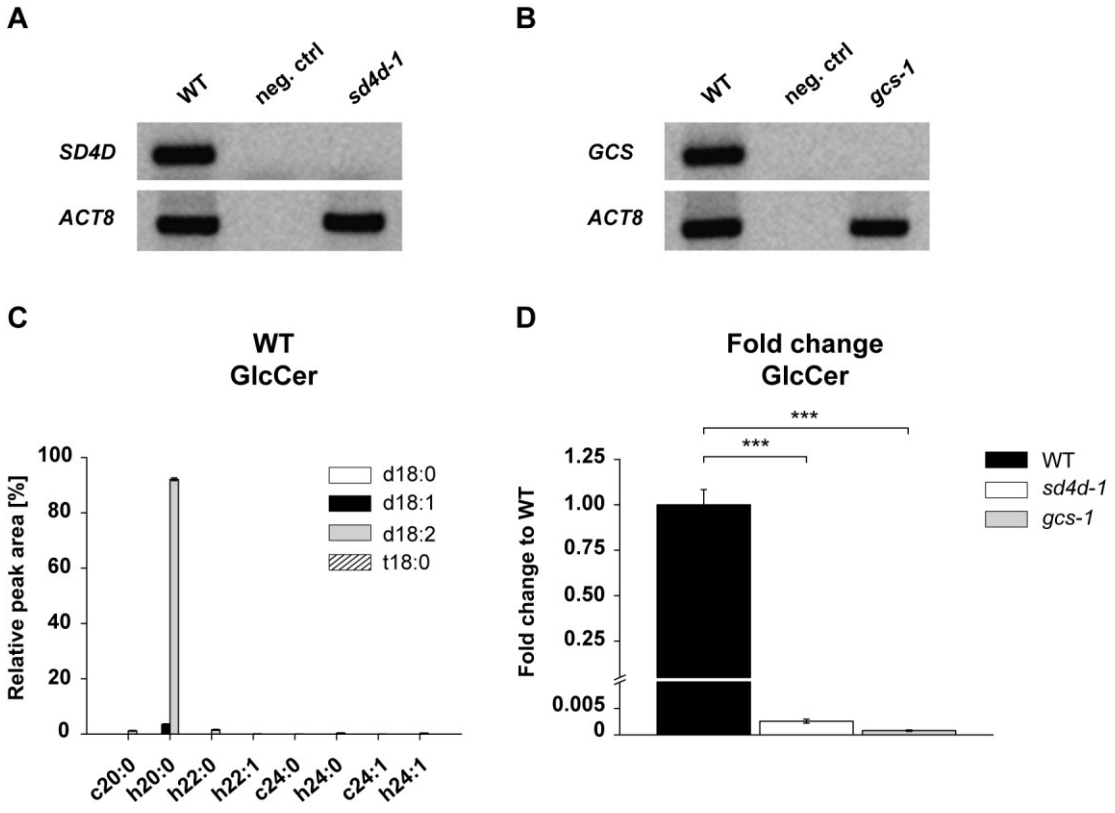

Fig. 1. *P. patens* s*d4d-1* and *gcs-1* mutant characterisation and GlcCer content of *P. patens* wild type, *sd4d-1*, and *gcs-1*. (A) *PpSD4D* and (B) *PpGCS* transcript determination by reverse transcriptase PCR. *ACTIN8* (*ACT8*) was used as reference gene and water as negative control (neg. ctrl). (C, D) Glycosylceramides (GlcCers) were extracted from protonema of ten-day-old wild type (WT), *sd4d-1*, and *gcs-1 P. patens* and analysed with UPLC-nanoESI-MS/MS. (C) Relative GlcCer profile of *P. patens* WT. GlcCers are shown with their LCB (column colour) and fatty acid (x-axis) moieties. Dihydroxy LCB moieties are indicated by a 'd' and trihydroxy LCB moieties are indicated by a 't'. Molecular species with an unhydroxylated fatty acid moiety are indicated by a 'c' and molecular species with an α-hydroxylated fatty acid moiety are indicated by an 'h'. Only molecular species with a peak area ≥ 0.1 % were included in the GlcCer graphs. Please note that this experiment was part of a larger experiment and the data for wild type protonema were shown recently in a different study as well (Gömann *et al*. 2021). (D) GlcCer fold changes to the WT were calculated using absolute peak areas. Fold changes are depicted in linear scale. The WT is set to 1. Sphingolipid data represent the mean ± SD of measurements from four independent cultivations each containing protonema material from eight cultivation plates. Statistical analysis was done using Student's *t*-test. Asterisks indicate different significance levels with *** significance at $P < 0.001$ compared to the WT.

Loss of GlcCers and of Δ4-unsaturated LCB moieties affects relative profiles of other sphingolipid classes

Sphingolipidomics revealed changes in profiles of other sphingolipid classes upon loss of either *Pp*SD4D or *Pp*GCS activity, including LCBs and ceramides (Fig. 2).

The most abundant LCB and LCB-P species in the wild type was t18:0, representing 94 % and 69 %, respectively (Fig. 2A, B). Lesser amounts of d18:0 was also found in LCB (6 %) and LCB-P (31 %). Although the overall LCB and LCB-P profiles were maintained in *sd4d-1* and *gcs-1* mutants, minor changes were observed in the relative abundances of individual species. In the *sd4d-1* mutant t18:0 LCB was reduced to 91 %, and the LCB-P to 60 %. *sd4d-1* plants further had a slight increase of d18:0 LCB to 8 % and the LCB-P to 40 %. The *gcs-1* mutant had reduced t18:0 LCB, at 82 %, and LCB-P, at 37 %. *gcs-1* plants

also had more d18:0 LCB, at 14 %, and LCB-P, at 51 %, compared to wild type. Additionally, d18:2, which was not found at all in the wild type, emerged as new LCB at 4 % of the total LCB content, and LCB-P at 12 % of the total LCB-P content in *gcs-1*.

In wild type, ceramides harbouring the t18:0 LCB moiety predominated, representing more than 90 % of all ceramides (Fig. 2C, F). Only minor amounts of ceramides with d18:0, d18:1, and d18:2 LCB moieties were detected. The most abundant fatty acid moiety at 52 % of the total, was h24:0, followed by fatty acid moieties with carbon chain lengths ranging from C20 to C26. *sd4d-1* plants had similar ceramide profiles as the wild type (Fig. 2D, G). However, no ceramide species with d18:1 and d18:2 LCB moieties were found. The *gcs-1* mutant also had comparable ceramide profiles to the wild type control (Fig. 2E, H). However, *gcs-1* specifically accumulated one ceramide species: d18:2/h20:0. This ceramide backbone is characteristic for the most abundant GlcCer species in *P. patens* wild type plants (Fig. 1C). Taken together, the data showed that *sd4d-1* lacked ceramides with d18:1 and d18:2 LCB moieties. *gcs-1* plants accumulated d18:2 LCBs and LCB-Ps, and the ceramide that is the characteristic backbone of wild type GlcCers, d18:2/h20:0, indicating that this might be the main substrate of *Pp*GCS.

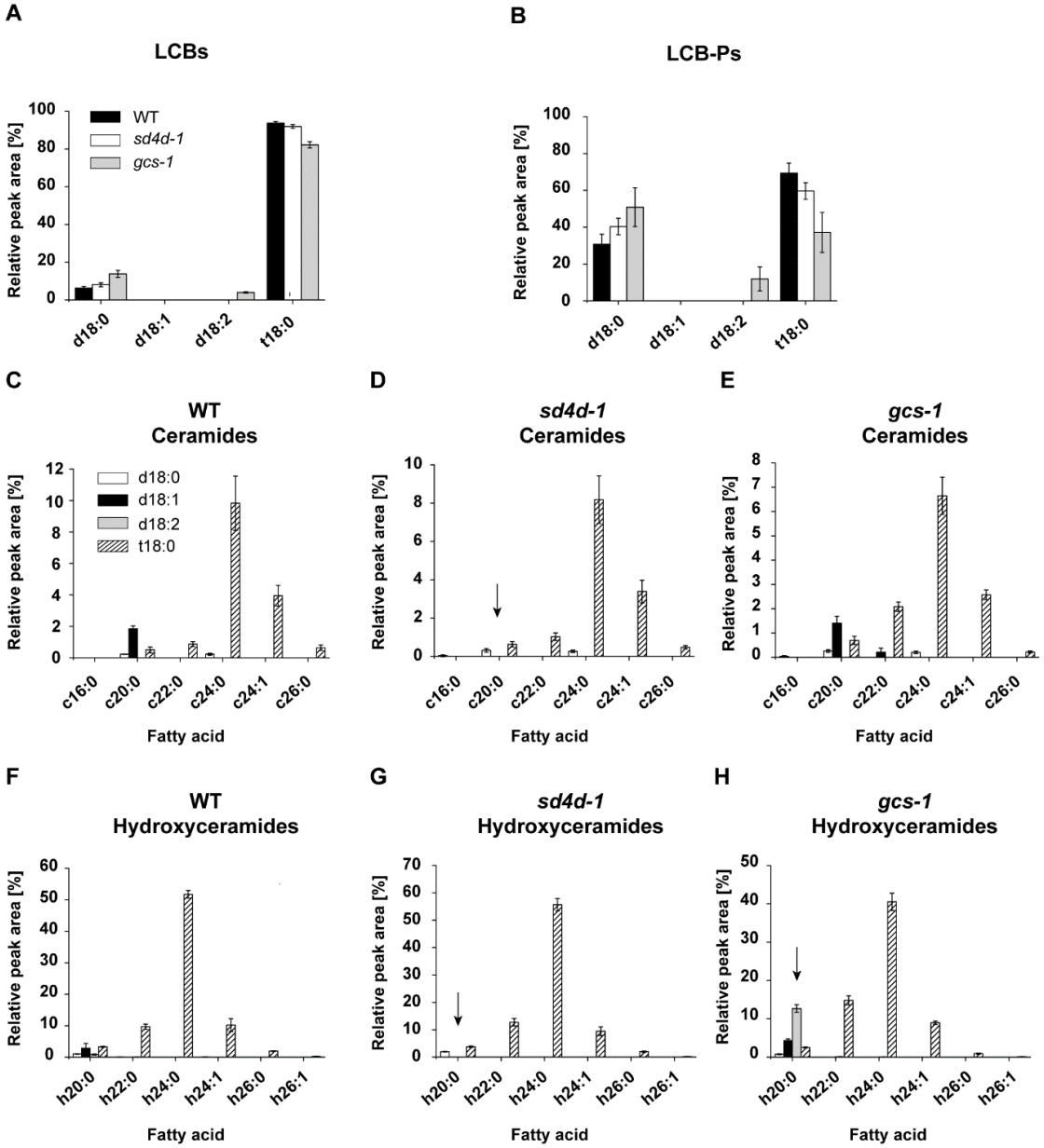

Fig. 2. Relative profiles of LCBs, LCB-Ps, and ceramides in *P. patens* wild type, *sd4d-1,* and *gcs-1*. Long-chain bases (LCBs), phosphorylated LCBs (LCB-Ps) and ceramides were extracted from protonema of ten-day-old wild type (WT), *sd4d-1*, and *gcs-1 P. patens* and analysed with UPLC-nanoESI-MS/MS. Relative profiles of (A) LCBs, (B) LCB-Ps, and (C-H) ceramides in WT, *sd4d-1*, and *gcs-1* lines. Dihydroxy LCB moieties are indicated by a 'd' and trihydroxy LCB moieties are indicated by a 't'. Molecular species with an unhydroxylated fatty acid moiety are indicated by a 'c' and molecular species with an α-hydroxylated fatty acid moiety are indicated by an 'h'. Please note that this experiment was part of a larger experiment and the data for wild type protonema were shown recently in a different study as well (Gömann *et al*. 2021). Relative profiles of (C-E) ceramide and (F-H) hydroxyceramide molecular species are shown with their LCB (column colour) and fatty acid (x-axis) moieties. Arrows highlight changes to the WT. Sphingolipid data represent the mean ± SD of measurements from four independent cultivations each containing protonema material from eight cultivation plates.

GlcCers and GIPCs are both complex sphingolipids that contain polar head groups at the C-1 position of the LCB moiety. Depending on the hydroxylation and desaturation state of the LCB moiety of ceramides, either GlcCers or GIPCs are synthesised. Therefore, GlcCer and GIPC formation represent alternative sphingolipid metabolic pathways. The blockage of GlcCer synthesis in *sd4d-1* and *gcs-1* mutants might result in changes of GIPC synthesis

and composition. This was confirmed in the study from Msanne *et al*. (2015) in which they demonstrated that *A. thaliana gcs-1* null mutants had a higher GIPC content compared to the wild type. To check this for *P. patens*, GIPCs with different head groups were analysed. Series A GIPCs include species with one hexose (Hex) moiety that may be converted to *N*-acetylhexosamine (HexNAc), that is connected to glucuronic acid (GlcA) linked IPC, Hex(NAc)-GlcA-IPCs. Series B GIPCs include species with two Hex moieties of which one may be be converted to HexNAc, Hex-Hex (NAc)-GlcA-IPCs. Changes in GIPC profiles were most prominent in the Hex-HexNAc-GlcA-IPC profile (Fig. 3, Fig. S4). The wild type Hex-HexNAc-GlcA-IPC profile consisted mainly of species with a t18:0 LCB moiety in their backbone (Fig. 3A). d18:0, d18:1, and d18:2 LCB moieties were only present in low amounts in the wild type. Most abundant fatty acid moieties in the wild type were h24:0 (53 %), h24:1 (17 %), h22:0 (9 %), and h20:0 (5 %). Other less abundant fatty acids ranged from acyl chain lengths of C20 to C26 that were mostly α-hydroxylated. In the *sd4d-1* Hex-HexNAc-GlcA-IPC profile, molecular species containing a d18:1 or d18:2 LCB moiety were missing (Fig. 3B). Otherwise, the Hex-HexNAc-GlcA-IPC profile looked similar to the wild type profile. *gcs-1* mutants had a comparable Hex-HexNAc-GlcA-IPC profile as the wild type (Fig. 3C). However, minimal amounts of species with d18:2/h20:0 (1.5 %) ceramide composition emerged in the mutant. Similar changes were observed for GIPC classes with a different head group composition; however, differences were not as prominent as for Hex-HexNAc-GlcA-IPCs (Fig. S4). To summarise, GIPC profiles were affected to a minor degree, which reflected the changes to the ceramide profiles in these mutants.

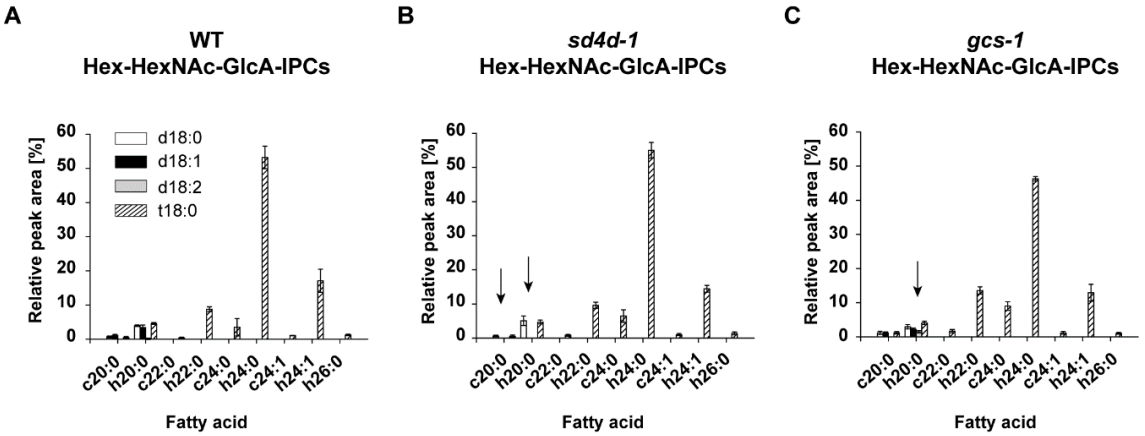

Fig. 3. Relative Hex-HexNAc-GlcA-IPC profiles in *P. patens* wild type, s*d4d-1,* and *gcs-1*. (A-C) Glycosyl inositolphosphorylceramides (GIPCs) with one hexose moiety and one *N*-acetylhexosamine unit (Hex-HexNAc-GlcA-IPCs) were extracted from protonema of ten-day-old wild type (WT), *sd4d-1*, and *gcs-1 P. patens* and analysed with UPLC-nanoESI-MS/MS. Hex-HexNAc-GlcA-IPC molecular species are shown with their LCB (column colour) and fatty acid (x-axis) moieties. Dihydroxy LCB moieties are indicated by a 'd' and trihydroxy LCB moieties are indicated by a 't'. Molecular species with an unhydroxylated fatty acid moiety are indicated by a 'c' and molecular species with an α-hydroxylated fatty acid moiety are indicated by an 'h'. (A-C) Relative Hex-HexNAc-GlcA-IPC profiles of (A) WT, (B) *sd4d-1*, and (C) *gcs-1*. Only molecular species with a peak area ≥ 0.5 % in at least one of the three lines were included in the Hex-HexNAc-GlcA-IPC graphs. Arrows highlight changes to the WT. Sphingolipid data represent the mean ± SD of measurements from four independent cultivations each containing protonema material from eight cultivation plates. Abbreviations are as follows: GlcA: glucuronic acid; Hex: hexose; HexNAc. *N*-acetylhexosamine, IPCs: inositolphosphorylceramides.

sd4d-1 and *gcs-1* mutants have altered sphingolipid contents

The loss of GlcCers and of sphingolipids with Δ4-unsaturated LCBs influenced the relative profiles of other sphingolipid classes in *gcs-1* and *sd4d-1* mutants (Fig. 2, Fig. 3). To investigate whether total sphingolipid contents were also affected, fold changes compared to the wild type were calculated for the individual sphingolipid classes using absolute peak areas of the analysed compounds (Fig. 4). In *sd4d-1* only LCBs were significantly increased compared to the wild type (Fig. 4A). *sd4d-1* also had two-fold higher levels of ceramides with d18:0 LCB moieties and lacked ceramides with d18:1 and d18:2 LCB moieties (Fig. S5A). Total amounts of all other sphingolipid classes were not significantly affected (Fig. 4B-D, Fig. S6). In contrast to that, *gcs-1* showed significant accumulation of LCBs, hydroxyceramides, and Hex-HexNAc-GlcA-IPCs compared to the wild type (Fig. 4A, C, D). *gcs-1* also had 25-fold more ceramides with a d18:2 LCB moiety than wild type (Fig. S5B). Total levels of ceramides, LCB-Ps, Hex-GlcA-IPCs, HexNAc-GlcA-IPCs, and Hex-Hex-GlcA-IPCs were not significantly affected in *gcs-1* compared to wild type (Fig. 4B, Fig. S6). These findings indicated that disruption of *Pp*GCS function influences the *P. patens* sphingolipidome more strongly than disruption of *Pp*SD4D.

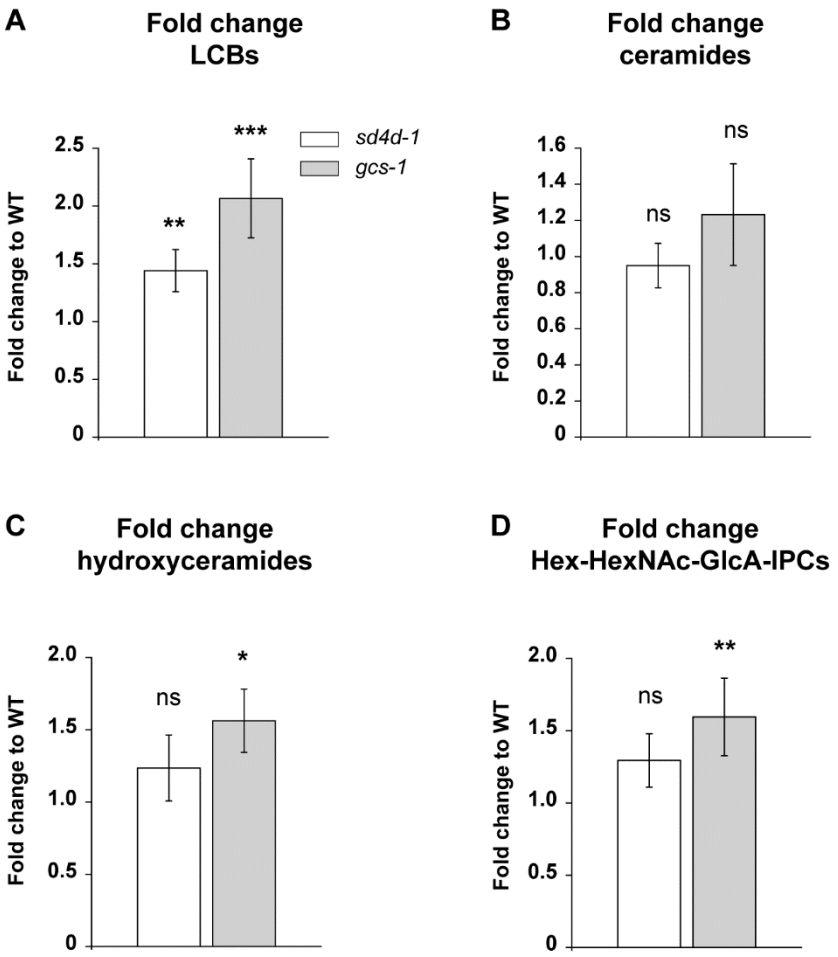

Fig. 4. Total contents of LCBs, ceramides, and GIPCs in *P. patens sd4d-1* and *gcs-1*. Long-chain bases (LCBs), ceramides, hydroxyceramides, and glycosyl inositolphosphorylceramides (GIPCs) were extracted from protonema of ten-day-old wild type (WT), *sd4d-1*, and *gcs-1 P. patens* and analysed with UPLC-nanoESI-MS/MS. Fold changes of (A) LCBs, (B) ceramides, C) hydroxyceramides, and (D) Hex-HexNAc-GlcA-IPCs to the WT were calculated using absolute peak areas. Fold changes are depicted in linear scale. The WT, which is not shown, is set to 1. Sphingolipid data represent the mean ± SD of measurements from four independent cultivations each containing protonema material from eight cultivation plates. Statistical analysis was done using Student's *t*-test. Asterisks indicate different significance levels with *** significance at $P < 0.001$, ** significance at $P < 0.01$, * significance at $P < 0.05$ and not significant (ns) at $P > 0.05$ compared to the WT. Abbreviations are as follows: GlcA: glucuronic acid; Hex: hexose, HexNAc: *N*-acetylhexosamine IPCs: inositolphosphorylceramides.

gcs-1 has a more severe growth and development phenotype than *sd4d-1*

The *A. thaliana* mutant whose LCB Δ4-desaturase activity is disrupted does not show any growth or development phenotype. This observation might be explained by its expression pattern which is restricted to *A. thaliana* pollen and floral tissue (Michaelson *et al.*, 2009). Although mutant pollen and floral tissue had reduced GlcCer levels, the knockout did not show reduced pollen viability. The plants further did not have any impairment in response to drought stress and in transpiration rate, leading the authors to conclude that sphingolipids with Δ4-unsaturated LCB moieties do not have an essential role in *A. thaliana* physiology (Michaelson *et al.*, 2009). Disruption of *A. thaliana* GCS, however, caused seedling lethality, impaired cell differentiation and organogenesis, and defects in pollen transmission (Msanne *et al.*, 2015). In *A. thaliana* most GlcCer species have either a t18:1 or a d18:1 LCB moiety

(Markham *et al.*, 2006). Given that in *P. patens* the d18:2 LCB moiety is the most abundant LCB moiety in the GlcCer pool and that this sphingolipid class was found throughout the plant, *Pp*SD4D and *Pp*GCS were both expected to have major physiological roles in the moss. The sphingolipid data from this study showed that both independent knockout mutants, *sd4d-1* and *gcs-1*, were devoid of GlcCers (Fig. 1D). It was therefore assumed that both knockout mutants would exhibit similar phenotypes. To perform phenotype investigations, colonies were started by placing protonema spot inocula of similar size (around 1 mm in diameter) onto BCD medium. After ten days of growth, wild type colonies developed long stretched and branched protonema filaments (Fig. 5). After 14 days, the emergence of gametophores was observed. After 52 days, wild type colonies consisted of fully expanded gametophores that overgrew the protonema tissue. *sd4d-1* showed similar protonema and gametophore development as the wild type control plants (Fig. 5). However, *sd4d-1* protonema filaments appeared shorter and in consequence, *sd4d-1* colony outreach was more restricted than in the wild type. *gcs-1* mutants had much shorter protonema filaments than wild type and *sd4d-1* plants and had dwarfed gametophores compared to the wild type and *sd4d-1* (Fig. 5). The shorter appearance of *sd4d-1* and *gcs-1* protonema filaments was also observed when the tissue was investigated under the microscope (Fig. S6). It further appeared that *gcs-1* plants developed brown patches in the centre of the colony and at the basis of gametophores.

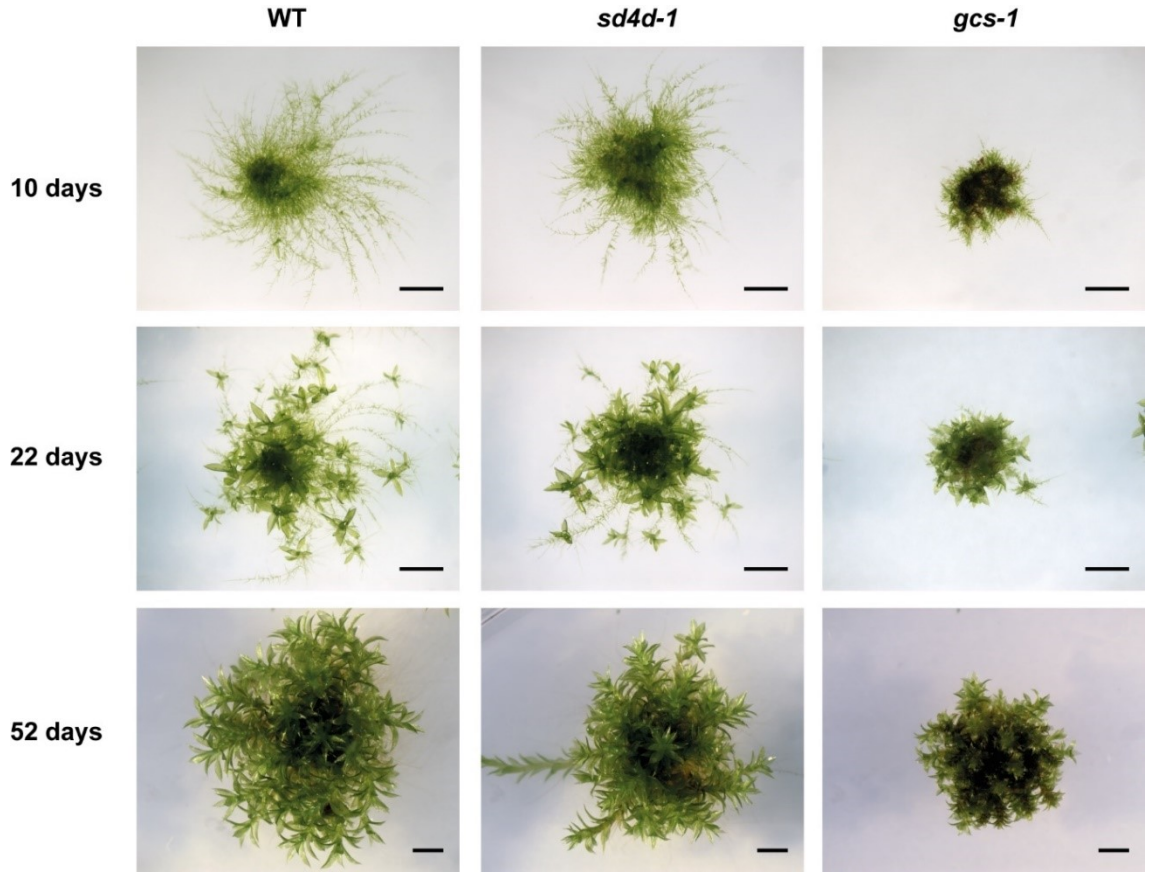

Fig. 5. Growth phenotypes of *P. patens* wild type, *sd4d-1*, and *gcs-1*. Gametophore and protonema growth of *P. patens* wild type (WT), *sd4d-1*, and *gcs-1*. Colonies were grown for seven weeks and imaged at the indicated time points. Scale bars are 2 mm.

The browning of the *gcs-1* gametophyte tissue indicated cell death induction in that mutant line. Therefore, gene expression levels of defence-related marker genes were determined. Genes that are involved in defence responses are often associated with PCD, which is a common defence strategy in plants (Zienkiewicz *et al.*, 2020). In Bressendorff *et al*. (2012) and Overdjik *et al*. (2016) several gene candidates were analysed and used as defence-related marker genes in *P. patens* (Bressendorff, 2012; Overdijk *et al.*, 2016). The gene expression of some of these genes was determined in ten-day-old protonema of *P. patens* wild type, *sd4d-1*, and *gcs-1*. Genes of interest were *CHS*, *ERF*, and *PAL4*. Appropriate reference genes for qRT PCR analyses in *P. patens* were investigated by Le Bail *et al*. (2013). Of the proposed reference gene candidates *Ade PRT* proved to be a stably expressed gene in all developmental tissues. Stable gene expression was confirmed before application for qRT PCR analysis in this study. Fold over reference was calculated in each line and for each gene of interest. Relative gene expression of *CHS*, *ERF5*, and *PAL4* in *sd4d-1* and *gcs-1* was normalised to the wild type. All three defence-related marker genes were upregulated in *gcs-1* plants but not in *sd4d-1* plants (Fig. 6A-C). This result is consistent with the different mutant morphologies and the observed tissue browning in *gcs-1* plants may therefore indeed indicate cell death.

It was speculated that changes might also be determined in phytohormones that are known to be involved in plant defence. Previous studies showed that 12-oxo-phytodienoic acid (OPDA) inhibits *P. patens* growth and that its production is induced upon wounding (Ponce De León *et al.*, 2012; Scholz *et al.*, 2012). *gcs-1* had significantly elevated levels of the oxylipin-derived phytohormones OPDA and *dinor*-OPDA (*dn*-OPDA) compared to the wild type (Fig.6D, E). Consistent with previous studies on OPDA function in *P. patens* was the observation that *gcs-1* plants appeared to have growth defects (Fig. 5). To quantify growth of the *P. patens* wild type, *sd4d-1*, and *gcs-1*, protonema was cultivated for ten days on cellophane-covered BCD plates. All cultivation plates were inoculated with the same amount of starting material. After harvesting, the material was weighed for fresh weight determination. *sd4d-1* and *gcs-1* mutants generated significantly less biomass than the wild type (Fig. 6F). After lyophilisation, the dry weight of the material was also determined, revealing the same effect (Fig. S7). This indicated that both mutant lines had quantifiable growth defects. However, the *gcs-1* growth defect was more severe than the *sd4d-1* growth defect, which was consistent with the determined OPDA and *dn*-OPDA levels.

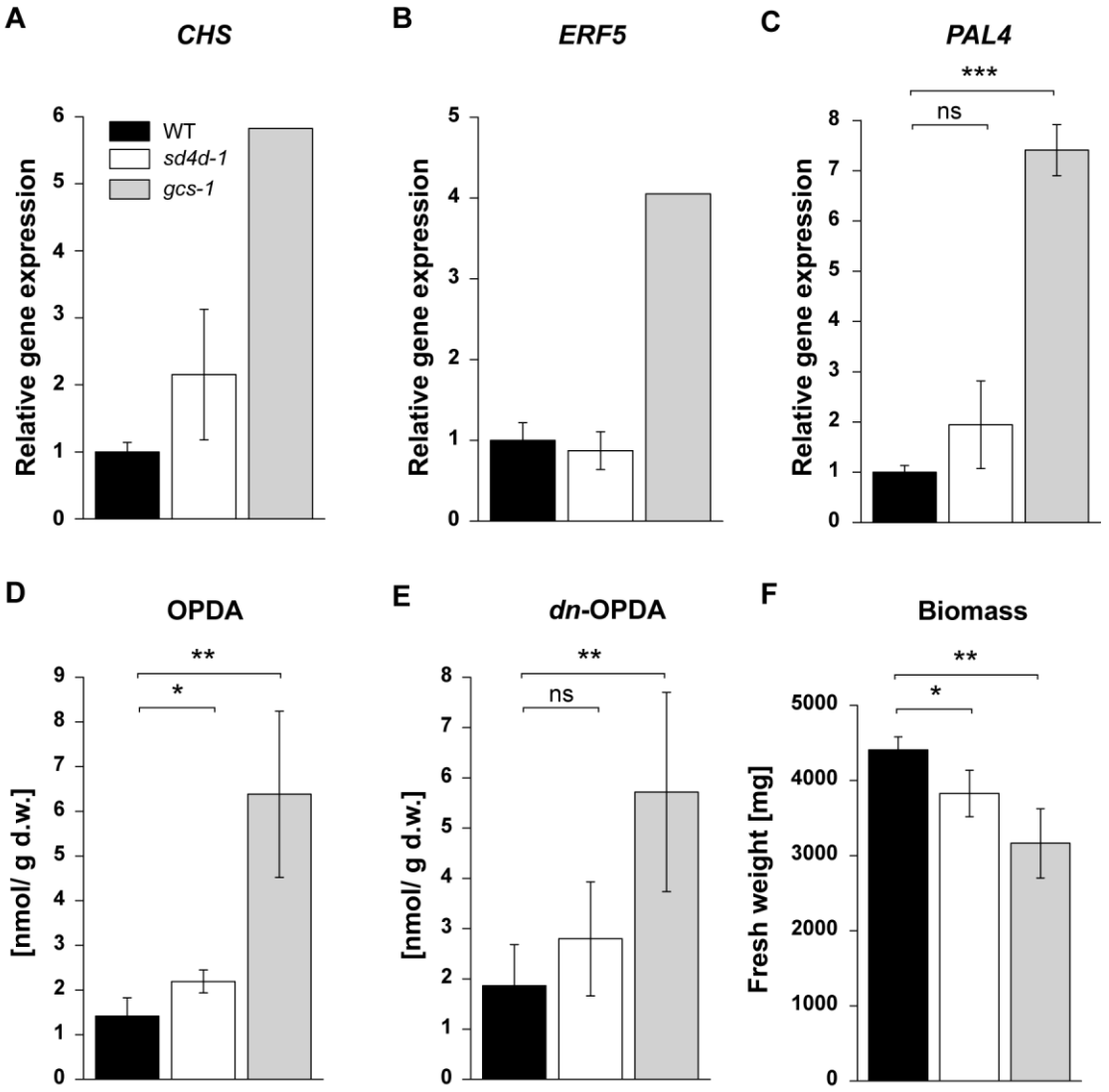

Fig. 6. Defence-related marker gene expression, OPDA and *dn*-OPDA levels, and biomass generation in *P. patens* wild type, *sd4d-1*, and *gcs-1* plants. (A-C) RNA was extracted from two-week-old wild type (WT), *sd4d-1*, and *gcs-1* protonema grown on cellophane-covered BCDAT medium. Gene expression of defence-related marker genes (A) chalcone synthase (*CHS*), (B) the transcription factor ethylene-responsive element-binding factor 5 (*ERF5*), and (C) phenylalanine lyase 4 (*PAL4*) was determined. Fold over reference was calculated using adenine phosphoribosyltransferase (Ade PRT) as reference gene. Data was normalised to gene expression in the WT, which is set to 1. (A, B) Data represent the mean ± SE of measurements of three (WT, *sd4d-1*) and two (*gcs-1*) replicates from one experiment. (C) Data represent the mean ± SE of measurements of three replicates from one experiment. (D) 12-oxo-phytodienoic acid (OPDA) and (E) *dinor*-OPDA (*dn*-OPDA) were extracted from ten-day-old protonema grown on cellophane-covered BCD medium and analysed using UPLC-nanoESI-MS/MS. (F) Growth of WT, *sd4d-1*, and *gcs-1* was quantified by collecting ten-day-old protonema tissue grown on cellophane-covered BCD medium and determining the fresh weight. Data represent the mean ± SD of measurements from four independent cultivations each containing protonema material from eight cultivation plates. Statistical analysis was done using Student's *t*-test. Asterisks indicate different significance levels with *** significance at $P < 0.001$, ** significance at $P < 0.01$, * significance at $P < 0.05$ and not significant (ns) at $P > 0.05$ compared to the WT.

gcs-1 has impaired protonema cell differentiation

The protonema is a two-dimensional filamentous network that consists of two cell types: chloronema cells that are rich in chloroplasts and caulonema cells that have fewer and less developed chloroplasts. The chloronema cells are the first ones to be generated from a germinating spore. They differentiate gradually into caulonema cells during development.

As mentioned, *A. thaliana gcs-1* plants were impaired in cell differentiation (Msanne *et al.*, 2015). To asses whether differentiation was also affected in *P. patens sd4d-1* and *gcs-1*, a dark growth assay was performed. During this assay, cultivation of a subtype of caulonema cells, specified as skotonema cells, is induced by growing plants in the dark. Protonema spot inocula were placed on medium supplemented with 2 % sucrose. Colonies were grown for one week under continuous light. Subsequently, culture plates were transferred to the dark, rotated into vertical orientation and cultivation was continued for another three weeks. After one week under continuous light, the wild type, the *sd4d-1,* and the *gcs-1* mutants developed into dense green protonema colonies of similar size (Fig. 7, upper row). After three more weeks of cultivation in the dark and in vertical orientation, the wild type developed long, brown, and unbranched filaments that reached upwards (Fig. 7 lower row). *sd4d-1* colonies looked similar to the wild type colonies. The mutant filaments, however, appeared to be slightly shorter than wild type filaments. In contrast to wild type and *sd4d-1* colonies, *gcs-1* colonies failed to develop any skotonema cells. Protonema differentiation ability therefore appeared to be strongly affected in *gcs-1* mutants but not in *sd4d-1* mutants.

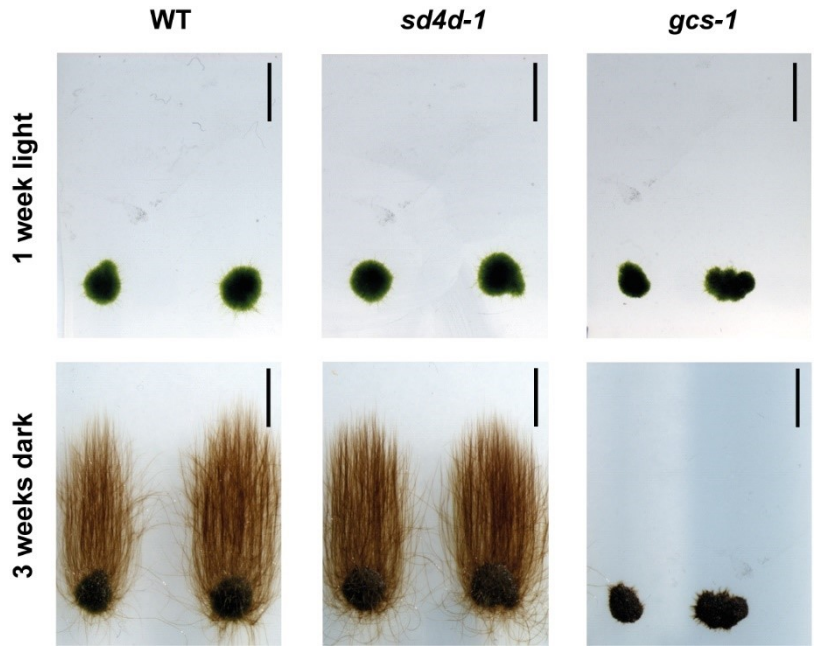

Fig. 7. Skotonema development of *P. patens* wild, type, *sd4d-1*, and *gcs-1*. 1 mm protonema spot inocula of wild type (WT), *sd4d-1*, and *gcs-1* lines were placed on BCDAT+2 % sucrose and grown under continuous light for one week (upper row). Plates were transferred to the dark and rotated into vertical orientation. Colonies were grown for another three weeks to induce skotonema development (lower row). The experiment was repeated three times with similar results. Scale bares are 0.5 cm.

sd4d-1 may be impaired in cell elongation

sd4d-1 mutants appeared to have slightly shorter skotonema filaments than the wild type (Fig. 7). The dark growth experiment was performed several times and the observed shorter *sd4d-1* filaments were in some experiments more obvious than in others. A possible explanation for the shortened filaments might be that *sd4d-1* cells were generally shorter.

To determine the cell lengths, the dark growth experiment was started with smaller spot inocula to obtain fewer filaments (Fig. 8A, upper row). This facilitated examination of individual filaments. The experiment was repeated with the same conditions as described. Photos of the filaments were additionally taken at higher magnification to identify individual cells (Fig. 8A, lower row) and the separating cross walls (Fig. 8B). 428 cells were measured for each plant line. At 0.17 mm, the mean *sd4d-1* cell length was significantly shorter than the mean wild type cell length at 0.2 mm (Fig. 8C). Although *sd4d-1* plants were not affected in their cell differentiation ability, they appeared to have impaired protonema cell elongation.

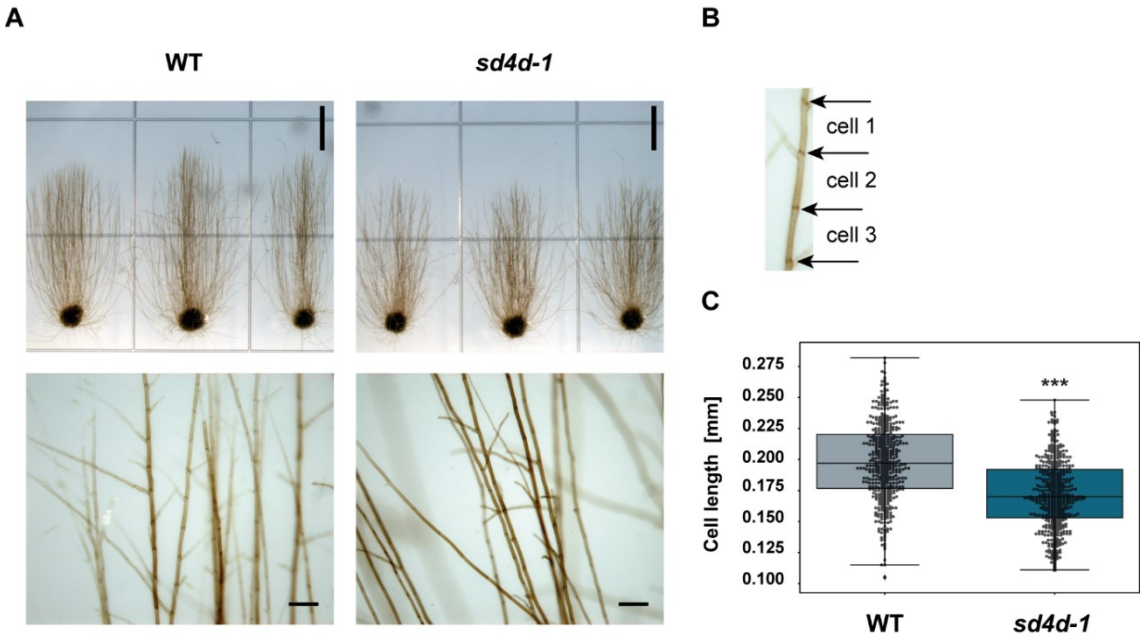

Fig. 8. Determination of skotonema cell length of *P. patens* wild type and *sd4d-1* plants. Wild type (WT) and *sd4d-1* protonema spot inocula were placed on BCDAT +2 % sucrose and grown under continuous light for one week. Plates were transferred to the dark and rotated to vertical orientation. (A) Colonies were grown for another three weeks to induce skotonema development. Pictures were taken at different magnifications. Scale bares in upper row are 0.5 cm. Scale bares in lower row are 0.2 mm. (B) Skotonema cells are separated by cross-walls. (C) Skotonema cell length measurements of *P. patens* WT and *sd4d-1* plants. The experiment was repeated twice with similar results. Statistical analysis was done using Student's *t*-test. Asterisks indicate different significance levels with *** significance at $P < 0.001$ compared to the WT.

gcs-1 gametophores develop cell death-like lesions when flooded with water

While in *A. thaliana* Δ4-desaturase mutants were not affected in pollen viability, *gcs-1* mutants were affected in pollen transmission (Michaelson *et al.*, 2009; Msanne *et al.*, 2015). According to the predicted gene expression of *PpSD4D* and *PpGCS* in *P. patens*, both genes were highly expressed in spores and the sporophyte generation (Fig. S1). The specific expression of both genes in *P. patens* reproductive organs raised the question whether *sd4d-1* and *gcs-1* were also affected in their fertilisation and sporulation efficiency. To test this, *P. patens* gametophores were induced to generate gametangia. After gametophores reached full size, cultivation plates were moved to short-day conditions. When gametangia were observed on the tip of the gametophores, the plants were flooded with water and placed for several weeks in short-day conditions. No spore capsules were

observed for either the *sd4d-1* or for the *gcs-1* mutant. The wild type, however, also showed a very low sporulation efficiency with only one- to two spore capsules per cultivation plate. The 'Gransden' strain, which has been used for decades as a wild type strain, is recognised to have low sporulation efficiency (Hiss *et al.*, 2017; Meyberg *et al.*, 2020). It is therefore not clear, whether the lack of spore capsules in *sd4d-1* and *gcs-1* colonies was due to the inability of the mutants to sporulate or if it was rather due to the general low sporulation ability of the selected wild type strain. However, the experiment led to another interesting observation. While wild type and *sd4d-1* gametophores looked alike with elongated stems and expanded leaflets at the gametophore tip, *gcs-1* gametophores had elongated brownish stems (Fig. 9). Leaflets of *gcs-1* gametophores were smaller in size the more elongated the stem was. Furthermore, the leaflets had brown patches that resembled PCD lesions in vascular plants.

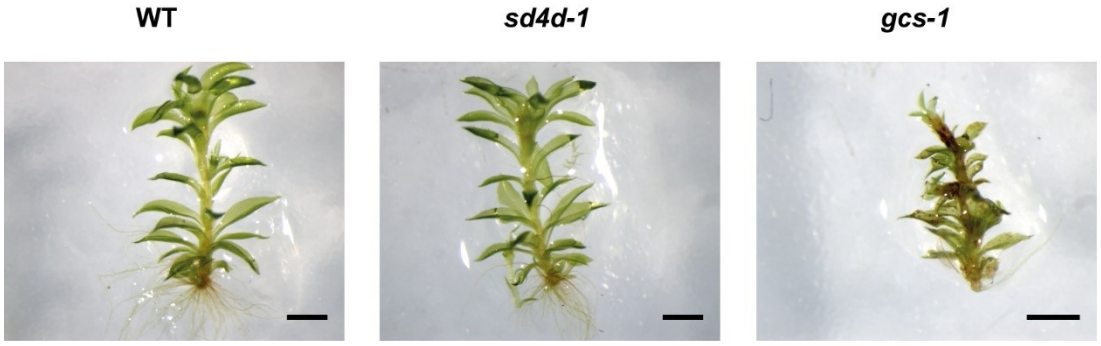

Fig. 9. Gametophore morphology during gametangia induction in *P. patens* wild type, *sd4d-1*, and *gcs-1*. Gametophore colonies were grown under normal conditions for five weeks. Gametophores were transferred to short-day conditions at 17 °C and flooded with water. Gametophores were kept in water for another month before pictures were taken. Scale bares are 1 mm.

Discussion

Sphingolipid metabolism has diversified across different plant lineages over the course of evolution. However, the causes and consequences of this divergent evolution are still unknown. An example of this is the LCB composition of GlcCers. In bryophytes and Solanaceae GlcCers are characterised by a Δ4,8-diunsaturated LCB moiety that is only present in the floral tissue sphingolipidome of *A. thaliana* (Sperling *et al.*, 2005; Markham *et al.*, 2006; Michaelson *et al.*, 2009; Resemann, 2018). While the Δ8-unsaturated LCB moiety predominates in *A. thaliana* sphingolipids and its physiological function has been thoroughly investigated, the role of the Δ4-unsaturated LCB moiety is not yet understood. The characterised *A. thaliana* LCB Δ4-desaturase only has a restricted expression pattern and is not physiologically relevant in the tested tissues and conditions. In contrast to *A. thaliana*, *P. patens* GlcCers have high levels of the Δ4,8-diunsaturated LCB moiety. It was therefore expected that LCB Δ4-desaturase activity is physiologically more relevant in *P. patens*. Investigation of the *P. patens* LCB Δ4-desaturase might therefore give new insights into the metabolic and physiological roles of Δ4-unsaturated molecular species in

plant GlcCers. Loss-of-function mutants of the *P. patens* LCB Δ4-desaturase and the GCS were generated and characterised. Both mutant lines lacked nearly all GlcCers but exhibited unexpectedly different phenotypes. Although both enzymes are located in the same metabolic pathway, their physiological impact appears to vary greatly.

Analysis on the *P. patens* lipidome conducted by Resemann (2018) included GlcCer composition. Over 94 % of the GlcCer pool consisted of a single molecular species with a Δ4,8-diunsaturated LCB moiety connected to a h20:0 fatty acid moiety, d18:2/h20:0 (Resemann, 2018). This composition indicated that GlcCers should be strongly affected by the loss of either *Pp*SD4D or *Pp*GCS. Initially, it was hypothesised that disruption of *PpSD4D* might result in 1) a structural change of the LCB moiety of *P. patens* GlcCers or 2) in loss of GlcCers. Disruption of *PpGCS* was expected to result in a depletion of all GlcCers. UPLC-nanoESI-MS/MS analyses revealed that GlcCers were nearly absent in *sd4d* as well as in *gcs* knockouts. The results were consistent with findings from the corresponding knockouts in *A. thaliana*. Knockouts of the *A. thaliana* LCB Δ4-desaturase had a significant reduction in GlcCer levels in pollen (Michaelson *et al.*, 2009) and *A. thaliana gcs* plants were devoid of all GlcCers (Msanne *et al.*, 2015).

Michaelson *et al*. (2009) already speculated that LCB Δ4-desaturation may have a significant role in channelling ceramide substrates into GlcCers in some plants and fungi. The observed metabolic changes in the *P. patens sd4d-1* and *gcs-1* mutants were similar to changes in sphingolipid profiles of the corresponding *P. pastoris* knockout mutants (Ternes *et al.*, 2011b). The *P. pastoris* LCB Δ4-desaturase knockout mutant, *Δ4Δ*, and the glucosylceramide synthase knockout mutant, *gcsΔ*, were also both devoid of GlcCers. Ternes *et al*., 2011b therefore confirmed the channelling function of LCB Δ4-desaturation for the yeast *P. pastoris*, whereas our study confirmed the function for the non-vascular plant *P. patens*.

In addition to the lack of GlcCers, *P. patens sd4d-1* plants were also devoid of d18:1 and d18:2 LCB moieties. This observation implied that double bond insertion into the *P. patens* LCB moiety follows a sequential order. The Δ4 double bond appears to be inserted first, followed by insertion of the Δ8 double bond. The d18:1$^{\Delta 4}$ LCB might therefore be the substrate for the LCB Δ8-desaturase. If the Δ4 double bond insertion is inhibited, as in case of the *sd4d-1* mutant, Δ8 double bond insertion could also not take place, and hence, no double bonds are present in *sd4d-1* LCB moieties. This suggestion is supported by the sphingolipid screen conducted by Islam *et al*., 2012. They investigated the double bond position in d18:1 LCB moieties and found that in the *P. patens* d18:1 LCB moiety, the double bond is present in Δ4 position.

An accumulation of putative substrate molecules of the LCB Δ4-desaturase reaction was observed in *P. patens sd4d-1*. The LCB Δ4-desaturase is assumed to use the d18:0

LCB moiety as substrate. Therefore, an enrichment of d18:0 LCBs or of ceramides with a d18:0 LCB moiety was expected. Significant increases were observed for d18:0 LCBs and for ceramides with a d18:0 LCB moiety in *sd4d-1* plants. The obtained data, however, does not indicate whether the *P. patens* LCB Δ4-desaturase preferably acts on LCBs or on LCBs bound in ceramides.

Interestingly, although in *sd4d-1* plants GlcCer formation was drastically reduced, residual GlcCers were still present. These leftover GlcCers contained a d18:0 moiety. This can be explained by the fact that GlcCers with a d18:0 LCB moiety were not affected by loss of the LCB Δ4-desaturase activity. However, in wild type and *sd4d-1* plants these molecular species were only present in trace amounts. Surprisingly, also the d18:2/h20:0 GlcCer species was detected in trace amounts in the *sd4d-1* mutant. This might be explained by the close functional relation of the LCB Δ4-desaturase to the LCB C-4 hydroxylase. Both enzymes have three characteristic histidine boxes in their active site and are part of a bifunctional enzyme complex in mammals (Ternes *et al.*, 2011a). The LCB C-4 hydroxylase might therefore have a low level of desaturase activity that is normally negligible in comparison to that of the desaturase. The LCB C-4 hydroxylase could have partially compensated for loss of the LCB Δ4-desaturase activity, however, the efficiency of the enzyme might only result in formation of trace amounts of the d18:2 LCB moiety.

Loss of almost all GlcCers in *sd4d-1* plants indicated that *Pp*GCS preferentially uses ceramides with a Δ4,8-diunsaturated LCB moiety as substrates. Furthermore, accumulation of the d18:2/h20:0 ceramide species in *gcs-1* mutants identified this compound as putative substrate of *Pp*GCS. *gcs-1* plants also accumulated d18:2 LCBs and d18:2 LCB-Ps. These sphingolipid compounds are upstream of the d18:2/h20:0 ceramide species; this result indicates that ceramide formation is a limiting step in sphingolipid biosynthesis.

Another interesting observation was the emergence of the d18:2/h20:0 species in the Hex-HexNAc-GlcA-IPC pool of the *gcs-1* mutant, which was associated with an increase of the total Hex-HexNAc-GlcA-IPC content. This implied that the *P. patens* enzymes involved in GIPC synthesis are able to metabolise ceramides with a d18:2 LCB moiety and are not restricted to ceramides with a t18:0 LCB moiety. As mentioned, GlcCer and GIPC synthesis are two alternative pathways within plant sphingolipid metabolism. The separation of these complex sphingolipids synthetic pathways likely relies on certain LCB modifications (Markham *et al.*, 2006). However, *P. patens* GIPC synthetic enzymes appear to be less restrictive in their substrate usage than *Pp*GCS. Further work is needed to better understand the regulation of complex sphingolipid biosynthesis in *P. patens*. Accumulation of GIPCs was also detected in the *A. thaliana gcs-1* null mutant. However, *A. thaliana gcs-1* cells did not accumulate the precursor ceramides (Msanne *et al.*, 2015). Instead, ceramides that were usually incorporated into GlcCers were channelled into GIPC formation

in *A. thaliana*. Consequently, this would indicate that GlcCer and GIPC synthetic enzymes compete more strongly for ceramide substrates in *A. thaliana* than in *P. patens*, in which the ceramide substrates of the corresponding complex sphingolipids enzymes are structurally more different. Consistent with the *P. patens* and *A. thaliana gcs* knockouts, *P. pastoris gcsΔ* had increased levels of the yeast equivalent for plant GIPCs: mannose-inositol-phosphoceramides (MIPCs) and mannose-(inositol phosphate)2-ceramides ($M(IP)_2Cs$) (Ternes *et al.*, 2011b). The similar metabolic changes observed in *gcs* mutants from different organisms indicate that channelling of ceramide substrates into complex sphingolipids formation underlies regulatory processes that are conserved in filamentous fungi and in plants.

Changes in the sphingolipid profiles also affected *gcs-1* and *sd4d-1* morphology. Since *sd4d-1* and *gcs-1* mutants were both deficient in GlcCer synthesis, it was expected that they would exhibit similar morphological phenotypes. However, surprisingly, while *sd4d-1* plants had almost normal growth and development in all investigated developmental stages, *gcs-1* plants had dwarfed gametophores and impaired protonema cell differentiation. Msanne *et al*., 2015 showed that *A. thaliana gcs* RNAi suppression lines with as little as 2 % of wild type GlcCer levels were fertile, whereas *gcs* null mutants were seedling lethal and had impaired organogenesis. As mentioned, *P. patens sd4d-1* plants had residual GlcCer levels. The cumulative findings from vascular and non-vascular plants suggest that plant performance and cell differentiation are not highly sensitive to GlcCer quantity, but a threshold level of GlcCers is required for normal growth and development (Melser *et al.*, 2011; König *et al.*, 2012; Msanne *et al.*, 2015).

Studies on *A. thaliana* mutants that had reduced GlcCer levels described defects in organ-specific cell differentiation and an altered Golgi morphology (Melser *et al.*, 2010; Krüger *et al.*, 2013; Msanne *et al.*, 2015). The authors therefore speculated about a role of GlcCers in Golgi-mediated protein trafficking. An impaired cell differentiation was also observed in *P. patens gcs-1* mutants which is consistent to the vascular plant studies. GlcCers may therefore potentially also be involved in endomembrane trafficking in *P. patens*.

P. patens gcs-1 mutants also developed cell death-like lesions, especially in chloronema cells and when gametophores were flooded with water and cultivated under short-day conditions at 17 °C. A strong indicator for cell death symptoms in *P. patens* is the upregulation of the defence-related marker genes *PAL4*, *CHS*, and *ERF5* (Bressendorff, 2012; Overdijk *et al.*, 2016) in *gcs-1* (Fig. 6A-C). The results further indicate that the *P. patens* sphingolipid metabolism may be associated with the initiation of defence responses and that metabolic changes in the *gcs-1* sphingolipidome may be specifically responsible for the induction of these plant defence mechanisms. However, it has to be

considered that all the analysed genes have multiple alleles in *P. patens* that are highly homologous to each other. Therefore, the gene fragments that were amplified during qRT PCR likely derived from gene families within the *P. patens* genome and not from a single gene. It is assumed that the alleles have redundant functions within the *P. patens* physiology and the results therefore allow for conclusions about their functional activity in the *gcs-1* mutant.

Which exact metabolic changes induce the defence signalling cascade still needs to be elucidated. In contrast to *sd4d-1*, *gcs-1* accumulated LCBs, hydroxyceramides and Hex-HexNAc-GlcA-IPCs. LCBs and ceramides are known signalling compounds that are able to induce PCD in *A. thaliana* (Greenberg *et al.*, 2000; Liang *et al.*, 2003; Shi *et al.*, 2007; Alden *et al.*, 2011). Their elevated levels in *P. patens gcs-1* plants might therefore also stimulate cell death induction. Especially the enrichment of hydroxyceramides appears to be specific for *gcs-1* mutants, putting this compound into the spotlight as potential inducer for the observed phenotype. (Fig. 5).

Previous studies showed that jasmonic acid (JA) is not produced by *P. patens*. However, its precursor molecules OPDA and *dn*-OPDA were determined (Stumpe *et al.*, 2010). This indicates that JA signalling in non-vascular plants differs from JA signalling in vascular plants with OPDA and *dn*-OPDA being the active compounds. For another bryophyte, *Marchantia polymorpha*, it was recently shown that *dn*-OPDA indeed binds instead to the JA receptor COI1 (Monte *et al.*, 2018). A connection between the sphingolipid metabolism and JA signalling was already described for vascular plants (Magnin-Robert *et al.*, 2015; Zienkiewicz *et al.*, 2020). Accumulation of JA-Ile was observed in response to pathogen infection and in developmentally controlled PCD (dPCD). Zienkiewicz *et al*. (2020) reported a correlation between hydroxyceramide accumulation in *A. thaliana* neutral ceramidase 1 knockout plant, *ncer1*, and elevated levels of jasmonate-isoleucine (JA-Ile). A correlation of JA signalling and sphingolipid metabolism has not yet been described for *P. patens* and was observed during this study for the first time. The accumulation of jasmonates in *P. patens gcs-1* plants may be associated with the observed accumulation of hydroxyceramides, which in combination might cause the cell death lesions in the mutant. As described, *gcs-1* plants showed PCD like lesions in chloronema cells and in gametophores that were flooded with water. Browning of the tissue may indicate early senescence symptoms. To fully elucidate the connection between JA signalling and sphingolipid metabolism in *P. patens*, more studies have to be conducted on other sphingolipid mutants.

Although *P. patens gcs-1* mutants were substantially impaired in growth and development, they could be maintained and investigated without major challenges. This was not the case for *A. thaliana gcs-1* null mutants whose development did not progress

beyond the seedling stage. However, it remains unclear whether fertility and reproduction were affected in *P. patens gcs-1* and *sd4d-1*. Their involvement in these processes is strongly indicated by their specific gene expression in spores an in the sporophyte generation. Future studies should therefore focus on identification of defects in reproductive tissue and in sporulation possibly by using the Reute ecotype which showed enhanced sporulation compared to the Gransden strain (Hiss *et al.*, 2017).

In summary, our findings show that LCB Δ4-desaturation is an important regulatory mechanism in *P: patens* to channel ceramides into GlcCer formation. Although *P. patens sd4d-1* and *gcs-1* plants were both mostly devoid of GlcCers, the two mutant lines had substantially different morphological phenotypes. Phenotype differences may be explained by the stronger accumulation of precursor LCBs and hydroxyceramides in *gcs-1* compared to *sd4d-1*. These sphingolipid compounds might act as signalling molecules that trigger induction of processes such as PCD. Even if GlcCers with a Δ4,8-diunsaturated LCB moiety are abundant membrane compounds in *P. patens*, their complete abolishment did not interfere with plant survival, which questions their quantitative relevance in plants. *P. patens* is a valuable model organism in the study and understanding of plant sphingolipid metabolism.

Acknowledgements

We are grateful to Dr. Ellen Hornung, Pia Meyer, and Dr. Hanno Resemann for generating the *sd4d* and *gcs-1* mutants. J.G. has been a doctoral student of the Ph.D. program "Microbiology and Biochemistry" from the Göttingen Graduate Center for Neurosciences, Biophysics, and Molecular Biosciences (GGNB) at the Georg August University Göttingen. I.F. acknowledges funding through the German Research Foundation (INST 186/822-1 and DFG, INST 186/1167-1).

Author Contribution

I.F. and J.G. designed the experiments. J.G. performed the experiments. K.Z. performed phytohormone mesurements. J.G. performed and analysed the lipid measurements with the assistance of C.H.. J.G. wrote the manuscript. T.M.H. and I.F. edited the manuscript and I.F. supervised the study.

Supplementary data

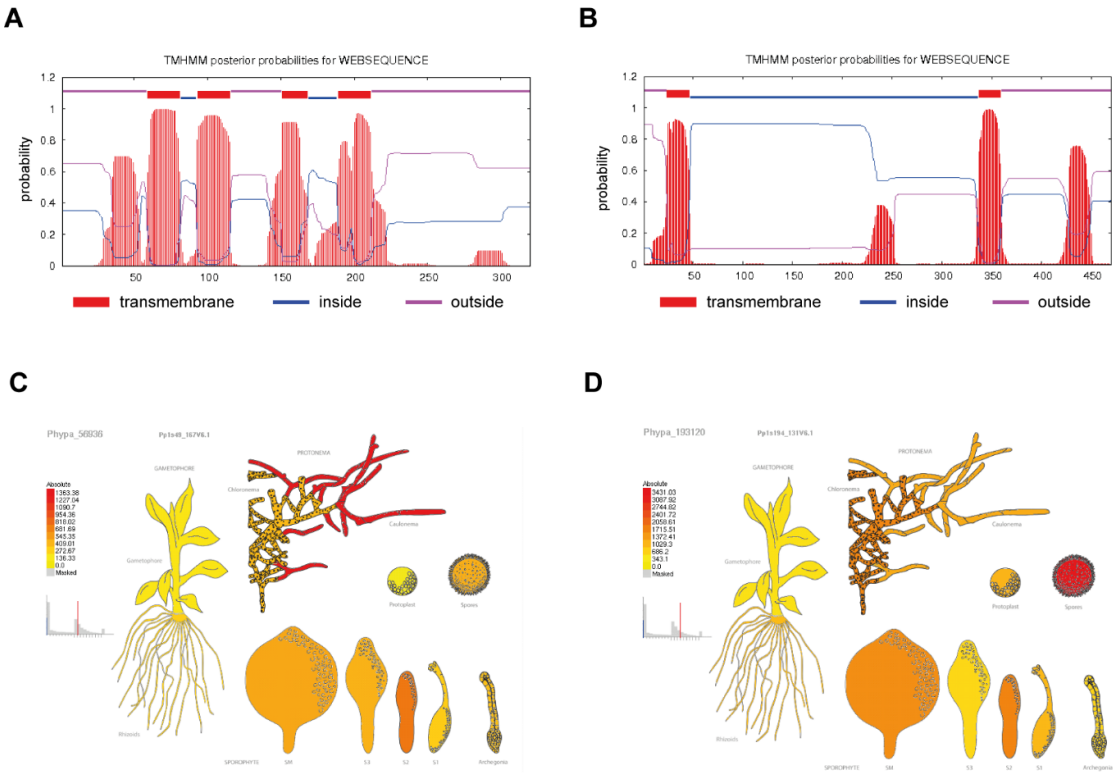

Fig. S1. Prediction data for transmembrane domains and gene expression. Transmembrane domain prediction was done for (A) *Pp*SD4D and (B) *Pp*GCS using TMHMM webtool. Gene expression for (C) *PpSD4D* and (D) *PpGCS* in *P. patens* organs was predicted using eFP browser.

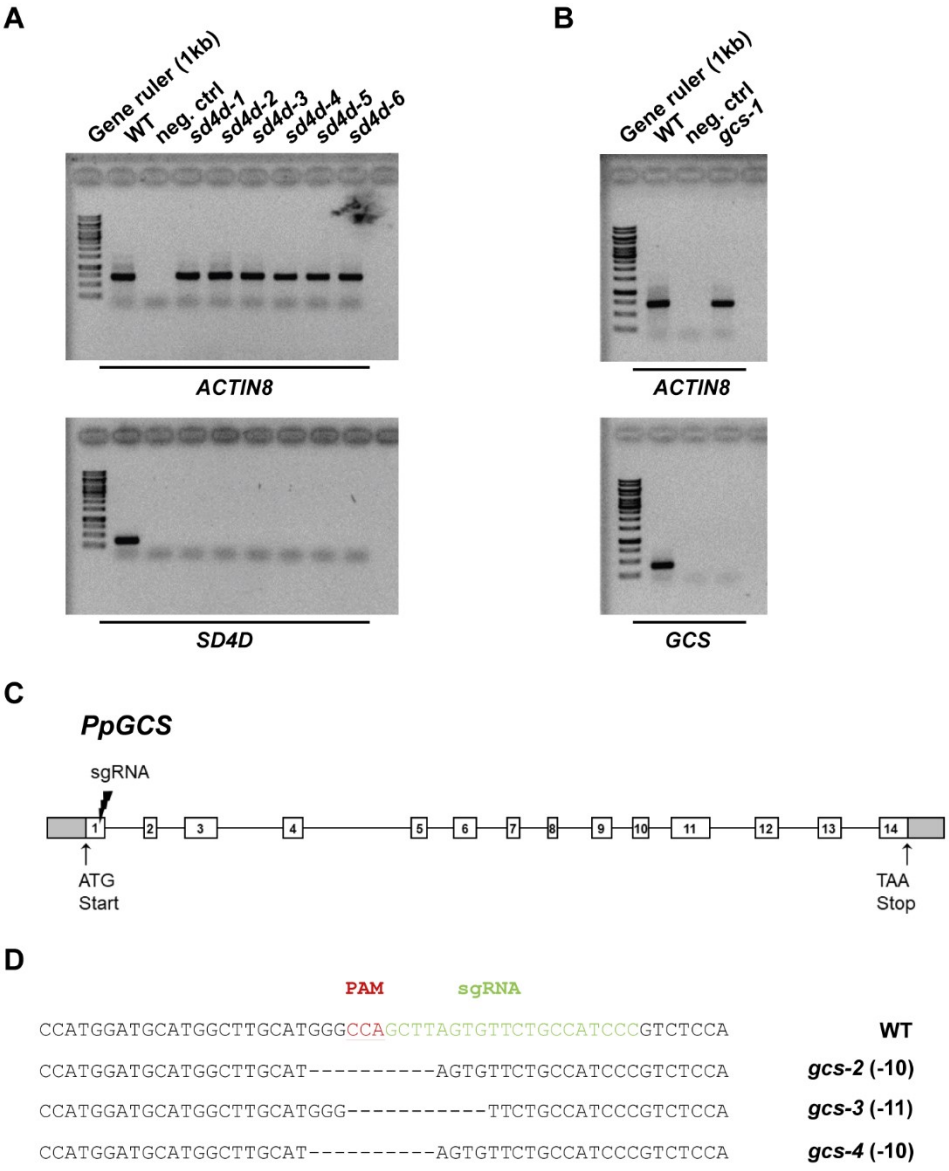

Fig. S2. *sd4d* and *gcs* mutant characterisation. Complete gel picture of (A) *PpSD4D* and (B) *PpGCS* transcript determination by real-time PCR. *ACTIN8* was used as reference gene and water as negative control (neg. ctrl). (C) CRISPR-Cas9 gene editing strategy for *PpGCS* targeting. Single-guide RNA (sgRNA) was designed to target the first exon of *PpGCS*. White boxes indicate exons, grey boxes indicate untranslated regions and lines indicate introns. (D) Sequencing of the targeted locus revealed three *gcs* mutants with frame shift deletions.

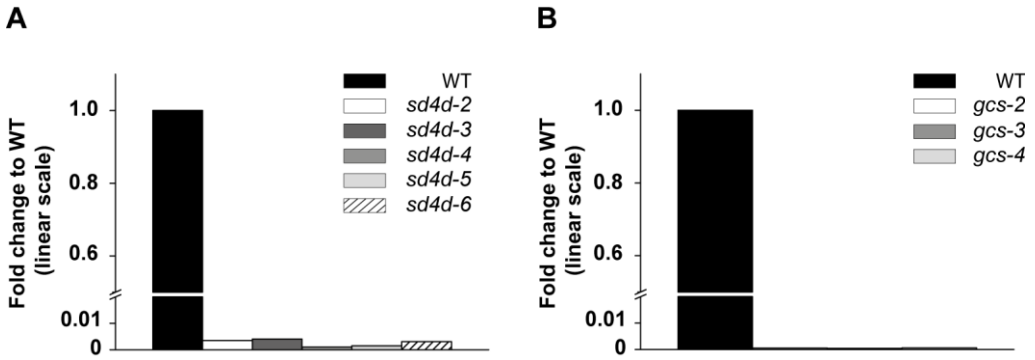

Fig. S3. GlcCer content of *P. patens* wild type, *sd4d,* and *gcs* mutants. Glycosylceramides (GlcCers) were extracted from protonema of ten-day-old wild type (WT), *sd4d-2, -3, -4, -5, -6* and *gcs-2, -3, -4 P. patens* and analysed with UPLC-nanoESI-MS/MS. Fold changes of (A) *sd4d* GlcCers and (B) *gcs* GlcCers to WT GlcCers were calculated using absolute peak areas. Fold changes are depicted in linear scale. The WT is set to 1. Sphingolipid data represent the measurement from one cultivation.

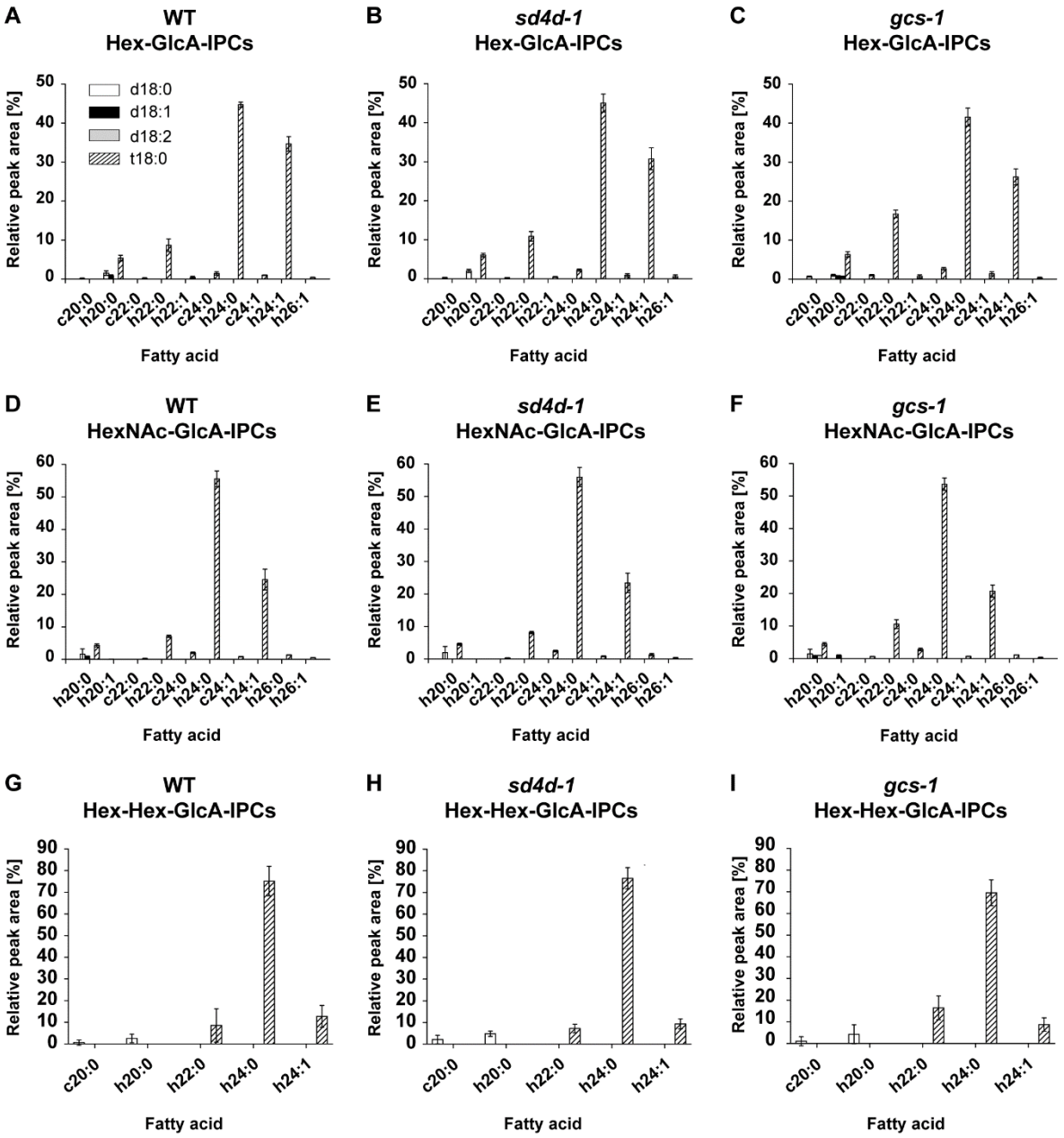

Fig. S4. GIPC profiles of *P. patens* wild type, *sd4d-1*, and *gcs-1*. (A-C) Glycosyl inositolphosphorylceramides (GIPCs) were extracted from protonema of ten-day-old wild type (WT), *sd4d-1*, and *gcs-1 P. patens* and analysed with UPLC-nanoESI-MS/MS. GIPC molecular species are shown with their LCB (column colour) and fatty acid (x-axis) moieties. Dihydroxy LCB moieties are indicated by a 'd' and trihydroxy LCB moieties are indicated by a 't'. Molecular species with an unhydroxylated fatty acid moiety are indicated by a 'c' and molecular species with an α-hydroxylated fatty acid moiety are indicated by an 'h'. (A-C) Relative Hex-GlcA-IPC profiles of (A) WT, (b) *sd4d-1*, and (C) *gcs-1*. (D-F) Relative HexNAc-GlcA-IPC profiles of (D) WT, (E) *sd4d-1*, and (F) *gcs-1*. (G-I) Relative Hex-Hex-GlcA-IPC profiles of (G) WT, (H) *sd4d-1*, and (I) *gcs-1*. Only molecular species with a peak area ≥ 0.5 % in at least one of the three lines were included in GIPC graphs. Sphingolipid data represent the mean ± SD of measurements from four independent cultivations each containing protonema material from eight cultivation plates. Abbreviations are as follows: GlcA: glucuronic acid; Hex: hexose; HexNAc. *N*-acetylhexosamine, IPCs: inositolphosphorylceramides.

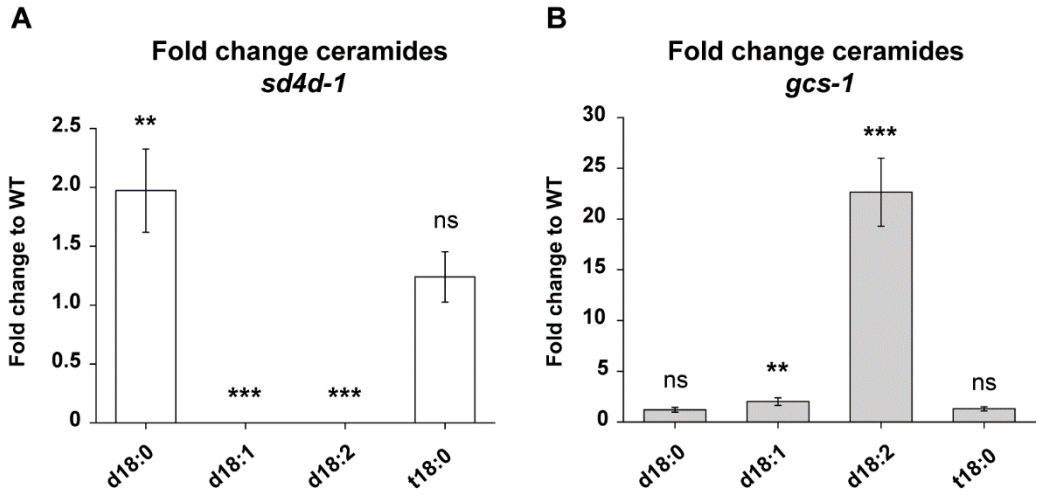

Fig. S5. Total content of LCB moieties in *P. patens sd4d-1* and *gcs-1* ceramides. Ceramides were extracted from protonema of ten-day-old wild type (WT), *sd4d-1*, and *gcs-1 P. patens* and analysed with UPLC-nanoESI-MS/MS. Species with the same LCB moiety were summed up. Fold changes of ceramide LCB moieties from (A) *sd4d-1* and (B) *gcs-1* to the WT were calculated using absolute peak areas. Fold changes are depicted in linear scale. The WT, which is not shown, is set to 1. Sphingolipid data represent the mean ± SD of measurements from four independent cultivations each containing protonema material from eight cultivation plates. Statistical analysis was done using Student's *t*-test. Asterisks indicate different significance levels with *** significance at $P < 0.001$, ** significance at $P < 0.01$, and not significant (ns) at $P > 0.05$ compared to the WT.

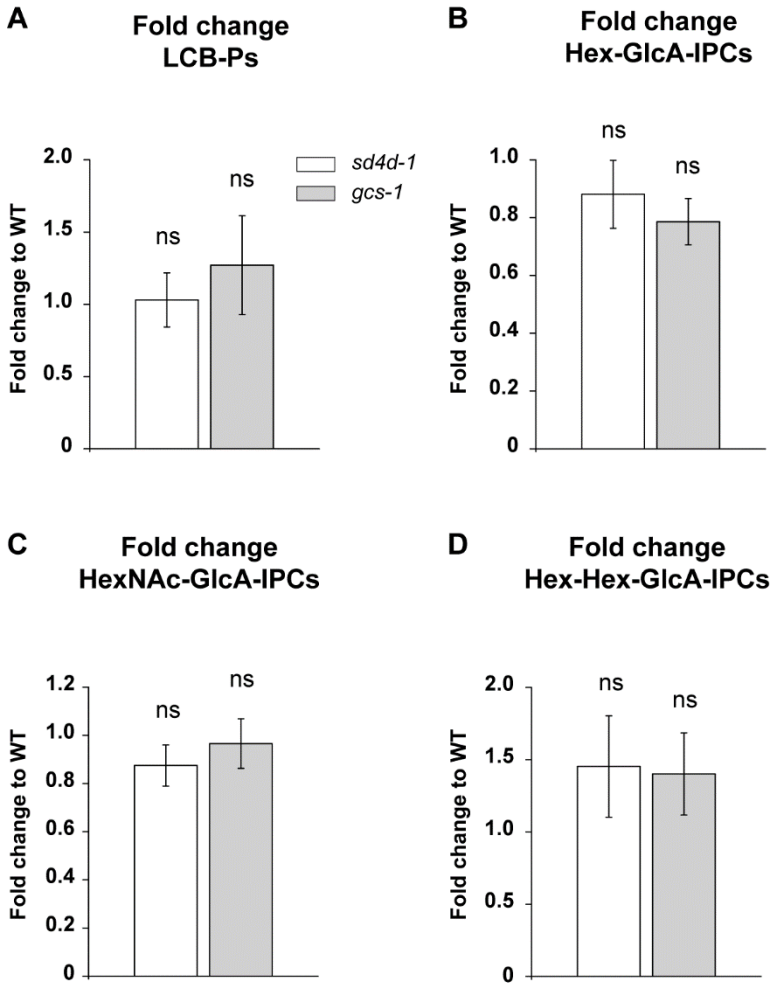

Fig. S6. Total contents of LCB-Ps and other GIPC classes in *sd4d-1* and *gcs-1*. Phosphorylated long-chain bases (LCB-Ps), and glycosyl inositolphosphorylceramide (GIPCs) were extracted from protonema of ten-day-old wild type (WT), *sd4d-1*, and *gcs-1 P. patens* and analysed with UPLC-nanoESI-MS/MS. Fold changes of (A) LCB-Ps, (B) Hex-GlcA-IPCs, (C) HexNAc-GlcA-IPCs, and (D) Hex-Hex-GlcA-IPCs to the WT were calculated using absolute peak areas. Fold changes are depicted in linear scale. The WT, which is not shown, is set to 1. Sphingolipid data represent the mean ± SD of measurements from four independent cultivations each containing protonema material from eight cultivation plates. Statistical analysis was done using Student's *t*-test. Letters indicate no significance (ns) to the WT with $P > 0.05$. Abbreviations are as follows: GlcA: glucuronic acid; Hex: hexose, HexNAc: *N*-acetylhexosamine, IPCs: inositolphosphate.

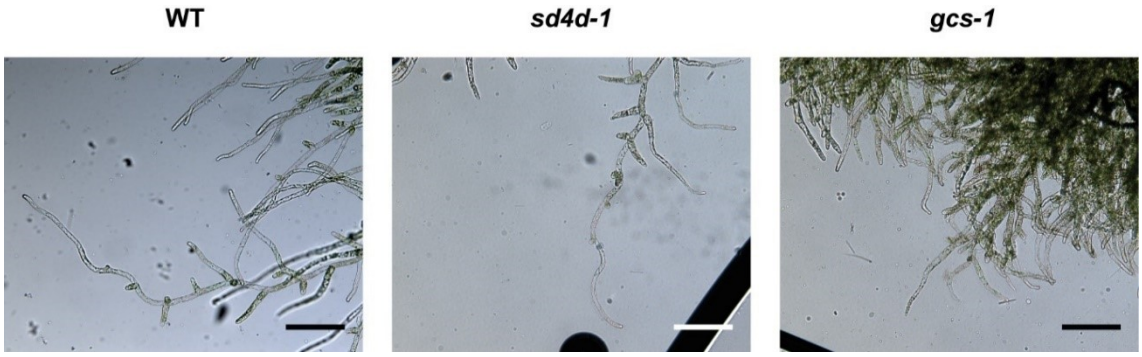

Fig. S7. Protonema filaments of *P. patens* wild type, *sd4d-1* and *gcs-1* plants. Pictures of wild type (WT), *sd4d-1*, and *gcs-1* protonema were captured after plants were grown for two weeks on cellophane-covered medium. Scale bars are 0.2 mm.

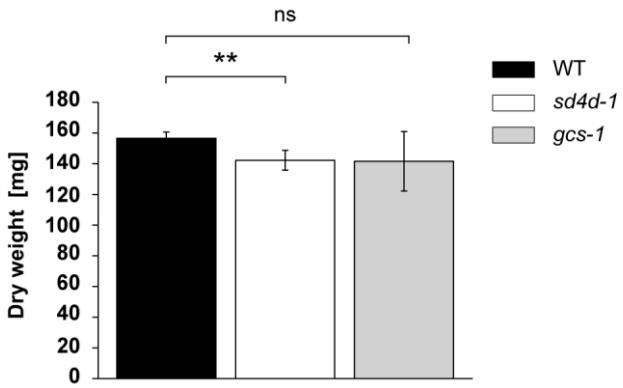

Fig. S8. Dry weight protonema biomass of *P. patens* wild type, *sd4d-1*, and *gcs-1*. Growth capacities of the wild type (WT), *sd4d-1*, and *gcs-1* lines were quantified by collecting and lyophilising ten-day-old protonema grown on cellophane-covered BCD medium and determining the dry weight. Data represent the mean ± SD of measurements from four independent cultivations each containing protonema material from eight cultivation plates. Statistical analysis was done using Student's *t*-test. Asterisks indicate significance level with ** significance at $P < 0.01$ and not significant (ns) at $P > 0.05$ compared with the WT.

6 Discussion

The plant PM is a highly dynamic and complex structure. It represents a semipermeable barrier that separates the inside of a cell to its external environment. Plants are constantly exposed to external stimuli and stresses and rely on intercellular communication to respond to these incoming signals appropriately. The PM therefore has a vital role during signal perception and transmission. Different membrane components are responsible for coordinating membrane-associated signal transduction processes. More and more evidence indicates a heterogenous lateral distribution of membrane lipids and proteins within the plant PM (Grison *et al.*, 2015; Grosjean *et al.*, 2015; Cacas *et al.*, 2016; Grosjean *et al.*, 2018). The plant PM is considered as a fluid and dynamic system with various lipid micro- and nanodomains. PM organisation needs to be orchestrated in a flexible manner and membrane domains are assumed to be key players in PM organisation. Some of these domains are enriched in sterols and sphingolipids (Grosjean *et al*., 2015; Grosjean *et al*., 2018; Cacas *et al*., 2016). This distinct lipid composition equips the membrane fractions with different biophysical properties, making them more ordered and thicker than the surrounding membrane regions (Mamode Cassim *et al*., 2019). These domains function as sorting platforms for membrane proteins and are therefore considered crucial for mediating signalling cascades (Mamode Cassim *et al*., 2019). GlcCers and GIPCs are the two most abundant sphingolipids in plants and are expected to be the main sphingolipids involved in membrane domain formation and other physiological processes (Borner *et al.*, 2005; Markham *et al.*, 2006; Grosjean *et al.*, 2015). The two classes have different head groups and ceramide backbones and are therefore assumed to have distinct physiological functions. However, their exact roles within the plant membrane system remain to be determined. The tissue and organ complexity of commonly used model plants are a challenge in the study of *in vivo* PM dynamics. Furthermore, disruption of genes that are involved in the formation of complex sphingolipids cause severe growth and development defects in vascular plants and in some cases even result in embryo lethality (Chen *et al.*, 2008; Msanne *et al.*, 2015; Gonzalez Solis *et al.*, 2020).

The bryophyte model *P. patens* has a simple anatomy compared to vascular plants, allowing for in-depth investigations of subcellular processes on a single cell level. A recent study determined the sphingolipidome composition of *P. patens* and revealed significant differences to the *A. thaliana* sphingolipidome (Markham *et al.*, 2006; Resemann, 2018). However, this comprehensive lipidomics analysis of about 700 lipid species was conducted on liquid-grown *P. patens* protonema and may therefore not reflect the sphingolipid composition under native conditions and in different tissues. The roles of individual sphingolipid classes during *P. patens* growth and development therefore remain elusive.

To determine the physiological functions of sphingolipids in distinct tissues and development stages of *P. patens*, a tightly controlled cultivation method is required. An appropriate cultivation system was therefore established and optimised for in-depth phenotype and chemotype examinations of sphingolipid mutants (chapter 1). Independent *P. patens* sphingolipid pathway mutants disturbed in GIPC or GlcCer synthesis were investigated. While *Pp*S4H is involved in GIPC formation (chapter 2), *Pp*SD4D and *Pp*GCS are involved in GlcCer formation (chapter 3). The cumulative findings from all three chapters allow first conclusions about the involvement of GIPCs and GlcCers in *P. patens* physiology. Table 2 summarises the findings from the three *P. patens* and the corresponding *A. thaliana* sphingolipid mutants.

Table 2. Comparison of three *P. patens* and *A. thaliana* sphingolipid mutants. Shown are their phenotypes, chemotypes and their suggested physiological impact.

Organism	Designated gene symbol	Gene ID	Phenotype	Chemotype	Physiological impact
LCB C-4 hydroxylase					
P. patens	*PpS4H*	XM_024507119.1	Severely dwarfed gametophores, stunted, shortened protonema, altered cross-walls	Change from t18:0 to d18:0 LCB species, drastic accumulation of LCBs and LCB-Ps	Impaired cell growth and tissue development, possibly cytokinesis defects
A. thaliana	*AtSBH1, AtSBH2* (Chen *et al*., 2008)	At1g69640, At1g14290	Growth reductions, cannot progress from vegetative to reproductive growth, upregulation of cell death-associated genes	Change from t18:1 to d18:1 and d18:0 LCB species, drastic accumulation of all sphingolipid classes, accumulation of dihydroxy/LCFA sphingolipids	Impaired plant growth and tissue development, cell extension and division defects
LCB Δ4-desaturase					
P. patens	*PpSD4D*	XM_024506175.1	Shorter protonema cells	Substantial reduction of GlcCers, accumulation of LCBs and ceramides	Cell elongation defects
A. thaliana	None (Michaelson *et al*., 2009)	At4g04930	No phenotype	Significant reduction of pollen GlcCers	
Glycosylceramide synthase/ Glucosylceramide synthase					
P. patens	*PpGCS*	XM_024543952.1	Dwarfed gametophores, cell differentiation defects, cell death-like lesions, upregulation of defence-related genes,	No GlcCers, increased levels of hydroxyceramides, LCBs, and GIPCs, accumulation of OPDA and *dn*-OPDA	Impaired cell differentiation, developmentally controlled PCD
A. thaliana	*AtGCS* (Msanne *et al*., 2015)	At2g19880	Seedling lethality, impaired Golgi morphology	No of GlcCers, increased levels of GIPCs	Impaired cell differentiation, organogenesis defects, possibly protein trafficking defects

The following sections discuss the results from this work and contextualise them with findings on sphingolipid function in vascular plants. The bryophyte *P. patens* is proposed as suitable model organism to investigate *in planta* membrane dynamics and to dissect the physiological roles of GlcCers and GIPCs. This non-vascular plant may also contribute to our understanding of how plant sphingolipid biosynthesis diversified during land colonisation.

6.1 LCB modifications determine the metabolic fate of *P. patens* sphingolipids

GIPCs and GlcCers can be structurally distinguished by their head group and ceramide backbone composition. The structural difference of their ceramide backbones is likely key for channelling substrates into the two alternative complex sphingolipid classes. In *A. thaliana*, GIPCs are highly enriched in molecular species with a t18:1 LCB moiety that is connected to VLCFAs (Markham *et al*., 2006). *A. thaliana* GlcCers, especially those found in pollen tissue, are, however, additionally enriched in 18:2 LCB moieties conjugated to LCFAs, mainly C16 (Markham *et al.*, 2006; Markham & Jaworski, 2007). In *P. patens*, GIPCs and GlcCers have different LCB and fatty acid compositions than in *A. thaliana* (Resemann, 2018). *P. patens* GIPCs are composed of a t18:0 LCB moiety that is conjugated to VLCFAs. *P. patens* GlcCers are mainly (up to 92 %) composed of one single species with a Δ4,8-diunsaturated LCB moiety that is conjugated to a h20:0 fatty acid moiety (d18:2/h20:0). Other species like d18:1/h20:0, d18:2/h22:0 or d18:2/c20:0 account for around 4 %, 2 %, and 1 % of *P. patens* GlcCers, respectively. The functional rationale of the diversification of plant sphingolipid metabolism among different plant lineages is, however, not understood.

*Pp*S4H and *Pp*SD4D activities are considered the first designated steps in GIPC and GlcCer synthesis, respectively. The following text therefore compares the lipid profiles of the respective knockout mutants of these two key enzymes.

GIPC and GlcCer synthesis represent alternative pathways in plant sphingolipid metabolism. Their syntheses therefore underlie specific control mechanisms. *Pp*S4H and *Pp*SD4D activities are considered key modifications for channelling ceramide substrates into either GIPC or GlcCer formation. They both act on the C-4 of the LCB moiety and are therefore mutually exclusive. *Pp*S4H catalyses C-4 hydroxylation of the LCB moiety and is therefore responsible for t18:0 LCB formation. *Pp*SD4D introduces a double bond between the C-4 and the C-5 of the LCB moiety and is therefore responsible for the formation of Δ4-unsaturated LCBs. While ceramides with a t18:0 LCB moiety are channelled into GIPC formation, ceramides with a Δ4,8-diunsaturated LCB moiety, d18:2, are shunted into GlcCer formation. A proposed scheme for ceramide channelling into complex sphingolipid formation in *P. patens* is depicted in Fig. 5.

Interestingly, disruption of the *P. patens* sphingolipid enzymes *Pp*S4H and *Pp*SD4D caused significantly different metabolic changes in the mutants. Loss of one hydroxyl group in the LCB moiety of *s4h* mutants caused a global shift in LCB moieties of GIPCs, ceramides, and LCBs (chapter 2). Consequently, the prevalent LCB moiety t18:0 in *P. patens* wild type plants was replaced by the d18:0 LCB moiety in *s4h* plants.

Furthermore, the head group composition of GIPCs was affected. Compared to the wild type, *s4h* mutants accumulated series B GIPCs. Disruption of *PpSD4D*, however, resulted in loss of all double bonds in the LCB moiety of *sd4d-1* plants and consequently in loss of almost all GlcCers (chapter 3). Only some minor species that represent < 1 % of *P. patens* GlcCers in the wild type were still detected in the *sd4d-1* mutant. However, these remaining species were only present in trace amounts. These observations give a deeper insight into GlcCer and GIPC biosynthesis in *P. patens*. The shift from a t18:0 to a d18:0 LCB moiety in *s4h* GIPCs demonstrates that enzymes catalysing the transfer of inositolphphate to the ceramide backbone are not exclusively using ceramide substrates with a t18:0 LCB moiety but can also act on ceramides with a d18:0 LCB moiety. Loss of almost all GlcCers in *sd4d-1* plants, however, indicates that the enzyme catalysing the synthesis of GlcCers, *Pp*GCS, is highly selective for ceramides containing dihydroxy LCB moieties but cannot act on ceramides with a trihydroxy LCB moiety.

It is likely that other factors also contribute to the channelling of ceramide substrates into either one of the two pathways, such as spatial and temporal separation. A spatial separation of GIPC synthesis is described for *A. thaliana* (Michaelson *et al.*, 2016). While almost all enzymes active in sphingolipid biosynthesis are located in the ER, enzymes assembling the head groups of GIPCs are located in the Golgi apparatus membrane (Wang *et al.*, 2008; Ishikawa *et al.*, 2018). Ceramides with a trihydroxy LCB unit thus need to be transported to the Golgi apparatus, where they are further incorporated into GIPCs. Spatial separation of enzymes that assemble glycan moieties of the GIPC head groups in the Golgi apparatus could be associated with the localisation of cell wall glycan biosynthesis enzymes in the Golgi membrane (Oikawa *et al.*, 2013). Co-presence of glycan synthetic and glycan transferring enzymes in the Golgi membrane might suggest a division of labor between enzymes involved in PM and cell wall biosynthesis. A similar separation system is likely also present in *P. patens* but should be confirmed in future studies. Spatial separation of GIPC synthetic enzymes from other sphingolipid enzymes allows them to be less specific for a certain ceramide substrate. Findings from the *s4h* mutant indicate that all ceramides exported to the Golgi apparatus are used for GIPC formation.

The *A. thaliana* glucosylceramide synthase, however, is located, like other enzymes of the sphingolipid pathway, in the ER membrane (Melser *et al.*, 2010). The t18:0 LCB moiety is prevalent in all *P. patens* sphingolipids, except for GlcCers. Its omnipresence in *P. patens* GIPCs, ceramides, and LCBs and the presence of *Pp*GCS in the ER might explain the necessity of the high substrate selectivity of *Pp*GCS. The Δ4,8-diunsaturated LCB moiety is only found in the GlcCer pool in high levels. It is likely that already small amounts of ceramides with a Δ4,8-diunsaturated LCB moiety are immediately metabolised by a

highly active and specific *Pp*GCS, instead of being transported to the Golgi for GIPC formation.

In *A. thaliana*, however, the GlcCer pool contains molecular species with d18:1, d18:2, and t18:1 LCB moieties (Markham *et al.*, 2006). This observation indicates that GCS enzymes from different plants might have varying substrate preferences. This might be due to the provision of structurally different ceramide substrates in individual plant species. For instance, t18:1 LCB moieties appear to be absent in *P. patens*. To determine GCS substrate preferences, *in vitro* enzyme assays might be performed in future studies.

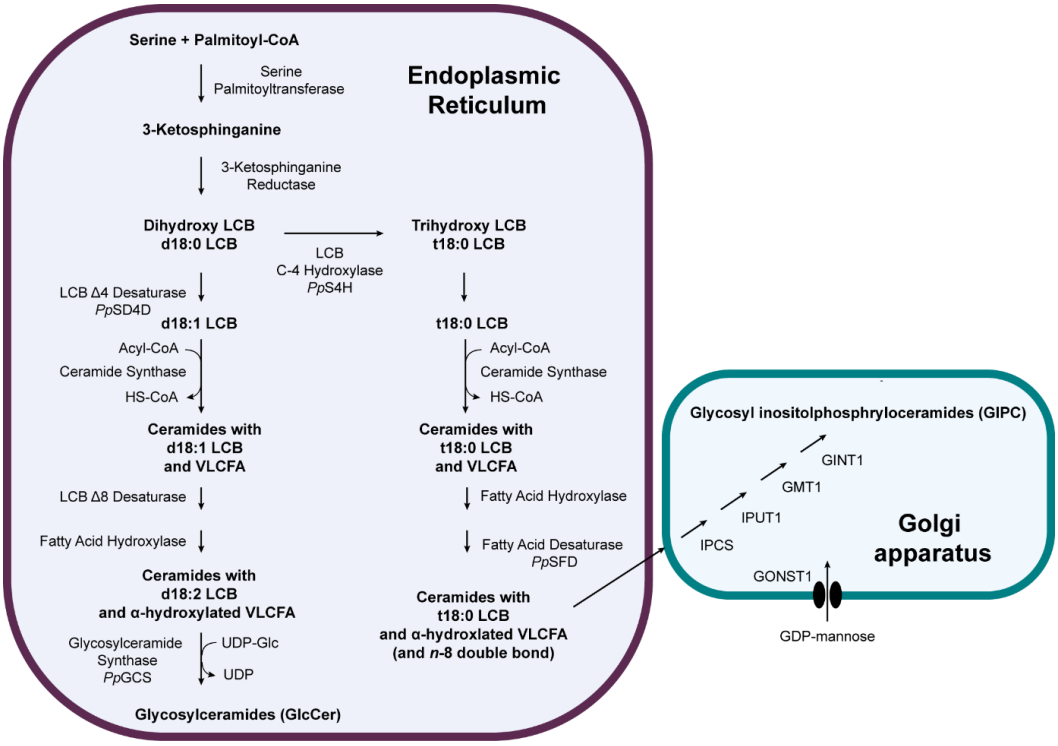

Fig. 5. Proposed abbreviated *de novo* sphingolipid biosynthesis in *P. patens*. The majority of reactions within sphingolipid biosynthesis most likely takes place in the endoplasmic reticulum (ER). During the initial steps, the simplest sphingolipid compound, the long-chain base (LCB) sphinganine (d18:0), is formed. The d18:0 LCB is subsequently applied to modifications such as Δ4-desaturation (*Pp*SD4D), or C-4 hydroxylation (*Pp*S4H). *N*-acylation of the LCB moiety results in ceramide formation. Depending on the structural features of the LCB, different substrate-specific ceramide synthases might be active. The ceramide backbone may subsequently be modified by fatty acid α-hydroxylation, or fatty acid *n*-8 desaturation (*Pp*SFD). The combination of structurally different LCB and fatty acid moieties causes channelling of distinct ceramide substrates into glycosylceramide (GlcCer) formation (*Pp*GCS) or glycosyl inositolphosphorylceramide (GIPC) formation. The demonstrated pathway is an abbreviated version of sphingolipid biosynthesis, not including reactions such as phosphorylation, de-phosphorylation or breakdown of complex sphingolipids. Abbreviations are as follows: CoA: Coenzyme A; GCS: Glycosylceramide Synthase; GDP-Man: Guanosine Diphosphate Mannose; GINT1: Glucosamine Inositolphosphorylceramide Synthase; GMT: GIPC Mannosyl Transferase; GONST1: GDP-Mannose Transporter; SFD: Sphingolipid Fatty acid Desaturase; IPCS: Inositolphosphorylceramide Synthase; IPUT: Inositolphosphorylceramide Glucuronosyl Transferase; SD4D: Sphingolipid delta 4 Desaturase; S4H: Sphinganine C-4 Hydroxylase; UDP-Glc: Uridine Diphosphate Glucose.

It should also be noted that loss of the *Pp*S4H activity caused a 60-fold accumulation of the putative substrate d18:0 LCB (chapter 2). LCB levels were also significantly increased (1.5-fold) upon loss of *Pp*SD4D activity, although to a much lesser degree than in *s4h* plants (chapter 3). As for the respective enzymes from *A. thaliana* it is assumed that *Pp*S4H may

preferably act on d18:0 LCBs, while *Pp*SD4D may act on d18:0 LCBs or ceramide-bound d18:0 LCBs. Nevertheless, previous studies on maize microsomes showed that the LCB C-4 hydroxylase can act on LCBs as well as on bound LCBs in ceramides (Wright *et al.*, 2003). While that assay showed the LCB hydroxylase activity on LCBs and ceramides *in vitro*, it is not clear whether it also reflects the *in vivo* situation. The *in vivo* LCB and/ or ceramide substrate preferences of *Pp*S4H and *Pp*SD4D therefore need to be determined in the future.

The different accumulation levels of the putative substrates in the two independent knockout mutants might give a hint about the physiological relevance of *Pp*S4H and *Pp*SD4D activities. The t18:0 LCB moiety is prevalent in LCBs, ceramides, and GIPCs. Loss of the LCB C-4 hydroxylation caused an exceptional accumulation of LCBs. In comparison to that, d18:1 and d18:2 LCB moieties are only detected in very low amounts in *P. patens* wild type LCBs and ceramides and in high levels in GlcCers. Loss of LCB Δ4-desaturation only caused a minor increase of LCBs. The precursor accumulation and the general prevalence of the t18:0 LCB moiety might suggest a more important physiological function for the LCB C-4 hydroxylase than for the LCB Δ4-desaturation in *P. patens*. Another aspect that would support this hypothesis is that the overall *s4h* phenotype was much more severe than the *sd4d-1* phenotype (Table 1).

Neither of the two enzymes was able to compensate for substrate accumulation caused by loss of the other, which would have prevented the observed accumulations in the *s4h* and *sd4d-1* knockout mutants (chapter 2, chapter 3). It is not clear how the activities of *Pp*S4H and *Pp*SD4D are regulated. Determination of kinetics of the two enzymes *in vitro* might give an idea of their conversion efficiencies. It could also be that *Pp*S4H and *Pp*SD4D reactions are spatially separated within the ER. The regulation and localisation of *Pp*S4H and *Pp*SD4D activities should therefore be addressed in future studies.

It is also unclear whether the prevalences of LCB moieties with different structural features in GIPCs and GlcCers play a role in their physiological functions. Studies on other plants suggest that the t18:0 LCB moiety of GIPCs is important for the interaction with other membrane components during membrane domain formation (Mamode Cassim *et al.*, 2019). LCB desaturation, however, has been correlated with low temperature tolerance (Chen *et al.*, 2012). The d18:2 LCB moiety of *P. patens* GlcCers may therefore play a role in cold stress adaptation by adjusting membrane fluidity.

6.2 *P. patens* GlcCer mutants have similar chemotypes but contradicting phenotypes

*Pp*S4H and *Pp*SD4D are alternative reactions that introduce different modifications to the LCB moiety and hence affect the downstream metabolic fate of sphingolipids. The third investigated sphingolipid mutant of this study had a disturbed *Pp*GCS function. *Pp*GCS

catalyses GlcCer formation. The metabolic differences between the *sd4d-1* and *gcs-1* mutants are discussed in chapter 3. The contradicting phenotypes and chemotypes of the two mutants, however, put the function of GlcCers in *P. patens* physiology into question. Although both *sd4d-1* and *gcs-1* mutants lacked most GlcCers, only *gcs-1* plants had a strong growth and development phenotype and showed cell death symptoms. An explanation for this might be the accumulation of hydroxyceramides in *gcs-1* mutants that is not observed in *sd4d-1* mutants. Ceramides are not only precursor molecules for GlcCer and GIPC synthesis, but they are also known as signalling molecules with the potential to elicit PCD in plants (Greenberg *et al.*, 2000; Liang *et al.*, 2003). A connection between hydroxyceramide accumulation, JA signalling, and developmentally controlled PCD (dPCD) was already discussed in chapter 3 (Zienkiewicz *et al.*, 2020). If indeed the accumulation of hydroxyceramides and not the absence of GlcCers is responsible for the observed cell death-like lesions and the growth inhibition of *gcs-1* plants, the question arises if GlcCers even have an essential function in *P. patens*. Although reduced in size, *gcs-1* mutants were still viable and only had defects in the differentiation into skotonema cells (Cove *et al.*, 1978; Rensing *et al.*, 2020). It might be that only very low GlcCer amounts are required for certain plant physiological processes such as cell differentiation. This would be supported by findings from *sd4d-1* mutants. In contrast to *P. patens gcs-1* plants *sd4d-1* plants still had trace amounts of GlcCers and showed almost no impairments.

The quantitative relevance of GlcCers in plants was already discussed by Msanne *et al*. (2015) who characterised the glucosylceramide synthase mutant, *gcs-1*, from *A. thaliana*. Together with other studies Msanne *et al*. (2015) provided evidence that strong GlcCer reduction to a certain threshold (down to 2 %) does not affect plant viability and a reduction of 50-75 % does barely even have an effect on plant growth (Melser *et al.*, 2011; Chen *et al.*, 2012; König *et al.*, 2012). They therefore speculated that excess production of GlcCers may serve as non-toxic sphingolipid reservoir that avoids a potential harmful accumulation of ceramides.

It might also be that GlcCers become quantitatively more important under unfavourable conditions, which were not investigated in the presented studies. In case of *P. patens*, another, although a rather unlikely, explanation might be that not all GlcCer species have yet been identified in the bryophyte. While the sphingolipidome of *A. thaliana* is thoroughly investigated and described, only one extensive study has been conducted on characterising the *P. patens* sphingolipidome (Resemann, 2018). The study was performed using a targeted MRM-based LC-MS method. This method was also used for the investigation of the three sphingolipid mutants in this study. The used strategy only screens for molecular species whose MRMs have been generated beforehand. Unexpected molecular species might therefore have been omitted in the measurements. The disruption

of *Pp*GCS ensures the abolishment of all GlcCers because hexose moieties cannot be conjugated to any possible ceramide backbone anymore. Disruption of *Pp*SD4D, however, only prevents LCB double bond introduction. That means that GlcCers with unexpected ceramide backbone compositions might exist in *P. patens* that have yet to be identified.

To address the question of the physiological impact of GlcCers in the future, a *P. patens* double knockout mutant could be generated that not only targets *Pp*GCS but also *Pp*SD4D function. Thereby, a complete abolishment of GlcCers would be achieved without initiating the unusual accumulation of the ceramide precursor d18:2/h20:0 that potentially induced the observed PCD symptoms in *gcs-1* plants. If the *gcs-1* mutant phenotype is rescued in that double knockout, it would mean that the cell death symptoms and development defects are indeed induced by the unusual hydroxyceramide accumulation in *gcs-1* plants. It would further indicate a less important physiological role for GlcCers in *P. patens* than expected.

6.3 Lipid profile comparison of *P. patens* and other plants

Complex sphingolipids, GIPCs and GlcCers, are the most abundant sphingolipids found in plants. GIPCs and GlcCers represent around 64 % and 34 %, respectively, of all sphingolipids in total *A. thaliana* leaf extract (Markham *et al.*, 2006). In tomato and soybean, however, both complex sphingolipid classes are found in equal quantities (Sperling *et al.*, 2005; Markham *et al.*, 2006). Depending on the analysed plant species and tissue type, the prevalence of both classes may vary (Sperling *et al.*, 2005; Markham *et al.*, 2006; Luttgeharm *et al.*, 2015b). The quantitative distribution of GIPCs and GlcCers in *P. patens* is, however, unknown. The functional significance of the diversification of plant sphingolipid metabolism among different plant lineages is poorly understood. The following sections discuss the general differences of sphingolipid profiles from different plants. Furthermore, the influence of other lipid classes on sphingolipid levels and *vice versa* is discussed.

As mentioned, the t18:0 LCB moiety is found in GIPCs and the d18:2 LCB moiety in GlcCers of *P. patens*. The t18:0 LCB moiety also predominates in the precursors LCBs and ceramides. It would thus be interesting to know whether the downstream sphingolipid classes GIPCs and GlcCers occur in different quantities in *P. patens*. Sphingolipid data from Resemann (2018) and from this work are represented as relative data within individual sphingolipid classes. Sphingolipid species and classes could not be compared quantitatively with each other because structural features of different molecular species in LCBs, ceramides, GlcCers, and GIPCs have different ionisation efficiencies in the applied UPLC-nanoESI-MS/MS approach. The different ionisation efficiencies may thus falsify quantification of individual sphingolipid species and classes. While the LC-MS approach is the method of choice in lipid analyses in terms of coverage, sensitivity, and selectivity it is

not appropriate for quantification. Future studies should therefore focus on combining LC-MS measurements with other techniques such as gas chromatography (GC), thin layer chromatography (TLC), or direct infusion mass spectrometry (DI-MS) that are more appropriate for absolute compound quantification.

Another idea would be the establishment of a set of lipid standards for structurally different molecular species in LC-MS measurements that would allow for direct comparison of molecular species quantities.

GIPCs and GlcCers are found in varying amounts in different tissues (Sperling *et al.*, 2005; Markham *et al.*, 2006; Luttgeharm *et al.*, 2015b). While GIPCs are considered the predominant class in *A. thaliana* leaves, GlcCers are enriched in *A. thaliana* pollen and floral tissue (Michaelson *et al.*, 2009; Luttgeharm *et al.*, 2015b). Therefore, it would be interesting to investigate the quantitative distribution of GIPCs and GlcCers in different *P. patens* tissues. The sphingolipid profiles of distinct tissues may indicate different physiological roles of GIPCs and GlcCers during *P. patens* development. The sporophyte tissue, which was not analysed in the studies presented in this thesis, would be of particular interest. The GlcCer specific enzymes *Pp*SD4D and *Pp*GCS are both highly expressed in *P. patens* sporophyte tissue as reported by the eFP browser (chapter 3). While gene expression may not necessarily be linked to a certain physiological function, studies from *A. thaliana* show an involvement of GlcCers in reproduction processes (Msanne *et al.*, 2015). In *A. thaliana*, Δ4,8-diunsaturated GlcCers are enriched in reproductive tissues, including pollen and floral tissue (Michaelson *et al.*, 2009). *A. thaliana* mutants that are deficient in GlcCer also show defects in pollen transmission (Msanne *et al.*, 2015). As discussed in chapter 3, the *P. patens* 'Gransden' strain that has been propagated for decades as wild type under laboratory conditions is acknowledged to have a low sporulation efficiency (Hiss *et al.*, 2017; Meyberg *et al.*, 2020). Therefore, it might be helpful to introduce the mutations into another ecotype with a higher sporulation rate and to determine sporophyte sphingolipid profiles in this other background. The 'Reute' ecotype was found to have a much higher sporulation efficiency than the 'Gransden' strain and therefore appears to be an appropriate candidate for future sporophyte studies in *P. patens* (Hiss *et al.*, 2017). If the sporophyte indeed has higher GlcCer levels, the 'Reute' ecotype could further be used for generating mutants that are disturbed in their GlcCer biosynthesis such as the *sd4d-1* and *gcs-1* mutants generated in the study of chapter 3 in the 'Gransden' background. Reproduction processes could then be monitored in *sd4d-1* and *gcs-1* mutants or even in the proposed *sd4d gcs* double knockout in the 'Reute' background.

GlcCer and GIPC localisation has also already been determined on a subcellular level in vascular plants. Both were found in membranes of the secretory pathway, with highest levels in the tonoplast and the PM (Moreau *et al.*, 1998; Cacas *et al.*, 2016).

Sphingolipids are considered to be located in the outer leaflet of the plant PM (Tjellström *et al.*, 2010; Cacas *et al.*, 2016). Most sphingolipid analyses conducted in this work were performed on crude lipid extract from *P. patens* protonema tissue. However, a better detection for GIPCs was achieved by analysing microsome fractions of *P. patens* (chapter 2). Microsomes are artificial vesicles that are rebuilt from intracellular membrane fragments, mostly ER and PM. They can be extracted from broken eukaryotic cells and reflect the cellular membrane composition. The increased detection of GIPCs in microsomes may indicate an enrichment of this lipid class in the extracted membrane fractions. *P. patens* GlcCers (mainly d18:2/h20:0) were detected with high signal intensity in crude lipid extracts as well as in microsome fractions. Whether that means that GlcCers are more abundant than GIPCs in *P. patens* is not clear and has to be confirmed with quantitative analytics. For an absolute quantification of complex sphingolipids in different membrane compartments, improvements in the lipid extraction and an internal standard use would be required.

Isolation of the plant PM would reveal whether GIPCs are especially enriched in the *P. patens* PM. An appropriate PM isolation method has been established for plant tissue and has already been applied for PM purification of *A. thaliana* leaf tissue (Larsson *et al.*, 1994). Even more details of the PM composition and especially about a putative plant PM lipid asymmetry might give selective analysis of the inner and outer leaflets of the *P. patens* PM. This would show whether complex sphingolipids are enriched in the outer PM leaflet in *P. patens*. Presence of complex sphingolipids in the outer leaflet would enforce their presumptive role in signal perception and transmission processes.

As explained in the introduction, DRM fractions may not necessarily reflect the lipid composition of *in vivo* membrane rafts. However, previous studies on animal and plant membrane rafts *in vivo* showed that although DRM preparation has clear technical limitations, the lipid compositions of DRMs and membrane rafts may indeed be similar (Pike, 2009; Cacas *et al.*, 2016). Therefore, it might be an idea to prepare DRM fractions of *P. patens* PM and investigate the lipid composition of these fragments. The three sphingolipid mutants might be useful tools in determining the contribution of GlcCers and GIPCs in membrane domain formation in *P. patens*.

Next to sphingolipids it could also be interesting to determine levels and compositions of other lipid classes in the three *P. patens* sphingolipid knockouts. It might be that metabolic changes in the complex sphingolipid pools and the associated reshaping of the membrane lipid composition are reflected in changes of other lipid classes such as phosphosglycerolipids, glycoglycerolipids, neutral glycerolipids, and sterol lipids (Table 1). *P. patens* GIPCs and GlcCers both contain VLCFAs. One idea would therefore be to check whether the VLCFA content of phosphoglycerolipids such as PS, PE, and PC is affected in the investigated sphingolipid mutants. Of particular interest would also be the composition

of free and conjugated sterols. Sterols and sphingolipids are considered the key components of membrane micro- and nanodomains (Simons & Ikonen, 1997; Mongrand *et al.*, 2010). Changes in the GIPC and GlcCer composition are hence expected to influence phytosterol composition and maybe to some extent the total sterol content. Both free sterols and conjugated sterols were found to induce microdomain formation in artificial vesicles from tobacco lipid mixtures (Grosjean *et al.*, 2015; Grosjean *et al.*, 2018). Grosjean *et al*. (2015) also examined the influence of GIPCs and GlcCers on lipid raft formation. Although both complex sphingolipid classes appeared to have a role in raft formation, GIPCs were described as the main sphingolipid components in lipid rafts. The studies were conducted on artificial vesicles built-up of different ratios of tobacco sterol and sphingolipid classes. Even though these are first indications for the involvement of different sphingolipids and phytosterols in membrane raft formation, it is not known how the situation is *in planta* and if the findings apply to all plant species. The observed changes in the glycosylated sterol composition in *P. patens s4h* microsomes (chapter 2) is a strong indication for the interaction between sphingolipids and sterols in *P. patens* membranes. Accordingly, the determination of acyl steryl glycosides (ASG) and free sterol levels in *P. patens s4h* plants might give even more details about the interaction network of GIPCs and sterols in *P. patens*. Sterol levels were not determined in *P. patens sd4d-1* and *gcs-1* plants in the presented study (chapter 3). To get an idea about the interaction between GlcCers and sterols in *P. patens*, microsomes should be prepared from these mutants and free and conjugated sterol levels should be determined. Finally, quantification of sterols and other lipids in the sphingolipid mutants might give even more detailed insights into the absolute *P. patens* membrane lipid composition.

Other lipids worth investigating in sphingolipid mutants are PIs and PIPs. PIs and PIPs are plant PM components that are involved in directional tip growth of pollen tubes, root hairs, and protonema filaments (Ischebeck *et al.*, 2008; Sousa *et al.*, 2008; Stenzel *et al.*, 2008; Saavedra *et al.*, 2015). Green fluorescent protein (GFP) fusions of phosphatidylinositol phosphate kinase (PIPK) and their transient overexpression in *P. patens* protoplasts located PIPK to the PM (Saavedra *et al.*, 2009). Furthermore, PIPs, were found to be enriched in DRM fractions, which indicates their localisation to distinct membrane domains (Furt *et al.*, 2010). PIPs were also described to be clustered in nanodomains in the PM (Furt *et al.*, 2010). Saavedra *et al*., (2011) described a role for PIPKs in rhizoid elongation and caulonema development in *P. patens*. Since *P. patens s4h*, *sd4d-1*, and *gcs-1* mutants investigated in this work all showed impaired cell elongation, cell differentiation, and general growth and development defects, it would be of interest to test whether PI and PIP levels in these mutants are also affected. The phenotype of PIPK mutants in *P. patens* showed stunted protonema and rhizoid growth. The PIPK mutant

growth phenotypes were remarkably similar to the described *s4h* and *gcs-1* mutant phenotypes from this work (Saavedra *et al.*, 2011). Future studies might reveal interactions between sphingolipids and PIPs during *P. patens* development. It is likely that PIPs as well as complex sphingolipids are located in distinct domains in the inner and outer leaflet of the plant PM, respectively (Cacas *et al.*, 2016; Gronnier *et al.*, 2017; Mamode Cassim *et al.*, 2019). These domains might interact through leaflet interdigitation during signal transduction processes. Future studies on *P. patens* membrane dynamics might reveal domain interaction among the two leaflets during signalling processes.

6.4 Differences in other sphingolipid enzyme activities of *A. thaliana* and *P. patens*

All three investigated *P. patens* sphingolipid mutants were also characterised in *A. thaliana* (Chen *et al.*, 2008; Michaelson *et al.*, 2009; Msanne *et al.*, 2015). The lipid profiles of the respective knockout mutants from both organisms were already compared and discussed in chapters 2 and 3. Comparing the results from *P. patens* sphingolipid mutants with results obtained from the respective *A. thaliana* mutants even give indications about other sphingolipid enzyme activities that were not the focus of the presented studies. In the following, differences between the lipid profiles of the *P. patens* and *A. thaliana* sphingolipid mutants are discussed that might give hints about functions of other *P. patens* sphingolipid enzymes. The findings may broaden our knowledge on the evolution of plant sphingolipid metabolism.

The following text discusses the putative presence of substrate-specific ceramide synthases in *P. patens*, based on the results from the *A. thaliana sbh1 sbh2* and the *P. patens s4h* mutants (chapter 2) and on the observed gametophore ceramide profile (chapter 1).

A. thaliana contains two classes of distinct ER-localised ceramide synthases that have different substrate preferences (Fig. 6). The class I ceramide synthase LOH2 prefers dihydroxy LCBs and LCFAs, mainly C16. Class II ceramide synthases, LOH1 and LOH3, prefer trihydroxy LCBs and VLCFAs (Marion *et al.*, 2008; Markham *et al.*, 2011; Ternes *et al.*, 2011a). LOH1 and LOH3 share high protein sequence similarity while the sequence of LOH2 is substantially different. The divergence of LOH2 from LOH1 and LOH3 likely occurred early in land plant evolution because phylogenetic clustering of distinct ceramide synthases was already observed in *P. patens* (Rensing *et al.*, 2008; Ternes *et al.*, 2011a). The activity of substrate-specific ceramide synthases in *A. thaliana* results in two distinct ceramide pools that have different structural features. While ceramide backbones with a trihydroxy LCB moiety and VLCFAs are detected in GlcCers and GIPCs in *A. thaliana*,

ceramide backbones with a dihydroxy LCB moiety and LCFAs are only enriched in GlcCers (Fig. 6).

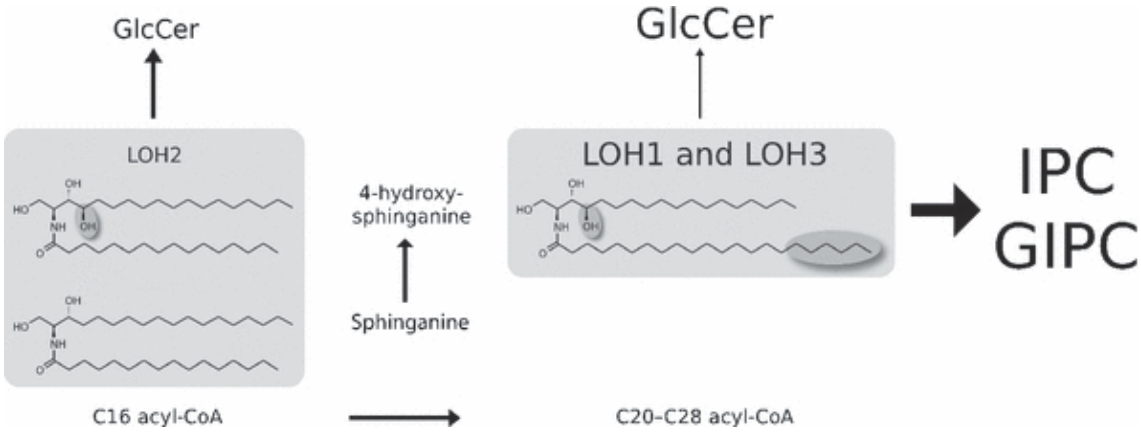

Fig. 6. Ceramide synthase activity of LOH1, LOH2, and LOH3 in *A. thaliana*. The ceramide synthases LOH1, LOH2, and LOH3 from *A. thaliana* have different substrate preferences for LCBs with specific hydroxylation status and fatty acids of different acyl chain lengths. LOH2 prefers dihydroxy LCB moieties (sphinganine) and C20 fatty acids, whereas LOH1 and LOH3 prefer trihydroxy LCB moieties (4-hydroxy-sphinganine) and VLCFAs. The glycosyl inositolphosphorylceramide (GIPC) pool contains ceramides from LOH1 and LOH3 ceramide synthases. The glucosylceramide (GlcCer) pool contains ceramides generated by all three ceramide synthases. Font sizes demonstrate the relative size of the complex sphingolipid pools. Different arrow thicknesses indicate estimated conversion efficiencies (not to scale). Figure taken from (Ternes *et al*., 2011).

According to Ternes *et al*. (2011a) two putative *P. patens* ceramide synthases show protein sequence similarity to *A. thaliana* LOH2 and three other putative *P. patens* ceramide synthases show sequence similarity to *A. thaliana* LOH1 and LOH3. Therefore, it was assumed that ceramide synthases in *P. patens* have similar substrate preferences as *A. thaliana* ceramide synthases.

First indications for the presence of substrate-specific ceramide synthases in *A. thaliana* were derived from observations made in the LCB C-4 hydroxylase mutant *sbh1 sbh2* (Chen *et al.*, 2008). The authors found that the absence of trihydroxy LCB moieties in the double knockout mutant caused an enrichment in sphingolipids with dihydroxy LCB moieties and a C16 fatty acid moiety. They therefore concluded that distinct ceramide synthases may act on different LCB and fatty acid substrates. Later studies confirmed this hypothesis by describing *A. thaliana* LOH1, LOH2, and LOH3 enzyme activities and metabolic changes in the respective knockout mutants (Markham *et al.*, 2011; Ternes *et al.*, 2011a). Comparison of the sphingolipid profiles from *A. thaliana sbh1 sbh2* and *P. patens s4h* revealed that in contrast to *sbh1 sbh2* plants, *s4h* mutants do not accumulate sphingolipids with dihydroxy LCB moieties and C16 LCBs (chapter 2). Sphingolipids with a C16 fatty acid moiety are in general minor species in *P. patens*. However, there is a clear distinction in the ceramide backbones of *P. patens* wild type GlcCers and GIPCs. Dihydroxy LCB moieties are mainly connected to a C20 fatty acid moiety in GlcCers, while the trihydroxy LCB moiety in GIPCs is connected to C20-C24 fatty

acid moieties (chapters 1-3). In addition to that, gametophore tissue is enriched in ceramide species with a C20 fatty acid moiety compared to protonema tissue (chapter 1). *A. thaliana* LOH1 and LOH3 showed highest homology to *P. patens* XP_024374569.1 while *A. thaliana* LOH2 showed highest homology to *P. patens* XP_024361685.1. The reported expression of the two putative *P. patens* ceramide synthases in the eFP browser revealed that the LOH2 *P. patens* homologue has higher expression in gametophore tissue than the LOH1, LOH3 homologue (Fig. S1). These predicted expression patterns strongly suggest that distinct substrate-specific ceramide synthases might be active in different developmental stages of *P. patens*.

Cumulative findings from different parts of this study strongly suggests the presence of functionally distinct ceramide synthases in *P. patens*. While this might be a similar situation to *A. thaliana* ceramide synthases, substrate preferences of ceramide synthases from both organisms are likely different. This might indicate a different evolutionary background of the enzyme activities in *A. thaliana* and *P. patens*. Future studies on *P. patens* ceramide synthase knockout mutants should focus on analysing different growth stages and will give more information about ceramide synthase activities in *P. patens*.

6.5 Metabolic changes in *P. patens* sphingolipid metabolism cause varying phenotypes

The functional relevance of complex plant sphingolipids is not yet fully understood. Recent studies have unravelled roles for GIPCs and GlcCers in multiple key physiological processes in vascular plants. The involvement of GIPCs and GlcCers in these processes is assumed partially due to their contribution in membrane domain formation in the PM. GIPCs are associated with sensing and responding to salt stress (Jiang *et al.*, 2019), are identified as receptors for NLP toxin (Lenarčič *et al.*, 2017), and have a crucial role in controlling plasmodesmal cell-to-cell transport (Yan *et al.*, 2019; Liu *et al.*, 2020). GlcCers, on the other hand, are essential in organogenesis, cell differentiation, pollen transmission, protein secretion, and in tolerance towards cold stress (Uemura *et al.*, 1995; Melser *et al.*, 2010; Msanne *et al.*, 2015).

Examination of knockout mutants is a useful tool to determine the physiological role of certain plant metabolites. Mutant phenotypes thereby give indications about the physiological relevance of the missing compound. In the following, the three investigated *P. patens* sphingolipid mutant phenotypes are discussed and compared with each other.

Of all three investigated sphingolipid mutants the *s4h* mutant, which is involved in GIPC formation in *P. patens*, showed the most severe growth phenotype (chapter 2). The plant was unable to develop fully grown gametophores and had a generally dwarfed morphology. Also, *s4h* protonema cross-walls were misshaped compared to the wild type.

The altered cross-walls might indicate an involvement of plant GIPCs in cytokinesis processes. The observed cross-wall morphology with strands reaching into the cytoplasm of both adjacent cells also resembled microtubule structures. Microtubules are part of the cytoskeletal network and are involved in vesicular transport of cell wall components to the phragmoplast during cytokinesis (de Keijzer *et al.*, 2017). It could be that the cell wall component callose is not properly transported to the cell plate destination site because of disturbed vesicle dynamics. To confirm a co-localisation of callose and microtubules in *s4h* mutants, the microtubule network would have to be visualised with the help of a tubulin-specific staining or with stable GFP marker lines. It is, however, not clear whether the observed growth defect is attributed to the changed GIPC structure, GlcCer structure, ceramide structure, or to the unusual increase of LCBs and LCB-Ps. Even though it is tempting to speculate that the observed growth and developmental *s4h* phenotype is attributed to the changed LCB moiety and the resulting biophysical changes in the plasma membrane, the exceptional drastic increase of LCBs and LCB-Ps must also be considered to have a strong effect on plant physiology. Especially the fact that LCBs are known signalling molecules during plant PCD (Abbas *et al.*, 1994; Shi *et al.*, 2007; Alden *et al.*, 2011) may indicate an involvement of these compounds in physiological changes in *s4h* plants.

The GlcCer-deficient *gcs-1* mutant also showed a dwarfed morphology even though it was less severe than the observed phenotype of *s4h* mutants (chapter 3). Moreover, the *gcs-1* mutant did not show an altered protonema cross-wall morphology. In contrast to the *s4h* mutant, the *gcs-1* mutant had PCD-like lesions in both protonema and gametophore tissue, that were accompanied with the up-regulation of defence-related marker genes. On top of that, *gcs-1* mutants had protonema cell differentiation defects that were not observed in *s4h* mutants. This reflects the metabolic differences between the *s4h* and in the *gcs-1* mutants and shows that these metabolic changes may have different effects on *P. patens* physiology. Potential inducers of physiological changes in *s4h* might be the drastic accumulation if LCBs, LCB-Ps or the change in GIPC structure. In *gcs-1* the resulting physiological defects might result from the accumulation of hydroxyceramides or the abolishment of GlcCers.

Unlike the *gcs-1* phenotype, the *sd4d-1* phenotype was surprisingly mild (chapter 3). Plant growth and development was very similar to the wild type. In contrast to *s4h* mutants, protonema cross-walls of *sd4d-1* did not have an altered morphology. *sd4d-1* plants were, however, impaired in skotonema cell elongation even though the observed defect was not very prominent. Although *Pp*SD4D and *Pp*GCS are located in the same complex sphingolipid pathway, the phenotypes significantly differed from each other. With respect to the similar underlying metabolic changes in the sphingolipid profiles this was a

surprising observation. The potential metabolic reasons for the different mutant phenotypes were discussed in chapter 3 and part 6.2 of the discussion.

All these findings indicate that GIPCs and GlcCers might have different functions in *P. patens* physiology. Changes in GIPC composition of *s4h* mutants caused severe growth defects, possibly by interfering with cytokinesis. Lack of GlcCers in the *gcs-1* plant caused cell differentiation defects and cell death induction that might derive from impaired endomembrane trafficking (Melser *et al.*, 2010; Msanne *et al.*, 2015). Strong reduction but not complete abolishment of GlcCers in the *sd4d-1* mutant, however, had almost no effect on plant physiology.

Analogous to the investigated GlcCer-deficient mutants it would be interesting to study sphingolipid mutants that are devoid of all GIPCs. Comparing these mutants with the *gcs-1* mutant would give an idea about the different physiological relevance of both complex sphingolipid compounds. However, the severe *s4h* growth defect suggests that GIPC-deficient mutants might be lethal.

6.6 GIPCs and GlcCers likely confer similar functions in *A. thaliana* and *P. patens*

Comparing the *P. patens* sphingolipid mutant phenotypes to phenotypes of the respective knockout mutants in *A. thaliana* may provide information about the conservation of GlcCer and GIPC function during land plant evolution. The following text discusses the physiological phenotypes observed in *A. thaliana* and *P. patens* sphingolipid mutants. An important aspect of *A. thaliana* sphingolipid mutants is that many plants that have a disturbed sphingolipid biosynthesis are embryo lethal or they are unable to reach reproductive maturity (Chen *et al.*, 2008; Msanne *et al.*, 2015; Gonzalez Solis *et al.*, 2020). This was the case for *A. thaliana gcs-1* and *sbh1 sbh2* mutants. For mutant studies in *A. thaliana* this is a great disadvantage because plant propagation relies on sexual reproduction. To overcome this issue, the authors mostly switch to RNAi suppressor lines that exhibit moderate phenotypes (Chen *et al.*, 2008). *P. patens*, however, can be propagated vegetatively. True knockout mutants that might be affected in their sexual reproduction can therefore still be easily propagated and phenotypes can be thoroughly examined.

P. patens s4h mutants and *A. thaliana sbh1 sbh2* mutants showed similar morphological phenotypes. Both plant mutants were severely dwarfed and likely had cytokinesis defects. Plant GIPCs mostly consist of a ceramide backbone with a trihydroxy LCB moiety and an α-hydroxylated fatty acid moiety (Cacas *et al.*, 2013; Buré *et al.*, 2014; Resemann, 2018). Thus, the hydroxylation status of the ceramide backbone appears to be an important structural feature for plant GIPCs. Free hydroxyl groups in the LCB moiety and

in the fatty acid moiety are considered important for the interaction of sphingolipids with surrounding membrane molecules, especially with sterols (Mamode Cassim *et al.*, 2019). Disruption of the hydroxylation, either on the LCB or on the fatty acid moiety, is therefore assumed to have major effects on GIPC structure and thus on the biophysical properties of the membrane. As mentioned, *P. patens s4h* mutants have a different GIPC composition than wild type plants (chapter 2). The t18:0 LCB moiety of *s4h* GIPCs is replaced by the d18:0 LCB moiety. Furthermore, *s4h* plants are enriched in series B GIPCs compared to the wild type. The *A. thaliana* LCB C-4 hydroxylase mutant *sbh1 sbh2* showed a similar switch from the t18:1 LCB moiety to the d18:1 LCB moiety. Both mutants were not investigated for defects in membrane dynamics or organisation. However, the *A. thaliana* fatty acid hydroxylase mutant, *fah1 fah2*, characterised by König *et al*. (2012), was described to have a disturbed membrane organisation (Lenarčič *et al.*, 2017). Membrane organisation was determined using the environment-sensitive, fluorescent probe di-4-ANEPPDHQ, which enables visualisation of membrane microdomains. The compound inserts into the lipid bilayer. Depending on the phase order of the surrounding membrane compartment, the dye exhibits either red fluorescence in a Lo phase-like structure or green fluorescence in a Ld phase-like structure. The emission shift between images taken in each emission spectrum is determined from the red and green ratio of the membrane. The ratio of the fluorescence spectrum consequently indicates the relative proportion of each distinct phase and hence gives an idea about the order level of the investigated membrane fraction. While *A. thaliana* wild type membranes are mostly found in an Lo phase, the *fah1 fah2* mutant membrane exhibited an Ld phase-like membrane order (Lenarčič *et al.*, 2017). The assay may also be applied for *P. patens s4h* plants. In *A. thaliana fah1 fah2* plants the experiment was performed on protoplasts. However, *P. patens* protonema cells are easily accessible for in-depth single-cell microscopic examinations and the lipid order may be directly determined in protonema cells, which have undergone minimal manipulation and retain their cell walls. This would give an idea about the impact of the structure change in *s4h* GIPCs on the overall membrane organisation and hence might explain the observed *s4h* development phenotype. Accordingly, it may also be helpful to generate *P. patens* mutants that are defective in fatty acid hydroxylation and to compare these mutant phenotypes with the *s4h* phenotype. Both of the mutants have an impaired ceramide backbone hydroxylation which may influence the hydrogen bond network between membrane components and hence the ability to form membrane domains (Slotte, 2016; Mamode Cassim *et al.*, 2019). Comparing the two mutants might clarify whether hydroxylation on the LCB moiety or on the fatty acid moiety is more important for membrane organisation processes. The two GlcCer mutants *sd4d-1* and *gcs-1* may also be examined

for their membrane lipid order to determine the effect of GlcCer loss on membrane organisation.

Recent studies show an involvement of sphingolipids and especially of GIPCs in plasmodesmal cell-to-cell transport (Grison *et al.*, 2015). It is assumed that callose synthesis and degradation enzymes are transported via membrane domains to the target region at plasmodesmal sites. Callose deposition is known to regulate the size exclusion limit of plasmodesmata. Since *s4h* mutants have an unusual callose accumulation at protonema cross-walls, it might be that plasmodesmal flux is affected in the mutants. Plasmodesmata ultrastructure could be examined by electron microscopy. This would reveal whether the symplastic channels are disrupted in the *s4h* mutants. Another way to determine whether plasmodesmal transport is disturbed is to track the distribution of metabolites within the protonema network. One idea for this is to bombard protonema cells with fluorescent proteins. If no signal peptide is attached to the fluorescent protein, it should locate to the cytoplasm. Cell-to-cell migration of the fluorescent signal may then be monitored and tracked using fluorescence microscopy.

The growth and differentiation phenotype of *gcs-1* plants might be caused by defects in Golgi-mediated protein trafficking. Studies on *A. thaliana* mutants whose GCS activity was inhibited, described growth and differentiation defects that might be caused by an altered Golgi morphology and hence by a disturbed endomembrane protein trafficking (Melser *et al.*, 2010; Krüger *et al.*, 2013; Msanne *et al.*, 2015). Although cell differentiation defects were also observed in *P. patens gcs-1* mutants, it is not known whether subcellular structures, such as the Golgi apparatus, were also affected. Future studies might apply electron microscopy to reveal whether the Golgi morphology in *P. patens gcs-1* was also altered. Together this would enforce the proposed role of GlcCer in endomembrane trafficking.

It is known that sphingolipids are involved in responses to biotic and abiotic stresses in vascular plants. Sphingolipid LCB and fatty acid desaturation is for example determined as an important feature in plant adaptation to cold stress to maintain membrane fluidity (Chen *et al.*, 2012). GlcCers have also been described to have a putative role in chilling and freezing tolerance in plants (Steponkus *et al.*, 1990; Uemura & Steponkus, 1994; Uemura *et al.*, 1995). A recent *P. patens* study showed a role for the sphingolipid fatty acid desaturase (*Pp*SFD) in the response to cold stress (Resemann, 2018). Sphingolipid profiling of the *sfd* knockout mutant confirmed loss of sphingolipid molecular species with an unsaturated fatty acid moiety. Mutant plants were also indeed more susceptible to cold stress. Analysis of sequence and domain annotation identified the *P. patens* desaturase as a front-end Cb5 desaturase whereas the characterised *A. thaliana* desaturase (*At*ADS) is a methyl-end *n*-9 desaturase. Although *Pp*SFD showed a conserved desaturase function, it

catalyses the introduction of a double bond mostly at the *n*-8 position of the fatty acid moiety instead of at the *n*-9 position as the *At*ADS does. These findings indicate an independent evolutionary background of the two desaturases. Nevertheless, the *Pp*SFD activity offers protection against cold stress in *P. patens* as well as in *A. thaliana* and therefore seems to confer the same physiological function. It might be interesting to investigate whether LCB Δ4-desaturation and GlcCer formation also play a role in cold adaptation in *P. patens*. The LCB Δ8-desaturase (SLD) was shown to be involved in chilling tolerance in *A. thaliana* and tomato (Chen *et al.*, 2012; Zhou *et al.*, 2016). *At*SLD catalyses the formation of the Δ8-unsaturated LCB moiety, t18:1$^{\Delta 8}$. t18:1$^{\Delta 8}$ is the predominating LCB moiety in all *A. thaliana* sphingolipids. In *P. patens*, however, the most abundant LCB moiety is t18:0. Δ8-desaturation occurs in *P. patens* only in combination with Δ4-desaturation and is only found in GlcCers but not in GIPCs. It is not known why Δ8-desaturation is an essential sphingolipid modification in vascular plants while it appears not to be essential in non-vascular plants. One hypothesis is that vascular land plants had to adapt to greater changes in the environmental conditions during land colonisation. This might include an increased tolerance towards cold stress. Future studies may target the characterisation of the *P. patens* LCB Δ8-desaturase and assessment of the role of LCB desaturation in cold stress adaptation in the moss. It is not known whether the *A. thaliana* LCB Δ4-desaturase has a similar function in the cold stress response as the LCB Δ8-desaturase. Since no obvious phenotypes were observed for *A. thaliana* and *P. patens* plants whose Δ4-desaturase activity was disturbed, it could also be interesting to check the Δ4-desaturase involvement in plant response to unfavourable environments, including cold temperatures.

6.7 Concluding remarks and outlook

Plant sphingolipid metabolism has been thoroughly investigated in the common vascular model *A. thaliana*. Although functional characterisation of *A. thaliana* sphingolipid enzymes gives us a first insight into sphingolipid function in plants, many aspects are still unknown. Several studies on sphingolipids from different plants indicate a diversification of plant sphingolipid biosynthesis in various land plant lineages. Together with the yeast *S. cerevisiae* and the vascular plant A. *thaliana*, *P. patens* has the potential to become a powerful model organism in the study of sphingolipid biosynthesis.

The aim of this work was to investigate the phenotypes and chemotypes of *P. patens* knockouts of the key sphingolipid enzymes LCB C-4 hydroxylase, LCB Δ4-desaturase, and glycosylceramide synthase. Prior to examination of the three *P. patens* sphingolipid mutants, appropriate cultivation systems and characterisation assays have been established. These establishments provide the basis for the performed mutant characterisations but also for future *P. patens* mutant studies (chapter 1). Sphingolipid

profiling of the *P. patens* knockout lines indicated that all three proteins are encoded by single genes. The lipid profiles also demonstrated that LCB C-4 hydroxylation and LCB Δ4-desaturation likely dictate the metabolic flux of sphingolipid substrates into GIPC and GlcCer formation in *P. patens*, respectively. Phenotype investigations showed that LCB C-4 hydroxylase knockout plants were strongly impaired in plant growth and development while LCB Δ4-desaturase knockout plants barely showed any defects. LCB C-4 hydroxylation therefore appears to have a more important physiological function than LCB Δ4-desaturation in *P. patens*. Loss of GlcCers and accumulation of precursor molecules in the glycosylceramide synthase mutant affected *P. patens* protonema cell differentiation and was associated with cell death-like lesions.

Comparison with corresponding *A. thaliana* mutants shows that despite their distinct structural features, complex sphingolipids appear to confer similar physiological functions in vascular and non-vascular plants. While observations from the three distinct *P. patens* sphingolipid mutants confirm certain features known from the *A. thaliana* sphingolipid biosynthesis, they also reveal novel aspects of *P. patens* sphingolipid biosynthesis.

Findings from these studies contribute to our understanding of sphingolipid biosynthesis and function in *P. patens*. However, the studies also uncovered questions concerning the regulation of plant sphingolipid biosynthesis: How are LCB C-4 hydroxylation and LCB Δ4-desaturation regulated in *P. patens* and in other plants? Do GlcCers and GIPCs have different roles in *P. patens* physiology? Do distinct ceramide backbone modifications influence the roles of GlcCers and GIPCs in *P. patens* physiology?

P. patens might represent a valuable plant model in answering these and other unanswered questions concerning sphingolipid biosynthesis in plants. Different developmental stages of *P. patens* have simple structures consisting either of a two-dimensional network of filamentous cells or of single cell layered leaflets (Prigge & Bezanilla, 2010). Membrane dynamics may therefore be visualised *in planta* with the help of advanced microscopic techniques in a plant system of lower complexity.

The less complex *P. patens* sphingolipidome may also help to dissect the involvement of GlcCers and GIPCs in the highly dynamic processes of membrane organisation and membrane-associated signal transduction processes. Furthermore, the *P. patens* genome is completely sequenced since 2008 and the toolbox for genetic manipulation of the moss is steadily growing (Rensing *et al.*, 2008; Rensing *et al.*, 2020). The extension of the genetic toolkit includes use of the CRISPR-Cas9 strategy which enables targeting of other sphingolipid genes encoded by gene families in future studies.

In addition to all these favourable aspects of *P. patens*, its unique evolutionary position which links plants with marine and terrestrial lifestyles offers the chance to

understand how sphingolipid biosynthesis has evolved and adapted throughout the evolution of land plants.

The demonstrated studies from this work contribute to our knowledge on sphingolipid biosynthesis in plants. However, sphingolipid metabolism in the bryophyte has only started to be elucidated. Macro- and microscopic investigations of other *P. patens* sphingolipid mutants in combination with advanced lipid purification methods and mass spectrometric approaches will be powerful tools in the future to finally solve the riddle of the plant sphingolipids.

7 References

Abas L, Luschnig C. 2010. Maximum yields of microsomal-type membranes from small amounts of plant material without requiring ultracentrifugation. *Analytical Biochemistry* **401**(2): 217-227.

Abbas HK, Tanaka T, Duke SO, Porter JK, Wray EM, Hodges L, Sessions AE, Wang E, Merrill Jr AH, Riley RT. 1994. Fumonisin- and AAL-toxin-induced disruption of sphingolipid metabolism with accumulation of free sphingoid bases. *Plant Physiology* **106**(3): 1085-1093.

Alden KP, Dhondt-Cordelier S, McDonald KL, Reape TJ, Ng CKY, McCabe PF, Leaver CJ. 2011. Sphingolipid long chain base phosphates can regulate apoptotic-like programmed cell death in plants. *Biochemical and Biophysical Research Communications* **410**(3): 574-580.

Altschul SF, Gish W, Miller W, Myers EW, Lipman DJ. 1990. Basic local alignment search tool. *J Mol Biol* **215**(3): 403-410.

Andersson MX, Larsson KE, Tjellstrom H, Liljenberg C, Sandelius AS. 2005. Phosphate-limited Oat: THE PLASMA MEMBRANE AND THE TONOPLAST AS MAJOR TARGETS FOR PHOSPHOLIPID-TO-GLYCOLIPID REPLACEMENT AND STIMULATION OF PHOSPHOLIPASES IN THE PLASMA MEMBRANE. *Journal of Biological Chemistry* **280**(30): 27578-27586.

Andersson MX, Stridh MH, Larsson KE, Liljenberg C, Sandelius AS. 2003. Phosphate-deficient oat replaces a major portion of the plasma membrane phospholipids with the galactolipid digalactosyldiacylglycerol. *FEBS Letters* **537**(1-3): 128-132.

Ashton NW, Cove DJ. 1977. The isolation and preliminary characterisation of auxotrophic and analogue resistant mutants of the moss, *Physcomitrella patens*. *Molecular and General Genetics MGG* **154**(1): 87-95.

Ashton NW, Grimsley NH, Cove DJ. 1979. Analysis of gametophytic development in the moss, Physcomitrella patens, using auxin and cytokinin resistant mutants. *Planta* **144**(5): 427-435.

Bach L, Gissot L, Marion J, Tellier F, Moreau P, Satiat-Jeunemaitre B, Palauqui J-C, Napier JA, Faure J-D. 2011. Very-long-chain fatty acids are required for cell plate formation during cytokinesis in Arabidopsis thaliana. *Journal of Cell Science* **124**(19): 3223-3234.

Bai Y, McCoy JG, Levin EJ, Sobrado P, Rajashankar KR, Fox BG, Zhou M. 2015. X-ray structure of a mammalian stearoyl-CoA desaturase. *Nature* **524**(7564): 252-256.

Balcke GU, Handrick V, Bergau N, Fichtner M, Henning A, Stellmach H, Tissier A, Hause B, Frolov A. 2012. An UPLC-MS/MS method for highly sensitive high-throughput analysis of phytohormones in plant tissues. *Plant Methods* **8**(1): 47.

Bayer EM, Mongrand S, Tilsner J. 2014. Specialized membrane domains of plasmodesmata, plant intercellular nanopores. *Frontiers in Plant Science* **5**(507).

Beike AK. 2013. *The transcriptomic and physiological cold stress response of Physcomitrella patens.* Inaugural Dissertation zur Erlangung der Doktorwürde, Albert-Ludwigs-Universität Freiburg.

Beike AK, Lang D, Zimmer AD, Wüst F, Trautmann D, Wiedemann G, Beyer P, Decker EL, Reski R. 2015. Insights from the cold transcriptome of *Physcomitrella patens*: global specialization pattern of conserved transcriptional regulators and identification of orphan genes involved in cold acclimation. *New Phytologist* **205**(2): 869-881.

Berdyshev EV, Gorshkova IA, Garcia JG, Natarajan V, Hubbard WC. 2005. Quantitative analysis of sphingoid base-1-phosphates as bisacetylated derivatives by liquid chromatography-tandem mass spectrometry. *Analytical Biochemistry* **339**(1): 129-136.

Berkey R, Bendigeri D, Xiao S. 2012. Sphingolipids and plant defense/disease: the "death" connection and beyond. *Frontiers in Plant Science* **3**: 68.

Bi F-C, Liu Z, Wu J-X, Liang H, Xi X-L, Fang C, Sun T-J, Yin J, Dai G-Y, Rong C, et al. 2014. Loss of ceramide kinase in Arabidopsis impairs defenses and promotes ceramide accumulation and mitochondrial H_2O_2 bursts. *The Plant Cell* **26**(8): 3449-3467.

Borner GHH, Sherrier DJ, Weimar T, Michaelson LV, Hawkins ND, MacAskill A, Napier JA, Beale MH, Lilley KS, Dupree P. 2005. Analysis of detergent-resistant membranes in Arabidopsis. Evidence for plasma membrane lipid rafts. *Plant Physiology* **137**(1): 104-116.

Bressendorff S. 2012. *Immunity in the moss Physcomitrella patens.* Ph.D. PhD thesis, University of Copenhagen COPENHAGEN.

Brodersen P, Petersen M, Pike HM, Olszak B, Skov S, Odum N, Jørgensen LB, Brown RE, Mundy J. 2002. Knockout of Arabidopsis accelerated-cell-death11 encoding a sphingosine transfer protein causes activation of programmed cell death and defense. *Genes & development* **16**(4): 490-502.

Buré C, Cacas JL, Mongrand S, Schmitter JM. 2014. Characterization of glycosyl inositol phosphoryl ceramides from plants and fungi by mass spectrometry. *Analytical and Bioanalytical Chemistry* **406**(4): 995-1010.

Buré C, Cacas JL, Wang F, Gaudin K, Domergue F, Mongrand S, Schmitter JM. 2011. Fast screening of highly glycosylated plant sphingolipids by tandem mass spectrometry. *Rapid Communications in Mass Spectrometry* **25**(20): 3131-3145.

Cacas J-L, Bure C, Furt F, Maalouf J-P, Badoc A, Cluzet S, Schmitter J-M, Antajan E, Mongrand S. 2013. Biochemical survey of the polar head of plant glycosylinositolphosphoceramides unravels broad diversity. *Phytochemistry* **96**(12): 191-200.

Cacas J-L, Buré C, Grosjean K, Gerbeau-Pissot P, Lherminier J, Rombouts Y, Maes E, Bossard C, Gronnier J, Furt F, et al. 2016. Revisiting plant plasma membrane lipids in tobacco: A focus on sphingolipids. *Plant Physiology* **170**(1): 367-384.

Cacas J-L, Furt F, Le Guédard M, Schmitter J-M, Buré C, Gerbeau-Pissot P, Moreau P, Bessoule J-J, Simon-Plas F, Mongrand S. 2012. Lipids of plant membrane rafts. *Progress in Lipid Research* **51**(3): 272-299.

Cahoon EB, Lynch DV. 1991. Analysis of glucocerebrosides of rye (*Secale cereale* L. cv Puma) leaf and plasma membrane. *Plant Physiology* **95**(1): 58.

Casares D, Escribá PV, Rosselló CA. 2019. Membrane lipid composition: Effect on membrane and organelle structure, function and compartmentalization and therapeutic avenues. *International Journal of Molecular Sciences* **20**(9): 2167.

Castel B, Tomlinson L, Locci F, Yang Y, Jones JDG. 2019. Optimization of T-DNA architecture for Cas9-mediated mutagenesis in Arabidopsis. *PLOS ONE* **14**(1): e0204778.

Chao D-Y, Gable K, Chen M, Baxter I, Dietrich CR, Cahoon EB, Guerinot ML, Lahner B, LÃ¼ S, Markham JE, et al. 2011. Sphingolipids in the root play an important role in regulating the leaf ionome in *Arabidopsis thaliana*. *The Plant Cell* **23**(3): 1061-1081.

Chen L-Y, Shi D-Q, Zhang W-J, Tang Z-S, Liu J, Yang W-C. 2015. The *Arabidopsis* alkaline ceramidase TOD1 is a key turgor pressure regulator in plant cells. *Nature Communications* **6**: 6030.

Chen M, Han G, Dietrich CR, Dunn TM, Cahoon EB. 2006. The Essential Nature of Sphingolipids in Plants as Revealed by the Functional Identification and Characterization of the *Arabidopsis* LCB1 Subunit of Serine Palmitoyltransferase. *Plant Cell* **18**(12): 3576-3593.

Chen M, Markham JE, Cahoon EB. 2012. Sphingolipid Δ8 unsaturation is important for glucosylceramide biosynthesis and low-temperature performance in Arabidopsis. *The Plant Journal* **69**(5): 769-781.

Chen M, Markham JE, Dietrich CR, Jaworski JG, Cahoon EB. 2008. Sphingolipid long-chain base hydroxylation is important for growth and regulation of sphingolipid content and composition in Arabidopsis. *The Plant Cell* **20**(7): 1862-1878.

Chen M, Thelen JJ. 2013. ACYL-LIPID DESATURASE2 is required for chilling and freezing tolerance in *Arabidopsis*. *The Plant Cell* **25**(4): 1430-1444.

Collonnier C, Epert A, Mara K, Maclot F, Guyon-Debast A, Charlot F, White C, Schaefer DG, Nogué F. 2017. CRISPR-Cas9-mediated efficient directed mutagenesis and RAD51-dependent and RAD51-independent gene targeting in the moss *Physcomitrella patens*. *Plant Biotechnology Journal* **15**(1): 122-131.

Coursol S, Fan LM, Le Stunff H, Spiegel S, Gilroy S, Assmann SM. 2003. Sphingolipid signalling in *Arabidopsis* guard cells involves heterotrimeric G proteins. *Nature* **423**(6940): 651-654.

Cove D. 2005. The moss *Physcomitrella patens*. *Annual Review of Genetics* **39**(1): 339-358.

Cove D, Bezanilla M, Harries P, Quatrano R. 2006. Mosses as model systems for the study of metabolism and development. *Annual Review of Plant Biology* **57**(1): 497-520.

Cove DJ, Schild A, Ashton NW, Hartmann E. 1978. Genetic and physiological studies of the effect of light on the development of the moss, *Physcomitrella patens*. *Photochemistry and Photobiology* **27**(2): 249-254.

Dai G-Y, Yin J, Li K-E, Chen D-K, Liu Z, Bi F-C, Rong C, Yao N. 2020. The *Arabidopsis At*GCD3 protein is a glucosylceramidase that preferentially hydrolyzes long-acyl-chain glucosylceramides. *Journal of Biological Chemistry* **295**(3): 717-728.

de Almeida RF, Fedorov A, Prieto M. 2003. Sphingomyelin/phosphatidylcholine/cholesterol phase diagram: boundaries and composition of lipid rafts. *Biophysical Journal* **85**(4): 2406-2416.

de Keijzer J, Kieft H, Ketelaar T, Goshima G, Janson ME. 2017. Shortening of microtubule overlap regions defines membrane delivery sites during plant cytokinesis. *Current Biology* **27**(4): 514-520.

De Storme N, Geelen D. 2014. Callose homeostasis at plasmodesmata: molecular regulators and developmental relevance. *Frontiers in Plant Science* **5**: 138.

Decker EL, Frank W, Sarnighausen E, Reski R. 2006. Moss systems biology en route: phytohormones in Physcomitrella development. *Plant Biolohy (Stuttgart)* **8**(3): 397-405.

Decker EL, Reski R. 2004. The moss bioreactor. *Current Opinion in Plant Biology* **7**(2): 166-170.

Desfarges L, Durrens P, Juguelin H, Cassagne C, Bonneu M, Aigle M. 1993. Yeast mutants affected in viability upon starvation have a modified phospholipid composition. *Yeast* **9**(3): 267-277.

Devaux PF, Morris R. 2004. Transmembrane asymmetry and lateral domains in biological membranes. *Traffic* **5**(4): 241-246.

Dickson RC. 2010. Roles for sphingolipids in *Saccharomyces cerevisiae*. *Advances in experimental medicine and biology* **688**: 217-231.

Dietrich CR, Han G, Chen M, Berg RH, Dunn TM, Cahoon EB. 2008. Loss-of-function mutations and inducible RNAi suppression of Arabidopsis LCB2 genes reveal the critical role of sphingolipids in gametophytic and sporophytic cell viability. *The Plant Journal* **54**(2): 284-298.

Dörmann P, Benning C. 2002. Galactolipids rule in seed plants. *Trends in Plant Science* **7**(3): 112-118.

Dorne AJ, Joyard J, Douce R. 1990. Do thylakoids really contain phosphatidylcholine? *Proceedings of the National Academy of Sciences USA* **87**(1): 71-74.

Dunn TM, Lynch DV, Michaelson LV, Napier JA. 2004. A post-genomic approach to understanding sphingolipid metabolism in *Arabidopsis thaliana*. *Annals of Botany* **93**(5): 483-497.

Dutilleul C, Benhassaine-Kesri G, Demandre C, Rézé N, Launay A, Pelletier S, Renou JP, Zachowski A, Baudouin E, Guillas I. 2012. Phytosphingosine-phosphate is a signal for AtMPK6 activation and Arabidopsis response to chilling. *New Phytologist* **194**(1): 181-191.

Engel PP. 1968. The induction of biochemical and morphological mutants in the moss *Physcomitrella patens*. *American Journal of Botany* **55**(4): 438-446.

Fang L, Ishikawa T, Rennie EA, Murawska GM, Lao J, Yan J, Tsai AY-L, Baidoo EEK, Xu J, Keasling JD, et al. 2016. Loss of inositol phosphorylceramide sphingolipid mannosylation induces plant immune responses and reduces cellulose content in Arabidopsis. *The Plant Cell* **28**(12): 2991-3004.

Frank W, Decker EL, Reski R. 2005. Molecular tools to study *Physcomitrella patens*. *Plant Biology* **7**: 220-227.

Fukuchi-Mizutani M, Savin K, Cornish E, Tanaka Y, Ashikari T, Kusumi T, Murata N. 1995. Senescence-induced expression of a homologue of D9 desaturase in rose petals. *Plant Molecular Biology* **29**: 627-635.

Furt F, König S, Bessoule J-J, Sargueil F, Zallot R, Stanislas T, Noirot E, Lherminier J, Simon-Plas F, Heilmann I, et al. 2010. Polyphosphoinositides Are Enriched in Plant Membrane Rafts and Form Microdomains in the Plasma Membrane. *Plant Physiology* **152**(4): 2173-2187.

Furt F, Simon-Plas F, Mongrand S 2011. Lipids of the Plant Plasma Membrane. In: Murphy AS, Schulz B, Peer W eds. *The Plant Plasma Membrane*. Berlin, Heidelberg: Springer Berlin Heidelberg, 3-30.

Gallagher KL, Sozzani R, Lee CM. 2014. Intercellular protein movement: deciphering the language of development. *Annual Review of Cell and Developmental Biology* **30**: 207-233.

Gerbeau-Pissot P, Der C, Thomas D, Anca I-A, Grosjean K, Roche Y, Perrier-Cornet J-M, Mongrand Sb, Simon-Plas Fo. 2014. Modification of Plasma Membrane Organization in Tobacco Cells Elicited by Cryptogein. *Plant Physiology* **164**(1): 273-286.

Gietz RD, Schiestl RH. 2007. High-efficiency yeast transformation using the LiAc/SS carrier DNA/PEG method. *Nature Protocols* **2**(1): 31-34.

Gömann J, Herrfurth C, Zienkiewicz A, Ischebeck T, Haslam TM, Hornung E, Feussner I. 2021. Sphingolipid long-chain base hydroxylation influences plant growth and callose deposition in Physcomitrium patens. *New Phytologist* **231**(1): 297-314.

Gómez-Gómez L, Boller T. 2000. FLS2: an LRR receptor-like kinase involved in the perception of the bacterial elicitor flagellin in Arabidopsis. *Molecular Cell* **5**(6): 1003-1011.

Gonzalez-Solis A, Han G, Gan L, Li Y, Markham JE, Cahoon RE, Dunn TM, Cahoon EB. 2020. Unregulated sphingolipid biosynthesis in gene-edited Arabidopsis ORM mutants results in nonviable seeds with strongly reduced oil content. *The Plant Cell* **32**(8): 2474.

Gonzalez Solis A, Han G, Gan L, Liu Y, Markham JE, Cahoon RE, Dunn TM, Cahoon EB. 2020. Unregulated Sphingolipid Biosynthesis in Gene-Edited Arabidopsis *ORM* Mutants Results in Nonviable Seeds with Strongly Reduced Oil Content. *The Plant Cell* **32**(8): 2474–2490.

Greenberg JT, Silverman FP, Liang H. 2000. Uncoupling salicylic acid-dependent cell death and defense-related responses from disease resistance in the Arabidopsis mutant *acd5*. *Genetics* **156**(1): 341-350.

Grillitsch K, Tarazona P, Klug L, Wriessnegger T, Zellnig G, Leitner E, Feussner I, Daum G. 2014. Isolation and characterization of the plasma membrane from the yeast *Pichia pastoris*. *Biochimica et Biophysica Acta* **1838**(7): 1889-1897.

Grison MS, Brocard L, Fouillen L, Nicolas W, Wewer V, Dörmann P, Nacir H, Benitez-Alfonso Y, Claverol S, Germain V, et al. 2015. Specific membrane lipid composition is important for plasmodesmata function in Arabidopsis. *The Plant Cell* **27**(4): 1228-1250.

Gronnier J, Crowet J-M, Habenstein B, Nasir MN, Bayle V, Hosy E, Platre MP, Gouguet P, Raffaele S, Martinez D, et al. 2017. Structural basis for plant plasma membrane protein dynamics and organization into functional nanodomains. *eLife* **6**: e26404.

Gronnier J, Germain V, Gouguet P, Cacas J-L, Mongrand S. 2016. GIPC: Glycosyl inositol phospho ceramides, the major sphingolipids on earth. *Plant Signaling & Behavior* **11**(4): e1152438.

Grosjean K, Der C, Robert F, Thomas D, Mongrand S, Simon-Plas F, Gerbeau-Pissot P. 2018. Interactions between lipids and proteins are critical for plasma membrane ordered domain organization in BY-2 cells. *Journal of Experimental Botany* **69**(15): 3545–3557.

Grosjean K, Mongrand S, Beney L, Simon-Plas F, Gerbeau-Pissot P. 2015. Differential effect of plant lipids on membrane organization: SPECIFICITIES OF PHYTOSPHINGOLIPIDS AND PHYTOSTEROLS. *Journal of Biological Chemistry* **290**(9): 5810-5825.

Guo L, Mishra G, Markham JE, Li M, Tawfall A, Welti R, Wang X. 2012. Connections between sphingosine kinase and phospholipase D in the abscisic acid signaling pathway in *Arabidopsis*. *Journal of Biological Chemistry* **287**(11): 8286-8296.

Guo L, Wang X. 2012. Crosstalk between phospholipase D and sphingosine kinase in plant stress signaling. *Frontiers in Plant Science* **3**.

Haak D, Gable K, Beeler T, Dunn T. 1997. Hydroxylation of *Saccharomyces cerevisiae* ceramides requires Sur2p and Scs7p. *Journal of Biological Chemistry* **272**(47): 29704-29710.

Haeussler M, Schönig K, Eckert H, Eschstruth A, Mianné J, Renaud J-B, Schneider-Maunoury S, Shkumatava A, Teboul L, Kent J, et al. 2016. Evaluation of off-target and on-target scoring algorithms and integration into the guide RNA selection tool CRISPOR. *Genome Biology* **17**(1): 148.

Hanada K, Nishijima M, Akamatsu Y, Pagano RE. 1995. Both sphingolipids and cholesterol participate in the detergent insolubility of alkaline phosphatase, a glycosylphosphatidylinositol-anchored protein, in mammalian membranes. *Journal of Biological Chemistry* **270**(11): 6254-6260.

Hedges SB. 2002. The origin and evolution of model organisms. *Nature Reviews Genetics* **3**(11): 838-849.

Heilmann I, Pidkowich MS, Girke T, Shanklin J. 2004. Switching desaturase enzyme specificity by alternate subcellular targeting. *Proceedings of the National Academy of Sciences USA* **101**(28): 10266-10271.

Herrfurth C, Feussner I 2020. Quantitative jasmonate profiling using a high-throughput UPLC-NanoESI-MS/MS method. In: Champion A, Laplaze L eds. *Jasmonate in Plant Biology: Methods and Protocols*. New York, NY: Springer US, 169-187.

Hiss M, Meyberg R, Westermann J, Haas FB, Schneider L, Schallenberg-Rüdinger M, Ullrich KK, Rensing SA. 2017. Sexual reproduction, sporophyte development and molecular variation in the model moss Physcomitrella patens: introducing the ecotype Reute. *The Plant Journal* **90**(3): 606-620.

Hohe A, Rensing SA, Mildner M, Lang D, Reski R. 2002. Day length and temperature strongly influence sexual reproduction and expression of a novel MADS-box gene in the moss Physcomitrella patens. *Plant Biology* **4**(5): 595-602.

Huang D, Sun Y, Ma Z, Ke M, Cui Y, Chen Z, Chen C, Ji C, Tran TM, Yang L, et al. 2019. Salicylic acid-mediated plasmodesmal closure via Remorin-dependent lipid organization. *Proceedings of the National Academy of Sciences* **116**(42): 21274-21284.

Huby E, Napier JA, Baillieul F, Michaelson LV, Dhondt-Cordelier S. 2020. Sphingolipids: towards an integrated view of metabolism during the plant stress response. *New Phytologist* **225**(2): 659-670.

Hunter JE, Brandsma J, Dymond MK, Koster G, Moore CM, Postle AD, Mills RA, Attard GS. 2018. Lipidomics of *Thalassiosira pseudonana* under phosphorus stress reveal underlying phospholipid substitution dynamics and novel diglycosylceramide substitutes. *Applied and Environmental Microbiology* **84**(6): e02034-02017.

Imai H, Nishiura H. 2005. Phosphorylation of sphingoid long-chain bases in Arabidopsis: functional characterization and expression of the first sphingoid long-chain base Kinase gene in plants. *Plant Cell Physiol* **46**(2): 375-380.

Imai H, Ohnishi M, Kinoshita M, Kojima M, Ito S. 1995. Structure and distribution of cerebroside containing unsaturated hydroxy fatty acids in plant leaves. *Bioscience, Biotechnology, and Biochemistry* **59**(7): 1309-1313.

Imai H, Yamamoto K, Shibahara A, Miyatani S, Nakayama T. 2000. Determining double-bond positions in monoenoic 2-hydroxy fatty acids of glucosylceramides by gas chromatography-mass spectrometry. *Lipids* **35**(2): 233.

Ipsen JH, Karlström G, Mouritsen OG, Wennerström H, Zuckermann MJ. 1987. Phase equilibria in the phosphatidylcholine-cholesterol system. *Biochim Biophys Acta* **905**(1): 162-172.

Ischebeck T, Stenzel I, Heilmann I. 2008. Type B Phosphatidylinositol-4-Phosphate 5-Kinases Mediate Arabidopsis and Nicotiana tabacum Pollen Tube Growth by Regulating Apical Pectin Secretion. *The Plant Cell* **20**(12): 3312-3330.

Ishikawa T, Fang L, Rennie EA, Sechet J, Yan J, Jing B, Moore W, Cahoon EB, Scheller HV, Kawai-Yamada M, et al. 2018. GLUCOSAMINE INOSITOLPHOSPHORYLCERAMIDE TRANSFERASE1 (GINT1) is a GlcNAc-containing glycosylinositol phosphorylceramide glycosyltransferase. *Plant Physiology* **177**(3): 938–952.

Islam MN, Jacquemot M-P, Coursol S, Ng CKY. 2012. Sphingosine in plants – more riddles from the Sphinx? *New Phytologist* **193**(1): 51-57.

Iven T, König S, Singh S, Braus-Stromeyer SA, Bischoff M, Tietze LF, Braus GH, Lipka V, Feussner I, Dröge-Laser W. 2012. Transcriptional activation and production of tryptophan-derived secondary metabolites in Arabidopsis roots contributes to the defense against the fungal vascular pathogen *Verticillium longisporum*. *Molecular Plant* **5**(6): 1389-1402.

Jarsch IK, Konrad SSA, Stratil TF, Urbanus SL, Szymanski W, Braun P, Braun K-H, Ott T. 2014. Plasma Membranes Are Subcompartmentalized into a Plethora of Coexisting and Diverse Microdomains in Arabidopsis and Nicotiana benthamiana. *The Plant Cell Online* **26**(4): 1698-1711.

Jiang Z, Zhou X, Tao M, Yuan F, Liu L, Wu F, Wu X, Xiang Y, Niu Y, Liu F, et al. 2019. Plant cell-surface GIPC sphingolipids sense salt to trigger Ca^{2+} influx. *Nature* **572**(7769): 341–346.

Joyard J, Teyssier E, Miege C, Bernyseigneurin D, Marechal E, Block MA, Dorne AJ, Rolland N, Ajlani G, Douce R. 1998. The biochemical machinery of plastid envelope membranes. *Plant Physiology* **118**(3): 715-723.

Klose C, Ejsing CS, García-Sáez AJ, Kaiser H-J, Sampaio JL, Surma MA, Shevchenko A, Schwille P, Simons K. 2010. Yeast lipids can phase-separate into micrometer-scale membrane domains. *Journal of Biological Chemistry* **285**(39): 30224-30232.

König S, Feussner K, Schwarz M, Kaever A, Iven T, Landesfeind M, Ternes P, Karlovsky P, Lipka V, Feussner I. 2012. Arabidopsis mutants of sphingolipid fatty acid α-hydroxylases accumulate ceramides and salicylates. *New Phytologist* **196**(4): 1086-1097.

Krogh A, Larsson B, von Heijne G, Sonnhammer ELL. 2001. Predicting transmembrane protein topology with a hidden markov model: application to complete genomes. *Journal of Molecular Biology* **305**(3): 567-580.

Krüger F, Krebs M, Viotti C, Langhans M, Schumacher K, Robinson DG. 2013. PDMP induces rapid changes in vacuole morphology in Arabidopsis root cells. *Journal of Experimental Botany* **64**(2): 529-540.

Landberg K, Pederson ERA, Viaene T, Bozorg B, Friml J, Jönsson H, Thelander M, Sundberg E. 2013. The moss *Physcomitrella patens* reproductive organ development is highly organized, Affected by the two *SHI/STY* genes and by the level of active auxin in the *SHI/STY* expression domain. *Plant Physiology* **162**(3): 1406-1419.

Larsson C, Sommarin M, Widell S 1994. Isolation of highly purified plant plasma membranes and separation of inside-out and right-side-out vesicles. *Methods in Enzymology*: Academic Press, 451-469.

Le Bail A, Scholz S, Kost B. 2013. Evaluation of reference genes for RT qPCR analyses of structure-specific and hormone regulated gene expression in *Physcomitrella patens* gametophytes. *PloS one* **8**(8): e70998-e70998.

Lefebvre B, Furt F, Hartmann M-A, Michaelson LV, Carde J-P, Sargueil-Boiron F, Rossignol M, Napier JA, Cullimore J, Bessoule J-J, et al. 2007. Characterization of lipid rafts from *Medicago truncatula* root plasma membranes: A proteomic study reveals the presence of a raft-associated redox system. *Plant Physiology* **144**(1): 402-418.

Leipelt M, Warnecke D, Zahringer U, Ott C, Muller F, Hube B, Heinz E. 2001. Glucosylceramide synthases, a gene family responsible for the biosynthesis of glucosphingolipids in animals, plants, and fungi. *Journal of Biological Chemistry* **276**(36): 33621-33629.

Lenarčič T, Albert I, Böhm H, Hodnik V, Pirc K, Zavec AB, Podobnik M, Pahovnik D, Žagar E, Pruitt R, et al. 2017. Eudicot plant-specific sphingolipids determine host selectivity of microbial NLP cytolysins. *Science* **358**(6369): 1431-1434.

Li J, Bi F-C, Yin J, Wu J-X, Rong C, Wu J-L, Yao N. 2015. An *Arabidopsis* neutral ceramidase mutant *ncer1* accumulates hydroxyceramides and is sensitive to oxidative stress. *Frontiers in Plant Science* **6**: 460.

Liang H, Yao N, Song JT, Luo S, Lu H, Greenberg JT. 2003. Ceramides modulate programmed cell death in plants. *Genes & Development* **17**(21): 2636-2641.

Lichtenberg D. 1985. Characterization of the solubilization of lipid bilayers by surfactants. *Biochim Biophys Acta* **821**(3): 470-478.

Lichtenberg D, Goñi FM, Heerklotz H. 2005. Detergent-resistant membranes should not be identified with membrane rafts. *Trends in Biochemical Sciences* **30**(8): 430-436.

Lin Q, London E. 2014. Preparation of artificial plasma membrane mimicking vesicles with lipid asymmetry. *PloS one* **9**(1): e87903-e87903.

Lisanti MP, Rodriguez-Boulan E. 1990. Glycophospholipid membrane anchoring provides clues to the mechanism of protein sorting in polarized epithelial cells. *Trends in Biochemical Sciences* **15**(3): 113-118.

Liu N-J, Zhang T, Liu Z-H, Chen X, Guo H-S, Ju B-H, Zhang Y-Y, Li G-Z, Zhou Q-H, Qin Y-M, et al. 2020. Phytosphinganine affects plasmodesmata permeability via facilitating PDLP5-stimulated callose accumulation in *Arabidopsis*. *Molecular Plant* **13**(1): 128-143.

Livak KJ, Schmittgen TD. 2001. Analysis of relative gene expression data using real-time quantitative PCR and the $2^{-\Delta\Delta CT}$ method. *Methods* **25**(4): 402-408.

Lopez-Obando M, Hoffmann B, Géry C, Guyon-Debast A, Téoulé E, Rameau C, Bonhomme S, Nogué F. 2016. Simple and efficient targeting of multiple genes through CRISPR-Cas9 in *Physcomitrella patens*. *G3: Genes|Genomes|Genetics* **6**(11): 3647-3653.

Lu S, Wang J, Chitsaz F, Derbyshire MK, Geer RC, Gonzales NR, Gwadz M, Hurwitz DI, Marchler GH, Song JS, et al. 2020. CDD/SPARCLE: the conserved domain database in 2020. *Nucleic Acids Research* **48**(D1): D265-D268.

Ludwig-Müller J, Jülke S, Bierfreund NM, Decker EL, Reski R. 2009. Moss (*Physcomitrella patens*) GH3 proteins act in auxin homeostasis. *New Phytologist* **181**: 323-338.

Luttgeharm KD, Chen M, Mehra A, Cahoon RE, Markham JE, Cahoon EB. 2015a. Overexpression of Arabidopsis ceramide synthases differentially affects growth, sphingolipid metabolism, programmed cell death, and mycotoxin resistance. *Plant Physiology* **169**(2): 1108-1117.

Luttgeharm KD, Kimberlin AN, Cahoon EB 2016. Plant Sphingolipid Metabolism and Function. In: Nakamura Y, Li-Beisson Y eds. *Lipids in Plant and Algae Development*. Cham: Springer International Publishing, 249-286.

Luttgeharm KD, Kimberlin AN, Cahoon RE, Cerny RL, Napier JA, Markham JE, Cahoon EB. 2015b. Sphingolipid metabolism is strikingly different between pollen and leaf in Arabidopsis as revealed by compositional and gene expression profiling. *Phytochemistry* **115**: 121-129.

Lynch DV, Dunn TM. 2004. An introduction to plant sphingolipids and a review of recent advances in understanding their metabolism and function. *New Phytologist* **161**(3): 677-702.

Magnin-Robert M, Le Bourse D, Markham J, Dorey S, Clément C, Baillieul F, Dhondt-Cordelier S. 2015. Modifications of sphingolipid content affect tolerance to hemibiotrophic and necrotrophic pathogens by modulating plant defense responses in Arabidopsis. *Plant Physiology* **169**(3): 2255-2274.

Mamode Cassim A, Gouguet P, Gronnier J, Laurent N, Germain V, Grison M, Boutté Y, Gerbeau-Pissot P, Simon-Plas F, Mongrand S. 2019. Plant lipids: Key players of plasma membrane organization and function. *Progress in Lipid Research* **73**(January): 1-27.

Marchler-Bauer A, Derbyshire MK, Gonzales NR, Lu S, Chitsaz F, Geer LY, Geer RC, He J, Gwadz M, Hurwitz DI, et al. 2015. CDD: NCBI's conserved domain database. *Nucleic acids research* **43**(Database issue): D222-226.

Marion J, Bach L, Bellec Y, Meyer C, Gissot L, Faure J-D. 2008. Systematic analysis of protein subcellular localization and interaction using high-throughput transient transformation of Arabidopsis seedlings. *The Plant Journal* **56**(1): 169-179.

Markham JE, Jaworski JG. 2007. Rapid measurement of sphingolipids from *Arabidopsis thaliana* by reversed-phase high-performance liquid chromatography coupled to electrospray ionization tandem mass spectrometry. *Rapid Communications in Mass Spectrometry* **21**(7): 1304-1314.

Markham JE, Li J, Cahoon EB, Jaworski JG. 2006. Separation and identification of major plant sphingolipid classes from leaves. *Journal of Biological Chemistry* **281**(32): 22684-22694.

Markham JE, Lynch DV, Napier JA, Dunn TM, Cahoon EB. 2013. Plant sphingolipids: Function follows form. *Current Opinion in Plant Biology* **16**(3): 350-357.

Markham JE, Molino D, Gissot L, Bellec Y, Hematy K, Marion J, Belcram K, Palauqui J-C, Satiat-JeuneMaitre B, Faure J-D. 2011. Sphingolipids containing very-long-chain fatty acids define a secretory pathway for specific polar plasma membrane protein targeting in *Arabidopsis*. *The Plant Cell* **23**(6): 2362-2378.

Matyash V, Liebisch G, Kurzchalia TV, Shevchenko A, Schwudke D. 2008. Lipid extraction by methyl-tert-butyl ether for high-throughput lipidomics. *Journal of Lipid Research* **49**(5): 1137-1146.

Melser S, Batailler B, Peypelut M, Poujol C, Bellec Y, Wattelet-Boyer V, Maneta-Peyret L, Faure J-D, Moreau P. 2010. Glucosylceramide Biosynthesis is Involved in Golgi Morphology and Protein Secretion in Plant Cells. *Traffic* **11**(4): 479-490.

Melser S, Molino D, Batailler B, Peypelut M, Laloi M, Wattelet-Boyer V, Bellec Y, Faure J-D, Moreau P. 2011. Links between lipid homeostasis, organelle morphodynamics and protein trafficking in eukaryotic and plant secretory pathways. *Plant Cell Reports* **30**(2): 177-193.

Menand B, Calder G, Dolan L. 2007. Both chloronemal and caulonemal cells expand by tip growth in the moss *Physcomitrella patens*. *Journal of Experimental Botany* **58**(7): 1843-1849.

Meyberg R, Perroud PF, Haas FB, Schneider L, Heimerl T, Renzaglia KS, Rensing SA. 2020. Characterisation of evolutionarily conserved key players affecting eukaryotic flagellar motility and fertility using a moss model. *New Phytologist* **227**(2): 440-454.

Michaelson LV, Napier JA, Molino D, Faure J-D. 2016. Plant sphingolipids: Their importance in cellular organization and adaption. *Biochimica et Biophysica Acta* **1861**(9, Part B): 1329-1335.

Michaelson LV, Zäuner S, Markham JE, Haslam RP, Desikan R, Mugford S, Albrecht S, Warnecke D, Sperling P, Heinz E, et al. 2009. Functional characterization of a higher plant sphingolipid Δ4-desaturase: Defining the role of sphingosine and sphingosine-1-phosphate in Arabidopsis. *Plant Physiology* **149**(1): 487-498.

Mina J, Okada Y, Wansadhipathi-Kannangara N, Pratt S, Shams-Eldin H, Schwarz R, Steel P, Fawcett T, Denny P. 2010. Functional analyses of differentially expressed isoforms of the Arabidopsis inositol phosphorylceramide synthase. *Plant Molecular Biology* **73**(4): 399-407.

Minami A, Fujiwara M, Furuto A, Fukao Y, Yamashita T, Kamo M, Kawamura Y, Uemura M. 2009. Alterations in detergent-resistant plasma membrane microdomains in *Arabidopsis thaliana* during cold acclimation. *Plant & Cell Physiology* **50**(2): 341-359.

Miquel M, James D, Dooner H, Browse J. 1993. Arabidopsis requires polyunsaturated lipids for low-temperature survival. *Proceedings of the National Academy of Sciences* **90**(13): 6208.

Mizutani Y, Kihara A, Igarashi Y. 2004. Identification of the human sphingolipid C4-hydroxylase, hDES2, and its up-regulation during keratinocyte differentiation. *FEBS Letters* **563**: 93-97.

Molino D, Van der Giessen E, Gissot L, Hématy K, Marion J, Barthelemy J, Bellec Y, Vernhettes S, Satiat-Jeunemaétre B, Galli T, et al. 2014. Inhibition of very long acyl chain sphingolipid synthesis modifies membrane dynamics during plant cytokinesis. *Biochimica et Biophysica Acta* **1841**(10): 1422-1430.

Mombelli E, Morris R, Taylor W, Fraternali F. 2003. Hydrogen-bonding propensities of sphingomyelin in solution and in a bilayer assembly: a molecular dynamics study. *Biophysical Journal* **84**(3): 1507-1517.

Mongrand S, Morel J, Laroche J, Claverol S, Carde J-P, Hartmann M-A, Bonneu M, Simon-Plas F, Lessire R, Bessoule J-J. 2004. Lipid rafts in higher plant cells: Purification and characterization of Triton X-100-insoluble microdomains from tobacco plasma membrane. *Journal of Biological Chemistry* **279**(35): 36277-36286.

Mongrand S, Stanislas T, Bayer EMF, Lherminier J, Simon-Plas F. 2010. Membrane rafts in plant cells. *Trends in Plant Science* **15**(12): 656-663.

Monte I, Ishida S, Zamarreño AM, Hamberg M, Franco-Zorrilla JM, García-Casado G, Gouhier-Darimont C, Reymond P, Takahashi K, García-Mina JM, et al. 2018. Ligand-receptor co-

evolution shaped the jasmonate pathway in land plants. *Nature Chemical Biology* **14**(5): 480-488.

Moreau P, Bessoule JJ, Mongrand S, Testet E, Vincent P, Cassagne C. 1998. Lipid trafficking in plant cells. *Progress in Lipid Research* **37**(6): 371-391.

Mortimer JC, Yu X, Albrecht S, Sicilia F, Huichalaf M, Ampuero D, Michaelson LV, Murphy AM, Matsunaga T, Kurz S, et al. 2013. Abnormal glycosphingolipid mannosylation triggers salicylic acid–mediated responses in Arabidopsis. *The Plant Cell* **25**(5): 1881.

Moscatelli A, Gagliardi A, Maneta-Peyret L, Bini L, Stroppa N, Onelli E, Landi C, Scali M, Idilli AI, Moreau P. 2015. Characterisation of detergent-insoluble membranes in pollen tubes of *Nicotiana tabacum* (L.). *Biology Open* **4**(3): 378-399.

Msanne J, Chen M, Luttgeharm KD, Bradley AM, Mays ES, Paper JM, Boyle DL, Cahoon RE, Schrick K, Cahoon EB. 2015. Glucosylceramides are critical for cell-type differentiation and organogenesis, but not for cell viability in Arabidopsis. *The Plant Journal* **84**(1): 188-201.

Nagano M, Ishikawa T, Ogawa Y, Iwabuchi M, Nakasone A, Shimamoto K, Uchimiya H, Kawai-Yamada M. 2014. Arabidopsis Bax inhibitor-1 promotes sphingolipid synthesis during cold stress by interacting with ceramide-modifying enzymes. *Planta* **240**(1): 77-89.

Napier JA, Michaelson LV, Dunn TM. 2002. A new class of lipid desaturase central to sphingolipid biosynthesis and signalling. *Trends in Plant Science* **7**(11): 475-478.

Napier JA, Sayanova O, Sperling P, Heinz E. 1999. A growing family of cytochrome b_5-domain fusion proteins. *Trends in Plant Science* **4**(1): 2-4.

Ng CK, Carr K, McAinsh MR, Powell B, Hetherington AM. 2001. Drought-induced guard cell signal transduction involves sphingosine-1-phosphate. *Nature* **410**(6828): 596-599.

Nishikawa M, Hosokawa K, Ishiguro M, Minamioka H, Tamura K, Hara-Nishimura I, Takahashi Y, Shimazaki K-i, Imai H. 2008. Degradation of Sphingoid Long-Chain Base 1-Phosphates (LCB-1Ps): Functional Characterization and Expression of AtDPL1 Encoding LCB-1P Lyase Involved in the Dehydration Stress Response in Arabidopsis. *Plant & Cell Physiology* **49**(11): 1758-1763.

Noirot E, Der C, Lherminier J, Robert F, Moricova P, Kiêu K, Leborgne-Castel N, Simon-Plas F, Bouhidel K. 2014. Dynamic changes in the subcellular distribution of the tobacco ROS-producing enzyme RBOHD in response to the oomycete elicitor cryptogein. *Journal of Experimental Botany* **65**(17): 5011-5022.

Oikawa A, Lund CH, Sakuragi Y, Scheller HV. 2013. Golgi-localized enzyme complexes for plant cell wall biosynthesis. *Trends in Plant Science* **18**(1): 49-58.

Ortiz-Ramírez C, Hernandez-Coronado M, Thamm A, Catarino B, Wang M, Dolan L, Feijó José A, Becker Jörg D. 2016. A Transcriptome Atlas of *Physcomitrella patens* Provides Insights into the Evolution and Development of Land Plants. *Molecular Plant* **9**(2): 205-220.

Overdijk EJR, De Keijzer J, De Groot D, Schoina C, Bouwmester K, Ketelaar T, Govers F. 2016. Interaction between the moss *Physcomitrella patens* and *Phytophthora*: a novel pathosystem for live-cell imaging of subcellular defence. *Journal of Microscopy* **263**(2): 171-180.

Peters C, Kim S-C, Devaiah S, Li M, Wang X. 2014. Non-specific phospholipase C5 and diacylglycerol promote lateral root development under mild salt stress in Arabidopsis. *Plant, Cell & Environment* **37**(9): 2002-2013.

Pike LJ. 2009. The challenge of lipid rafts. *Journal of Lipid Research* **50 Suppl**(Suppl): S323-S328.

Pinto SN, Laviad EL, Stiban J, Kelly SL, Merrill AH, Jr., Prieto M, Futerman AH, Silva LC. 2014. Changes in membrane biophysical properties induced by sphingomyelinase depend on the sphingolipid N-acyl chain. *Journal of lipid research* **55**(1): 53-61.

Ponce De León I, Schmelz EA, Gaggero C, Castro A, ÁLvarez A, Montesano M. 2012. Physcomitrella patens activates reinforcement of the cell wall, programmed cell death and accumulation of evolutionary conserved defence signals, such as salicylic acid and 12-oxo-phytodienoic acid, but not jasmonic acid, upon Botrytis cinerea infection. *Molecular Plant Pathology* **13**(8): 960-974.

Prigge MJ, Bezanilla M. 2010. Evolutionary crossroads in developmental biology: *Physcomitrella patens*. *Development* **137**(21): 3535-3543.

Quinn PJ, Wolf C. 2009. The liquid-ordered phase in membranes. *Biochimica et Biophysica Acta* **1788**(1): 33-46.

Raffaele S, Bayer E, Lafarge D, Cluzet S, German Retana S, Boubekeur T, Leborgne-Castel N, Carde J-P, Lherminier J, Noirot E, et al. 2009. Remorin, a Solanaceae Protein Resident in Membrane Rafts and Plasmodesmata, Impairs Potato virus X Movement. *The Plant Cell* **21**(5): 1541-1555.

Recktenwald DJ, McConnell HM. 1981. Phase equilibria in binary mixtures of phosphatidylcholine and cholesterol. *Biochemistry* **20**(15): 4505-4510.

Rennie EA, Ebert B, Miles GP, Cahoon RE, Christiansen KM, Stonebloom S, Khatab H, Twell D, Petzold CJ, Adams PD, et al. 2014. Identification of a Sphingolipid a-Glucuronosyltransferase That Is Essential for Pollen Function in *Arabidopsis*. *The Plant Cell* **26**(8): 3314-3325.

Rensing SA, Goffinet B, Meyberg R, Wu S-Z, Bezanilla M. 2020. The Moss *Physcomitrium* (*Physcomitrella*) *patens*: A Model Organism for Non-Seed Plants. *The Plant Cell* **32**(5): 1361-1376.

Rensing SA, Lang D, Zimmer AD, Terry A, Salamov A, Shapiro H, Nishiyama T, Perroud P-F, Lindquist EA, Kamisugi Y, et al. 2008. The Physcomitrella genome reveals evolutionary insights into the conquest of land by plants. *Science* **319**(5859): 64-69.

Resemann H. 2018. *Sphingolipids in Physcomitrella patens.* Doctor rerum naturalium, Georg-August-Universität Göttingen Göttingen.

Reski R, Abel WO. 1985. Induction of budding on chloronemata and caulonemata of the moss, *Physcomitrella patens*, using isopentenyladenine. *Planta* **165**(3): 354-358.

Reutter K, Atzorn R, Hadeler B, Schmülling T, Reski R. 1998. Expression of the bacterial ipt gene in Physcomitrella rescues mutations in budding and in plastid division. *Planta* **206**(2): 196-203.

Riezman H. 2006. Organization and functions of sphingolipid biosynthesis in yeast. *Biochemical Society Transactions* **34**(Pt 3): 367-369.

Roche Y, Gerbeau-Pissot P, Buhot B, Thomas D, Bonneau L, Gresti J, Mongrand S, Perrier-Cornet J-M, Simon-Plas F. 2008. Depletion of phytosterols from the plant plasma membrane provides evidence for disruption of lipid rafts. *The FASEB Journal* **22**(11): 3980-3991.

Ryan PR, Liu Q, Sperling P, Dong B, Franke S, Delhaize E. 2007. A higher plant Δ8 sphingolipid desaturase with a preference for (*Z*)-isomer formation confers aluminum tolerance to yeast and plants. *Plant Physiology* **144**(4): 1968-1977.

Saavedra L, Balbi V, Dove SK, Hiwatashi Y, Mikami K, Sommarin M. 2009. Characterization of phosphatidylinositol phosphate kinases from the moss *Physcomitrella patens*: PpPIPK1 and PpPIPK2. *Plant & Cell Physiology* **50**(3): 595-609.

Saavedra L, Balbi V, Lerche J, Mikami K, Heilmann I, Sommarin M. 2011. PIPKs are essential for rhizoid elongation and caulonemal cell development in the moss *Physcomitrella patens*. *The Plant Journal* **67**(4): 635-647.

Saavedra L, Catarino R, Heinz T, Heilmann I, Bezanilla M, Malho R. 2015. Phosphatase and tensin homolog Is a growth repressor of both rhizoid and gametophore development in the moss *Physcomitrella patens*. *Plant Physiology* **169**(4): 2572-2586.

Sackmann E. 1990. Molecular and global structure and dynamics of membranes and lipid bilayers. *Canadian Journal of Physics* **68**(9): 999-1012.

Sanabria NM, Huang J-C, Dubery IA. 2010. Self/non-self perception in plants in innate immunity and defense. *Self/Nonself* **1**(1): 40-54.

Sandhoff K, Harzer K. 2013. Gangliosides and Gangliosidoses: Principles of Molecular and Metabolic Pathogenesis. *The Journal of Neuroscience* **33**(25): 10195.

Sato M, Nagano M, Jin S, Miyagi A, Yamaguchi M, Kawai-Yamada M, Ishikawa T. 2019. Plant-Unique *cis/trans* Isomerism of Long-Chain Base Unsaturation is Selectively Required for

Aluminum Tolerance Resulting from Glucosylceramide-Dependent Plasma Membrane Fluidity. *Plants* **9**(1): 19.

Schaefer, Zryd, Knight, Cove. 1991. Stable transformation of the moss *Physcomitrella patens*. *Molecular and General Genetics MGG* **226**(3): 418-424.

Schaefer DG, Delacote F, Charlot F, Vrielynck N, Guyon-Debast A, Le Guin S, Neuhaus JM, Doutriaux MP, Nogué F. 2010. RAD51 loss of function abolishes gene targeting and de-represses illegitimate integration in the moss *Physcomitrella patens*. *DNA Repair (Amst)* **9**(5): 526-533.

Schaefer DG, Zrÿd J-P. 1997. Efficient gene targeting in the moss Physcomitrella patens. *The Plant Journal* **11**(6): 1195-1206.

Scheiffele P, Roth MG, Simons K. 1997. Interaction of influenza virus haemagglutinin with sphingolipid–cholesterol membrane domains via its transmembrane domain. *The EMBO Journal* **16**(18): 5501-5508.

Scherp P, Grotha R, Kutschera U. 2001. Occurrence and phylogenetic significance of cytokinesis-related callose in green algae, bryophytes, ferns and seed plants. *Plant Cell Reports* **20**(2): 143-149.

Schneider CA, Rasband WS, Eliceiri KW. 2012. NIH Image to ImageJ: 25 years of image analysis. *Nature Methods* **9**(7): 671-675.

Scholz J, Brodhun F, Hornung E, Herrfurth C, Stumpe M, Beike A, Faltin B, Frank W, Reski R, Feussner I. 2012. Biosynthesis of allene oxides in *Physcomitrella patens*. *BMC Plant Biology* **12**(1): 228.

Schuette S, Wood AJ, Geisler M, Geisler-Lee J, Ligrone R, Renzaglia KS. 2009. Novel localization of callose in the spores of *Physcomitrella patens* and phylogenomics of the callose synthase gene family. *Annals of Botany* **103**(5): 749-756.

Shanklin J, Cahoon EB. 1998. Desaturation and related modifications of fatty acids. *Annual Review of Plant Physiology and Plant Molecular Biology* **49**: 611-641.

Shi L, Bielawski J, Mu J, Dong H, Teng C, Zhang J, Yang X, Tomishige N, Hanada K, Hannun YA, et al. 2007. Involvement of sphingoid bases in mediating reactive oxygen intermediate production and programmed cell death in *Arabidopsis*. *Cell Research* **17**(12): 1030-1040.

Simons, Ikonen. 1997. Functional rafts in cell membranes. *Nature* **387**(6633): 569-572.

Simons K, Toomre D. 2000. Lipid rafts and signal transduction. *Nature Reviews Molecular Cell Biology* **1**(1): 31-39.

Simons K, Vaz WLC. 2004. Model systems, lipid rafts, and cell membranes. *Annual Review of Biophysics and Biomolecular Structure* **33**(1): 269-295.

Simpson C, Thomas C, Findlay K, Bayer E, Maule AJ. 2009. An Arabidopsis GPI-anchor plasmodesmal neck protein with callose binding activity and potential to regulate cell-to-cell trafficking. *Plant Cell* **21**(2): 581-594.

Singer SJ, Nicolson GL. 1972. The fluid mosaic model of the structure of cell membranes. *Science* **175**(4023): 720-731.

Slotte JP. 1999. Sphingomyelin-cholesterol interactions in biological and model membranes. *Chemistry and Physics of Lipids* **102**(1-2): 13-27.

Slotte JP. 2016. The importance of hydrogen bonding in sphingomyelin's membrane interactions with co-lipids. *Biochima et Biophysica Acta* **1858**(2): 304-310.

Smith WL, Merrill AH, Jr. 2002. Sphingolipid metabolism and signaling minireview series. *Journal of Biological Chemistry* **277**(29): 25841-25842.

Sonnhammer E, von Heijne G, Krogh A. 1998. A hidden Markov model for predicting transmembrane helices in protein sequences. *Proceedings on the International Conference on Intelligent Systems Molecular Biology* **6**: 175-182.

Sousa E, Kost B, Malho R. 2008. Arabidopsis Phosphatidylinositol-4-Monophosphate 5-Kinase 4 Regulates Pollen Tube Growth and Polarity by Modulating Membrane Recycling. *The Plant Cell* **20**(11): 3050-3064.

Sperling P, Franke S, Luthje S, Heinz E. 2005. Are glucocerebrosides the predominant sphingolipids in plant plasma membranes? *Plant Physiology and Biochemistry* **43**(12): 1031-1038.

Sperling P, Heinz E. 2003. Plant sphingolipids: structural diversity, biosynthesis, first genes and functions. *Biochimica et Biophysica Acta* **1632**(1-3): 1-15.

Sperling P, Ternes P, Moll H, Franke S, Zähringer U, Heinz E. 2001. Functional characterization of sphingolipid C4-hydroxylase genes from *Arabidopsis thaliana*. *FEBS Letters* **494**(1-2): 90-94.

Sperling P, Ternes P, Zank TK, Heinz E. 2003. The evolution of desaturases. *Prostaglandins, Leukotrienes & Essential Fatty Acids* **68**(2): 73-95.

Sperling P, Zähringer U, Heinz E. 1998. A sphingolipid desaturase from higher plants - Identification of a new cytochrome b_5 fusion protein. *Journal of Biological Chemistry* **273**(44): 28590-28596.

Stenzel I, Ischebeck T, König S, Holubowska A, Sporysz M, Hause B, Heilmann I. 2008. The Type B Phosphatidylinositol-4-Phosphate 5-Kinase 3 Is Essential for Root Hair Formation in *Arabidopsis thaliana*. *The Plant Cell* **20**(1): 124-141.

Steponkus PL, Lynch DV, Uemura M, Heber U, Pearce RS, Laws RM, Franks F. 1990. The influence of cold acclimation on the lipid composition and cryobehaviour of the plasma membrane of isolated rye protoplasts. *Philosophical Transactions of the Royal Society of London. B, Biological Sciences* **326**(1237): 571-583.

Stone JM, Heard JE, Asai T, Ausubel FM. 2000. Simulation of fungal-mediated cell death by fumonisin B1 and selection of fumonisin B1-resistant (*fbr*) Arabidopsis mutants. *The Plant Cell* **12**(10): 1811-1822.

Strotbek C, Krinninger S, Frank W. 2013. The moss *Physcomitrella patens*: methods and tools from cultivation to targeted analysis of gene function. *The International Journal of Developmental Biology* **57**(6-8): 553-564.

Stumpe M, Göbel C, Faltin B, Beike AK, Hause B, Himmelsbach K, Bode J, Kramell R, Wasternack C, Frank W, et al. 2010. The moss *Physcomitrella patens* contains cyclopentenones but no jasmonates: mutations in allene oxide cyclase lead to reduced fertility and altered sporophyte morphology. *New Phytologist* **188**(3): 740-749.

Szule JA, Fuller NL, Rand RP. 2002. The effects of acyl chain length and saturation of diacylglycerols and phosphatidylcholines on membrane monolayer curvature. *Biophysical Journal* **83**(2): 977-984.

Tarazona P, Feussner K, Feussner I. 2015. An enhanced plant lipidomics method based on multiplexed liquid chromatography–mass spectrometry reveals additional insights into cold- and drought-induced membrane remodeling. *The Plant Journal* **84**(3): 621-633.

Tartaglio V, Rennie EA, Cahoon R, Wang G, Baidoo E, Mortimer JC, Cahoon EB, Scheller HV. 2017. Glycosylation of inositol phosphorylceramide sphingolipids is required for normal growth and reproduction in Arabidopsis. *The Plant Journal* **89**(2): 278-290.

Teng C, Dong H, Shi L, Deng Y, Mu J, Zhang J, Yang X, Zuo J. 2008. Serine Palmitoyltransferase, a Key Enzyme for de Novo Synthesis of Sphingolipids, Is Essential for Male Gametophyte Development in Arabidopsis. *Plant Physiology* **146**(3): 1322-1332.

Ternes P, Feussner K, Werner S, Lerche J, Iven T, Heilmann I, Riezman H, Feussner I. 2011a. Disruption of the ceramide synthase LOH1 causes spontaneous cell death in *Arabidopsis thaliana*. *New Phytologist* **192**(4): 841-854.

Ternes P, Franke S, Zähringer U, Sperling P, Heinz E. 2002. Identification and characterization of a sphingolipid D4-desaturase family. *Journal of Biological Chemistry* **277**(28): 25512-25518.

Ternes P, Sperling P, Albrecht S, Franke S, Cregg JM, Warnecke D, Heinz E. 2006. Identification of Fungal Sphingolipid C9-methyltransferases by Phylogenetic Profiling. *Journal of Biological Chemistry* **281**(9): 5582-5592.

Ternes P, Wobbe T, Schwarz M, Albrecht S, Feussner K, Riezman I, Cregg JM, Heinz E, Riezman H, Feussner I, et al. 2011b. Two pathways of sphingolipid biosynthesis are separated in the yeast *Pichia pastoris*. *Journal of Biological Chemistry* **286**(13): 11401-11414.

Thelander M, Landberg K, Sundberg E. 2018. Auxin-mediated developmental control in the moss *Physcomitrella patens*. *Journal of Experimental Botany* **69**(2): 277-290.

Thelander M, Olsson T, Ronne H. 2005. Effect of the energy supply on filamentous growth and development in *Physcomitrella patens*. *Journal of Experimental Botany* **56**(412): 653-662.

Thudichum JLW. 1884. A treatise on the chemical constitution of the brain: Based throughout upon original researches. *Glasgow Medical Journal* **22**(5): 363-364.

Tilsner J, Nicolas W, Rosado A, Bayer EM. 2016. Staying Tight: Plasmodesmal Membrane Contact Sites and the Control of Cell-to-Cell Connectivity in Plants. *Annual Review of Plant Biology* **67**(1): 337-364.

Tjellström H, Hellgren LI, Wieslander A, Sandelius AS. 2010. Lipid asymmetry in plant plasma membranes: phosphate deficiency-induced phospholipid replacement is restricted to the cytosolic leaflet. *FASEB Journal* **24**(4): 1128-1138.

Tsegaye Y, Richardson CG, Bravo JE, Mulcahy BJ, Lynch DV, Markham JE, Jaworski JG, Chen M, Cahoon EB, Dunn TM. 2007. *Arabidopsis* mutants lacking long chain base phosphate lyase are Fumonisin-sensitive and accumulate trihydroxy-18:1 long chain base phosphate. *Journal of Biological Chemistry* **282**(38): 28195-28206.

Uemura M, Joseph RA, Steponkus PL. 1995. Cold acclimation of *Arabidopsis thaliana*. *Plant Physiology* **109**(1): 15-30.

Uemura M, Steponkus PL. 1994. A contrast of the plasma membrane lipid composition of oat and rye leaves in relation to freezing tolerance. *Plant Physiology* **104**(2): 479-496.

van Hooren M, Munnik T 2017. Plant Plasma Membrane. *eLS*: John Wiley & Sons, Ltd.

van Meer G, Simons K. 1982. Viruses budding from either the apical or the basolateral plasma membrane domain of MDCK cells have unique phospholipid compositions. *The EMBO Journal* **1**(7): 847-852.

Vatén A, Dettmer J, Wu S, Stierhof YD, Miyashima S, Yadav SR, Roberts CJ, Campilho A, Bulone V, Lichtenberger R, et al. 2011. Callose biosynthesis regulates symplastic trafficking during root development. *Developmental Cell* **21**(6): 1144-1155.

Viaene T, Landberg K, Thelander M, Medvecka E, Pederson E, Feraru E, Cooper ED, Karimi M, Delwiche CF, Ljung K, et al. 2014. Directional auxin transport mechanisms in early diverging land plants. *Current Biology* **24**(23): 2786-2791.

von Schwartzenberg K, Núñez MF, Blaschke H, Dobrev PI, Novák O, Motyka V, Strnad M. 2007. Cytokinins in the bryophyte *Physcomitrella patens*: analyses of activity, distribution, and cytokinin oxidase/dehydrogenase overexpression reveal the role of extracellular cytokinins. *Plant Physiology* **145**(3): 786-800.

Voxeur A, Fry SC. 2014. Glycosylinositol phosphorylceramides from Rosa cell cultures are boron-bridged in the plasma membrane and form complexes with rhamnogalacturonan II. *The Plant Journal* **79**(1): 139-149.

Wang W, Yang X, Tangchaiburana S, Ndeh R, Markham JE, Tsegaye Y, Dunn TM, Wang G-L, Bellizzi M, Parsons JF, et al. 2008. An inositolphosphorylceramide synthase is involved in regulation of plant programmed cell death associated with defense in Arabidopsis. *The Plant Cell* **20**(11): 3163-3179.

Wesołowska O, Michalak K, Maniewska J, Hendrich AB. 2009. Giant unilamellar vesicles - a perfect tool to visualize phase separation and lipid rafts in model systems. *Acta Biochimica Polonica* **56**(1): 33-39.

Winter D, Vinegar B, Nahal H, Ammar R, Wilson GV, Provart NJ. 2007. An "Electronic Fluorescent Pictograph" browser for exploring and analyzing large-scale biological data sets. *PLoS One* **2**(8): e718.

Worrall D, Liang Y-K, Alvarez S, Holroyd GH, Spiegel S, Panagopulos M, Gray JE, Hetherington AM. 2008. Involvement of sphingosine kinase in plant cell signalling. *The Plant Journal* **56**(1): 64-72.

Wright BS, Snow JW, O'Brien TC, Lynch DV. 2003. Synthesis of 4-hydroxysphinganine and characterization of sphinganine hydroxylase activity in corn. *Archives of Biochemistry and Biophysics* **415**(2): 184-192.

Wu J-X, Li J, Liu Z, Yin J, Chang Z-Y, Rong C, Wu J-L, Bi F-C, Yao N. 2015. The Arabidopsis ceramidase *At*ACER functions in disease resistance and salt tolerance. *The Plant Journal* **81**(5): 767-780.

Xu C, Shanklin J. 2016. Triacylglycerol Metabolism, Function, and Accumulation in Plant Vegetative Tissues. *Annual Review of Plant Biology* **67**(1): 179-206.

Yan D, Liu Y. 2020. Diverse regulation of plasmodesmal architecture facilitates adaptation to phloem translocation. *Journal of Experimental Botany* **71**(9): 2505-2512.

Yan D, Yadav SR, Paterlini A, Nicolas WJ, Petit JD, Brocard L, Belevich I, Grison MS, Vaten A, Karami L, et al. 2019. Sphingolipid biosynthesis modulates plasmodesmal ultrastructure and phloem unloading. *Nature Plants* **5**(6): 604-615.

Yanagawa D, Ishikawa T, Imai H. 2017. Synthesis and degradation of long-chain base phosphates affect fumonisin B_1-induced cell death in *Arabidopsis thaliana*. *Journal of Plant Research* **130**(3): 571-585.

Yu RK, Ariga T. 1998. The role of glycosphingolipids in neurological disorders. Mechanisms of immune action. *Annals of the New York Academy of Sciences* **845**: 285-306.

Zavaliev R, Ueki S, Epel BL, Citovsky V. 2011. Biology of callose (β-1,3-glucan) turnover at plasmodesmata. *Protoplasma* **248**(1): 117-130.

Zhou Y, Zeng L, Fu X, Mei X, Cheng S, Liao Y, Deng R, Xu X, Jiang Y, Duan X, et al. 2016. The sphingolipid biosynthetic enzyme Sphingolipid delta8 desaturase is important for chilling resistance of tomato. *Scientific Reports* **6**: 38742.

Zienkiewicz A, Gömann J, König S, Herrfurth C, Liu Y-T, Meldau D, Feussner I. 2020. Disruption of Arabidopsis neutral ceramidases 1 and 2 results in specific sphingolipid imbalances triggering different phytohormone-dependent plant cell death programs. *New Phytologist* **226**(1): 170-188.

8 Supplemental material

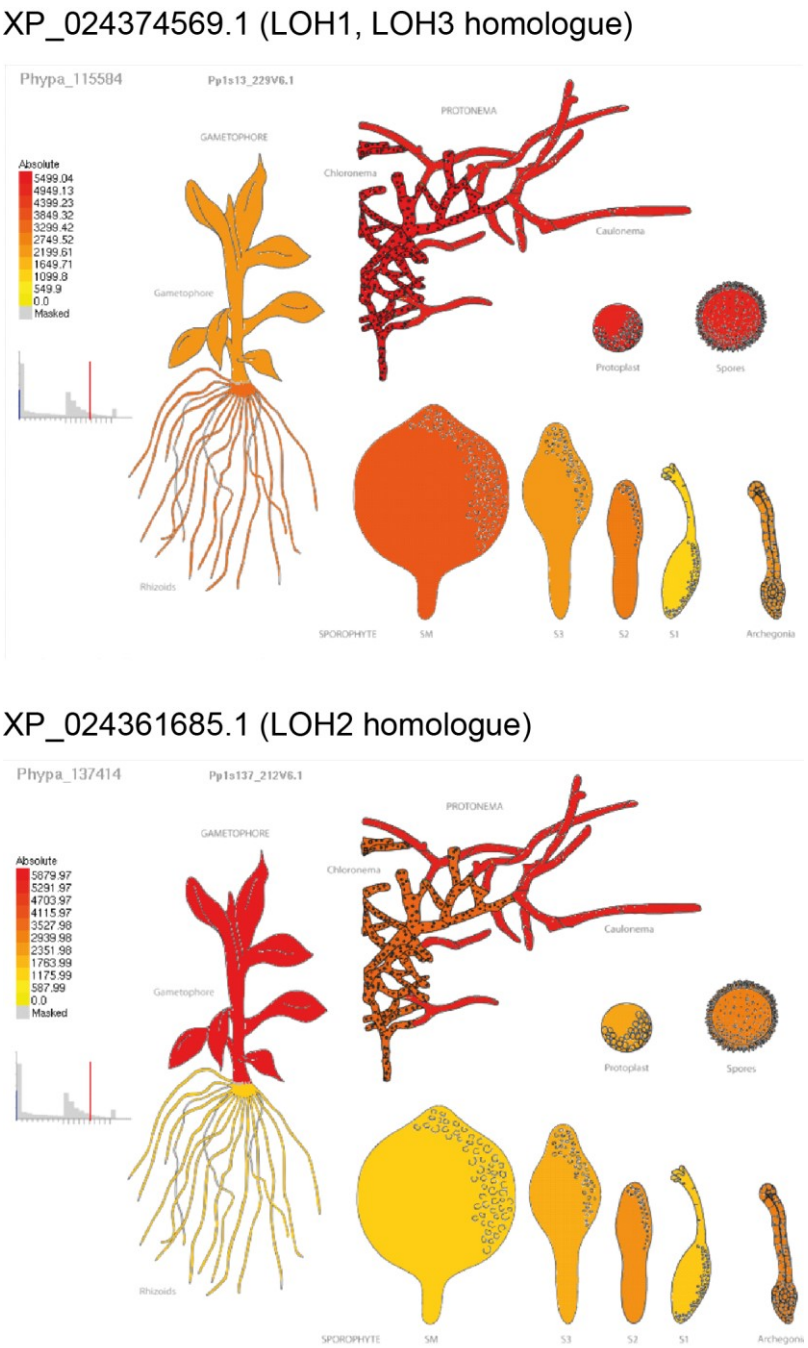

Fig. S1. Predicted expression pattern of putative ceramide synthases in *P. patens* tissues. The putative *P. patens* ceramide synthase with highest sequence homology to *A. thaliana* LOH1 and LOH3 (XP_024374569.1) has higher expression in protonema tissue. The putative *P. patens* ceramide synthase with highest sequence homology to *A. thaliana* LOH2 (XP_024361685.1) has high expression in gametophore and protonema tissue. The expression patterns in *P. patens* were predicted using the eFP browser at bar.utoronto.ca (Winter *et al*., 2007/ Ortiz-Ramirez *et al*., 2015).

9 Acknowledgements

First of all, I would like to thank Prof. Feußner for encouraging me to to pursue my doctor's degree and for offering me this challenging but highly exciting project. He trusted and supported my ideas throughout the course of this project and constantly motivated me during this time.

I am also thankful to Prof. Lipka and Prof Polle for their advisory role as members of my thesis committee.

Many thanks also go to the GGNB Office team who have always been a great support with all administrative issues.

I would also like to express my gratitude to Prof. Feußner and Dr. Kirstin Feußner for their incredible support and understanding during the first months of this project, which were overshadowed by a difficult event in my personal life.

Greatest thanks go to Dr. Kirstin Feußner for always taking the time to discuss with me different aspects of this project, for never getting tired of proofreading all the abstracts, posters, and other texts I wrote during the past three years, and for her kind motivational words when I needed them.

Special thanks also go to Dr. Cornelia Herrfurth for her great guidance in handling the UPLC-nanoESI-MS/MS machine and for her constant assistance in processing and discussing all the lipid data of this work.

I am also incredibly grateful to Dr. Ellen Hornung whose unlimited scientific expertise was helpful in many parts of this work. Although Physcomitrella is not her favorite model organism (yet) she always showed great interest in the progress of this project and patiently helped and motivated me when I got lost.

Greatest thanks also go to my fellow moss researcher in the lab Dr. Tegan Haslam. I am incredibly happy that she has joined our little moss team and it was the greatest pleasure working with her for the past two years. I am beyond grateful for our numerous discussions, for her detailed proofreading of this thesis, and for her valuable input on many parts of this work. Tegan, I wish you all the best for your own project, and I am confident that together with Pauline you will be able to crack some of the riddles of the Physcomitrella sphingolipids.

I would also like to thank Pia Meyer who introduced me to the work with Physcomitrella in the beginning of this project and Dr. Hanno Resemann from whom I took over the project and two of the mutant lines.

Many thanks also go to Dr. Agnieszka and Dr. Krzysztof Zienkiewicz who not only helped me with their technical expertise in microscopy and phytohormone measurements but who also became dear friends of mine during our shared time in the AG Feußner.

Great thanks also go to Sabine Freitag for helping me with all extraction-related questions and for her technical support in the lab. She has also offered me great moral support during this time, and I enjoyed being able to discuss everything and anything with her.
I am further thankful to my students Lina Helwig and Nina Zaremba for their assistance in parts of this work and for giving me the opportunity of learning how to be a teacher myself.
It was a great pleasure working with the people in Ellen's lab, including Ellen, Kathi, Benedikt, Andrea, Tegan, and all the other temporary members. It has always been a joyful atmosphere that I have already missed these past few months and that I will also miss in the future.
A shoutout goes to the Ph.D. girls Milena, Franzi, Anna, Yi-Tse, but especially to Kathi and Elisa. I am happy to have gone through all phases of this experience together with you two. Our mutual support has been invaluable to me during this time and I am glad to have found some true friends in you.
I would also like to thank all the other past and present members of the AG Feußner and AG Ischebeck who accompanied me during this time. I will miss all the (Christmas) movie nights and entertaining coffe breaks.
Greatest thanks also go to my friends outside the lab, Liese, Inka, Alina, Sandra, and the Göttingen gang who made sure that I got my timeouts from the scientific world every once in a while.
Mein größter Dank gilt jedoch meiner Familie, insbesondere meinen Eltern. Ihr habt mir in meinem Leben bisher jede Tür geöffnet und mir mehr als einmal den nötigen Stoß gegeben, um diese Türen auch zu durchschreiten. Die letzten Jahre haben uns mehr als einmal gezeigt was im Leben wirklich wichtig ist. Ich bin unendlich dankbar für eure bedinungslose Unterstützung in all den Jahren und das ich dieses Ereignis mit euch beiden teilen kann.
In the end I would like to thank Benji, the person who has always been closest to the happening and who has gone with me through all ups and downs of this eventful time. Your kindness, resilience, energy, and optimism amaze me and cheer me up on the darkest days. Thank you for this!